Advances in High Energy Physics

Properties of Chemical and Kinetic Freeze-Outs in High-Energy Nuclear Collisions

Lead Guest Editor: Fu-Hu Liu
Guest Editors: Sakina Fakhraddin, Roy A. Lacey, Raghunath Sahoo, Edward Sarkisyan-Grinbaum, and Bhartendu K. Singh

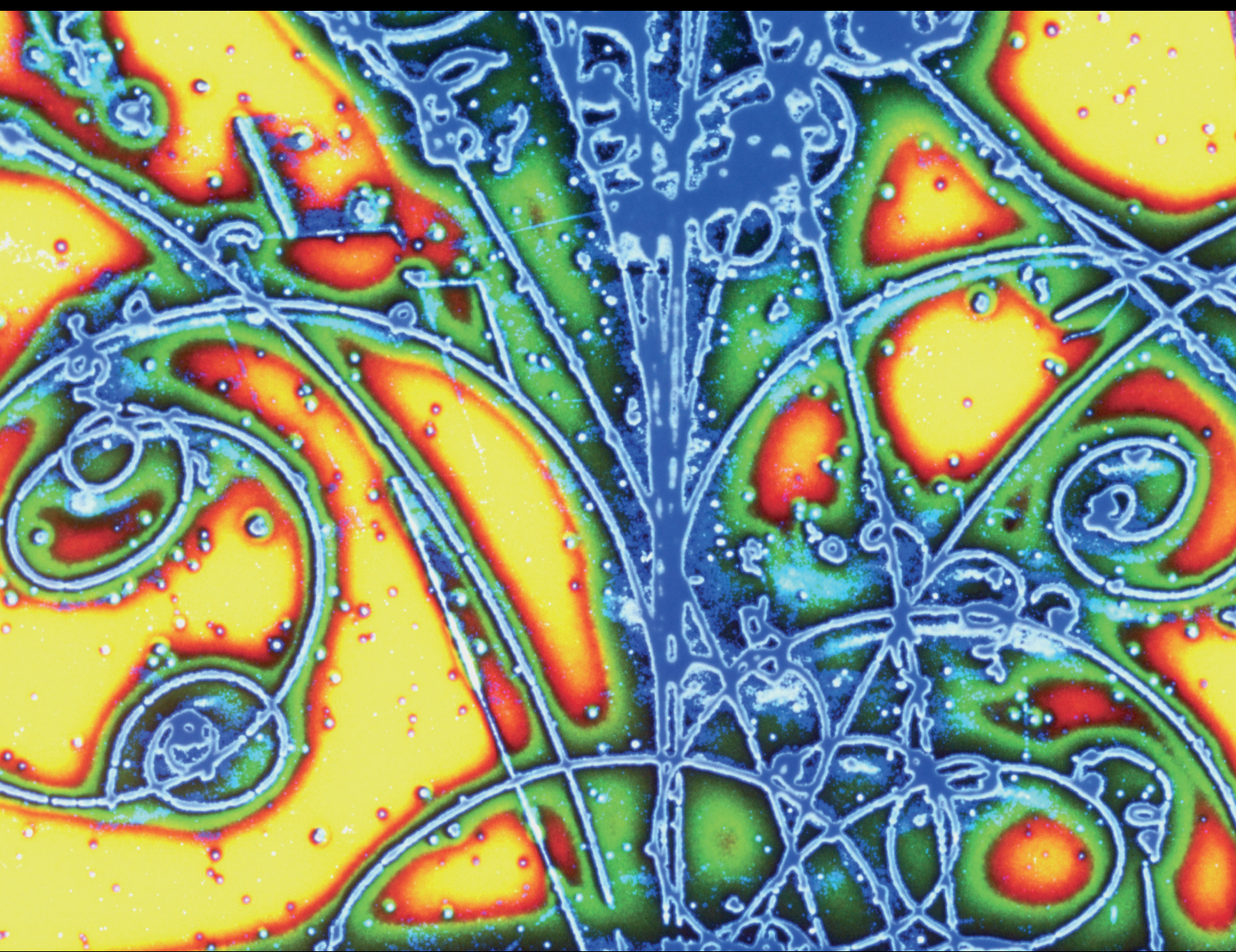

Properties of Chemical and Kinetic Freeze-Outs in High-Energy Nuclear Collisions

Advances in High Energy Physics

Properties of Chemical and Kinetic Freeze-Outs in High-Energy Nuclear Collisions

Lead Guest Editor: Fu-Hu Liu
Guest Editors: Sakina Fakhraddin, Roy A. Lacey, Raghunath Sahoo, Edward Sarkisyan-Grinbaum, and Bhartendu K. Singh

Editorial Board

Contents

Properties of Chemical and Kinetic Freeze-Outs in High-Energy Nuclear Collisions
Fu-Hu Liu, Sakina Fakhraddin, Roy A. Lacey, Raghunath Sahoo, Edward K. Sarkisyan-Grinbaum, and Bhartendu K. Singh
Editorial (3 pages), Article ID 9184574, Volume 2018 (2018)

Angular Dependence of η Photoproduction in Photon-Induced Reaction
Jun-Zhen Wang and Bao-Chun Li
Research Article (9 pages), Article ID 1260124, Volume 2018 (2018)

HBT Radii: Comparative Studies on Collision Systems and Beam Energies
Debasish Das
Review Article (5 pages), Article ID 3794242, Volume 2018 (2018)

Multifractal Analysis of Charged Particle Multiplicity Distribution in the Framework of Renyi Entropy
Swarnapratim Bhattacharyya, Maria Haiduc, Alina Tania Neagu, and Elena Firu
Research Article (15 pages), Article ID 6384357, Volume 2018 (2018)

Radial Flow in a Multiphase Transport Model at FAIR Energies
Soumya Sarkar, Provash Mali, Somnath Ghosh, and Amitabha Mukhopadhyay
Research Article (9 pages), Article ID 7453752, Volume 2018 (2018)

Entropy and Multifractality in Relativistic Ion-Ion Collisions
Shaista Khan and Shakeel Ahmad
Research Article (11 pages), Article ID 2136908, Volume 2018 (2018)

Correlations and Event-by-Event Fluctuations in High Multiplicity Events Produced in ^{208}Pb-^{208}Pb Collisions
Shakeel Ahmad, Shaista Khan, Ashwini Kumar, Arpit Singh, A. Ahmad, and B. K. Singh
Research Article (11 pages), Article ID 6914627, Volume 2018 (2018)

A Description of the Transverse Momentum Distributions of Charged Particles Produced in Heavy Ion Collisions at RHIC and LHC Energies
Jia-Qi Hui, Zhi-Jin Jiang, and Dong-Fang Xu
Research Article (9 pages), Article ID 7682325, Volume 2018 (2018)

Renormalization Group Equation for Tsallis Statistics
Airton Deppman
Research Article (4 pages), Article ID 9141249, Volume 2018 (2018)

Comparing Standard Distribution and Its Tsallis Form of Transverse Momenta in High Energy Collisions
Rui-Fang Si, Hui-Ling Li, and Fu-Hu Liu
Research Article (12 pages), Article ID 7895967, Volume 2018 (2018)

Azimuthal Anisotropy in High-Energy Nuclear Collision: An Approach Based on Complex Network Analysis
Susmita Bhaduri and Dipak Ghosh
Research Article (9 pages), Article ID 8347408, Volume 2018 (2018)

A Description of Pseudorapidity Distributions of Charged Particles Produced in Au+Au Collisions at RHIC Energies
Z. J. Jiang, Dongfang Xu, and Yan Huang
Research Article (8 pages), Article ID 1369098, Volume 2018 (2018)

A Comparative Study of $K^{\pm}/\pi^{\pm}$ Ratio in Proton-Proton Collisions at Different Energies: Experimental Results versus Model Simulation
Swarnapratim Bhattacharyya, Maria Haiduc, Alina Tania Neagu, and Elena Firu
Research Article (7 pages), Article ID 6307205, Volume 2018 (2018)

Mean Field Approximation for the Dense Charged Drop
S. Bondarenko and K. Komoshvili
Research Article (5 pages), Article ID 7374909, Volume 2017 (2018)

Chiral Phase Transition in Linear Sigma Model with Nonextensive Statistical Mechanics
Ke-Ming Shen, Hui Zhang, De-Fu Hou, Ben-Wei Zhang, and En-Ke Wang
Research Article (7 pages), Article ID 4135329, Volume 2017 (2018)

Hindawi
Advances in High Energy Physics
Volume 2018, Article ID 9184574, 3 pages
https://doi.org/10.1155/2018/9184574

Editorial

Properties of Chemical and Kinetic Freeze-Outs in High-Energy Nuclear Collisions

Fu-Hu Liu,[1] **Sakina Fakhraddin**,[2,3] **Roy A. Lacey**,[4] **Raghunath Sahoo**,[5] **Edward K. Sarkisyan-Grinbaum**,[6,7] **and Bhartendu K. Singh**[8]

[1] *Institute of Theoretical Physics, Shanxi University, Taiyuan, Shanxi 030006, China*
[2] *Physics Department, College of Science & Arts in RK, Qassim University, Buraidah 51452, Qassim, Saudi Arabia*
[3] *Physics Department, Faculty of Science, Sana'a University, P.O. Box 1247, Sana'a, Yemen*
[4] *Departments of Chemistry & Physics, Stony Brook University, Stony Brook, NY 11794, USA*
[5] *Discipline of Physics, School of Basic Sciences, Indian Institute of Technology Indore, Indore 453552, India*
[6] *Experimental Physics Department, CERN, 1211 Geneva 23, Switzerland*
[7] *Department of Physics, The University of Texas at Arlington, Arlington, TX 76019, USA*
[8] *Physics Department, Banaras Hindu University, Varanasi 221005, India*

Correspondence should be addressed to Fu-Hu Liu; fuhuliu@163.com

Received 25 September 2018; Accepted 26 September 2018; Published 17 October 2018

The search for a new state of matter and understanding of the conditions of its formation in the extreme conditions of the dense and high-temperature environment is the main goal of the ongoing heavy ion investigations at the CERN LHC experiments such as ALICE, ATLAS, and CMS where heavy-ions are smashed at unprecedented high energies ever reached. The study of these high-energy nuclear collisions is also believed to approach the conditions close to those at the formation of the early Universe which has been undergoing under extreme dense and temperature. The understanding of the formed nuclear matter is a main topic of the today's most theoretical and phenomenological models aimed to describe the conditions and to find the equation of state of the matter formed in heavy ion collisions at the LHC believed to be the quark-gluon plasma, predicted by the theory of strong interaction Quantum Chromodynamics (QCD) being currently under extensive development. The understanding of the features observed in nuclear collisions at high energies at the LHC and at RHIC is also believed to provide keys explaining the observations in nuclear collisions at lower energies of the studies planned and ongoing worldwide as well as unexpected nuclear-type findings in proton-proton collisions at LHC.

To clarify the above points it is crucial to understand the space-time evolution of the system formed during the collision and resulted into the observed particles, mostly hadrons. In these studies, one distinguishes the two so-called freeze-outs, namely, the chemical freeze-out and the kinetic freeze-out, so that the momentum spectra of produced particles are frozen in time. The understanding of this picture is still under wide discussion and attracts lot of interest, as on the one hand, one assumes the chemical and kinetic freeze-outs to occur without any time lag, while on the other hand, there are models considering time interval so that the kinetic freeze-out comes after the chemical one.

This special issue concerns many topics on properties of chemical and kinetic freeze-outs in high-energy nuclear (and particle) collisions, for example, (i) describing particle distributions and correlations and studying statistical laws and dynamical properties related to the special topic; (ii) extracting thermal and dynamical properties of interacting system and formed matters and real thermodynamic parameters of chemical and kinetic freeze-outs; (iii) extracting radial flow velocity and describing elliptic flow and other anisotropic flow; (iv) searching for the softest points of the equation of state and the critical point of hadronic matter to

quark-gluon plasma; and (v) studying collective behavior in small system.

In the article "Chiral Phase Transition in Linear Sigma Model with Nonextensive Statistical Mechanics," K.-M. Shen et al. investigate the chiral phase transition at finite temperature and baryon chemical potential in the framework of the linear sigma model. The corresponding nonextensive distribution is characterized by a nonextensive parameter and the results in the usual Boltzmann-Gibbs case are recovered when the nonextensive parameter levels off to one. The thermodynamics of the linear sigma model and its corresponding phase diagram are analyzed. Some behaviors of the critical temperature, chemical potential, and nonextensive parameter are studied in the phase diagram.

In the article "Mean Field Approximation for the Dense Charged Drop," S. Bondarenko and K. Komoshvili consider the mean field approximation for the description of the probe charged particle in a dense charged drop, solve the corresponding Schrödinger equation for the drop with spherical symmetry in the first order of mean field approximation, and discuss the obtained results. This work is useful for the clarification of the spectrum of the produced particles, which is influenced by the quantum-mechanical properties of the QCD fireball. This approach also provides the connection between the data obtained in the LHC and RHIC experiments and microscopic fields inside the collision region.

In the article "A Comparative Study of $K^{\pm}/\pi^{\pm}$ Ratio in Proton-Proton Collisions at Different Energies: Experimental Results versus Model Simulation," S. Bhattacharyya et al. present a systematic study of K^{+}/π^{+}, K^{-}/π^{-}, and $(K^{+} + K^{-})/(\pi^{+} + \pi^{-})$ ratio in proton-proton collisions as a function of the bombarding energy from 6.3 GeV to 7 TeV using the UrQMD model and DPMJET III model. Comparisons of the simulated results with the available experimental data are also presented. Dependence of K^{+}/π^{+} and K^{-}/π^{-} on energy shows different behaviors for the UrQMD and DPMJET III models. The presence of the horn-like structure in the variation of K^{+}/π^{+} and K^{-}/π^{-} with energy for the experimental data is supported by the DPMJET III model.

In the article "A Description of Pseudorapidity Distributions of Charged Particles Produced in Au+Au Collisions at RHIC Energies," Z. J. Jiang et al. assume that the hot and dense matter expands according to the hydrodynamic model including phase transition and decouples into particles via the prescription of Cooper-Frye. The leading particles are as usual supposed to have Gaussian rapidity distributions with the number equaling that of participants. This investigation shows that the leading particles are essential in describing the pseudorapidity distributions of charged particles produced in high energy heavy ion collisions. This might be due to the different transparencies of nuclei at different energies.

In the article "Azimuthal Anisotropy in High-Energy Nuclear Collision: An Approach Based on Complex Network Analysis," S. Bhaduri and D. Ghosh attempt to find deterministic information on the anisotropy in azimuthal distribution by means of precise determination of topological parameter from a complex network perspective. They construct visibility graphs from their corresponding azimuthal space or ϕ-data sets. From each visibility graph, a number of cluster data sets are extracted, and then again visibility graphs are constructed for each cluster data set and its Monte Carlo simulated counterpart. Each of these clusters is self-similar and scale-free and is of fractal structure.

The article "Comparing Standard Distribution and Its Tsallis Form of Transverse Momenta in High Energy Collisions" investigates the experimental (simulated) transverse momentum spectra of π^{-} produced at midrapidity in central nucleus-nucleus collisions at the SIS, RHIC, and LHC energies obtained by different collaborations, where a few simulated data are taken from the results of FOPI Collaboration which uses the IQMD transport code based on Quantum Molecular Dynamics. A two-component standard distribution and the Tsallis form of standard distribution are used to fit these data in the framework of a multisource thermal model. The excitation functions of main parameters in the two distributions are analyzed.

The article "Renormalization Group Equation for Tsallis Statistics" investigates the scaling properties of thermofractals through the renormalization group equation, known as Callan-Symanzik equation. The Callan-Symanzik equation associated with Tsallis statistics is derived in this article in association with the thermofractal scale-free structure, setting new grounds for the interpretation of nonextensive thermodynamics in terms of renormalization group theory and opening new possibilities of its application in QCD related problems. In addition, this article can be also associated with the nonthermal phase transition of hadronic matter associated with quark-gluon plasma.

The article "A Description of the Transverse Momentum Distributions of Charged Particles Produced in Heavy Ion Collisions at RHIC and LHC Energies" uses nonextensive statistics together with relativistic hydrodynamics including phase transition to discuss the transverse momentum distributions of charged particles produced in heavy ion collisions, by assuming the existence of memory effects and long-range interactions. The combined contributions from nonextensive statistics and hydrodynamics can give a good description of the experimental data in Au+Au collisions at 200 GeV and in Pb+Pb collisions at 2.76 TeV for $\pi^{\pm}$ and $K^{\pm}$ in wide transverse momentum region and for $p(\overline{p})$ in narrow transverse momentum region.

The article "Correlations and Event-by-Event Fluctuations in High Multiplicity Events Produced in ^{208}Pb-^{208}Pb Collisions" analyzes high multiplicity events produced in 158A GeV/c ^{208}Pb-^{208}Pb collisions to study the event-by-event fluctuations. The findings reveal that the method of scaled factorial moments can be used to identify the events having densely populated narrow phase space bins. A few events sorted out by adopting this approach are individually analyzed. It is observed that these events do exhibit large fluctuations in their pseudorapidity and azimuthal angle distributions arising due to some dynamical reasons. Some complex two-dimensional structures render some dynamical origins.

In the article "Entropy and Multifractality in Relativistic Ion-Ion Collisions," S. Khan and S. Ahmad investigate entropy production in multiparticle systems by analyzing the experimental data on ion-ion collisions at AGS and SPS

energies and comparing the findings with those reported earlier for hadron-hadron, hadron-nucleus, and nucleus-nucleus collisions. It is observed that the entropy produced in limited and full phase space, when normalized to maximum rapidity, exhibits a kind of scaling which is nicely supported by Monte Carlo model HIJING. The findings reveal that Rényi's order information entropy could be another way to investigate the fluctuations in multiplicity distributions in terms of spectral function.

In the article "Radial Flow in a Multiphase Transport Model at FAIR Energies," S. Sarkar et al. compare azimuthal distributions of radial velocities of charged hadrons produced in nucleus-nucleus collisions with the corresponding azimuthal distribution of charged hadron multiplicity in the framework of a multiphase transport (AMPT) model at two different collision energies. The mean radial velocity seems to be a good probe for studying radial expansion. While the anisotropic parts of the distributions indicate a kind of collective nature in the radial expansion of the intermediate "fireball" and their isotropic parts characterize a thermal motion, these simulation results at FAIR are also interesting to compare with those at RHIC and LHC.

In the article "Multifractal Analysis of Charged Particle Multiplicity Distribution in the Framework of Renyi Entropy," S. Bhattacharyya et al. present an analysis of multifractality and multifractal specific heat in the frame work of Rényi entropy analysis for the produced shower particles in ^{16}O-AgBr, ^{28}Si-AgBr, and ^{32}S-AgBr interactions at 4.5A GeV/c. Experimental results are compared with the prediction of the UrQMD model. Qualitative information about the multifractal dynamics of particle production process are extracted and reported. The investigation of quark-hadron phase transition in the mentioned interactions in the framework of Ginzburg-Landau theory are also presented.

The article "HBT Radii: Comparative Studies on Collision Systems and Beam Energies" reviews shortly the experimental results on the two-particle Hanbury-Brown-Twiss (HBT) interferometry which is an important probe for understanding the space-time structure of particle emission sources in high energy heavy ion collisions. The HBT radii in central Pb+Pb collisions at 17.3 GeV, in central Au+Au collisions at 19.6 GeV, and in central Cu+Cu collisions at 22.4 GeV are compared with each other. A similarity in the R_{out}/R_{side} ratio with transverse mass across the collision systems is found at the energy bridge from the SPS to RHIC. A rise of the R_{out}/R_{side} ratio at this energy bridge is not observed.

The article "Angular Dependence of η Photoproduction in Photon-induced Reaction" studies the angular dependence of η photoproduction in the photon-induced reaction in the framework of multisource thermal model. The photoproduction of η mesons from nucleons can provide valuable information about the excitation spectrum of the nucleons. The model results are in good agreement with the experimental data from $\eta \longrightarrow 3\pi^0 \longrightarrow 6\gamma$ decay mode. It is shown that the movement factor increases linearly with the photon beam energies. The deformation and translation of emission sources are visually given in the formalism.

This issue brings together a collection of articles on properties of chemical and kinetic freeze-outs in high energy nuclear collisions. We hope this will be a useful issue for researchers working in related areas. Meanwhile, we regret that more manuscripts submitted for publication in this issue have not been accepted according to reviewer's reports.

Conflicts of Interest

The authors declare that they have no conflicts of interest or private agreements with companies.

Acknowledgments

We sincerely thank all the authors who contributed to this issue and all the reviewers who reviewed to this issue.

Fu-Hu Liu
Sakina Fakhraddin
Roy A. Lacey
Raghunath Sahoo
Edward K. Sarkisyan-Grinbaum
Bhartendu K. Singh

Hindawi
Advances in High Energy Physics
Volume 2018, Article ID 1260124, 9 pages
https://doi.org/10.1155/2018/1260124

Research Article

Angular Dependence of η Photoproduction in Photon-Induced Reaction

Jun-Zhen Wang and Bao-Chun Li

Department of Physics, Shanxi University, Taiyuan, Shanxi 030006, China

Correspondence should be addressed to Bao-Chun Li; libc2010@163.com

Received 23 April 2018; Accepted 13 September 2018; Published 30 September 2018

Guest Editor: Sakina Fakhraddin

Photoproduction of η mesons from nucleons can provide valuable information about the excitation spectrum of the nucleons. The angular dependence of η photoproduction in the photon-induced reaction is investigated in the multisource thermal model. The results are compared with experimental data from the $\eta \longrightarrow 3\pi^0 \longrightarrow 6\gamma$ decay mode. They are in good agreement with the experimental data. It is shown that the movement factor increases linearly with the photon beam energies. And the deformation and translation of emission sources are visually given in the formalism.

1. Introduction

The excitation spectrum of nucleons is important to understanding the nonperturbative behavior of the fundamental theory of strong interactions, Quantum Chromodynamics (QCD) [1–4]. The photon-induced meson production off nucleons is mainly used to achieve more information from the excitation spectrum of nucleons. It is very important for missing resonances that the η meson production in photon-induced and hadron-induced reactions on free (and quasi-free) nucleons and on nuclei [5–8]. The advantage of photon-induced reactions is that the electromagnetic couplings can provide valuable information related to the details of the model wave functions. Because the electromagnetic excitations are isospin dependent, we need perform meson-production reactions off the neutron.

Recently, the photoproduction of η mesons from quasi-free protons and neutrons was measured in $\eta \longrightarrow 3\pi^0 \longrightarrow 6\gamma$ decay mode by the CBELSA/TAPS detector at the electron accelerator ELSA in Bonn [9]. At different incident photon energies, the experiments are performed by the incident photon beam on a liquid deuterium target. A great number of η mesons are produced in the photon-induced reaction. The experimental data are regarded as a multiparticle system. And, their angular distributions represent an obvious regularity at different incident photon energies. In order to explain the abundant experimental results, some statistical methods are proposed and developed [10–16]. In this work, we will extend a multi-source thermal model to the statistical investigation of the angular distributions in the photon-induced reaction and try to understand the η photoproduction in the reaction. In our previous wok [17–21], the model was focused on the investigation of the particle production in intermediate-energy and high-energy collisions.

2. η Meson Distribution in the Multi-Source Thermal Model

In the multi-source thermal model [17–21], many emission sources are expected to be formed at the final stage of the photon-induced reaction. Every source emits particles isotropically in the source rest frame. The observed η mesons are from different emission sources. The incident beam direction is defined as an oz axis and the reaction plane is defined as yoz plane. In the source rest frame, the meson momentum p_x, p_y, and p_z obeys a normal distribution. The corresponding transverse momentum $p_T = \sqrt{p_x^2 + p_y^2}$ obeys a Rayleigh distribution:

$$f_{p_T}(p_T) = \frac{p_T}{\sigma^2} e^{-p_T^2/2\sigma^2}, \quad (1)$$

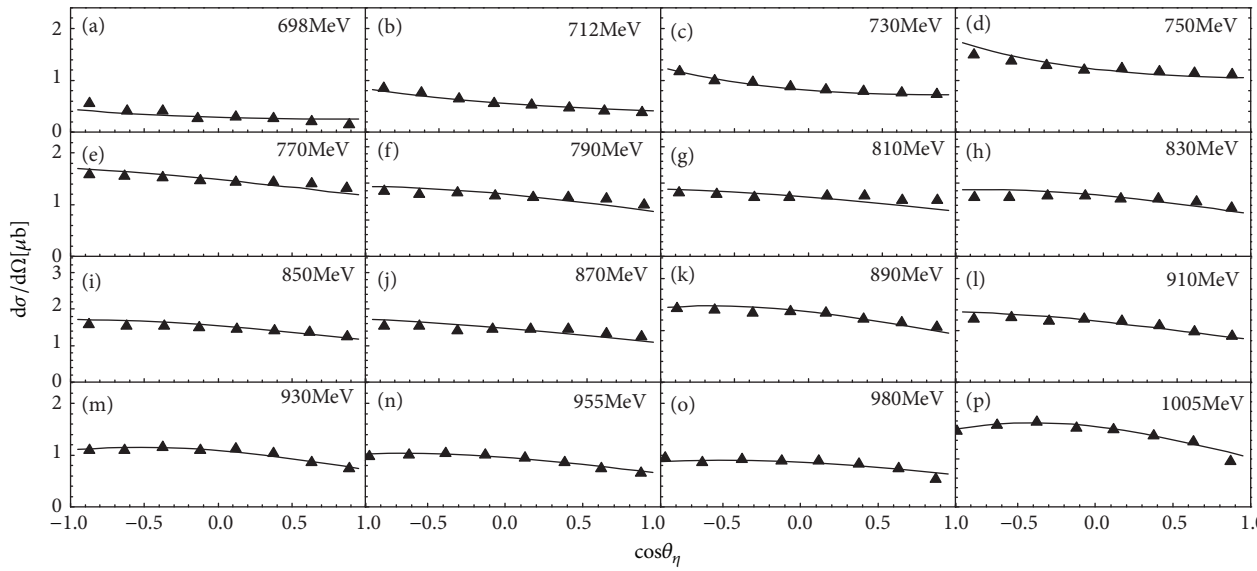

Figure 1: Angular distributions for different bins of incident photon energy 698 MeV ≤ E_γ ≤ 1005MeV as a function of $\cos\theta_\eta$ in the beam-target cm system assuming the initial state nucleon at rest. The symbols represent the experimental data from the CBELSA/TAPS detector at the electron accelerator ELSA in Bonn [9]. The results in the multi-source thermal model are shown with the curves.

where σ represents a distribution width. The distribution function of the polar angle θ is

$$f_\theta(\theta) = \frac{1}{2}\sin\theta \tag{2}$$

Because of the interactions with other emission sources, the considered source deforms and translates along the oz axis. Then, the momentum component is revised to

$$p_z' = a_z p_z + b_z \sigma \tag{3}$$

where a_z and b_z represent the coefficients of the source deformation and translation along the oz axis, respectively. The mathematical description of the deformable translational source is formulized simply as a linear relationship between p_z' and p_z, which reflects the mean result of the source interaction. For $a_z \neq 1$ or $b_z \neq 0$, the p_z' distribution of η mesons is anisotropic along the oz axis.

By using Monte Carlo method, p_T and p_z' are given by

$$p_T = \sigma\sqrt{-2\ln r_1}, \tag{4}$$

$$p_z' = a_z\sigma\sqrt{-2\ln r_2}\cos(2\pi r_3) + b_z\sigma, \tag{5}$$

where r_1, r_2, and r_3 are random numbers from 0 to 1. The polar angle θ is revised to

$$\theta' = \arctan\frac{p_T}{p_z'} = \arctan\frac{\sqrt{-2\ln r_1}}{a_z\sqrt{-2\ln r_2}\cos(2\pi r_3) + b_z}. \tag{6}$$

We can calculate a new distribution function of the polar angle by this formula.

3. Angular Dependencies of η Photoproduction in the Photon-Induced Reaction

Figures 1(a)–1(p) show the angular distributions of η mesons for different bins of incident photon energy 698 MeV ≤ E_γ ≤ 1005 MeV as a function of $\cos\theta_\eta$. θ_η is the polar angle of η meson in the beam-target cm system assuming the initial state nucleon at rest. The symbols represent the experimental data from the CBELSA/TAPS detector at the electron accelerator ELSA in Bonn [9]. The results obtained by using the multi-source thermal model are shown with the curves, which behave in the same way as the experimental data in the 16 bins of incident photon energy. By minimizing χ^2 per degree of freedom (χ^2/dof), we determine the corresponding parameters a_z and b_z, which are presented in Table 1. It is found that there is an almost linear relationship between the b_z and E_γ. As representative energies of Figure 1, we give a schematic sketch of these emission sources at the four different energies in Figure 7(a). The deformations and translations can be seen intuitively in the figure.

In Figures 2(a)–2(p) and Figures 3(a)–3(p), we present the angular distributions of η mesons for different bins of incident photon energy 1035 MeV ≤ E_γ ≤ 1835 MeV as a function of $\cos\theta_\eta$. θ_η is the polar angle of η meson in the beam-target cm system assuming the initial state nucleon at rest. Same as Figure 1, the symbols represent the experimental data from the CBELSA/TAPS detector at the electron accelerator ELSA in Bonn [9]. The results obtained by using the multisource thermal model are shown with the curves, which behave in the same way as the experimental data in the 28 bins of incident photon energy. Parameters a_z and b_z are presented in Tables 2 and 3. As the representative energies of Figures 1 and

Table 1: Values of a_z and b_z taken in Figure 1 model results.

Figure 1	E_γ (MeV)	a_z	b_z	χ^2/dof
(a)	698	1.050	-0.170	0.118
(b)	712	1.020	-0.210	0.105
(c)	730	1.050	-0.170	0.090
(d)	750	1.040	-0.155	0.134
(e)	770	0.985	-0.105	0.182
(f)	790	0.970	-0.125	0.179
(g)	810	0.979	-0.110	0.194
(h)	830	0.960	-0.120	0.192
(i)	850	0.970	-0.110	0.200
(j)	870	0.980	-0.130	0.211
(k)	890	0.950	-0.120	0.175
(l)	910	0.970	-0.140	0.261
(m)	930	0.940	-0.110	0.179
(n)	955	0.950	-0.120	0.154
(o)	980	0.950	-0.090	0.138
(p)	1005	0.920	-0.110	0.150

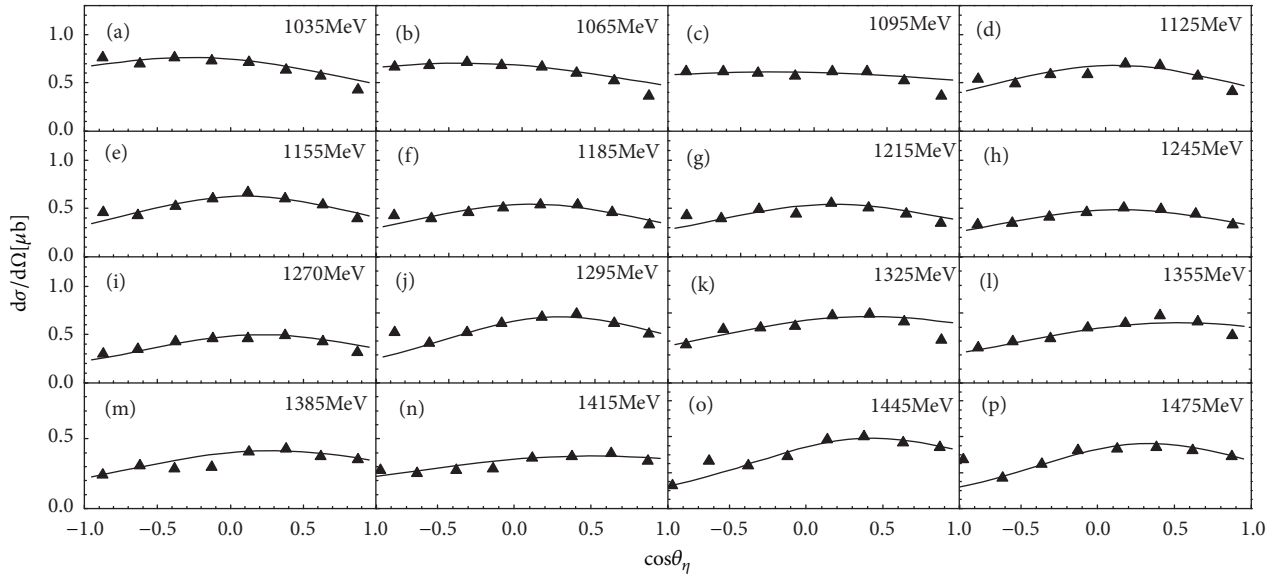

Figure 2: Same as Figure 1, but showing angular distributions for different bins of incident photon energy 1035 MeV ≤ E_γ ≤ 1475MeV.

2, the schematic sketches of the emission sources are given at different energies in Figures 7(b) and 7(c).

In Figures 4, 5, and 6, we show angular distributions in the η-nucleon cm system for $\gamma p \longrightarrow p\eta$ reaction for the different bins of final state energy 1488 MeV ≤ W ≤ 1625 MeV, 1635 MeV ≤ W ≤ 1830 MeV and 1850 MeV ≤ W ≤ 2070 MeV, respectively. Same as Figure 1, the model results and experimental data are indicated by the curves and symbols, respectively. The model results can also agree with the experimental data. In the same way, the deformations and translations of these emission sources are given in Tables 4–6 and Figures 7(d)–7(f). All the parameter values taken in the above calculations are also given in Figures 8 and 9. It can be found that a_z keeps almost invariable and fluctuates around 1.0 with the increasing E_γ. The parameter b_z increases linearly with the increasing E_γ and their relationship can be expressed by a linearly function, $b_z = (0.541 \pm 0.005) \times 10^{-3} E_\gamma - (0.622 \pm 0.011)$. There are similar relationships between the parameters and different final state energies W in Figure 9, where the fitting function of b_z is $b_z = (0.808 \pm 0.003) \times 10^{-3} W - (1.322 \pm 0.007)$.

4. Discussion and Conclusions

The excitation spectrum of nucleons can especially help us to understand the strong interaction in the nonperturbative regime. Before, the hadron induced reactions is a main experimental method in the investigation. In the last two

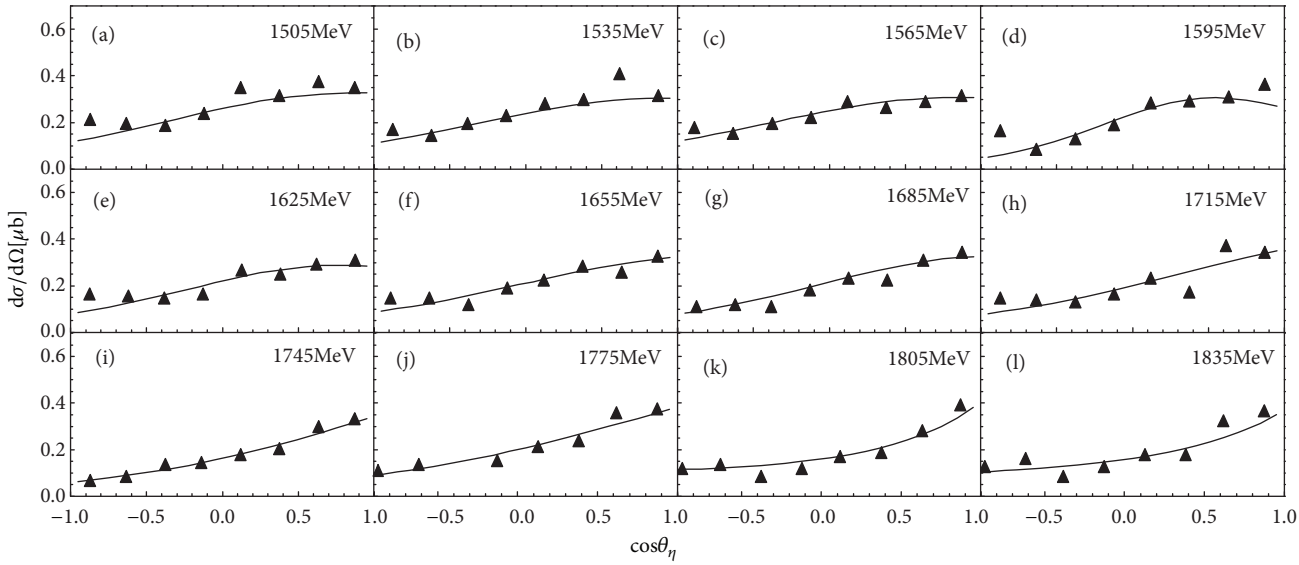

Figure 3: Same as Figure 1, but showing angular distributions for different bins of incident photon energy 1505 MeV ≤ E_γ ≤ 1835MeV.

Table 2: Values of a_z and b_z taken in Figure 2 model results.

Figure 2	E_γ (MeV)	a_z	b_z	χ^2/dof
(a)	1035	0.920	-0.080	0.124
(b)	1065	0.940	-0.090	0.118
(c)	1095	0.970	-0.030	0.132
(d)	1125	0.870	0.030	0.165
(e)	1155	0.850	0.050	0.170
(f)	1185	0.850	0.030	0.168
(g)	1215	0.860	0.070	0.173
(h)	1245	0.860	0.050	0.122
(i)	1270	0.850	0.110	0.121
(j)	1295	0.830	0.150	0.145
(k)	1325	0.910	0.120	0.147
(l)	1355	0.910	0.160	0.142
(m)	1385	0.890	0.110	0.115
(n)	1415	0.930	0.130	0.106
(o)	1445	0.830	0.250	0.122
(p)	1475	0.810	0.210	0.091

Table 3: Values of a_z and b_z taken in Figure 3 model results.

Figure 3	E_γ (MeV)	a_z	b_z	χ^2/dof
(a)	1505	0.915	0.260	0.243
(b)	1535	0.920	0.260	0.190
(c)	1565	0.920	0.240	0.158
(d)	1595	0.800	0.360	0.315
(e)	1625	0.890	0.310	0.179
(f)	1655	0.930	0.340	0.190
(g)	1685	0.910	0.360	0.206
(h)	1715	0.940	0.400	0.235
(i)	1745	0.960	0.460	0.085
(j)	1775	0.960	0.410	0.144
(k)	1805	1.090	0.400	0.132
(l)	1835	1.060	0.390	0.140

Table 4: Values of a_z and b_z taken in Figure 4 model results.

Figure 4	W (MeV)	a_z	b_z	χ^2/dof
(a)	1488	0.956	-0.098	0.086
(b)	1492	0.968	-0.069	0.125
(c)	1498	0.966	-0.058	0.101
(d)	1505	0.959	-0.063	0.114
(e)	1515	0.965	-0.052	0.205
(f)	1525	0.952	-0.048	0.192
(g)	1535	0.960	-0.063	0.143
(h)	1545	0.967	-0.066	0.206
(i)	1555	0.948	-0.060	0.174
(j)	1565	0.941	-0.072	0.168
(k)	1575	0.934	-0.059	0.170
(l)	1585	0.955	-0.068	0.235
(m)	1595	0.925	-0.051	0.260
(n)	1605	0.934	-0.039	0.251
(o)	1615	0.942	-0.045	0.307
(p)	1625	0.961	-0.058	0.293

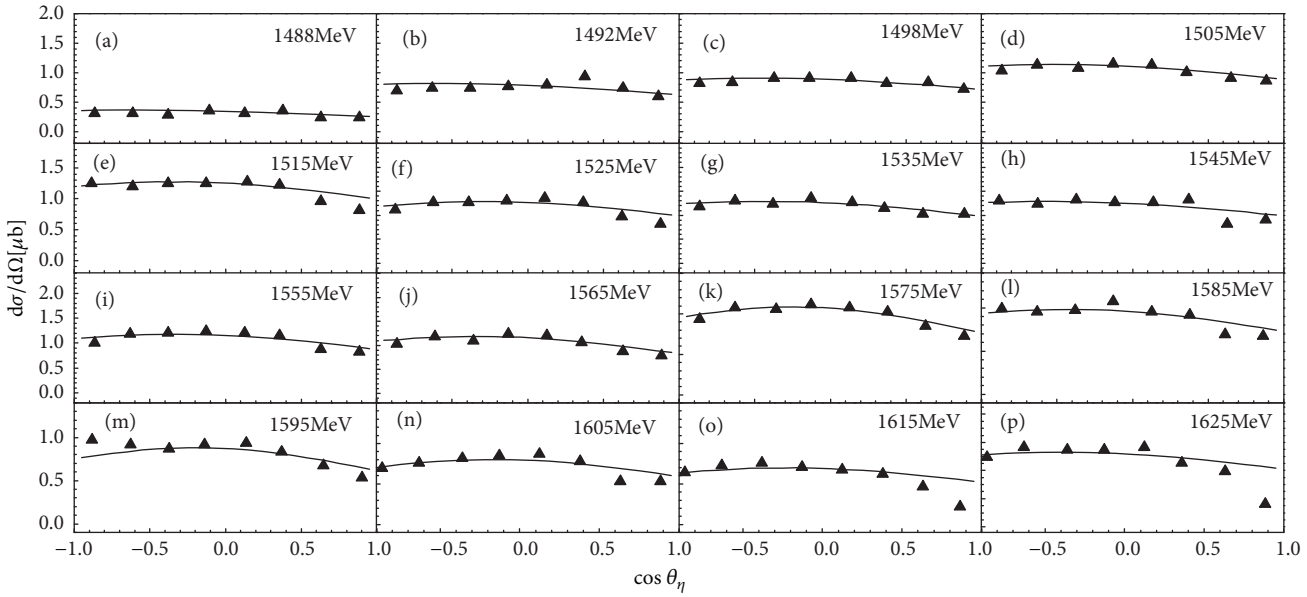

Figure 4: Angular distributions in the η-nucleon cm system for the reaction $\gamma p \longrightarrow p\eta$ for the different bins of final state energy 1488 MeV $\leq W \leq$ 1625 MeV. The symbols represent the experimental data from the CBELSA/TAPS detector at the electron accelerator ELSA in Bonn [9]. The results in the multisource thermal model are shown with the curves.

decades, the photon-induced reaction and electron scattering experiment are applied to study the electromagnetic excitation of baryons. Recently, the photoproduction of η mesons from quasi-free protons and neutrons are measured by the CBELSA/TAPS detector. In the paper, we theoretically study the angular distribution of η mesons for different incident photon energies E_γ and for different final state energies W. Then, the results are compared with the experimental data in detail. The deformation coefficient a_z and translation coefficient b_z are extracted by the comparison. a_z is almost independent of incident photon energies and final state energies. b_z is linearly dependent on incident photon energies and final state energies. In particular, we visually give the deformation and translation of the emission sources by schematic sketches. From the patterns, it is intuitive and easy to better understand the motion and configuration of the emission sources.

A great number of η mesons are produced in the photon-induced reaction. These η mesons are regarded as a multiparticle system, which can be analyzed by the statistical method. In recent years, we develop such a model, which is called multisource thermal model. Some emission sources of final-state particles are formed in the reaction. Each emission source emits particles isotropically in the rest frame of the emission

Table 5: Values of a_z and b_z taken in Figure 5 model results.

Figure 5	W (MeV)	a_z	b_z	χ^2/dof
(a)	1635	0.958	-0.042	0.305
(b)	1645	0.940	-0.028	0.350
(c)	1655	0.920	-0.021	0.263
(d)	1670	0.925	-0.009	0.187
(e)	1690	0.902	0.022	0.240
(f)	1710	0.899	0.047	0.209
(g)	1730	0.868	0.095	0.181
(h)	1750	0.843	0.102	0.194
(i)	1770	0.853	0.115	0.235
(j)	1790	0.879	0.125	0.170
(k)	1810	0.855	0.142	0.152
(l)	1830	0.867	0.159	0.138

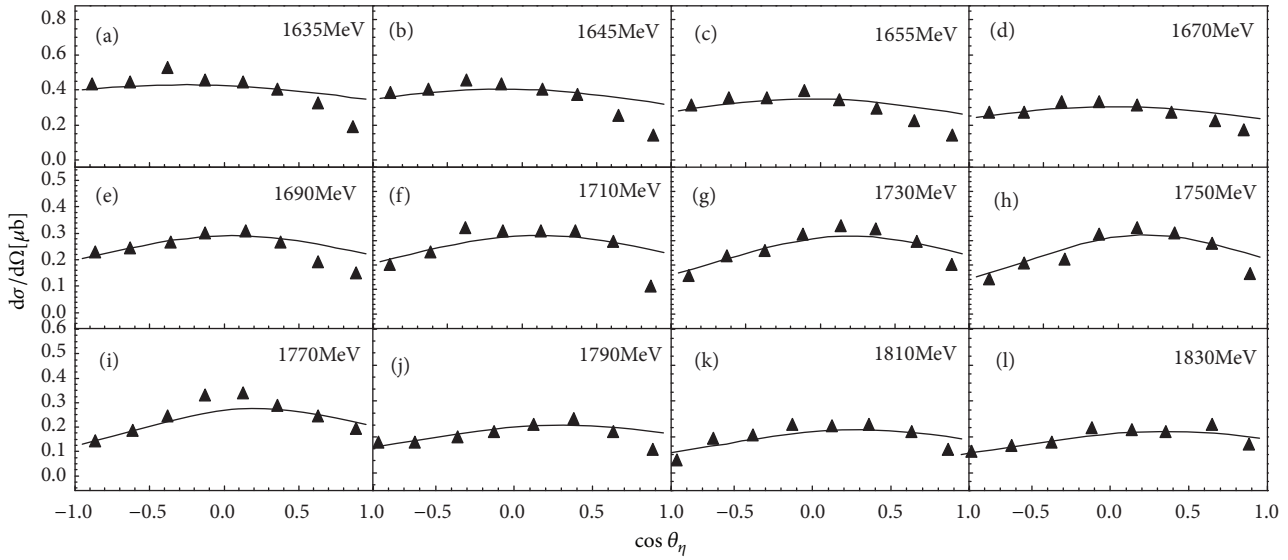

Figure 5: Same as Figure 4, but showing angular distributions for the different bins of final state energy 1635 MeV ≤ W ≤ 1830 MeV.

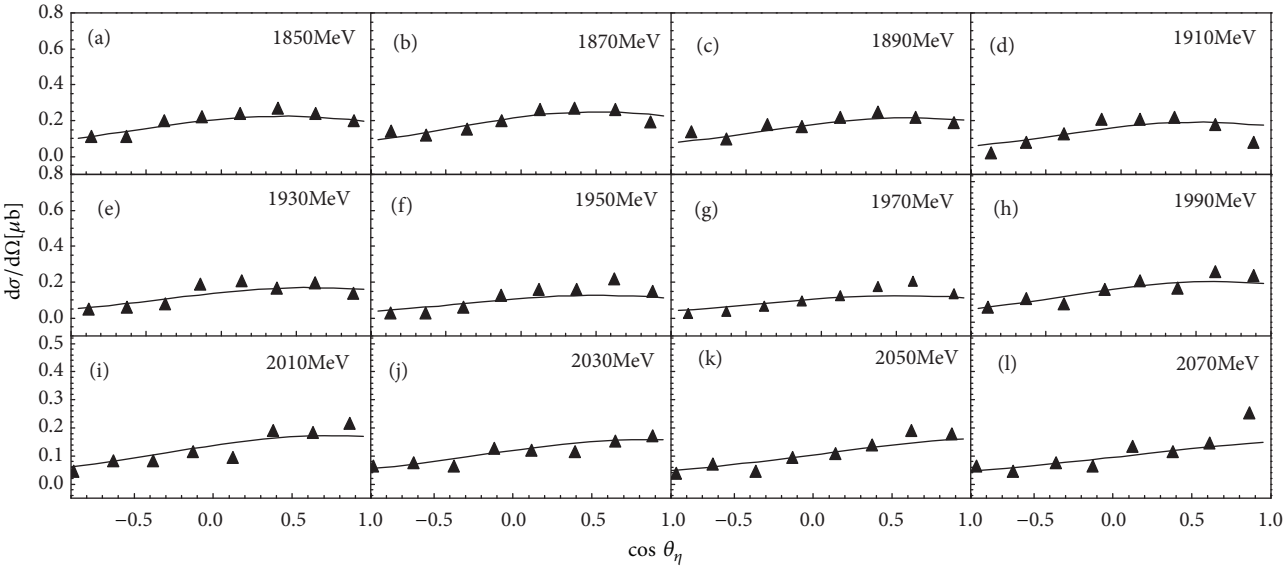

Figure 6: Same as Figure 4, but showing angular distributions for the different bins of final state energy 1850 MeV ≤ W ≤ 2070 MeV.

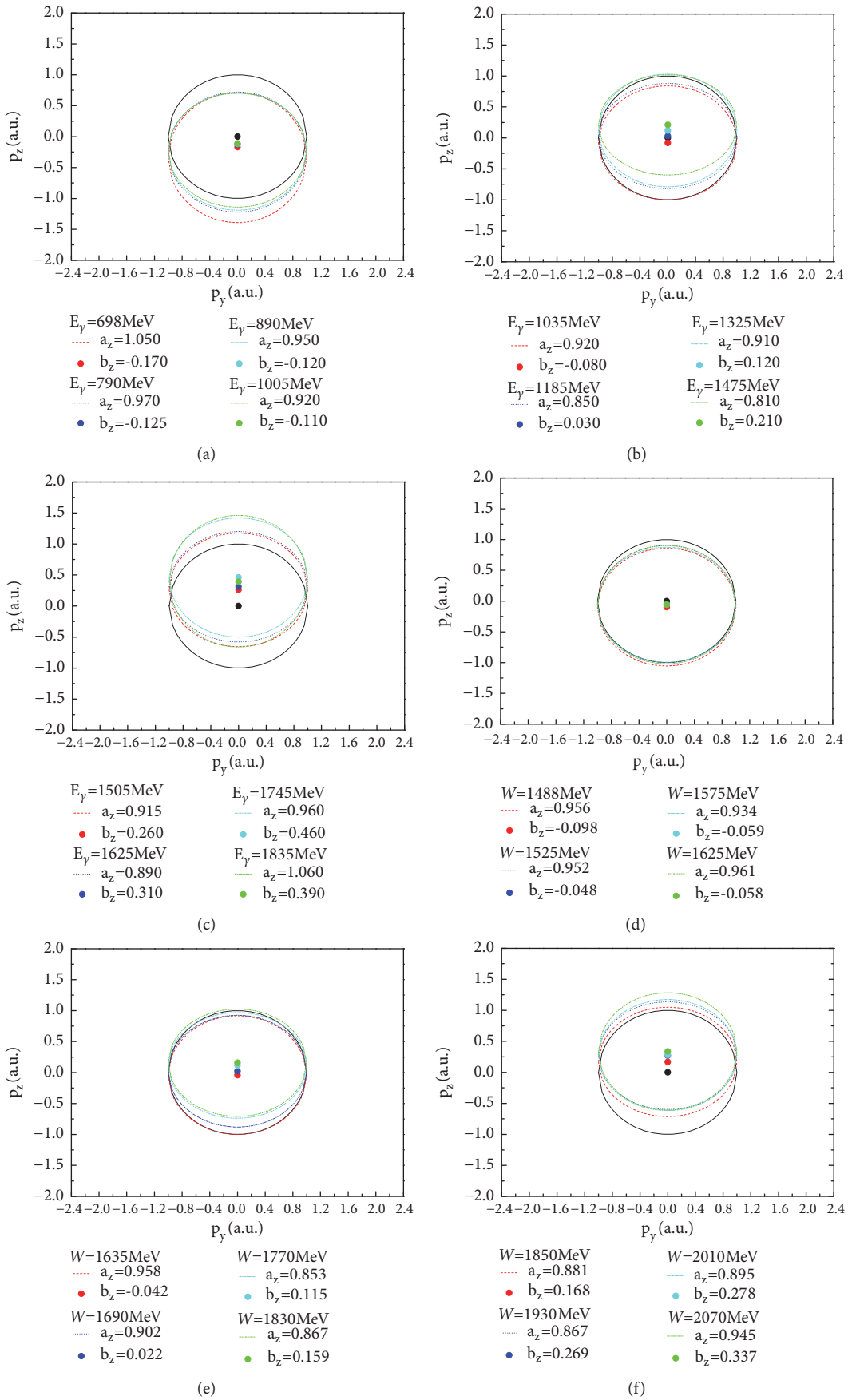

FIGURE 7: The deformable and translational source in the reaction plane for different bins of incident photon energy E_γ or final state energy W.

Table 6: Values of a_z and b_z taken in Figure 6 model results.

Figure 6	W (MeV)	a_z	b_z	χ^2/dof
(a)	1850	0.881	0.168	0.127
(b)	1870	0.872	0.221	0.132
(c)	1890	0.883	0.241	0.135
(d)	1910	0.856	0.252	0.153
(e)	1930	0.867	0.269	0.218
(f)	1950	0.853	0.253	0.295
(g)	1970	0.860	0.249	0.321
(h)	1990	0.875	0.261	0.184
(i)	2010	0.895	0.278	0.359
(j)	2030	0.906	0.299	0.337
(k)	2050	0.932	0.348	0.285
(l)	2070	0.945	0.337	0.304

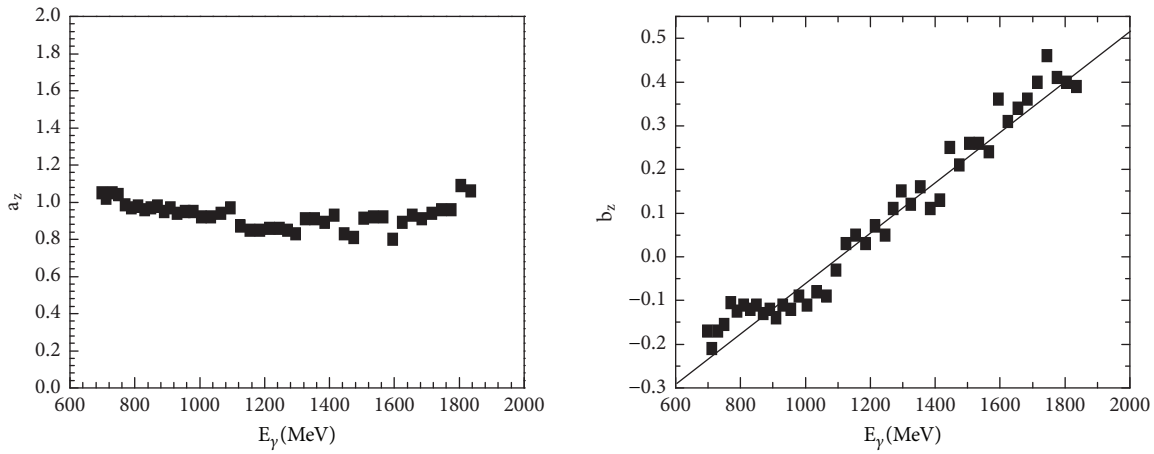

Figure 8: a_Z and b_Z for different bins of incident photon energy E_γ. The symbols are the values taken in Figures 1–3. The straight line is a fitted curve.

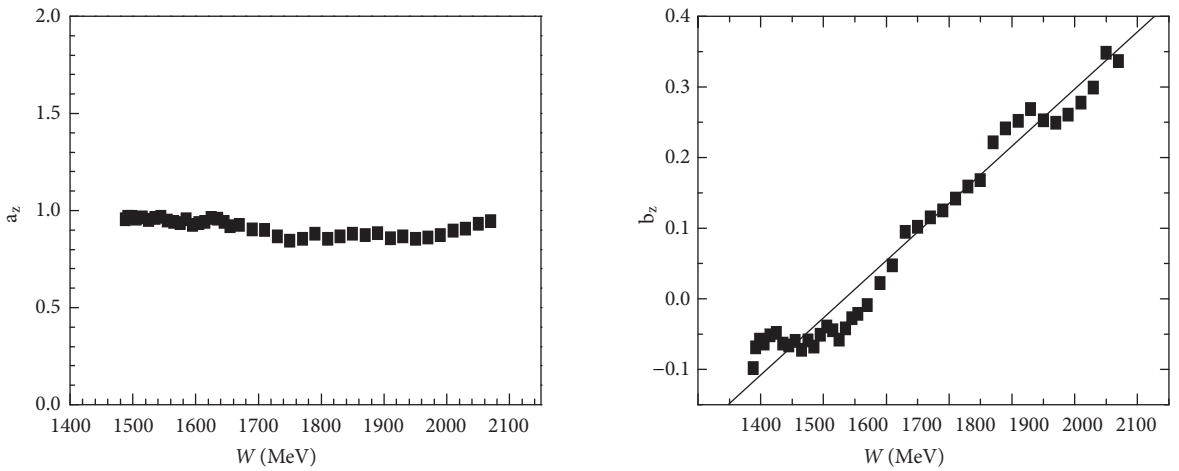

Figure 9: The a_Z and b_Z values taken for different bins of final state energy W. The symbols are the values taken in Figures 4–6. The straight line is a fitted curve.

source. Due to the source interaction, the sources emit particles anisotropically. The η mesons are emitted from these sources. In our previous work, the model can successfully describe transverse momentum spectra and pseudorapidity spectra of final-state particles produced in proton-proton (pp) collisions, proton-nucleus (pA) collisions, and nucleus -nucleus (AA) collisions at intermediate energy and at high energy [17–21]. In this work, we extend the multisource thermal model to the statistical investigation of final-state particles produced in the photon-induced reaction. The model is improved to describe the angular dependence of the η photoproduction from quasi-free protons and neutrons. The information of the source deformation and translation is obtained with different beam energies. It is helpful for us to understand the η photoproduction.

Data Availability

The theoretical results are compared with experimental data, which are from [9].

Conflicts of Interest

The authors declare that they have no conflicts of interest.

Acknowledgments

This work is supported by National Natural Science Foundation of China under Grants No. 11247250 and No. 11575103, Shanxi Provincial Natural Science Foundation under Grant No. 201701D121005, and Scientific and Technological Innovation Programs of Higher Education Institutions in Shanxi (STIP) Grant No. 201802017.

References

[1] B. Krusche, C. Wilkin, and Prog. Part, "Production of η and η' mesons on nucleons and nuclei," *Progress in Particle and Nuclear Physics*, vol. 80, pp. 43–95, 2014.

[2] M. Dieterle, "First measurement of the polarization observable E and helicity-dependent cross sections in single π^0 photoproduction from quasi-free nucleons," *Phys. Lett. B*, vol. 770, no. 523, 2017.

[3] B. C. Li, Y. Y. Fu, L. L. Wang, and F.-H. Liu, "Dependence of elliptic flows on transverse momentum and number of participants in Au+Au collisions at $\sqrt{s_{NN}}$=200 GeV," *Journal of Physics G: Nuclear and Particle Physics*, vol. 40, no. 2, Article ID 025104, 2013.

[4] T. Sekihara, H. Fujioka, and T. Ishikawa, "Possible η'd bound state and its bound state and its s-channel formation in the γd $\longrightarrow$ ηd reaction," *Physical Review C*, vol. 97, Article ID 045202, 2018.

[5] A. V. Anisovich, "Neutron helicity amplitudes," *Physical Review C*, vol. 96, Article ID 055202, 2017.

[6] V. Kuznetsov, "Observation of Narrow $N^+(1685)$ and N^o Resonances in $_\gamma N \longrightarrow \pi\eta N$ Reactions," *JETP Lett*, vol. 106, no. 11, pp. 693–699, 2017.

[7] J. D. Holt, J. Menéndez, J. Simonis, and A. Schwenk, "Three-nucleon forces and spectroscopy of neutron-rich calcium isotopes," *Physical Review C: Nuclear Physics*, vol. 90, no. 2, Article ID 024312, 2014.

[8] S. A. Voloshin, "Collective phenomena in ultra-relativistic nuclear collisions: anisotropic flow and more," *Progress in Particle and Nuclear Physics*, vol. 67, no. 2, pp. 541–546, 2012.

[9] L. Witthauer, "Photoproduction of η mesons from the neutron: Cross sections and double polarization observable E," *The European Physical Journal A*, vol. 53, no. 58, 2017.

[10] J. Rafelski and J. Letessier, "Testing limits of statistical hadronization," *Nuclear Physics A*, vol. 715, p. 98, 2003.

[11] A. Andronic, P. Braun-Munzinger, and J. Stachel, "Thermal hadron production in relativistic nuclear collisions: The hadron mass spectrum, the horn, and the QCD phase transition," *Physics Letters B*, vol. 673, no. 2, pp. 142–145, 2009.

[12] J. Cleymans, H. Oeschler, K. Redlich, and S. Wheaton, "Comparison of chemical freeze-out criteria in heavy-ion collisions," *Physical Review C: Nuclear Physics*, vol. 73, no. 4, Article ID 034905, 2006.

[13] P. Braun-Munzinger, J. Stachel, and C. Wetterich, "Chemical freeze-out and the QCD phase transition temperature," *Physics Letters B*, vol. 596, no. 1-2, pp. 61–69, 2004.

[14] A. Adare, S. Afanasiev, and C. Aidala, "Measurement of neutral mesons in p+p collisions at $\sqrt{s}$=200 GeV and scaling properties of hadron production," *Physical Review D: Particles, Fields, Gravitation and Cosmology*, vol. 83, Article ID 052004, 2011.

[15] K. Aamodt, N. Abel, and U. Abeysekara, "Transverse momentum spectra of charged particles in proton–proton collisions at $\sqrt{s}$ = 900 GeV with ALICE at the LHC," *Physics Letters B*, vol. 693, no. 2, pp. 53–68, 2010.

[16] C. Y. Wong and G. Wilk, "Tsallis fits to p_T spectra and multiple hard scattering in pp collisions at the LHC," *Physical Review D: Particles, Fields, Gravitation and Cosmology*, vol. 87, Article ID 114007, 2013.

[17] B. C. Li, Y. Y. Fu, E. Q. Wang, L. L. Wang, and F. H. Liu, "Transverse momentum dependence of charged and strange hadron elliptic flows in Cu–Cu collisions," *Journal of Physics G: Nuclear and Particle Physics*, vol. 39, no. 8, Article ID 025009, 2012.

[18] S. Andringa, E. Arushanova, and S. Asahi, "Current status and future prospects of the SNO+ experiment," *Advances in High Energy Physics*, vol. 2016, Article ID 6194250, 21 pages, 2016.

[19] B.-C. Li, Y.-Z. Wang, F.-H. Liu, X.-J. Wen, and Y.-E. Dong, "Particle production in relativistic pp and AA collisions at RHIC and LHC energies with Tsallis statistics using the two-cylindrical multisource thermal model," *Physical Review D: Particles, Fields, Gravitation and Cosmology*, vol. 89, Article ID 054014, 2014.

[20] B. C. Li, Y. Z. Wang, and F. H. Liu, "Formulation of transverse mass distributions in Au–Au collisions at $\sqrt{s}$NN = 200 GeV/nucleon," *Physics Letters B*, vol. 725, no. 4-5, pp. 352–356, 2013.

[21] B.-C. Li, Z. Zhang, J.-H. Kang, G.-X. Zhang, and F.-H. Liu, "Tsallis statistical interpretation of transverse momentum spectra in high-energy pA collisions," *Advances in High Energy Physics*, vol. 2015, Article ID 741816, 10 pages, 2015.

Hindawi
Advances in High Energy Physics
Volume 2018, Article ID 3794242, 5 pages
https://doi.org/10.1155/2018/3794242

Review Article

HBT Radii: Comparative Studies on Collision Systems and Beam Energies

Debasish Das

Saha Institute of Nuclear Physics, HBNI, 1/AF, Bidhannagar, Kolkata 700064, India

Correspondence should be addressed to Debasish Das; dev.deba@gmail.com

Received 12 February 2018; Revised 14 June 2018; Accepted 28 June 2018; Published 15 July 2018

Academic Editor: Fu-Hu Liu

Two-particle Hanbury-Brown-Twiss (HBT) interferometry is an important probe for understanding the space-time structure of particle emission sources in high energy heavy ion collisions. We present the comparative studies of HBT radii in Pb+Pb collisions at $\sqrt{s_{\mathrm{NN}}}$ = 17.3 GeV with Au+Au collisions at $\sqrt{s_{\mathrm{NN}}}$ = 19.6 GeV. To further understand this specific energy regime, we also compare the HBT radii for Au+Au collisions at $\sqrt{s_{\mathrm{NN}}}$ = 19.6 GeV with Cu+Cu collisions at $\sqrt{s_{\mathrm{NN}}}$ = 22.4 GeV. We have found interesting similarity in the $R_{\mathrm{out}}/R_{\mathrm{side}}$ ratio with m_{T} across the collision systems while comparing the data for this specific energy zone which is interesting as it acts as a bridge from SPS energy regime to the RHIC energy domain.

1. Introduction

A phase transition from a hadronic state to a "plasma" of deconfined quarks and gluons when the energy density exceeds a critical value is predicted from Quantum Chromo-Dynamics (QCD). The complicated structure of nuclear matter at low temperatures, where it is composed of a multitude of hadronic particles, baryons, and mesons, is thus expected to give way at high temperatures to a plasma of weakly composed quarks and gluons, the *Quark–Gluon Plasma* (*QGP*). QGP is a thermalized system where the properties of the system are governed by the quark and gluon degrees of freedom [1].

Understanding the deconfining phase transition in hadronic matter and the QGP properties is a challenging task. For systems created in the relativistic heavy ion collider (RHIC) and large hadron collider (LHC), energy region with high temperatures, and low baryon-chemical potential, Lattice QCD calculations predict a crossover transition between the hadron gas and the QGP phase. Lattice QCD predicts a phase transformation to a quark-gluon plasma at a temperature of approximately $T \approx 170\ MeV (1\ MeV \approx 1.1604 \times 10^{10} K)$ ([1]) corresponding to an energy density $\epsilon \approx 1\ GeV/fm^3$, which is nearly an order of magnitude larger than normal nuclear matter.

Experimental studies in relativistic heavy ion physics aim to study the QCD nature of matter under the conditions of extreme temperature and high energy density both at RHIC and at LHC. The discovery of the QGP can describe the system (governed by the quarks and gluons) in which the degrees of freedom are no more the color neutral hadron states.

The equation of state (EoS) of nuclear matter enables us to understand the relationship between the pressure and the energy at a given net-baryon density. Phase transitions from the hadronic resonance gas phase to the color-deconfined QGP (see, e.g., [2, 3]) contribute to the changes of the EoS. The experimental measurements should also be able to determine the physical characteristics of the transition, for example, the critical temperature, the order of the phase transition, and the speed of the sound along with the nature of the quasi-particles. The EoS of hot and dense QCD matter is still not precisely understood. Modern nuclear physics, has an important goal, that is, to explore the phase diagram of quark matter in various temperatures and baryon density so as to confirm the existence of the new phase of quark matter [4, 5].

The intermediate Super Proton Synchrotron (SPS) energy regime still remains interesting since the onset of deconfinement is expected to happen at those energies. Possibility of a

critical endpoint [6, 7] and a first-order phase transition is yet not excluded. Several beam-energy dependent observables such as the particle ratios [8, 9], the flow [10, 11], and the HBT parameters [12, 13] show a nonmonotonic behavior, for which the interpretation still remains unclear. The beam-energy scan (BES) programs at RHIC show that directed flow is strong for both the lowest and the highest RHIC energies as shown by results from STAR experiment [14]. The net-proton $v_1(y)$ slope has a minimum between 11.5 and 19.6 GeV and changing sign twice between 7.7 and 39 GeV, which is quite contrary to the UrQMD transport model predictions for that energy regime. The vanishing of directed flow when the expansion stops and its appearance when the matter has passed through the change constitute the "latent heat", where the predicted "softest point disappearance" of flow can become a possible signature of a first-order phase transition between hadronic matter and a deconfined QGP phase.

Assuming a first-order phase transition, there is a mixed phase of the QGP and hadronic gas. A slow-burning fireball is expected in the absence of pressure gradient, when the initial system is at rest in the mixed phase, and this leads to a time-delay in the system evolution [12, 15–17]. Investigation of the time-delay signatures for the first-order phase transition is henceforth a subject of interest.

Two-particle Hanbury-Brown-Twiss (HBT) interferometry is an important tool for detecting the space-time structure of particle emission sources in high energy heavy ion collisions [18–20]. The occurrence of first-order phase transition between the QGP and hadronic matter will lead to the time-delay of the system evolution, hence making the emission duration of particles more prolonged [12, 15–17]. As explained in [12, 15–17] the three HBT radius parameters, $R_{\text{out}}, R_{\text{side}}, R_{\text{long}}$, describe the dimensions of a Gaussian source in longitudinal comoving system (LCMS) framework. The $R_{\text{out}}/R_{\text{side}}$ ratio can be related to the emission time [12, 15–17]. We have explored in this paper the energy region of 17.3 GeV to 22.4 GeV through comparative studies of two-pion HBT radii. This energy region has shown interesting results in STAR experiment [14] for other correlation measurements (like flow).

2. Results

The intensity interferometry technique for measuring sizes of stars [21] was formulated by Robert Hanbury Brown and Richard Twiss and is also known as the "Hanbury-Brown-Twiss (HBT) effect". Such technique was extended to particle physics [22] for understanding the angular distributions of pion pairs in $p\overline{p}$ annihilations and thus the quantum statistics causing an enhancement in pairs with low relative momentum. In HBT analyses the method has henceforth evolved into a precision tool for measuring the space-time properties of the regions of homogeneity at kinetic freeze-out in heavy ion collisions [23].

Two-pion interferometry yields HBT radii that describe the geometry of these regions of homogeneity (regions that emit correlated pion pairs). The HBT radii increase for more central collisions due to the increasing volume of the source and hence demonstrate how HBT can probe spatial sizes and shapes [24]. The decrease of HBT radii with mean pair transverse momentum, $k_T(=|\overrightarrow{p}_{1\text{T}} + \overrightarrow{p}_{2\text{T}}|)/2)$, has been due to transverse and longitudinal flow [24]. Flow causes space-momentum correlations since the sizes of the regions emitting the particles do not correspond to the entire fireball created in a relativistic heavy ion collision [24].

In this paper, the results of two-pion HBT analyses of Pb+Pb at 17.3 GeV from NA49 experiment [25] are compared in Figure 1 and discussed with other STAR HBT results from Au+Au 19.6 GeV [26]. Figure 1 shows the HBT radii of SPS and RHIC collision species where Pb+Pb 17.3 GeV(NA49) and Au+Au 19.6 GeV(STAR) show similar trend for R_{side} and R_{long} with m_{T}. For R_{out} the SPS data has a flatter slope when compared with RHIC, but the $R_{\text{out}}/R_{\text{side}}$ ratios with m_{T} $(= \sqrt{k_{\text{T}}^2 + m_\pi^2})$ are very similar for the top central data of both experiments. The $R_{\text{out}}/R_{\text{side}}$ ratios of NA49 and STAR show weak m_{T} dependence and have values close to unity.

The HBT radii from Au+Au 19.6 GeV and Cu+Cu 22.4 GeV, both from STAR experiment, are also included in this paper since they are different collision species with close collision energies. Reference [27] explains the analysis methodology for Cu+Cu collisions at $\sqrt{s_{\text{NN}}}$ = 22.4 GeV. In Figure 2 we present this comparison of two-pion HBT radii to include central (0-5%) Au+Au collisions at $\sqrt{s_{\text{NN}}}$ = 19.6 GeV and central (0-10%) Cu+Cu collisions at $\sqrt{s_{\text{NN}}}$ = 22.4 GeV from the STAR experiment.

The HBT radii for Cu+Cu collisions at $\sqrt{s_{\text{NN}}}$ = 22.4 GeV are smaller than those for Au+Au collisions at $\sqrt{s_{\text{NN}}}$ = 19.6 GeV. The variations of the $R_{\text{out}}/R_{\text{side}}$ ratios with m_{T} are similar for the Au+Au and Cu+Cu collision data as we see in Figure 2. The ratios also show weak m_{T} dependence with the values close to unity.

In Figure 3 we present the m_{T} dependence of the ratios of two-pion HBT radii for the most-central Au+Au at $\sqrt{s_{\text{NN}}}$=19.6 GeV and Cu+Cu collisions at $\sqrt{s_{\text{NN}}}$ = 22.4 GeV. Details about the Cu+Cu systems are explained in [27] and references therein. As seen in Figure 3 the ratios of radii for Au+Au to those for Cu+Cu collisions are ~1.5. Although we see that the individual HBT radii decrease significantly with increasing m_{T}, the ratios in Figure 3 show that the HBT radii for Au+Au and Cu+Cu collisions at 19.6 GeV and 22.4 GeV share a common m_{T} dependence. Such trends can be understood in terms of models [28, 29] where participant scaling is used to predict the HBT radii in Cu+Cu collisions from the measured radii for Au+Au collisions at $\sqrt{s_{\text{NN}}}$ = 200 GeV, assuming the radii are proportional to $A^{1/3}$, where A is the atomic mass number of the colliding nuclei.

3. Summary

The $R_{\text{out}}/R_{\text{side}}$ ratio is important since it is able to provide the information of the emission duration. We also know that the HBT radii are affected by transverse and longitudinal flow. The SPS energy regime is still zone of interest where the recent flow results from STAR experiment [14] (within 11.5 and 19.6 GeV) have shown some new and interesting features. When we compare the HBT (two-particle correlation) radii in Pb+Pb collisions at $\sqrt{s_{\text{NN}}}$ = 17.3 GeV with Au+Au collisions at

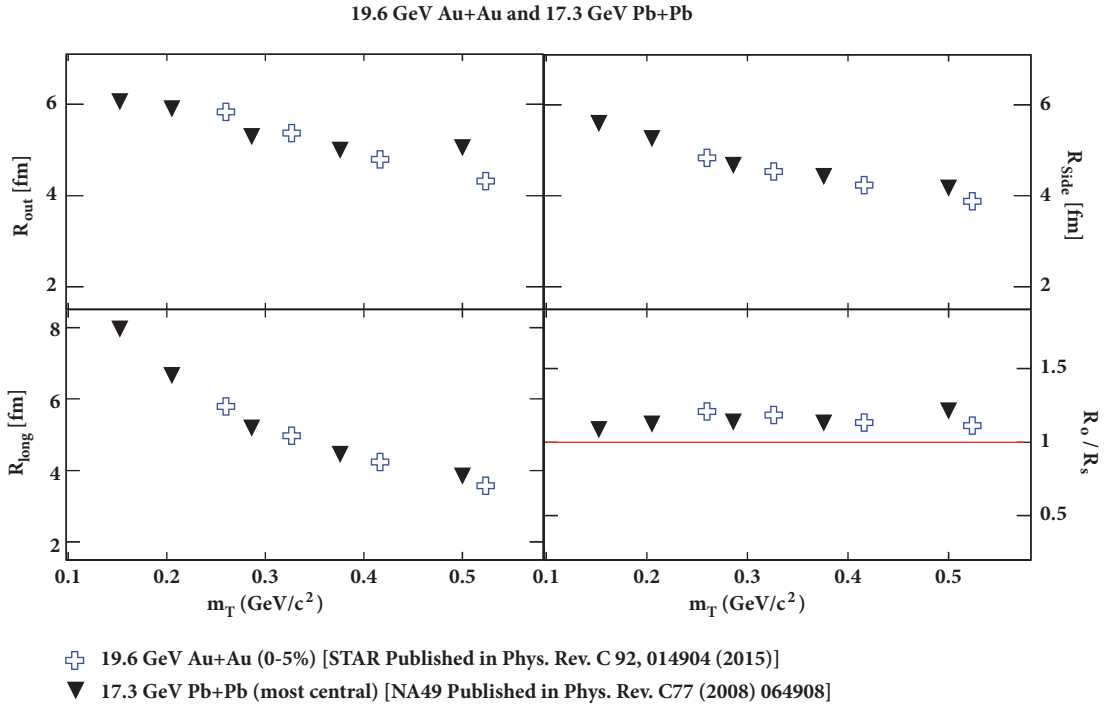

FIGURE 1: The comparison of system size dependence in HBT radii of STAR Au+Au collisions at $\sqrt{s_{NN}}$ = 19.6 GeV with NA49 Pb+Pb collisions for 17.3 GeV. Only statistical errors are shown for the top central data of both experiments.

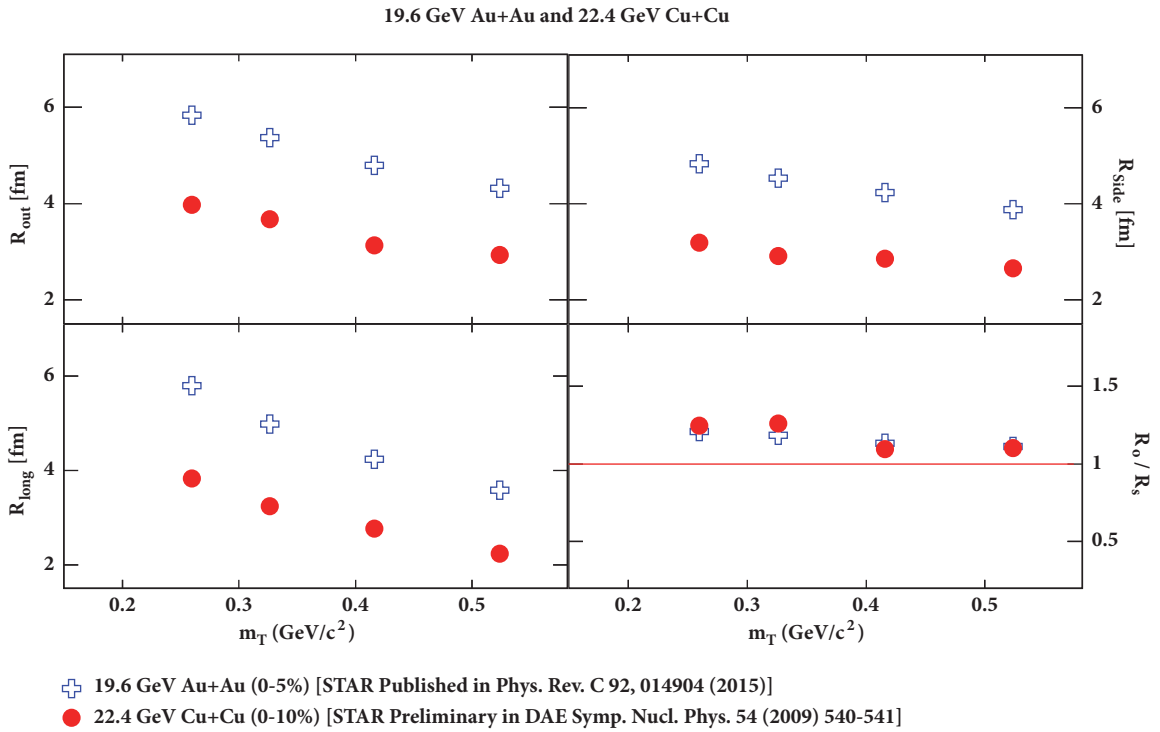

FIGURE 2: The comparison of system size dependence in HBT radii of STAR Au+Au collisions at $\sqrt{s_{NN}}$ = 19.6 GeV with Cu+Cu collisions at $\sqrt{s_{NN}}$ = 22.4 GeV. Only statistical errors are shown for the top central data of both the Au+Au and Cu+Cu datasets.

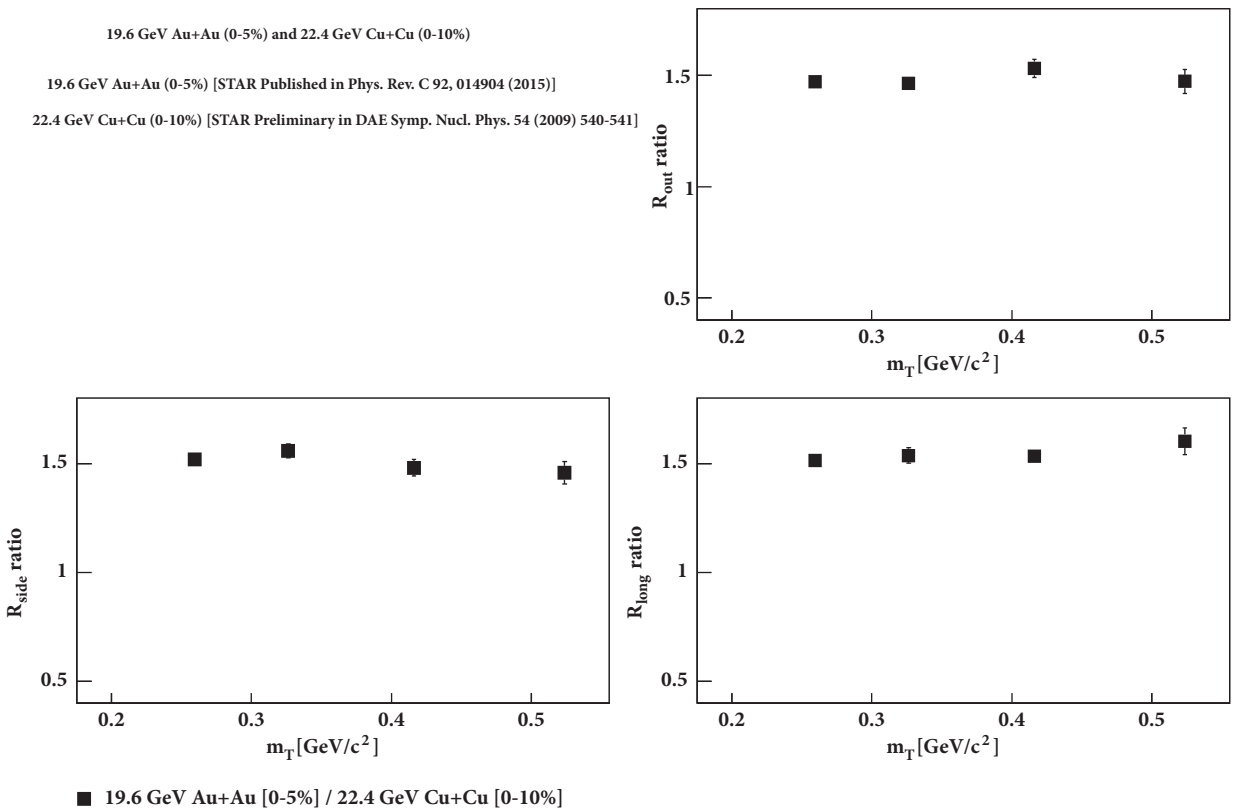

FIGURE 3: Ratios of HBT radii at top centralities for Au+Au and Cu+Cu collisions at $\sqrt{s_{NN}}$ = 19.6 and 22.4 GeV versus m_T. Only statistical errors are shown for Au+Au collisions at $\sqrt{s_{NN}}$ = 19.6 GeV and Cu+Cu collisions at $\sqrt{s_{NN}}$ = 22.4 for their top central datasets.

$\sqrt{s_{NN}}$ = 19.6 GeV, we find very similar R_{out}/R_{side} ratio with m_T. To explore this interesting energy regime we have compared the HBT radii for Au+Au collisions at $\sqrt{s_{NN}}$ = 19.6 GeV with Cu+Cu collisions at $\sqrt{s_{NN}}$ = 22.4 GeV. The similarity in the R_{out}/R_{side} ratio with m_T persists across the collision systems from SPS to RHIC energies and even in close RHIC energies for Au+Au and Cu+Cu systems as well. The rise of the ratio R_{out}/R_{side} with collision energy which was predicted [12] due to a possible phase transition is not observed. Such inferences establish that HBT radii R_{out}/R_{side} ratios are very much comparable and consistent across the different colliding species in (an exciting zone of interest of the RHIC BES program) the energy region of 17.3 GeV to 22.4 GeV.

Conflicts of Interest

The author declares that there are no conflicts of interest regarding the publication of this paper.

Acknowledgments

The author acknowledges the facilities of Saha Institute of Nuclear Physics, Kolkata, India.

References

[1] F. Karsch, "Lecture Notes in Physics," in *Nuclear Physics A*, F. Karsch, Ed., vol. 698, p. 199, 2002.

[2] C. Spieles, H. Stöcker, and C. Greiner, "Phase transition of a finite quark-gluon plasma," *Physical Review C: Nuclear Physics*, vol. 57, no. 2, pp. 908–915, 1998.

[3] M. Bluhm, B. Kämpfer, R. Schulze, D. Seipt, and U. Heinz, "A Family of equations of state based on lattice QCD: impact on flow in ultrarelativistic heavy-ion collisions," *Physical Review C: Nuclear Physics*, vol. 76, no. 3, Article ID 034901, 2007.

[4] Z. Fodor and S. D. Katz, "Lattice determination of the critical point of QCD at finite T and μ," *Journal of High Energy Physics*, vol. 2002, no. 3, p. 14, 2002.

[5] P. d. Forcrand and O. Philipsen, "The chiral critical line of," *Journal of High Energy Physics*, vol. 2007, no. 1, pp. 77-77, 2007.

[6] R. A. Lacey, N. N. Ajitanand, J. M. Alexander et al., "Has the QCD Critical Point Been Signaled by Observations at the BNL Relativistic Heavy Ion Collider?" *Physical Review Letters*, vol. 98, Article ID 092301, 2007.

[7] "Searching for Minimum in Dependence of Squared Speed-of-Sound on Collision Energy," *Advances in High Energy Physics*, vol. 2016, Article ID 9467194, 9 pages, 2016.

[8] S. V. Afanasiev, "Energy dependence of pion and kaon production in central Pb+Pb collisions," *Physical Review C*, vol. 66, Article ID 054902, 2002.

[9] C. Alt et al., "Pion and kaon production in central Pb+Pb collisions at 20A and 30A GeV: Evidence for the onset of deconfinement," *Physical Review C*, vol. 77, no. 4, Article ID 024903, 2008.

[10] P. F. Kolb, P. Huovinen, U. Heinz, and H. Heiselberg, "Elliptic flow at SPS and RHIC: from kinetic transport to hydrodynamics," *Physics Letters B*, vol. 500, no. 3-4, pp. 232–240, 2001.

[11] H. Petersen, Q. Li, X. Zhu, and M. Bleicher, " Directed and elliptic flow in heavy-ion collisions from ," *Physical Review C: Nuclear Physics*, vol. 74, no. 6, 2006.

[12] D. H. Rischke and M. Gyulassy, "The time-delay signature of quark-gluon plasma formation in relativistic nuclear collisions," *Nuclear Physics A*, vol. 608, pp. 479–512, 1996.

[13] D. Adamova et al., "Universal Pion Freeze-Out in Heavy-Ion Collisions," *Physical Review Letters*, vol. 90, Article ID 022301, 2003.

[14] L. Adamczyk, " Publisher's Note: Dielectron Mass Spectra from ," *Physical Review Letters*, vol. 113, no. 4, 2014.

[15] S. Pratt, "Pion interferometry of quark-gluon plasma," *Physical Review D: Particles, Fields, Gravitation and Cosmology*, vol. 33, Article ID 1314, 1986.

[16] G. Bertsch and G. E. Brown, "Temporal development of the plasma phase transition," *Physical Review C: Nuclear Physics*, vol. 40, no. 4, pp. 1830–1832, 1989.

[17] S. Soff, S. A. Bass, D. H. Hardtke, and S. Y. Panitkin, "Kaon Interferometry: A Sensitive Probe of the QCD Equation of State?" *Physical Review Letters*, vol. 88, no. 7, 2002.

[18] C. Wong, *Introduction to High-Energy Heavy-Ion Collisions*, World Scientific, 1994.

[19] U. A. Wiedemann and U. Heinz, "Particle interferometry for relativistic heavy-ion collisions," *Physics Reports*, vol. 319, no. 4-5, pp. 145–230, 1999.

[20] R. M. Weiner, "Boson interferometry in high-energy physics," *Physics Reports*, vol. 327, no. 5, pp. 249–346, 2000.

[21] R. Hanbury Brown and R. Q. Twiss, "A test of a new type of stellar interferometer on Sirius," *Nature*, vol. 178, no. 4541, pp. 1046–1048, 1956.

[22] G. Goldhaber, S. Goldhaber, W. Lee, and A. Pais, "Influence of Bose-Einstein statistics on the antiproton-proton annihilation process," *Physical Review A: Atomic, Molecular and Optical Physics*, vol. 120, no. 1, pp. 300–312, 1960.

[23] M. A. Lisa, S. Pratt, R. Soltz, and U. Wiedemann, "Femtoscopy in relativistic heavy ion collisions: two decades of progress," *Annual Review of Nuclear and Particle Science*, vol. 55, pp. 357–402, 2005.

[24] S. Pratt and J. Vredevoogd, "Femtoscopy in relativistic heavy ion collisions and its relation to bulk properties of QCD matter," *Physical Review C*, vol. 78, Article ID 069901, 2008.

[25] C. Alt, "Bose-Einstein correlations of $\pi - \pi-$ pairs in central Pb+Pb collisions at 20A,30A,40A,80A, and 158A GeV," *Physical Review C*, vol. 77, Article ID 064908, 2008.

[26] L. Adamczyk et al., "Beam-energy-dependent two-pion interferometry and the freeze-out eccentricity of pions measured in heavy ion collisions at the STAR detector," *Physical Review C*, vol. 92, 2015.

[27] D. Das, "Nuclear Physics," in *Proceedings of the DAE International Symposium on Nuclear Physics*, vol. 54, Bhabha Atomic Research Centre, Mumbai, India, 2009.

[28] J. G. Cramer, G. A. Miller, J. M. S. Wu, and J. H. S. Yoon, "Quantum Opacity, the RHIC Hanbury Brown–Twiss Puzzle, and the Chiral Phase Transition," *Physical Review Letters*, vol. 94, Article ID 102302, 2005.

[29] G. A. Miller and J. G. Cramer, "Polishing the lens: I. Pionic final state interactions and HBT correlations: distorted wave emission-function (DWEF) formalism and examples," *Journal of Physics G: Nuclear and Particle Physics*, vol. 34, p. 703, 2007.

Hindawi
Advances in High Energy Physics
Volume 2018, Article ID 6384357, 15 pages
https://doi.org/10.1155/2018/6384357

Research Article

Multifractal Analysis of Charged Particle Multiplicity Distribution in the Framework of Renyi Entropy

Swarnapratim Bhattacharyya,[1] **Maria Haiduc**,[2] **Alina Tania Neagu**,[2] **and Elena Firu**[2]

[1]*Department of Physics, New Alipore College, L Block, New Alipore, Kolkata 700053, India*
[2]*Institute of Space Science, Bucharest, Romania*

Correspondence should be addressed to Swarnapratim Bhattacharyya; swarna_pratim@yahoo.com

Received 3 March 2018; Accepted 22 May 2018; Published 26 June 2018

Academic Editor: Sakina Fakhraddin

A study of multifractality and multifractal specific heat has been carried out for the produced shower particles in nuclear emulsion detector for ^{16}O-AgBr, ^{28}Si-AgBr, and ^{32}S-AgBr interactions at 4.5AGeV/c in the framework of Renyi entropy. Experimental results have been compared with the prediction of Ultra-Relativistic Quantum Molecular Dynamics (UrQMD) model. Our analysis reveals the presence of multifractality in the multiparticle production process in high energy nucleus-nucleus interactions. Degree of multifractality is found to be higher for the experimental data and it increases with the increase of projectile mass. The investigation of quark-hadron phase transition in the multiparticle production in ^{16}O-AgBr, ^{28}Si-AgBr, and ^{32}S-AgBr interactions at 4.5 AGeV/c in the framework of Ginzburg-Landau theory from the concept of multifractality has also been presented. Evidence of constant multifractal specific heat has been obtained for both experimental and UrQMD simulated data.

1. Introduction

The study of nonstatistical fluctuations and correlations in relativistic and ultra-relativistic nucleus-nucleus collisions has become a subject of major interest among the particle physicists. Bialas and Peschanski [1, 2] proposed a new phenomenon called intermittency to study the nonstatistical fluctuations in terms of the scaled factorial moment. In high energy physics intermittency is defined as the power law behavior of scaled factorial moment with the size of the considered phase space [1, 2]. This method has its own advantage that it can extract nonstatistical fluctuations after extricating the normal statistical noise [1, 2]. The study of nonstatistical fluctuations by the method of scaled factorial moment leads to the presence of self-similar fractal structure in the multiparticle production of high energy nucleus-nucleus collisions [3]. The self-similarity observed in the power law dependence of scaled factorial moments reveals a connection between intermittency and fractality. The observed fractal structure is a consequence of self-similar cascade mechanism in multiparticle production process. The close connection between intermittency and fractality prompted the scientists to study fractal nature of multiparticle production in high energy nucleus-nucleus interactions. To get both qualitative and quantitative idea concerning the multiparticle production mechanism fractality study in heavy-ion collisions is expected to be very resourceful.

2. Fractals-Multifractals and Monofractals

The term "fractal" was coined by Mandelbrot [4] from the Latin word fractus which means broken or fractured. Mandelbrot introduced the new geometry called the fractal geometry to look into the world of apparent irregularities. A fractal pattern is one that scales infinitely to reproduce itself such that the traditional geometry does not define it. In other words a fractal is generally a rough or fragmented geometrical shape that can be split into parts, each of which is at least approximately reduced size copy of the whole [4]. Sierpinski triangle, Koch snow flack, Peano curve, Mandelbrot set, and Lorentz attractor are the well-known mathematical structures that exhibit fractal geometry [4]. Fractals also describe many real world objects such as clouds, mountains, coastlines, etc.;

those do not corresponds to simple geometrical shape [4]. Fractals can be classified into two categories: multifractals and monofractals [4]. Multifractals are complicated self-similar objects that consist of differently weighted fractals with different noninteger dimensions. The fundamental characteristic of multifractality is that the scaling properties may be different in different regions of the systems [4]. Monofractals are those whose scaling properties are the same in different regions of the system [4]. As the scaling properties are dissimilar in different parts of the system, multifractal systems require at least more than one scaling exponent to describe the scaling behavior of the system [5]. A distinguishing feature of the processes that have multifractal characteristics is that various associated probability distributions display power law properties [6, 7]. Multifractal theory is essentially rooted in probability theory though draws on complex ideas from each of physics, mathematics, probability theory, and statistics [6]. Apart from multiparticle production in high energy physics, multifractal analysis has proved to be a valuable method of capturing the underlying scaling structure present in many types of systems including diffusion limited aggregation [8–10], fluid flow through random porous media [11], atomic spectra of rare-earth elements [12], cluster-cluster aggregation [13], and turbulent flow [14]. In physiology, multifractal structures have been found in heart rate variability [15] and brain dynamics [16]. Multifractal analysis has been helpful in distinguishing between healthy and pathological patients [17]. Multifractal measures have also been found in man-made phenomena such as the Internet [18], art [19], and the stock market [20–22]. Multifractals have also been used in a wide range of application areas like the description of dynamical systems, rainfall modelling, spatial distribution of earthquakes and insect populations, financial time series modelling, and Internet traffic modelling [6, 7].

It should be mentioned here that the most important property of fractals is their dimensions [4, 6, 7]. Fractal dimension is used to describe the size of the fractal sets [4, 6, 7]. For example, the dimension of an irregular coastline may be greater than one but less than two, indicating that it is not like a simple line and has space filling characteristics in the plane. Likewise, the surface area of a snowflake may be greater than two but less than three, indicating that its surface is more complex than regular geometrical shapes and is partially volume filling [4, 6, 7]. Fractal dimension can be calculated by taking the limit of the quotient of the log change in object size and the log change in measurement scale, as the measurement scale approaches to zero [4]. The differences came in what is meant by the measurement scale and how to get an average number out of many different parts of the geometrical objects [4, 6, 7]. Fractal dimension quantifies the static geometry of an object [4].

Generalized fractal dimension $\mathbf{D_q}$ is a well-known parameter which reflects the nature of fractal structure [4]. From the dependence of generalized fractal dimension $\mathbf{D_q}$ on the order q a distinguishable characterization of fractality is possible [4]. Decrease of generalized fractal dimension $\mathbf{D_q}$ with the order of moment $\mathbf{q}$ signals the presence of multifractality. On the other hand if $\mathbf{D_q}$ remains constant with the increase of order q monofractality occurs. It has been pointed out in [23] that if Quark-Gluon-Plasma (QGP) state is created in hadronic collisions, a phase transition to hadronic matter will take place. The hadronic system will show monofractality in contrast to an order dependence of generalized fractal dimension $\mathbf{D_q}$, when a cascade process occurs [23].

Hwa [24] was the first to provide the idea of using multifractal moments G_q, to study the multifractality and self-similarity in multiparticle production. According to the method enunciated by Hwa [24] if the particle production process exhibits self-similar behavior, the G_q moments show a remarkable power law dependence on phase space bin size. However, if the multiplicity is low, the G_q moments are dominated by statistical fluctuations. In order to suppress the statistical contribution, a modified form of G_q moments in terms of the step function was suggested by Hwa and Pan [25]. Takagi [26] also proposed a new method called Takagi moment method (T_q moment) for studying the fractal structure of multiparticle production. Both the G_q and the T_q techniques have been applied extensively to analyze several high energy nucleus-nucleus collision data [27–35]. Very recently some sophisticated methods have also been applied to study the fractal nature of multiparticle production process [36–45].

3. Entropy and Fractality

In high energy nucleus-nucleus collisions, entropy measurement of produced shower particles may provide important information in studying the multiparticle production mechanism [46]. In high energy collisions, entropy is an important parameter and it is regarded as the most significant characteristic of a system having many degrees of freedom [46]. As entropy reflects how the effective degrees of freedom change from hadronic matter at low temperature to the quark-gluon plasma state at high temperature, it is regarded as a useful probe to study the nature of deconfinement phase transition [46]. Entropy plays a key role in the evolution of the high temperature quark-gluon plasma in ultra-relativistic nucleus-nucleus interactions in Relativistic Heavy-Ion Collider (RHIC) experiments and in Large Hadron Collider (LHC) experiments [46]. In nucleus-nucleus collisions, entropy measurement can be used to not only search for the formation of Quark-Gluon-Plasma (QGP) state but it may also serve as an additional tool to investigate the correlations and event-by-event fluctuations [47]. Different workers have investigated the evolution of entropy in high energy nucleus-nucleus collisions at different times [48–64]. The entropy of produced particles can easily be calculated from the multiplicity distribution of the data. If P_n is the probability of producing n particles in a high energy interaction the entropy S is defined by the relation $S = -\sum_n P_n \ln P_n$ [65]. Mathematically this entropy S is called the Shannon entropy [66].

Apart from studying the well-known Shannon entropy, people are interested to explore the hidden physics of Renyi entropy [66–69] as well, mainly motivated by the inspiration of A. Bialas and W. Czyż [51, 64, 70]. According to C.W Ma

Table 1: This represents the average multiplicities of the shower particles for all the interactions in case of the experimental and the UrQMD data.

Interactions	Average Multiplicity	
	Experimental	UrQMD
^{16}O-AgBr (4.5AGeV/c)	18.05±0.22	17.79±0.21
^{28}Si-AgBr (4.5AGeV/c)	23.62±0.21	27.55±0.22
^{32}S-AgBr (4.5AGeV/c)	28.04±.14	30.84±0.17

and Y.G. Ma [71] the difference between qth order Renyi entropy and 1st order Renyi entropy is found just to be a q dependent constant but which is very sensitive to the form of probability distribution. Renyi entropy can play a potential role to investigate the fractal characteristics of multiparticle production process [72, 73]. The advantage of this method to study the fractal properties of multiparticle production process is that it is not related to the width and resolution of the phase space interval [72, 73]. This method can be applied to events having higher as well as lower multiplicity. This method never suffers from the drawback of lower statistics.

In terms of the probability of multiplicity distribution $\mathbf{P_n}$, the q th order Renyi entropy can be defined as [51, 64, 70]

$$\mathbf{H_q} = \frac{\mathbf{1}}{(\mathbf{q-1})}\mathbf{ln}\left[\sum_{\mathbf{n}}(\mathbf{P_n})^{\mathbf{q}}\right] \quad (1)$$

If $\mathbf{C_q} = \sum_{\mathbf{n}}(\mathbf{P_n})^{\mathbf{q}}$, then (1) can be written as

$$\mathbf{H_q} = \frac{\mathbf{1}}{(\mathbf{q-1})}\mathbf{ln}\left[\mathbf{C_q}\right] \quad (2)$$

Generalized fractal dimension $\mathbf{D_q}$ can be evaluated from the concept of Renyi entropy according to the relation

$$\mathbf{D_q} = \frac{\mathbf{H_q}}{\mathbf{Y_m}} \quad (3)$$

where $\mathbf{Y_m}$ is the central rapidity value in the centre of mass frame and is given by

$$\mathbf{Y_m} = \mathbf{ln}\left[\left(\sqrt{\mathbf{s}} - \frac{\mathbf{2m_n}\left\langle\mathbf{n_p}\right\rangle}{\mathbf{m_\pi}}\right)\right]. \quad (4)$$

Here $\sqrt{\mathbf{s}}$ is the centre of mass energy of the concerned collision process, $\mathbf{m_\pi}$ is the rest mass of pions, and $\langle\mathbf{n_p}\rangle$ denotes the average number of participating nucleons.

The generalized fractal dimension $\mathbf{D_q}$ is related to the anomalous fractal dimension $\mathbf{d_q}$ by a simple mathematical relation [74]

$$\mathbf{d_q} = \mathbf{1} - \mathbf{D_q}. \quad (5)$$

Goal of our present study is to carry out an investigation of multifractality and multifractal specific heat in shower particle multiplicity distribution from the concept of Renyi entropy measurements in ^{16}O-AgBr, ^{28}Si-AgBr, and ^{32}S-AgBr interactions at 4.5AGeV/c. We have compared our experimental results with the prediction of Ultra-Relativistic Quantum Molecular Dynamics (UrQMD) model. Importance of this study is that so far very few attempts have been made to explore the presence of multifractality in multiparticle production process in the framework of higher-order Renyi entropy in high energy nucleus-nucleus interactions.

4. Experimental Details

In order to collect the data used for the present analysis, stacks of NIKFI-BR2 emulsion pellicles of dimensions 20cm×10 cm×600$\boldsymbol{\mu}$**m** were irradiated by the ^{16}O, ^{28}Si, and ^{32}S beam at 4.5 AGeV/c obtained from the Synchrophasotron at the Joint Institute of Nuclear Research (JINR), Dubna, Russia [75–78]. According to Powell [79], in nuclear emulsion detector particles emitted and produced from an interaction are classified into four categories, namely, the shower particles, the grey particles, the black particles, and the projectile fragments. Details of scanning and measurement procedure of our study along with the characteristics of these emitted and produced particles in nuclear emulsion can be found from our earlier publications [75–78].

One of the problem encountered in interpreting results from nuclear emulsion is the nonhomogeneous composition of emulsion which contain both light (H,C,N, and O) and heavy target nuclei (Ag, Br). In emulsion experiments it is very difficult to identify the exact target nucleus [75]. Based on the number of heavy tracks (N_h) total number of inelastic interactions can be divided into three broad target groups H, CNO, and AgBr in nuclear emulsion [75]. Detailed method of target identification has been described in our earlier publication [75]. For the present analysis we have not considered the events which are found to occur due to collisions of the projectile beam with H and CNO target present in nuclear emulsion. Our analysis has been carried out for the interactions of three different projectile ^{16}O, ^{28}Si, and ^{32}S at 4.5 AGeV/c with the AgBr target only. Applying the criteria of selecting AgBr events (N_h >8) we have chosen 1057 events of ^{16}O-AgBr interactions, 514 events of ^{28}Si-AgBr, and 434 events of ^{32}S-AgBr interactions at 4.5 AGeV/c [75]. Our analysis has been performed on the shower tracks only. We have calculated the average multiplicity of shower tracks in each interaction and presented the values in Table 1 [75–78].

Table 2: This represents the experimental and UrQMD simulated values of Renyi entropy $\mathbf{H_q}$ for ^{16}O-AgBr, ^{28}Si-AgBr, and ^{32}S-AgBr interactions at 4.5AGeV/c.

Interactions	Order	**Experimental** values of Renyi Entropy $\mathbf{H_q}$	**UrQMD** simulated values of Renyi Entropy $\mathbf{H_q}$
^{16}O-AgBr	2	3.47±.04	3.05±.02
	3	3.41±.**03**	2.99±.**04**
	4	3.37±.**02**	2.95±.**02**
	5	3.34±.**02**	2.92±.**02**
^{28}Si-AgBr	2	3.76±.05	3.29±.06
	3	3.69±.**02**	3.21±.**02**
	4	3.63±.**03**	3.17±.**02**
	5	3.59±.**03**	3.13±.**03**
^{32}S-AgBr	2	3.91±.04	3.36±.08
	3	3.84±.**03**	3.28±.**03**
	4	3.79±.**03**	3.24±.**03**
	5	3.74±.**03**	3.20±.**02**

Table 3: This represents the experimental and UrQMD simulated values of generalized fractal dimension $\mathbf{D_q}$ for ^{16}O-AgBr, ^{28}Si-AgBr, and ^{32}S-AgBr interactions at 4.5AGeV/c.

Interactions	Order	**Experimetal** values of Generalized fractal dimension $\mathbf{D_q}$	**UrQMD** simulated values of Generalized fractal dimension $\mathbf{D_q}$
^{16}O-AgBr	2	.892±.007	.826±.002
	3	.877±.**006**	.810±.**003**
	4	.866±.**009**	.799±.**004**
	5	.858±.**008**	.791±.**005**
^{28}Si-AgBr	2	.897±.**004**	.829±.**002**
	3	.880±.**004**	.808±.**002**
	4	.866±.**007**	.798±.**004**
	5	.857±.**007**	.788±.**005**
^{32}S-AgBr	2	.924±.**004**	.836±.**003**
	3	.907±.**007**	.815±.**004**
	4	.896±.**008**	.805±.**005**
	5	.884±.**008**	.796±.**006**

5. Analysis and Results

In a very recent paper [80] we have investigated the Renyi entropy of second order of shower particles using ^{16}O, ^{28}Si, and ^{32}S projectiles on interaction with AgBr and CNO target present in nuclear emulsion at an incident momentum of 4.5 AGeV/c. In this paper we have extended our analysis of Renyi entropy to the study of fractality in multiparticle production of ^{16}O-AgBr, ^{28}Si-AgBr, and ^{32}S-AgBr interactions at 4.5AGeV/c.

In order to study the fractal nature of multiparticle production from the concept of Renyi entropy we have calculated the Renyi entropy values of order q=2-5 from relations (1) and (2) for all the three interactions. The calculated values of Renyi entropy of different orders of the produced shower particles in ^{16}O-AgBr, ^{28}Si-AgBr, and ^{32}S-AgBr interactions at 4.5AGeV/c have been presented in Table 2. It may be mentioned here that the values of the second-order Renyi entropy have been taken from our recent publication [80]. From the table it can be noted that for all the interactions Renyi entropy values are found to decrease as the order number increases. The variation of Renyi entropy $\mathbf{H_q}$with order q has been presented in Figure 1 for ^{16}O-AgBr, ^{28}Si-AgBr, and ^{32}S-AgBr interactions. Error bars drawn to every experimental point are statistical errors only. Using (3) and (4) we have calculated the values of generalized fractal dimension $\mathbf{D_q}$ for ^{16}O-AgBr, ^{28}Si-AgBr, and ^{32}S-AgBr interactions. Calculated values of generalized fractal dimension $\mathbf{D_q}$ for ^{16}O-AgBr, ^{28}Si-AgBr, and ^{32}S-AgBr interactions have been presented in Table 3. From the table it may be noted that the values of generalized fractal dimension $\mathbf{D_q}$ decrease with the increase of order number suggesting the presence of

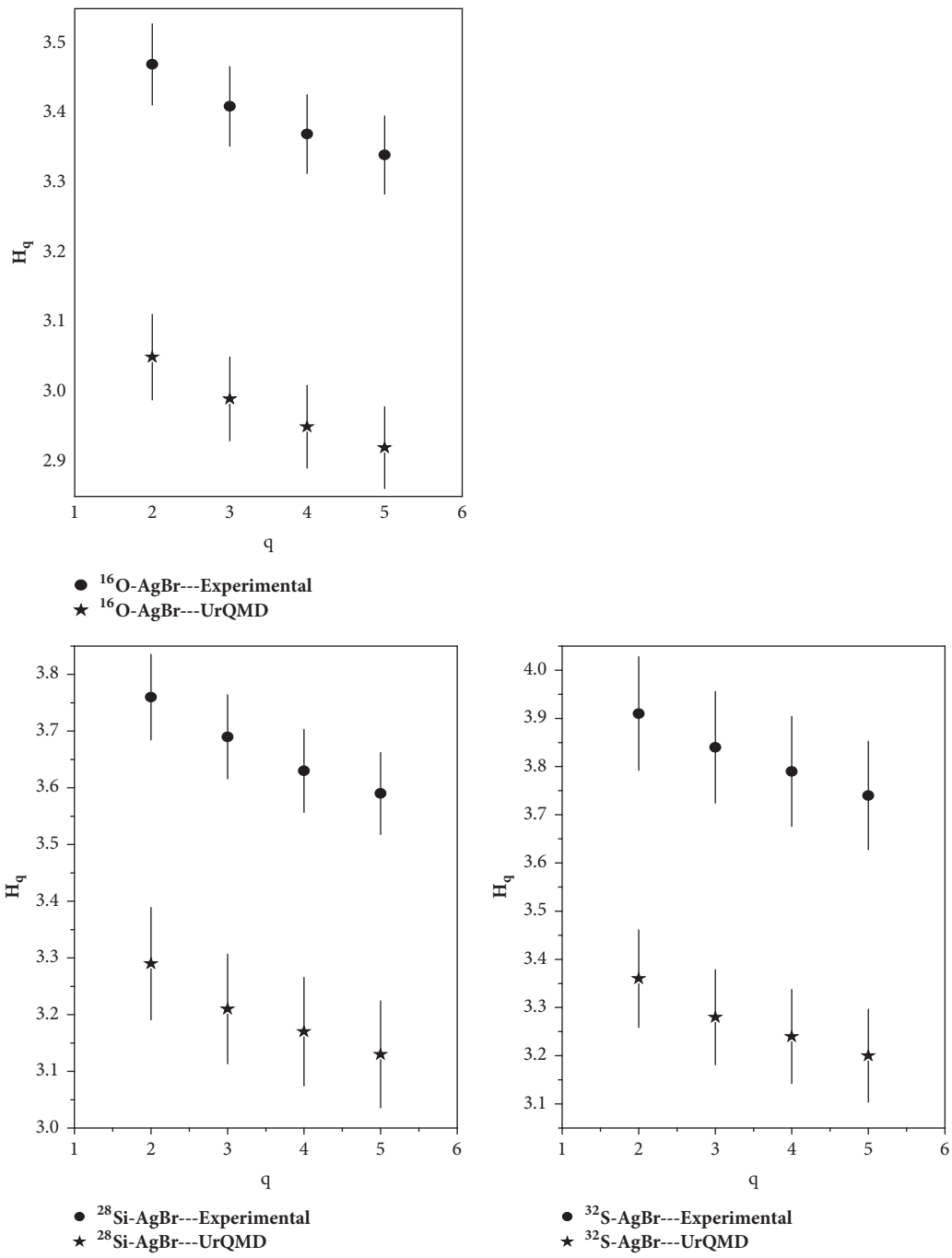

Figure 1: It represents the variation of Renyi entropy with order number q for ^{16}O-AgBr, ^{28}Si-AgBr, and ^{32}S-AgBr interactions at 4.5AGeV/c in case of experimental and UrQMD simulated events.

multifractality in multipion production mechanism. Presence of multifractality during the production of shower particles indicates the occurrence of cascade mechanism in particle production process. From Table 3 it may also be noted that the values of the generalized fractal dimension remain almost the same within the experimental error for ^{16}O-AgBr and ^{28}Si-AgBr interactions. But for ^{32}S-AgBr interactions the $\mathbf{D_q}$ values are higher in comparison to the other two interactions. The variation of $\mathbf{D_q}$ against the order q has been shown in Figure 2 for ^{16}O-AgBr, ^{28}Si-AgBr, and ^{32}S-AgBr interactions.

Now it will be interesting to see how the analysis will look like if one uses Shannon entropy instead of Renyi entropy. However, Shannon entropy cannot be calculated for different orders and hence we can only calculate the values of information fractal dimension for ^{16}O-AgBr, ^{28}Si-AgBr, and ^{32}S-AgBr interactions. We have calculated the values of Shannon entropies derived from the concept of

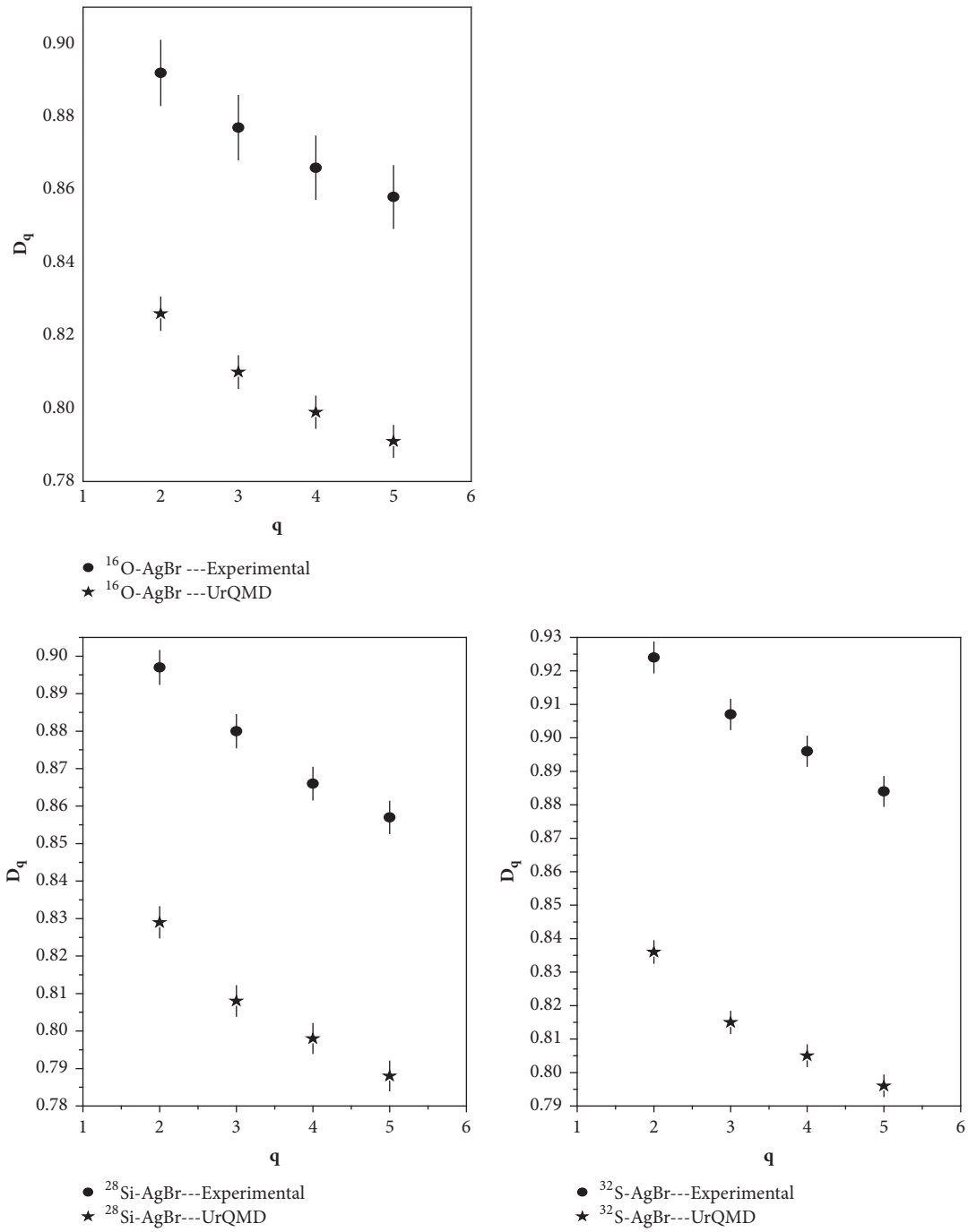

FIGURE 2: It represents the variation of generalized fractal dimension with order number q for ^{16}O-AgBr, ^{28}Si-AgBr, and ^{32}S-AgBr interactions at 4.5AGeV/c in case of experimental and UrQMD simulated events.

Gibbs-Boltzmann theories of entropy and tabulated the values in Table 4. The values of information fractal dimension for the three interactions have also been calculated and presented in the same table. Comparing Tables 2 and 4 it may be noticed that the values of Shannon entropy for ^{16}O-AgBr, ^{28}Si-AgBr, and ^{32}S-AgBr interactions are little higher than those of Renyi entropies.

From the values of the generalized fractal dimension calculated from Renyi entropy values we have evaluated the values of anomalous fractal dimension and hence the ratio of $\mathbf{d_q/d_2}$ has been calculated. In Table 5 the calculated values of $\mathbf{d_q/d_2}$ have been presented for ^{16}O-AgBr, ^{28}Si-AgBr, and ^{32}S-AgBr interactions. It is worthwhile to point out that the spiky structure of density distribution of shower particles

Table 4: This represents the values of Shannon entropy S and Information dimension for all the three interactions in case of the experimental as well as the UrQMD simulated data.

Interactions	Shannon Entropy S **Experimental value**	Information dimension Experimental data	Shannon Entropy S **UrQMD simulated Value**	Information dimension UrQMD data
$^{16}O - AgBr$	3.59±.12	.922±.001	3.19±.01	.864±.002
$^{28}Si - AgBr$	3.87±.14	.924±.002	3.44±.06	.866±.003
$^{32}S - AgBr$	4.00±.16	.924±.002	3.50±.09	.870±.003

Table 5: This represents the experimental and UrQMD simulated values of $\mathbf{d_q/d_2}$ and $\boldsymbol{\beta_q}$ for ^{16}O-AgBr, ^{28}Si-AgBr, and ^{32}S-AgBr interactions at 4.5AGeV/c.

Interactions	Order	**Experimental** values of $\frac{\mathbf{d_q}}{\mathbf{d_2}}$	**Experimental** values of $\boldsymbol{\beta_q}$	**UrQMD** simulated values of $\frac{\mathbf{d_q}}{\mathbf{d_2}}$	**UrQMD** simulated values of $\boldsymbol{\beta_q}$
^{16}O-AgBr	2	1.00±.02	1.00±.02	1.00±.03	1.00±.02
	3	1.14±.**03**	2.28±.**03**	1.09±.**02**	2.18±.**02**
	4	1.24±.**05**	3.72±.**05**	1.15±.**03**	3.45±.**03**
	5	1.31±.**05**	5.24±.**05**	1.20±.**04**	4.80±.**04**
^{28}Si-AgBr	2	1.00±.02	1.00±.02	1.00±.02	1.00±.02
	3	1.16±.**03**	2.32±.**03**	1.12±.**02**	2.24±.**02**
	4	1.30±.**05**	3.90±.**05**	1.18±.**03**	3.54±.**03**
	5	1.39±.**06**	5.56±.**05**	1.24±.**04**	4.96±.**04**
^{32}S-AgBr	2	1.00±.02	1.00±.02	1.00±.02	1.00±.02
	3	1.22±.**04**	2.44±.**03**	1.13±.**03**	2.26±.**02**
	4	1.37±.**04**	4.11±.**05**	1.19±.**03**	3.57±.**02**
	5	1.53±.**08**	6.12±.**05**	1.24±.**04**	4.96±.**02**

Table 6: This represents the **r** value characterizing the degree of multifractality obtained from the plot $\mathbf{d_q/d_2}$ with order number q for ^{16}O-AgBr, ^{28}Si-AgBr, and ^{32}S-AgBr interactions at 4.5AGeV/c in case of experimental and UrQMD simulated events.

Interactions	**r** value characterizing the degree of multifractality obtained from the plot $\frac{\mathbf{d_q}}{\mathbf{d_2}}$ with order number q	
	Experimental	UrQMD
^{16}O-AgBr (4.5AGeV/c)	.206±0.011	.132±0.006
^{28}Si-AgBr (4.5AGeV/c)	.262±.011	.156±0.017
^{32}S-AgBr (4.5AGeV/c)	.348±.014	.156±0.019

can also be investigated with the help of a set of bunching parameters [81]. The higher-order bunching parameters can be expressed in terms of lower-order parameters resulting in a linear expression for the anomalous fractal dimension [82].

$$\mathbf{d_q} = (\mathbf{1} - \mathbf{r})\,\mathbf{d_2} + \frac{\mathbf{q}}{\mathbf{2}}\mathbf{d_2 r} \tag{6}$$

so that

$$\frac{\mathbf{d_q}}{\mathbf{d_2}} = (\mathbf{1} - \mathbf{r}) + \frac{\mathbf{qr}}{\mathbf{2}} \tag{7}$$

A nonzero value of the **r** implies the multifractal behavior [82]. We have applied this theory to our study in order to quantify the fractal nature of shower particle production. We have plotted the variation of $\mathbf{d_q/d_2}$ against the order number **q** in Figure 3 for ^{16}O-AgBr, ^{28}Si-AgBr, and ^{32}S-AgBr interactions. The calculated values of **r from** the slope parameter have been presented in Table 6 for our data. The value of **r** signifies the degree of multifractality. From the table it may be seen that for all the interactions the **r** value is greater than zero. This reconfirms the multifractal nature of multiparticle production mechanism. Moreover, **r**

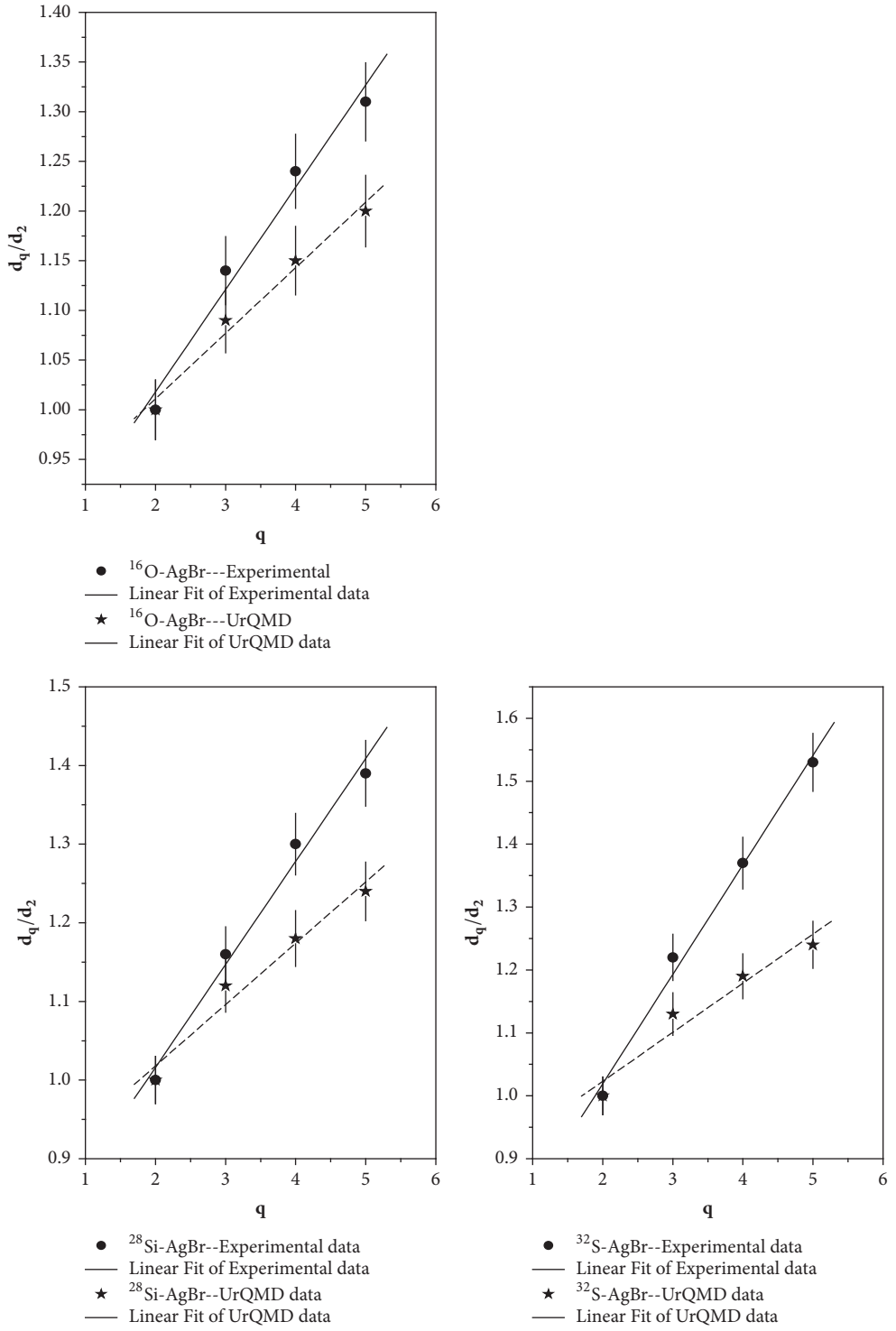

FIGURE 3: It represents the variation of $\mathbf{d_q/d_2}$ with order number q for ^{16}O-AgBr, ^{28}Si-AgBr, and ^{32}S-AgBr interactions at 4.5AGeV/c in case of experimental and UrQMD simulated events.

value characterizing the degree of multifractality is found to depend on the mass number of the projectile beam. Degree of multifractality is found to increase with the increase of projectile mass as evident from Table 6.

R.C Hwa suggested that [83] from the concept of multifractality a qualitative and quantitative investigation of quark-hadron phase transition in high energy nucleus-nucleus collisions is possible. In analogy with the photo count problem at the onset of lasing in nonlinear optics, the coherent state description in high energy nucleus-nucleus interactions can be used in the frame work of Ginzburg-Landau theory [83, 84]. A quantity $\boldsymbol{\beta_q}$ in terms of the ratio

Table 7: This represents the values of ν the critical value for the Ginzburg-Landau phase transition for ^{16}O-AgBr, ^{28}Si-AgBr, and ^{32}S-AgBr interactions at 4.5 AGeV/c for experimental and UrQMD simulated events calculated from the concept of Renyi entropy.

Interactions	data	ν (Calculated From Renyi entropy values)
^{16}O-AgBr interaction at 4.5 AGeV/c	Experimental	1.197 ± 0.003
	UrQMD	1.136 ± 0.004
^{28}Si-AgBr interaction at 4.5 AGeV/c	Experimental	1.248 ± 0.010
	UrQMD	1.152 ± 0.007
^{32}S-AgBr interaction at 4.5 AGeV/c	Experimental	1.327 ± 0.022
	UrQMD	1.144 ± 0.007

of higher-order anomalous fractal dimension to the second-order anomalous fractal dimension can be defined by the following relation [83, 84]:

$$\beta_q = \frac{d_q}{d_2}(q-1) \tag{8}$$

According to Ginzburg-Landau model [84] β_q is related to (q-1) by the relation

$$\beta_q = (q-1)^{\nu}. \tag{9}$$

Relation (8) and relation (9) are found to be valid for all systems which can be described by the Ginzburg-Landau (GL) theory and also are independent of the underlying dimension of the parameters of the model [84]. If the value of the scaling exponent ν is equal to or close enough (within the experimental error) to 1.304 then a quark-hadron phase transition is expected for the experimental data [84]. If the measured value of ν is different from the critical value 1.304 considering the experimental errors then the possibility of the quark-hadron phase transition has to be ruled out [84]. ν is a universal quantity valid for all systems describable by the Ginzburg-Landau (GL) theory. It is independent of the underlying dimension or the parameters of the model. The critical exponent ν is an important parameter to investigate the possibility of quark-hadron phase transition, since neither the transition temperature nor the other important parameters are known there [3, 84]. If the signature of quark-hadron phase transition depends on the details of the heavy-ion collisions, e.g., nuclear sizes, collision energy, transverse energy, etc., even after the system has passed the thresholds for the creation of quark-gluon plasma, such a signature is likely to be sensitive to the theoretical model used [3, 84]. But the critical exponent ν is independent of such details. The value of the critical exponent depends only on the validity of the Ginzburg-Landau (GL) description of the phase transition for the problem concerned. Here lies the importance of this critical exponent.

We have calculated the values of β_q using relation (8) and presented the values in Table 5 for ^{16}O-AgBr, ^{28}Si-AgBr, and ^{32}S-AgBr interactions. In order to search for the Ginzburg-Landau second-order phase transition we have studied the variation of β_q with (q-1) in Figures 4, 5, and 6 in case of ^{16}O-AgBr, ^{28}Si-AgBr, and ^{32}S-AgBr interactions at 4.5 AGeV/c for the experimental data. The variations of β_q with (q-1) have been fitted with the function $\beta_q=(q-1)^{\nu}$ in order to extract the critical exponent ν. In Table 7 we have shown the calculated values of the critical exponent ν for ^{16}O-AgBr, ^{28}Si-AgBr, and ^{32}S-AgBr interactions for experimental events. Table 7 reflects that the calculated values of critical exponents obtained from our analysis increase with the increase of projectile mass. The experimental values of the critical exponent ν for ^{16}O-AgBr and ^{28}Si-AgBr interactions are found to be lower than the critical value 1.304 while for ^{32}S-AgBr interaction the critical exponent is higher than the critical value signifying the absence of quark-hadron phase transition in our data.

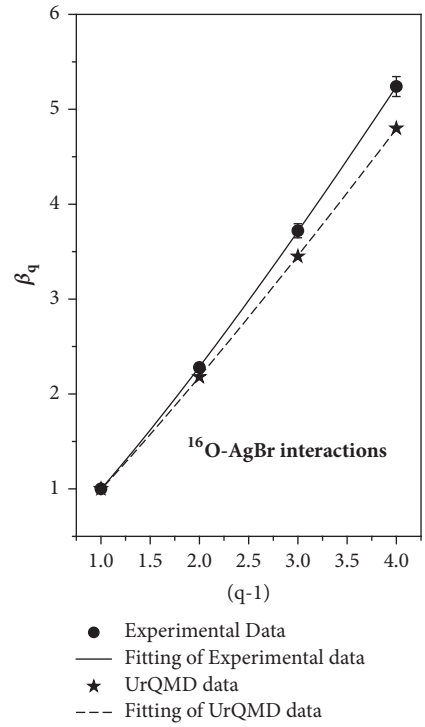

Figure 4: It represents the fitting of $\beta_q = (q-1)^{\nu}$ in case of ^{16}O-AgBr interactions for the experimental and UrQMD simulated data.

Interpretation of multifractality from the thermodynamical point of view allows us to study the fractal properties of stochastic processes with the help of standard concept of thermodynamics. In thermodynamics the constant-specific-heat approximation is widely applicable in many important

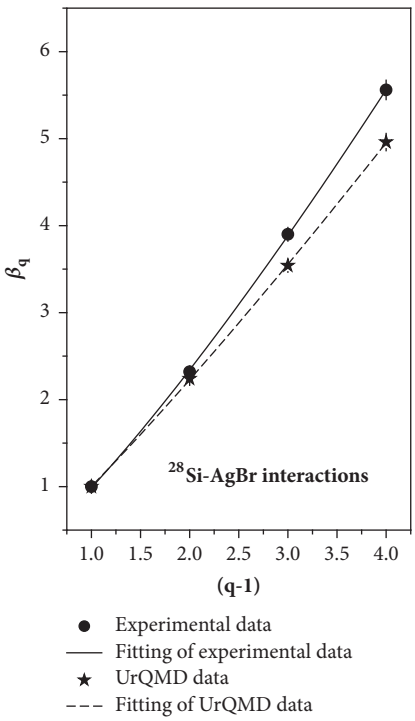

FIGURE 5: It represents the fitting of $\boldsymbol{\beta_q = (q-1)^{\gamma}}$ in case of ^{28}Si-AgBr interactions for the experimental and UrQMD simulated data.

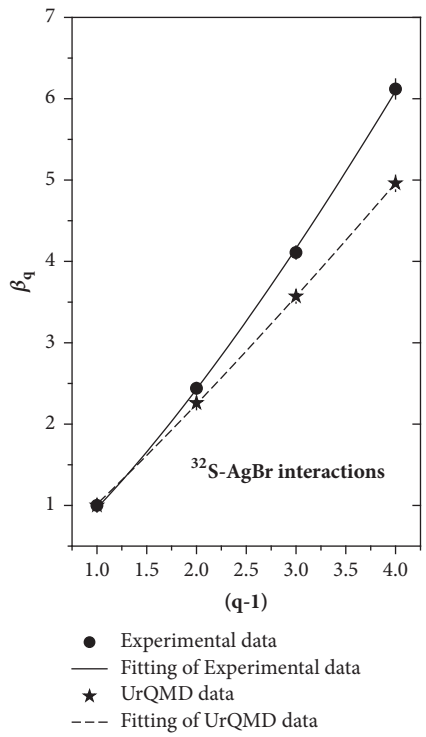

FIGURE 6: It represents the fitting of $\boldsymbol{\beta_q = (q-1)^{\gamma}}$ in case of ^{32}S-AgBr interactions for the experimental and UrQMD simulated data.

cases; for example, the specific heat of gases and solids is constant, independent of temperature over a larger or smaller temperature interval [85]. This approximation is also applicable to multifractal data of multiparticle production processes proposed by Bershadskii [86]. Bershadskii pointed out that [87] regions of the temperature where the constant-specific-heat approximation is applicable are usually far away from the phase transition regimes. For the considered interactions the phase-transition-like phenomena can occur in the vicinity of q=0, where q is the inverse of temperature. Such situation is expected at the onset of chaos of the dynamical attractors [87]. Barshadskii argued that [86] multiparticle production in high energy nucleus-nucleus collisions is related to phase-transition-like phenomena [3]. He introduced a multifractal Bernoulli distribution which appears in a natural way at the morphological phase transition from monofractality to multifractality. Multifractal Bernoulli distribution plays an important role in multiparticle production at higher energies. It has been pointed out that [11] multifractal specific heat can be derived from the relation $\mathbf{D_q = D_\infty + Clnq/(q-1)}$ if the monofractal to multifractal transition is governed by the Bernoulli distribution. The slope of the linear best fit curve showing the variation of $\mathbf{D_q}$ against $\mathbf{lnq/(q-1)}$ has been designated as multifractal specific heat. The gap at the multifractal specific heat at the multifractality to monofractality transition allows us to consider this transition as a thermodynamic phase transition [88, 89].

We have studied the variation of $\mathbf{D_q}$ against $\mathbf{lnq/(q-1)}$ for ^{16}O-AgBr, ^{28}Si-AgBr, and ^{32}S-AgBr interactions in Figure 7. The experimental points have been fitted with the best linear behavior and the slope of the best linear behavior reflects the values of multifractal specific heat. The linear behavior in Figure 7 indicates approximately good agreement between the experimental data and the multifractal Bernoulli representation. The calculated values of the multifractal specific heat for all the three interactions have been presented in Table 8. From Table 8 it may be noted that within the experimental error multifractal specific heat remains almost constant for the three interactions.

The experimental results have been compared with those obtained by analyzing events generated by the Ultra-Relativistic Quantum Molecular Dynamics (UrQMD) model. UrQMD is a hadronic transport model and this model can be used in the entire available range of energies to simulate nucleus-nucleus interactions. For more details about this model, readers are requested to consult [81, 90]. In our earlier papers [78, 80] we have utilized the UrQMD model to simulate ^{16}O-AgBr, ^{28}Si-AgBr, and ^{32}S-AgBr interactions at 4.5 AGeV/c. As described in our previous papers [78, 80] we have generated a large sample of events using the UrQMD code (UrQMD 3.3p1) for ^{16}O-AgBr, ^{28}Si-AgBr, and ^{32}S-AgBr interactions at 4.5AGeV/c. We have also calculated the average multiplicities of the shower tracks for all the three interactions in case of the UrQMD data sample [78]. Average multiplicities of the shower tracks in case of UrQMD data sample have been presented in Table 1 along with the average multiplicity values of shower particles in the case of the experimental events. Table 1 shows that the average multiplicities of the shower tracks for the UrQMD events are comparable with those of the experimental values for all the interactions

Table 8: This represents the values of multifractal specific heat of the produced shower particles in ^{16}O-AgBr, ^{28}Si-AgBr, and ^{32}S-AgBr interactions at 4.5AGeV/c in case of experimental and UrQMD simulated events.

Interactions	Multifractal Specific heat	
	Experimental	UrQMD
^{16}O-AgBrv (4.5AGeV/c)	.116±0.004	.119±0.003
^{28}Si-AgBr (4.5AGeV/c)	.138±.007	.138±.005
^{32}S-AgBr (4.5AGeV/c)	.133±.010	.136±.004

[78]. We have calculated the values of Renyi entropy of order q=2-5 for all the three interactions using the UrQMD simulated data. The calculated values of Renyi entropy have been presented in Table 2 along with the experimental values. For the UrQMD simulated data also second-order Renyi entropy values have been taken from our recent publication [80]. From the table it may be seen that the experimentally calculated values of Renyi entropy are higher than those of their UrQMD counterparts signifies the presence of more disorderness for the experimental data. The variation of $\mathbf{H_q}$ with order q for the UrQMD simulated data has been presented in Figure 1 along with the experimental plots for each interaction. For the UrQMD simulated events we have calculated the values of the generalized fractal dimension $\mathbf{D_q}$ from the values of Renyi entropy using relations (3) and (4). The calculated values of generalized fractal dimension for the UrQMD simulated events of ^{16}O-AgBr, ^{28}Si-AgBr, and ^{32}S-AgBr interactions at 4.5AGeV/c have been presented in Table 3 along with the corresponding experimental values. From the table it is seen that for the UrQMD simulated events also the generalized fractal dimension $\mathbf{D_q}$ decreases with order q signifying the presence of multifractality for the simulated events. But the values of $\mathbf{D_q}$ for the simulated events are lower than the corresponding experimental counterparts for all the interactions. The variation of $\mathbf{D_q}$ with order q has been shown in Figure 2 for ^{16}O-AgBr, ^{28}Si-AgBr, and ^{32}S-AgBr interactions along with the experimental plots. We have calculated the values of Shannon entropies and information dimension for the UrQMD data set of ^{16}O-AgBr, ^{28}Si-AgBr, and ^{32}S-AgBr interactions. The calculated values of Shannon entropy and information dimension have been presented in Table 4. From Table 4 it may be noticed that the Shannon entropy and information dimension for the UrQMD simulated events in case of ^{16}O-AgBr, ^{28}Si-AgBr, and ^{32}S-AgBr interactions are lower than the corresponding experimental values.

As in the case of experimental data in case of UrQMD simulated data also we have calculated the values of $\mathbf{d_q/d_2}$ and presented the values in Table 5. From the table it may be noticed that the experimentally obtained values of $\mathbf{d_q/d_2}$ are little higher than the corresponding UrQMD simulated values. To quantify the multifractality in case of UrQMD simulated data we have studied the variation of $\mathbf{d_q/d_2}$ with order q in Figure 3 for ^{16}O-AgBr, ^{28}Si-AgBr, and ^{32}S-AgBr interactions. From the slope of the plot of $\mathbf{d_q/d_2}$ against q we have calculated the value of **r** which signifies the degree of multifractality. The extracted value **of r** has been presented in Table 6 for the UrQMD simulated events. From the table it may be seen that the **r** value characterizing the degree of multifractality calculated for the UrQMD simulated events is significantly lower than the corresponding experimental value for all the three interactions. This observation signifies the presence of stronger multifractality for the experimental data. We have also studied the Ginzburg-Landau phase transition with UrQMD simulated events of ^{16}O-AgBr, ^{28}Si-AgBr, and ^{32}S-AgBr interactions. The variations of $\boldsymbol{\beta_q}$ with (q-1) for the UrQMD simulated data have been presented in Figures 4, 5, and 6 in case of ^{16}O-AgBr, ^{28}Si-AgBr, and ^{32}S-AgBr interactions, respectively, at 4.5 AGeV/c along with the experimental plot. The variations of $\boldsymbol{\beta_q}$ with (q-1) have been fitted with the function $\boldsymbol{\beta_q}=(\mathbf{q-1})^{\boldsymbol{\nu}}$ in order to extract the critical exponent $\boldsymbol{\nu}$. In Table 7 we have shown the calculated values of the critical exponents for ^{16}O-AgBr, ^{28}Si-AgBr, and ^{32}S-AgBr interactions for the experimentally simulated events. From Table 7 it may be seen that the critical exponent values for the simulated events are lower than those of the experimental events and there is no evidence of quark-hadron phase transition for the simulated data also. The values of the critical exponent calculated from the multifractal analysis in case of UrQMD simulated data remain almost constant with respect to the mass number of the projectile beam.

We have studied the variation of $\mathbf{D_q}$ against $\mathbf{lnq/(q-1)}$ in Figure 7 for the UrQMD data sample of ^{16}O-AgBr, ^{28}Si-AgBr, and ^{32}S-AgBr interactions in order to calculate the multifractal specific heat. From the slope of the best linear behavior of the plotted points the multifractal specific heat of the shower particles for the UrQMD data sample has been evaluated and presented in Table 8 for all the three interactions. From the table it may be seen that the values of the multifractal specific heat for the experimental and simulated data agree reasonably well with each other. This observation signifies the constancy of multifractal specific heat for the UrQMD simulated events also.

6. Conclusions and Outlook

In this paper we have presented an analysis of multifractality and multifractal specific heat in the frame work of Renyi entropy analysis for the produced shower particles in nuclear

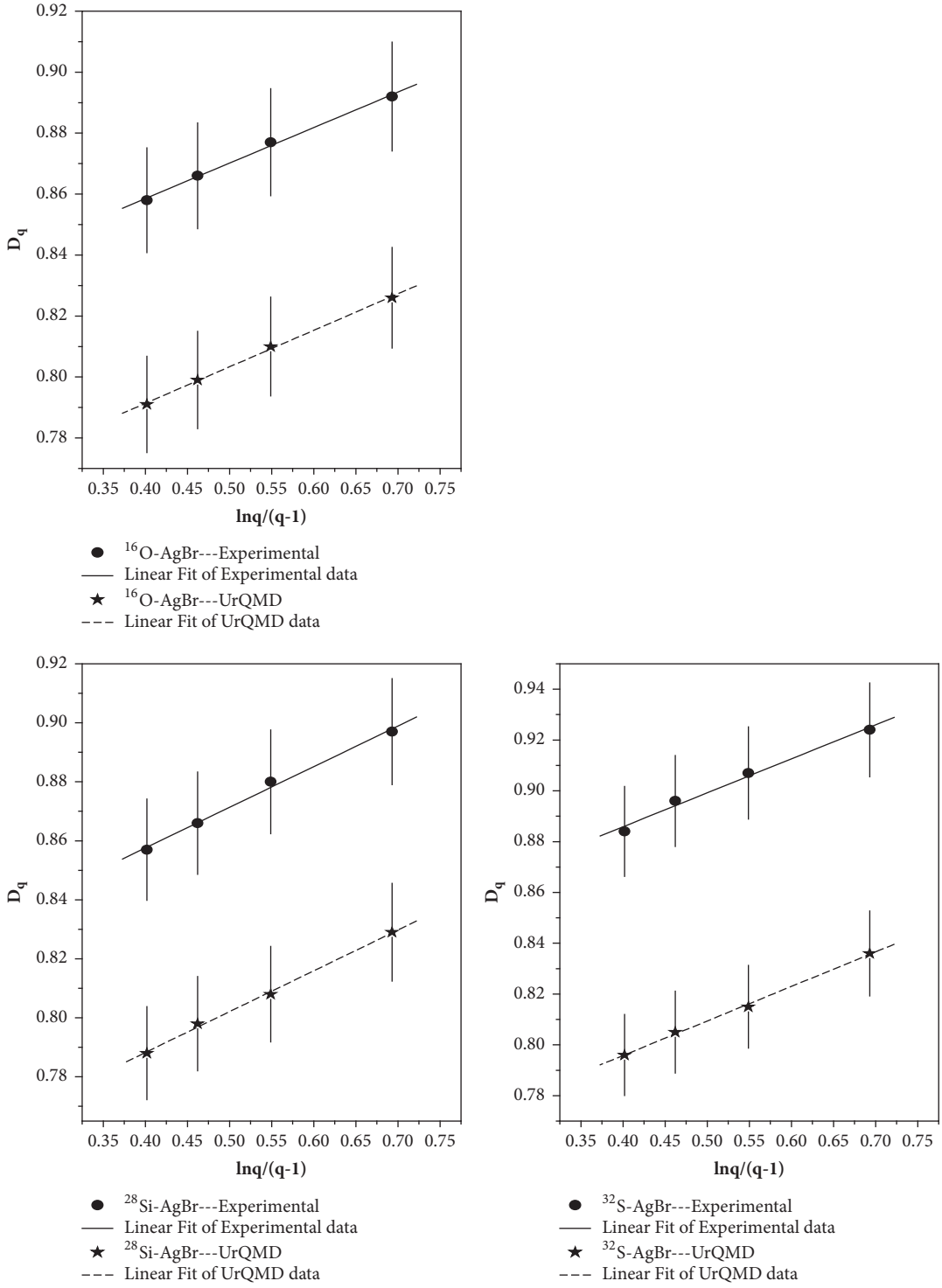

FIGURE 7: It represents the variation of D_q against $\ln q/(q-1)$for ^{16}O-AgBr, ^{28}Si-AgBr, and ^{32}S-AgBr interactions at 4.5AGeV/c in case of experimental and UrQMD simulated events.

emulsion detector for ^{16}O-AgBr, ^{28}Si-AgBr, and ^{32}S-AgBr interactions at 4.5AGeV/c. Experimental results have been compared with the prediction of Ultra-Relativistic Quantum Molecular Dynamics (UrQMD) model. Qualitative information about the multifractal dynamics of particle production process has been extracted and reported in the present analysis. The significant conclusions of this analysis are as follows:

(1) Renyi entropy values of all the interactions decrease with the order number q for both experimental and UrQMD simulated data. Renyi entropy values

for UrQMD data are less than the corresponding experimental values.

(2) Generalized fractal dimension calculated from Renyi entropy for both experimental and UrQMD simulated data decreases with the increase of order q suggesting the presence of multifractality in multiparticle production process.

(3) The values of Shannon entropy for ^{16}O-AgBr, ^{28}Si-AgBr, and ^{32}S-AgBr interactions are little higher than those of Renyi entropies.

(4) Degree of multifractality is found to be higher for the experimental data in comparison to the simulated data and it increases with the increase of projectile mass for the experimental data.

(5) The experimental values of the critical exponents for ^{16}O-AgBr and ^{28}Si-AgBr interactions are lower than the critical value 1.304 required for a quark-hadron phase transition to occur while for ^{32}S-AgBr interaction the experimentally obtained values of critical exponent are higher than the critical value 1.304 signifying the absence of quark-hadron phase transition. Absence of quark-hadron phase transition is prominent for the simulated events also.

(6) The calculated values of critical exponents obtained from our analysis increase with the increase of projectile mass for the experimental data. UrQMD predicted values of the critical exponent $\boldsymbol{\nu}$ remain almost constant with the increase of projectile mass.

(7) Multifractal specific heat for the simulated data agrees well with the experimental data. Constancy of multifractal specific heat is reflected from our analysis.

It is true that there are many papers available in the literature where presence of multifractality has been tested experimentally in multiparticle production in high energy nucleus-nucleus interactions by different methods. But the method adopted in this paper to study multifractality seems to be simple and interesting and in this regard our study deserves attention. The observed multifractal behavior of the produced shower particles may be viewed as an experimental fact.

Data Availability

The data used to support the findings of this study are available from the corresponding author upon request.

Conflicts of Interest

There are no conflicts of interest in publishing the paper

Acknowledgments

The authors are grateful to Professor Pavel Zarubin of the Joint Institute of Nuclear Research (JINR), Dubna, Russia, for providing them the required emulsion data. Dr. Bhattacharyya acknowledges Professor Dipak Ghosh, Department of Physics, Jadavpur University, and Professor Argha Deb, Department of Physics, Jadavpur University, for their inspiration in the preparation of this manuscript.

References

[1] A. Bialas and R. Peschanski, "Moments of rapidity distributions as a measure of short-range fluctuations in high-energy collisions," *Nuclear Physics B*, vol. 273, no. 3-4, pp. 703–718, 1986.

[2] A. Bialas and R. Peschanski, "Intermittency in multiparticle production at high energy," *Nuclear Physics B*, vol. 308, no. 4, pp. 857–867, 1988.

[3] E. A. De Wolf, I. M. Dremin, and W. Kittel, "Scaling laws for density correlations and fluctuations in multiparticle dynamics," *Physics Reports*, vol. 270, no. 1-2, pp. 1–141, 1996.

[4] B. B. Mandelbrot, *The Fractal Geometry of Nature*, Henry Holt and Company, San Francisco, Calif, USA, 1982.

[5] Z. Chen, P. Ivanov, k. Hu, and H. E. Stanley, "Effect of nonstationarities on detrended fluctuation analysis," *Physical Review E*, vol. 65, Article ID 041107, 2002.

[6] D. S. Harte, *Multifractals: Theory and Applications*, Chapman & Hall/crc, 2001.

[7] K. J. Falconer, *The Geometry of Fractal Sets*, vol. 85 of *Cambridge Tracts in Mathematics*, Cambridge University Press, Cambridge, UK, 1985.

[8] T. C. Halsey, P. Meakin, and I. Procaccia, "Scaling structure of the surface layer of diffusion-limited aggregates," *Physical Review Letters*, vol. 56, no. 8, pp. 854–857, 1986.

[9] W. G. Hanan and D. M. Heffernan, "Multifractal analysis of the branch structure of diffusion-limited aggregates," *Physical Review E: Statistical, Nonlinear, and Soft Matter Physics*, vol. 85, no. 2, 2012.

[10] W. G. Hanan and D. M. Heffernan, "Global structure and finite-size effects in the $f(\alpha)$ of diffusion-limited aggregates," *Physical Review E: Statistical, Nonlinear, and Soft Matter Physics*, vol. 77, no. 1, 2008.

[11] H. E. Stanley and P. Meakin, "Multifractal phenomena in physics and chemistry," *Nature*, vol. 335, no. 6189, pp. 405–409, 1988.

[12] A. Cummings, G. O'Sullivan, W. G. Hanan, and D. M. Heffernan, "Multifractal analysis of selected rare-earth elements," *Journal of Physics B: Atomic, Molecular and Optical Physics*, vol. 34, 2001.

[13] W. G. Hanan, D. M. Heffernan, and J. C. Earnshaw, "Left-sided Multifractality of the Harmonic Measure on 2-D Cluster - Cluster Aggregates," *Chaos, Solitons & Fractals*, vol. 9, no. 6, pp. 875–880, 1998.

[14] B. B. Mandelbrot, "Intermittent turbulence in self-similar cascades: divergence of high moments and dimension of the carrier," *Journal of Fluid Mechanics*, vol. 62, pp. 331–358, 1974.

[15] P. C. Ivanov, L. A. Nunes Amaral, A. L. Goldberger et al., "Multifractality in human heartbeat dynamics," *Nature*, vol. 399, no. 6735, pp. 461–465, 1999.

[16] Y. Zheng, J. Gao, J. C. Sanchez, J. C. Principe, and M. S. Okun, "Multiplicative multifractal modeling and discrimination of human neuronal activity," *Physics Letters A*, vol. 344, no. 2-4, pp. 253–264, 2005.

[17] E. A. Ihlen, "Introduction to multifractal detrended fluctuation analysis in matlab," *Front. Physiol*, vol. 3, p. 141, 2012.

[18] A. Feldmann, A. C. Gilbert, and W. Willinger, "Data networks as cascades: investigating the multifractal nature of Internet

WAN traffic," in *Proceedings of the the ACM SIGCOMM '98 conference on Applications, technologies, architectures, and protocols for computer communication*, pp. 42–55, Vancouver, British Columbia, Canada, August 1998.

[19] N. Sala, "Fractal Geometry in the Arts: An Overview Across the Different Cultures," in *Thinking in Patterns: Fractals and Related Phenomena in Nature*, M. M. Novak, Ed., World Scientific, Singapore, 2004.

[20] B. B. Mandelbrot and R. L. Hudson, *The (Mis)Behavior of Markets: A Fractal View of Risk, Ruin, and Reward*, Basic Books, New York, NY, USA, 2004.

[21] Ł. Czarnecki and D. Grech, "Multifractal dynamics of stock markets," *Acta Physica Polonica A*, vol. 117, no. 4, pp. 623–629, 2010.

[22] A. Turiel and C. J. Pérez-Vicente, "Multifractal geometry in stock market time series," *Physica A: Statistical Mechanics and its Applications*, vol. 322, no. 1-4, pp. 629–649, 2003.

[23] A. Bialas and R. C. Hwa, "Intermittency parameters as a possible signal for quark-gluon plasma formation," *Physics Letters B*, vol. 253, no. 3-4, pp. 436–438, 1991.

[24] R. C. Hwa, "Fractal measures in multiparticle production," *Physical Review D: Particles, Fields, Gravitation and Cosmology*, vol. 41, no. 5, pp. 1456–1462, 1990.

[25] R. C. Hwa and J. Pan, "Fractal behavior of multiplicity fluctuations in high-energy collisions," *Physical Review D: Particles, Fields, Gravitation and Cosmology*, vol. 45, no. 5, pp. 1476–1483, 1992.

[26] F. Takagi, "Multifractal structure of multiplicity distributions in particle collisions at high energies," *Physical Review Letters*, vol. 72, no. 1, pp. 32–35, 1994.

[27] R. Saha, A. Deb, and D. Ghosh, "Study of phase transition and its dependence on target excitation using fractal properties of pionization process," *Canadian Journal of Physics*, vol. 95, no. 8, pp. 699–710, 2017.

[28] N. Parashar, "Nuclear effects and intermittency in two dimensions," *Journal of Physics G: Nuclear and Particle Physics*, vol. 22, p. 59, 1996.

[29] M. K. Ghosh, A. Mukhopadhyay, and G. Singh, "Intermittency and multiplicity moments of charged particles produced in ^{32}S–Ag/Br interaction at 200 A GeV/c," *Journal of Physics G: Nuclear and Particle Physics*, vol. 32, p. 2293, 2006.

[30] S. Ahmad and M. A. Ahmed, "A comparative study of multifractal moments in relativistic heavy-ion collisions," *Journal of Physics G: Nuclear and Particle Physics*, vol. 32, p. 1279, 2006.

[31] S. Bhattacharyya, A. T. Neagu, and M. Haiduc, "Multifractality analysis of crack images from indirect thermal drying of thin-film dewatered sludge," *Physica A: Statistical Mechanics and its Applications*, vol. 390, no. 14, pp. 2678–2685, 2011.

[32] S. Ahmad, A. R. Khan, M. Zafar, and M. Irfan, "On multifractality and multifractal specific heat in ion-ion collisions," *Chaos, Solitons & Fractals*, vol. 42, no. 1, pp. 538–547, 2009.

[33] D. Ghosh, A. Deb, and M. B. Lahiri, "Pion production and multifractality in ultrarelativistic nuclear collision – evidence of constant specific heat," *Canadian Journal of Physics*, vol. 83, pp. 1169–1175, 2005.

[34] A. Kamal, S. Ahmad, and N. Ahmad, "Evidence of deconfined phase transition in multiparticle production in relativistic nuclear collisions," *International Journal of Modern Physics A*, vol. 23, Article ID 1450016, 2014.

[35] S. Bhattacharyya, M. Haiduc, A. T. Neagu, and E. Firu Fractals, "A study of multifractality and phase transition in heavy-ion collisions — experimental data versus model simulation," *Fractals*, vol. 26, Article ID 1850015, 2018.

[36] S. Dutta, D. Ghosh, and S. Chatterjee, "Multifractal detrended fluctuation analysis of pseudorapidity and azimuthal distribution of pions emitted in high energy nuclear collisions," *International Journal of Modern Physics A*, vol. 29, Article ID 1450084, 2014.

[37] Y. X. Zhang, W. Y. Qian, and C. B. Yang, "Multifractal structure of pseudorapidity and azimuthal distributions of the shower particles in Au + Au collisions at 200 A geV," *International Journal of Modern Physics A*, vol. 23, no. 18, pp. 2809–2816, 2008.

[38] S. Bhaduri and D. Ghosh, "Fractal study of pion void probability distribution in ultrarelativistic nuclear collision and its target dependence," *Modern Physics Letters A*, vol. 31, no. 27, Article ID 1650152, 2016.

[39] S. Bhaduri and D. Ghosh, "A new approach of chaos and complex network method to study fluctuation and phase transition in nuclear collision at high energy," *The European Physical Journal A*, vol. 53, p. 135, 2017.

[40] G. Bhoumik, "Comparative Multifractal Detrended Fluctuation Analysis of Heavy Ion Interactions at a Few GeV to a Few Hundred GeV," *Advances in High Energy Physics*, vol. 2016, Article ID 7287803, 9 pages, 2016.

[41] P. Mali, A. Mukhopadhyay, and G. Singh, "Multifractal detrended moving average analysis of particle density functions in relativistic nuclear collisions," *Physica A*, vol. 450, pp. 323–332, 2016.

[42] P. Mali, "Multifractal analysis of multiparticle emission data in the framework of visibility graph and sandbox algorithm," *Physica A: Statistical Mechanics and its Applications*, vol. 493, pp. 253–266, 2018.

[43] P. Mali, A. Mukhopadhyay, and G. Singh, "Detrended analysis of shower track distribution in nucleus-nucleus interactions at CERN SPS energ," *Chaos Solitons & Fractals*, vol. 94, p. 86, 2017.

[44] P. Mali, A. Mukhopadhyay, S. K. Manna, P. K. Haldar, and G. Singh, "Multifractal analysis of charged particle distributions using horizontal visibility graph and sandbox algorithm," *Modern Physics Letters A*, vol. 32, Article ID 1750024, 2017.

[45] P. Mali, S. Sarkar, S. Ghosh, A. Mukhopadhyay, and G. Singh, "Multifractal detrended fluctuation analysis of particle density fluctuations in high-energy nuclear collisions," *Physica A: Statistical Mechanics and its Applications*, vol. 424, pp. 25–33, 2015.

[46] K. Yamazaki, T. Matsui, and g. Baym, "Entropy in the quark–hadron transition," *Nuclear Physics A*, vol. 933, pp. 245–255, 2015.

[47] S. Ahmad, A. Ahmad, A. Chandra, M. Zafar, and M. Irfan, "Entropy analysis in relativistic heavy-ion collisions," *Advances in High Energy Physics*, vol. 2013, Article ID 836071, 10 pages, 2013.

[48] S. Pal and S. Pratt, "Entropy production at RHIC," *Physics Letters*, vol. 578, no. 3, pp. 310–317, 2004.

[49] A. Bialas, W. Czyz, and J. Wosiek, "Studying thermodynamics in heavy ion collisions," *Acta Phys. Pol .B*, vol. 30, pp. 107–118, 1999.

[50] K. Fialkowski and R. Wit, "Entropy in hadron-hadron collisions," *Physical Review D: Particles, Fields, Gravitation and Cosmology*, vol. 62, no. 11, 2000.

[51] A. Bialas and W. Czyz, "Event by event analysis and entropy of multiparticle systems," *Physical Review D: Particles, Fields, Gravitation and Cosmology*, vol. 61, no. 7, 2000.

[52] M. Y. Sinyukov and S. V. Akkelin Acta, "Pion entropy and phase-space densities in A + A collisions," *Acta Physica Hungarica Series A*, vol. 22, no. 1-2, pp. 171–178, 2005.

[53] D. Ghosh, A. Deb, and S. Bhattacharyya, "Entropy scaling in high-energy nucleus–nucleus interactions," *Journal of Physics G: Nuclear and Particle Physics*, vol. 22, pp. 263–1114, 2005.

[54] M. Reiter, A. Dumitru, J. Brachmann, J. A. Maruhn, H. Stöcker, and W. Greiner, "Entropy production in collisions of relativistic heavy ions — a signal for quark-gluon plasma phase transition?" *Nuclear Physics A*, vol. 643, pp. 99–112, 1998.

[55] D. Ghosh, A. Deb, P. K. Haldar, S. R. Sahoo, and D. Maity, "Validity of the negative binomial multiplicity distribution in case of ultra-relativistic nucleus-nucleus interaction in different azimuthal bins," *Europhysics Letters*, vol. 65, p. 311, 2004.

[56] Y. K. Vermani and R. K. Puri, "Entropy and light cluster production in heavy-ion collisions at intermediate energies," *Nuclear Physics A*, vol. 847, no. 3-4, pp. 243–252, 2010.

[57] M. R. Atayan, "Entropy Analysis in π^+p and K^+p Collisions at $\sqrt{s}$ = 22 GeV," *Acta physica polonica B*, vol. 36, p. 2969, 2005.

[58] K. Eskola, H. Paukkunena, and C. Salgado, "From 0 to 5000 in 2×10^{-2}4 seconds: Entropy production in relativistic heavy-ion collisions," *Nuclear Physics A*, vol. 830, no. 1-4, pp. 519c–522c, 2009.

[59] Y. G. Ma, "Application of Information Theory in Nuclear Liquid Gas Phase Transition," *Physical Review Letters*, vol. 83, no. 18, pp. 3617–3620, 1999.

[60] D. Ghosh, A. Deb, S. Bhattacharyya, and U. Datta, "Multiplicity dependence of entropy in different rapidity bins in high-energy nucleus–nucleus interactions," *Physica Scripta*, vol. 85, Article ID 065205, 2012.

[61] D. Ghosh, A. Deb, and S. Bhattacharyya, "Entropy scaling in high-energy nucleus–nucleus interactions," *Journal of Physics G: Nuclear and Particle Physics*, vol. 38, Article ID 065105, 2011.

[62] S. Ahmad, A. Chandra, M. Zafar, and M. Irfan, "Entropy scaling in ion-ion collisions at AGS and SPS energies," *International Journal of Modern Physics E*, vol. 22, Article ID 1350088, 2013.

[63] M. Mohisin Khan, N. Ahmad, and M. Irfan, "Evidence of Entropy Scaling in Relativistic Nucleus–Nucleus Collisions," *International Journal of Modern Physics E*, vol. 21, Article ID 1250068, 2012.

[64] A. Bialas, W. Czyż, and A. Białas, "Renyi Entropies in Multiparticle Production," *Acta Physica Polonica B*, vol. 31, p. 2803, 2000.

[65] V. Simak, "Entropy in Multiparticle Production and Ultimate Multiplicity Scaling," *Physics Letters B*, vol. 206, pp. 159–162, 1988.

[66] C. E. Shannon, *The Mathematical Theory of Communication*, The University of Illinois Press, Urbana, Ill, USA, 1948.

[67] A. Rényi, "On Measurements of Entropy and Information," in *Proceedings of the 4th Berkeley Symp on Math. Stat. Prob*, pp. 547–561, University of California Press.

[68] C. Beck and F. Schloegl, *Thermodynamics of chaotic systems*, vol. 4 of *Cambridge Nonlinear Science Series*, Cambridge University Press, Cambridge, UK, 1993.

[69] I. M. Dremin and J. W. Gary, "Hadron multiplicities," *Physics Reports*, vol. 349, pp. 301–393, 2001.

[70] A. Bialas and W. Czyz, "Measurement of entropy of a multiparticle system: a do-list," *High Energy Physics - Phenomenology*, vol. 31, p. 687, 2000.

[71] C. W. Ma and Y. G. Ma, "Shannon information entropy in heavy-ion collisions," *Progress in Particle and Nuclear Physics*, vol. 99, pp. 120–158, 2018, rogress in Particle and Nuclear Physics.

[72] M. Pachr, V. Simak, M. Sumbera, and I. Zborovsky, "Entropy, dimensions and other multifractal characteristics of multiplicity distributions," *Modern Physics Letters A*, vol. 07, no. 25, pp. 2333–2339, 1992.

[73] A. Mukhopadhyay, P. L. Jain, and G. Singh, "Entropy and fractal characteristics of multiparticle production at relativistic heavy ion interactions," *Physical Review C*, vol. 47, p. 410, 1993.

[74] W. Ochs and J. Wosiek, "Multiparton correlations and fractal structure in QCD jets," *Physics Letters B*, vol. 305, no. 1-2, pp. 144–150, 1993.

[75] S. Bhattacharyya, M. Haiduc, A. T. Neagu, and E. Firu, "Target dependence of clan model parameters at Dubna energy-chaotic pion production," *Journal of Physics G: Nuclear and Particle Physics*, vol. 40, Article ID 025105, 2013.

[76] S. Bhattacharyya, M. Haiduc, A. T. Neagu, and E. Firu, "Event-by-event pseudo-rapidity fluctuations in high energy nucleus–nucleus interactions," *Physics Letters B*, vol. 726, no. 1-3, pp. 194–205, 2013.

[77] S. Bhattacharyya, M. Haiduc, A. T. Neagu, and E. Firu, "Forward–backward multiplicity correlation in high-energy nucleus–nucleus interactions at a few AGeV/c," *Journal of Physics G: Nuclear and Particle Physics*, vol. 41, Article ID 075106, 2014.

[78] S. Bhattacharyya, M. Haiduc, A. T. Neagu, and E. Firu Euro, "Multiplicity distribution of shower particles in nucleus-nucleus collisions at 4.1-4.5 A GeV/c," *The European Physical Journal Plus*, vol. 132, p. 229, 2017.

[79] C. F. Powell, P. H. Fowler, and D. H. Perkins, *The study of elementary particles by photographic method*, Oxford, 1959.

[80] S. Bhattacharyya, M. Haiduc, A. T. Neagu, and E. Firu, "An investigation of Renyi entropy in high-energy nucleus–nucleus collisions," *Canadian Journal of Physics*, vol. 95, p. 715, 2017.

[81] M. Bleicherdag, E. Zabrodin, C. Spieles, and S. A. Bass, "Relativistic hadron-hadron collisions in the ultra-relativistic quantum molecular dynamics model," *Journal of Physics G: Nuclear and Particle Physics*, vol. 25, no. 9, p. 1859, 1999.

[82] S. V. Chekanov and V. I. Kuvshinov Acta, "Bunching Parameter and Intermittency in High-Energy Collisions," *Acta Physica Polonica B*, vol. 25, p. 1189, 1994.

[83] R. C. Hwa, "Scaling exponent of multiplicity fluctuation in phase transition," *Physical Review D*, vol. 47, p. 2773, 1993.

[84] R. C. Hwa and M. T. Nazirov, "Intermittency in second-order phase transitions," *Physical Review Letters*, vol. 69, no. 5, pp. 741–744, 1992.

[85] L. D. Landau and E. M. Lifshitz, *Statistical Physics*, Pergamon Press, 1980.

[86] A. Bershadskii, "Anomalous distributions in heavy ion collisions at high energies," *Physical Review C: Nuclear Physics*, vol. 59, no. 1, pp. 364–368, 1999.

[87] A. Bershadskii, "Multifractal statistics of multiparticle production at high energies," *Journal of Physics A*, vol. 2, p. 225, 1998.

[88] A. Bershadskii, "Multifractal critical thermodynamics in nucleus-nucleus collisions," *Journal of Physics A*, vol. 4, p. 283, 1999.

[89] R. Peschanski, "Intermittency in Particle Collisions," *International Journal of Modern Physics A*, vol. 6, no. 18, p. 325681, 1991.

[90] S. A. Bass, M. Belkacem, M. Bleicher, and M. Brandstetter, "Microscopic Models for Ultrarelativistic Heavy Ion Collisions," *Nuclear Theory*, vol. 41, p. 225, 1998.

Hindawi
Advances in High Energy Physics
Volume 2018, Article ID 7453752, 9 pages
https://doi.org/10.1155/2018/7453752

Research Article

Radial Flow in a Multiphase Transport Model at FAIR Energies

Soumya Sarkar,[1,2] **Provash Mali**,[1] **Somnath Ghosh**,[1] **and Amitabha Mukhopadhyay**[1]

[1]*Department of Physics, University of North Bengal, Siliguri 734013, India*
[2]*Department of Physics, Siliguri College, Siliguri 734001, India*

Correspondence should be addressed to Amitabha Mukhopadhyay; amitabha_62@rediffmail.com

Received 13 October 2017; Revised 15 January 2018; Accepted 6 March 2018; Published 22 April 2018

Academic Editor: Raghunath Sahoo

Azimuthal distributions of radial velocities of charged hadrons produced in nucleus-nucleus (AB) collisions are compared with the corresponding azimuthal distribution of charged hadron multiplicity in the framework of a multiphase transport (AMPT) model at two different collision energies. The mean radial velocity seems to be a good probe for studying radial expansion. While the anisotropic parts of the distributions indicate a kind of collective nature in the radial expansion of the intermediate "fireball," their isotropic parts characterize a thermal motion. The present investigation is carried out keeping the upcoming Compressed Baryonic Matter (CBM) experiment to be held at the Facility for Antiproton and Ion Research (FAIR) in mind. As far as high-energy heavy-ion interactions are concerned, CBM will supplement the Relativistic Heavy-Ion Collider (RHIC) and Large Hadron Collider (LHC) experiments. In this context our simulation results at high baryochemical potential would be interesting, when scrutinized from the perspective of an almost baryon-free environment achieved at RHIC and LHC.

1. Introduction

When two heavy nuclei collide with each other at high-energy it is expected that a color deconfined state composed of strongly coupled quarks and gluons is formed. The properties of such a state, formally known as Quark-Gluon Plasma (QGP) [1], are governed by the rules of quantum chromodynamics (QCD). In order to understand the bulk properties of this extended QCD state and to understand the dynamical processes that might be involved in its formation and subsequent decay, over last three decades or so QGP has been widely searched in many high-energy experiments [2]. Of all the efforts in this regard, the study on the emission of final state particles with respect to the reaction plane of an AB collision, a plane spanned by the beam direction and the impact parameter vector, has been a popular technique that can characterize the thermodynamic and hydrodynamic properties of the QGP matter [3, 4]. In this technique the Fourier decomposition of the anisotropic azimuthal distribution has been widely employed to explore the collective behavior of the final state particles. More specifically, the second harmonic coefficient, traditionally known as the elliptic flow parameter (v_2), is of special interest [5]. The v_2 results obtained from the RHIC and LHC experiments show considerable hydrodynamical behavior of the matter present in the overlapping zone of the colliding nuclei, an intermediate "fireball" that gets thermalized within a very short time interval (<1 fm/c) and subsequently expands almost like a "perfect fluid" having a very small ratio of shear viscosity to entropy density [6–8]. In RHIC [9–13] and LHC [14–17] experiments the v_2 parameter has been widely studied as a function of the centrality of the collision, transverse momentum (p_T), and rapidity (y) or pseudorapidity (η) of the produced particles, for different colliding systems and at varying collision energies. Using the AMPT model, presence of anisotropy in the azimuthal distribution of transverse rapidity (y_T) has been investigated in Au + Au collision at $\sqrt{s_{\mathrm{NN}}} = 200$ GeV [18]. Recently, we have reported some simulation results on the anisotropy present in the azimuthal distribution of p_T of the emitted charged hadrons that has relevance to the radial flow of charged hadrons produced at FAIR energies [19]. The CBM experiment is dedicated to explore the deconfined QCD matter at high baryon density and low to moderate temperature. It is a fixed target experiment being designed with incident beam energy range $E_{\mathrm{lab}} = 10$–40 GeV per nucleon, which is expected to produce

partonic matter of density 6 to 12 times the normal nuclear matter density at the central rapidity region [20]. But at the same time it should be kept in mind that our present understanding of the collective flow of hadronic/partonic matter at this energy region is constrained by the availability of only a few experimental results [21]. Therefore, to get an idea about the expected behavior of any variable or parameter that is relevant in this regard, we have to rely mostly upon the event generators and models. In this article we present some basic simulated results on the (an)isotropy of the radial velocity of charged hadrons produced in Au + Au collisions at $E_{\text{lab}} = 10$ A and 40 A GeV using the AMPT model [22, 23]. The paper is organized as follows: a brief description of the methodology used in this analysis is given in Section 2, the AMPT model is summarily described in Section 3, our simulation based results are discussed in Section 4, and finally in Section 5 our observations are listed.

2. Methodology

Before the collision, the nucleons belonging to individual nucleus possess only longitudinal degrees of freedom. Transverse degrees of freedom are excited into them only after an interaction takes place. In mid-central collisions the overlapping area of the colliding nuclei is almond shaped in the transverse plane. This initial asymmetry in the geometrical shape gives rise to different pressure gradients along the long and the short axis of the overlapping zone and correspondingly to a momentum space asymmetry in the final state. As a result, if the matter present in the intermediate "fireball" exhibits a fluid-like behavior, then a collective flow of final state particles is observed, which is reflected in the azimuthal distribution of the particle number as well as in the azimuthal distribution of an appropriate kinematic variable like p_T, y_T and the transverse or radial velocity v_T [24]. The radial velocity has two components, the radial flow velocity and the velocity due to the random thermal motion of the particles constituting the intermediate fireball. For an ideal fluid the radial flow velocity should be isotropic. However, for a nonideal viscous fluid, the shear tension is proportional to the gradient of the radial velocity along the azimuthal direction, which again is related to the anisotropy of radial velocity [18]. An analysis of the v_2 results over the energy range $E_{\text{lab}} \cong$ 1–160 GeV has shown that the observed v_2 values are lower than what is expected from a phenomenology based on the three-fluid dynamics [25]. The difference has been attributed to dissipative effects like viscosity. A single parameter (the Knudsen number) fit of the v_2 results over a wide range of collision energy suggests that the upper limit of the shear viscosity to specific entropy ratio $\eta/s \sim$ 1-2, a value much higher than what is estimated for an almost ideal fluid created at RHIC or LHC energies. However, to understand the exact nature of the flow characteristics or the nature of the fluid created at FAIR energies, we shall have to wait till the CBM results in this regard become available.

We introduce the transverse (radial) velocity as

$$v_T = \frac{p_T}{E} = \frac{p_T}{m_T \cosh y}, \tag{1}$$

where $E = m_T \cosh y$ is the energy of the particle, $m_T = \sqrt{m_0^2 + p_T^2}$ is its transverse mass, m_0 is the particle rest mass, and y is its rapidity. For a large sample of events the total radial velocity $\langle V_T(\phi_m)\rangle$ of all particles falling within the mth azimuthal bin is defined as

$$\langle V_T(\phi_m)\rangle = \frac{1}{N_{\text{ev}}} \sum_{j=1}^{N_{\text{ev}}} \sum_{i=1}^{n_m} v_{T,i}(\phi_m), \tag{2}$$

where $v_{T,i}(\phi_m)$ is the radial velocity of the ith particle, n_m is the total number of particles present in the mth bin, N_{ev} is the number of events under consideration, and $\langle\,\rangle$ denotes an averaging over events. In this paper we have chosen the transverse velocity as the basic variable in terms of which the azimuthal asymmetry has been studied and compared the results obtained thereof with those of the azimuthal asymmetry associated with the charged particle multiplicity distribution. An azimuthal distribution of $\langle V_T(\phi_m)\rangle$ contains information of the asymmetry in the multiplicity distribution as well as that of the radial expansion. By taking an average over the particle number the mean transverse velocity $\langle\langle v_T(\phi_m)\rangle\rangle$ is introduced as

$$\langle\langle v_T(\phi_m)\rangle\rangle = \frac{1}{N_{\text{ev}}} \sum_{j=1}^{N_{\text{ev}}} \frac{1}{N_m} \sum_{i=1}^{N_m} v_{T,i}(\phi_m), \tag{3}$$

where $\langle\langle\,\rangle\rangle$ represents first an average over all particles present in the mth azimuthal bin and then over all events present in the sample. This double averaging reduces the multiplicity influences significantly, and the corresponding distribution measures only the radial expansion. In this context we must mention that the mean radial velocity actually consists of contributions coming from three different sources, the average isotropic radial velocity, the average anisotropic radial velocity, and the average velocity associated with thermal motion. It should be noted that both radial and thermal motion contribute to the isotropic velocity of the distribution. Like the azimuthal distribution of charged particle multiplicity $d\langle N_{\text{ch}}\rangle/d\phi$, it is also possible to expand the azimuthal distributions of the total and mean transverse velocities in Fourier series as

$$\begin{aligned} \frac{d\langle V_T\rangle}{d\phi} &\approx v_0\left(\langle V_T\rangle\right)\left[1 + 2v_2\left(\langle V_T\rangle\right)\cos(2\phi)\right], \\ \frac{d\langle\langle v_T\rangle\rangle}{d\phi} &\approx v_0\left(\langle\langle v_T\rangle\rangle\right)\left[1 + 2v_2\left(\langle\langle v_T\rangle\rangle\right)\cos(2\phi)\right]. \end{aligned} \tag{4}$$

In these expansions only the leading order terms ($n = 0$ and 2) are retained. The anisotropy present in any of the distributions [see (4)] is quantified by the second Fourier coefficient v_2, whereas v_0 is a measurement of the isotropic flow.

3. AMPT Model

Transport models are best suited to study AB collisions at the energy range under our consideration. Since transport models treat chemical and thermal freeze-out dynamically,

they have the ability to describe the space-time evolution of the hot and dense "fireballs" created in collision between two heavy nuclei at relativistic energy. As mentioned before, in this simulation study we use the AMPT model with partonic degrees of freedom, the so-called string melting version, with the expectation that under the FAIR conditions transitions from the initial nuclear matter to the QGP state (if any) and then from the QGP state to the final hadronic state will take place at high baryon density and low to moderate temperature. Previous calculations have shown that flow parameters consistent with experiment can be developed through AMPT and the model can successfully describe different aspects of the collective behavior of hadronic/partonic matter produced in AB interactions [26–32]. The string melting version of AMPT should be even more appropriate to model particle emission data, where a transition from nuclear matter to deconfined QCD state is expected. AMPT is a hybrid model where the primary particle distribution and other initial conditions are taken from the heavy-ion jet interaction generator (HIJING) [33], and Zhang's parton cascade (ZPC) formalism [34] is used in subsequent stages. Note that the ZPC model includes only parton-parton elastic scattering with an in-medium cross section derived from pQCD, the effective gluon screening mass being taken as an adjustable parameter. In the string melting version of the AMPT model, all hadrons are produced from string fragmentation like that in the HIJING model. The strings are converted into valence quarks and antiquarks. They are subsequently allowed to interact through the ZPC formalism and propagate according to a relativistic transport model [23]. Finally, the quarks and antiquarks are converted to hadrons via a quark coalescence formalism.

4. Results and Discussion

In this section we describe our results obtained from the Au + Au minimum bias events simulated by the AMPT model (string melting version) at $E_{\text{lab}} = 10$ A and 40 A GeV. A representative value of the parton scattering cross section ($\sigma = 3$ mb) is used in this analysis. The σ value is chosen so as to match with a previously studied collective behavior at FAIR energies [31]. We have indeed compared the NA49 results [21] on the p_T dependence of elliptic flow parameter v_2 by varying σ over a range of 0.1 to 6 mb. We have seen that even though the σ values differ almost by two orders of magnitude, the corresponding differences in the simulated v_2 values are not that significant [35]. The size of each sample of Au + Au events used in this analysis is one million. We begin with the multiplicity distribution of charged hadrons, represented schematically in Figure 1. The nature of the distributions is more or less similar at both energies considered. However, the average and the highest multiplicities are naturally quite larger at $E_{\text{lab}} = 40$ A GeV. In Figure 2 we plot the p_T distributions of charged hadrons. As expected, with increasing p_T we observe an approximately exponential fall in the particle number density. It is interesting to note that, at low p_T values, up to $p_T \approx 1.5$ GeV/c, the slopes of the distributions at both energies hardly differ, but at high p_T, beyond $p_T = 2.0$ GeV/c, the slope values are considerably

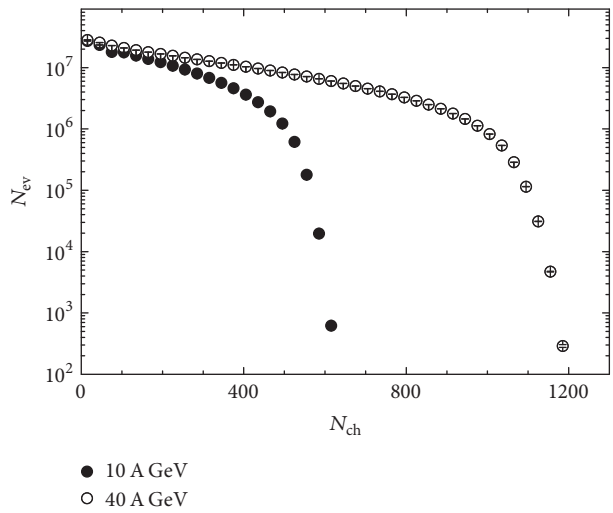

Figure 1: Charged hadron multiplicity distribution in Au + Au collisions at $E_{\text{lab}} = 10$ A and 40 A GeV.

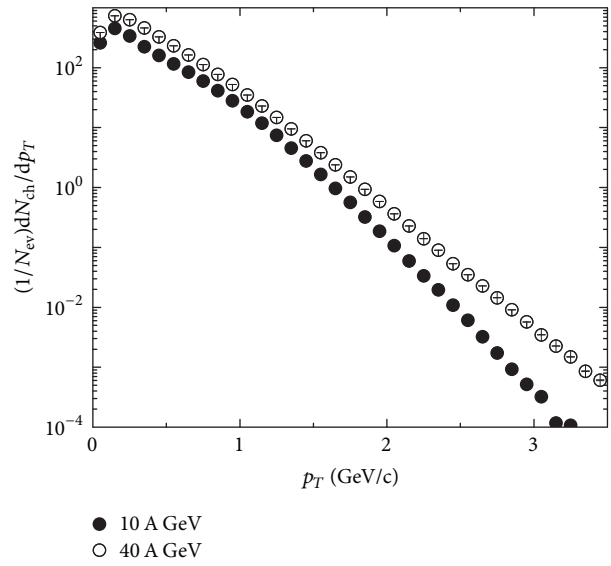

Figure 2: Charged hadron p_T distribution in Au + Au collisions at $E_{\text{lab}} = 10$ A and 40 A GeV.

different, this being stiffer at $E_{\text{lab}} = 10$ A GeV. The inverse slope can be related to the temperature of the intermediate "fireball" as and when it achieves a thermal equilibrium. With varying collision energies, the particles produced in soft processes, therefore, correspond to almost same source temperature, irrespective of the collision energy. A Monte Carlo Glauber (MCG) model [36] is employed to characterize the geometry of an AB collision. Using the MCG model the average transverse momentum $\langle p_T \rangle$ of particles produced in AB collisions belonging to a particular centrality can be determined. In Figure 3 such a plot of $\langle p_T \rangle$ against the number of participating nucleons (N_{part}), a measure of the centrality of the collision, is graphically shown. At both the collision energies considered in this analysis, at low N_{part} the $\langle p_T \rangle$ values are significantly different, $\langle p_T \rangle$

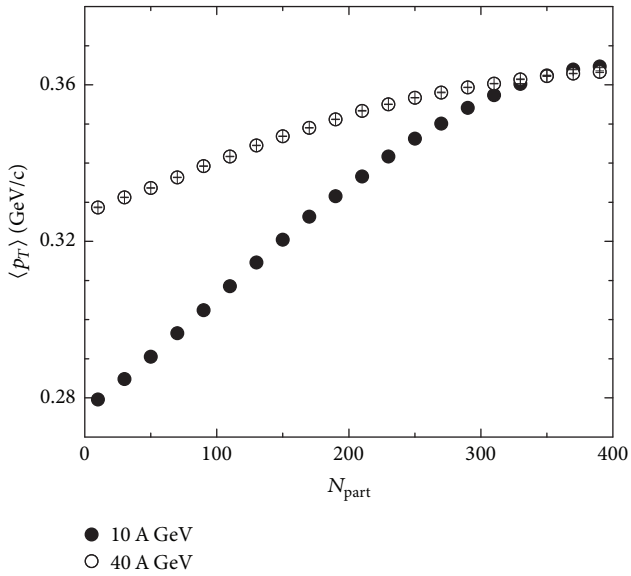

FIGURE 3: Average transverse momentum of charged hadrons as a function of N_{part} in Au + Au collisions at E_{lab} = 10 A and 40 A GeV.

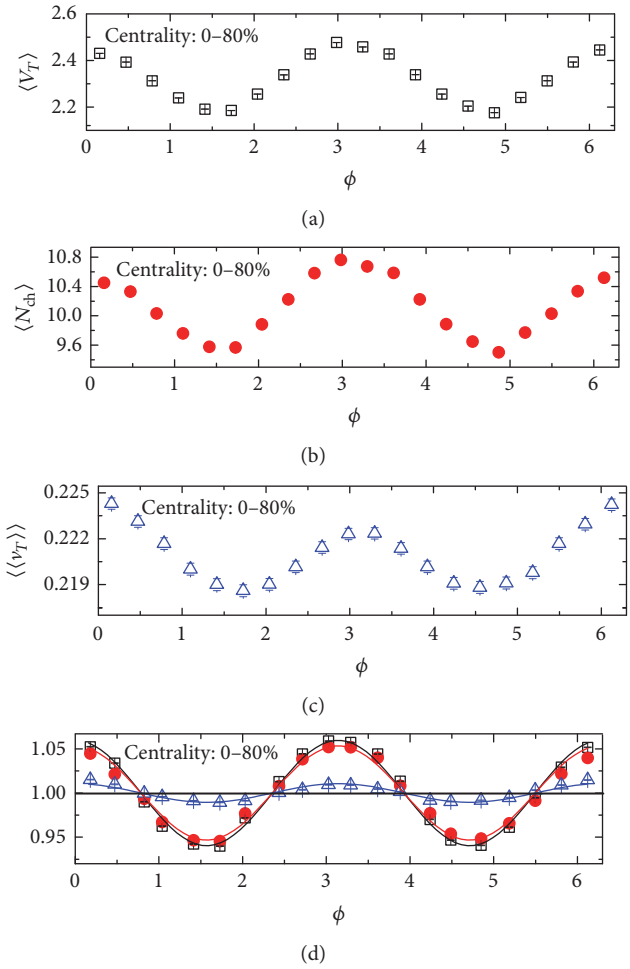

FIGURE 4: Azimuthal distribution of (a) total radial velocity, (b) multiplicity, (c) mean radial velocity, and (d) all the aforesaid quantities properly normalized for charged hadrons produced in Au + Au collisions at E_{lab} = 40 A GeV.

increases almost linearly with increasing centrality, and each distribution saturates at similar value, $\langle p_T \rangle \approx 0.365$ GeV/c. The fact that at the highest centrality the saturation value of $\langle p_T \rangle$ of produced particles is almost independent of the incident beam energy is perhaps due to kinematic reasons. The transverse degree of freedom that was absent before the collision took place is excited into the interacting AB system due to multiple nucleon-nucleon (NN) scattering and rescattering. Our results indicate that the degree of such excitations, which predominantly depends on the number of binary collisions N_{coll}, appears to remain almost same for the most central collisions of the Au + Au system in the FAIR energy region. In Figure 4 we present the azimuthal distributions of (a) the total radial velocity $\langle V_T \rangle$, (b) the multiplicity (N_{ch}), and (c) the mean radial velocity $\langle\langle v_T \rangle\rangle$ of charged hadrons produced at E_{lab} = 40 A GeV in the mid-rapidity region, within $\Delta y = \pm 1.0$ symmetric about the central value y_0 and within the 0–80% centrality range. Presence of anisotropy in all three distributions is clearly visible. It is also observed that while all three distributions exhibit same periodicity, their amplitudes are quite different. In order to show that all three distributions can analytically be described by a single function like $N[1 + \alpha \cos(2\phi)]$ without significant contributions coming from other harmonics, we fit the distributions with exactly the same relative vertical axis range with respect to the value of the parameter α centred around the same value of the other parameter N (here $N = 1.0$) and plot them together in Figure 4(d) along with the respective fitted lines. When appropriately scaled, we find that the elliptic anisotropy present in the distribution of total radial velocity is almost equal in magnitude to that coming from the anisotropy in multiplicity distribution. In comparison, corresponding anisotropy in the mean radial velocity is quite small. The results at E_{lab} = 10 A and 40 A GeV are qualitatively similar.

4.1. Centrality Dependence of v_2 and v_0. Elliptic flow results from interactions between particles comprising the intermediate "fireball," and hence it is a useful probe for the identification of local thermodynamic equilibrium. The v_2 values are smaller for the extreme central and peripheral collisions, which can be explained in terms of the initial geometric effects and the pressure gradient produced thereof [37]. In the hydrodynamical limit v_2 is proportional to the elliptic eccentricity (ε_2) of the overlapping region of the colliding nuclei, whereas in the low density limit v_2/ε_2 is proportional to the product of the rapidity density of charged particles $d\langle N_{\text{ch}} \rangle / dy$ and inverse of the overlapping area of the colliding nuclei. It is believed that the centrality dependence of elliptic flow provides valuable information regarding the degree of equilibration achieved by the intermediate "fireball" and also regarding the characteristics of (re)scattering effects present therein [38]. Some model based results at FAIR energies can be found in [19, 31, 35].

In Figure 5 we compare the centrality dependence of the v_2 parameter obtained from distributions of all three variables under consideration. The overall centrality dependence is

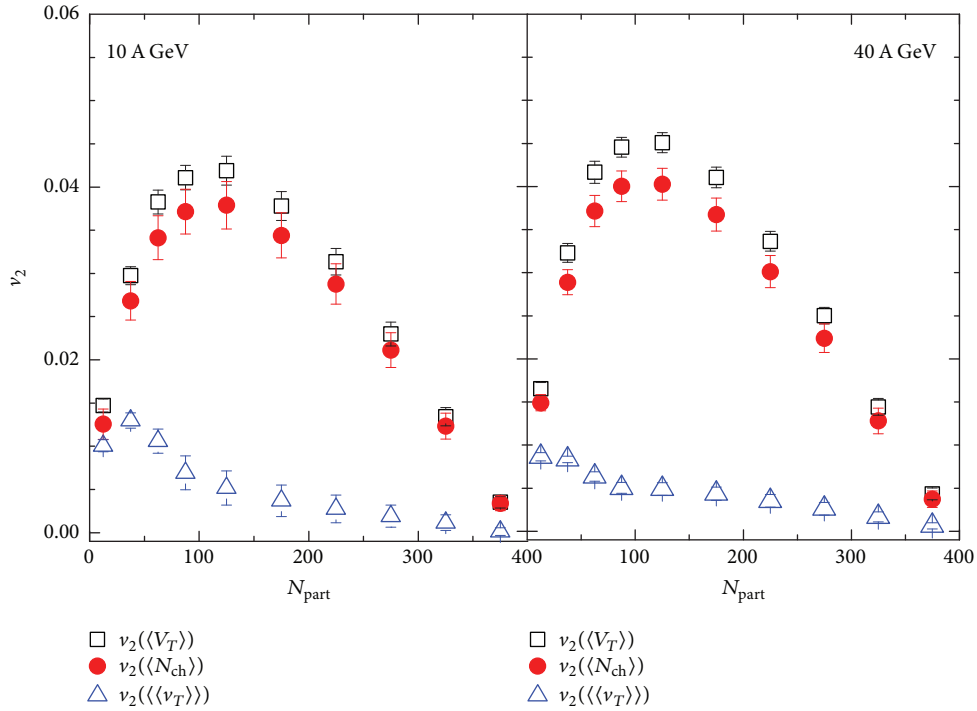

FIGURE 5: Centrality dependence of anisotropy parameter v_2 obtained from the azimuthal distributions of total radial velocity, multiplicity, and mean radial velocity in Au + Au collision at E_{lab} = 10 A and 40 A GeV.

found to be similar for $v_2(\langle V_T\rangle)$ and $v_2(\langle N_{\text{ch}}\rangle)$. However, $v_2(\langle\langle v_T\rangle\rangle)$, which in magnitude is quite small in comparison with the v_2 values obtained from the other two variables, behaves quite differently. All three variations are consistent with our observations of Figure 4(d). It is to be noted that the anisotropy in mean radial velocity, which describes the radial expansion, is significantly smaller than that of the corresponding multiplicity distribution in the mid-central region. In this regard we also intend to scrutinize the effects of the collision energy involved. It is observed that $v_2(\langle V_T\rangle)$ and $v_2(\langle N_{\text{ch}}\rangle)$ at E_{lab} = 40 A GeV are marginally higher than those obtained at E_{lab} = 10 A GeV, a general feature of any v_2 result, which has been confirmed over a wide energy range. The $v_2(\langle\langle v_T\rangle\rangle)$ values are not significantly different at the two collision energies involved either. We expect that the isotropy parameter (v_0) of all aforesaid distributions is also of certain importance and we graphically plot the results in Figure 6. The v_0 values associated with $\langle V_T\rangle$ and $\langle N_{\text{ch}}\rangle$ distributions show a linear dependence with increasing N_{part}, being highest in the most central events. This feature of v_0 can be ascribed to the fact that the azimuthally integrated magnitude of transverse flow increases with increasing centrality of the collisions. On the contrary, an increasing trend in the $v_0(\langle\langle v_T\rangle\rangle)$ values with increasing N_{part} is restricted only to the peripheral collisions, and beyond $N_{\text{part}} \approx 80$ the $v_0(\langle\langle v_T\rangle\rangle)$ values achieve a saturation, being nearly independent of the centrality of the collisions. A significant energy dependence of v_0 is also observed for all three variables considered in this analysis. We do not see any significant energy dependence in the variation of $v_0(\langle\langle V_T\rangle\rangle)$ with N_{part}. The $v_0(\langle N_{\text{ch}}\rangle)$ values are however consistently higher at E_{lab} = 40 A GeV than those at E_{lab} = 10 A GeV, the difference becoming larger with increasing N_{part}. Once again $v_0(\langle\langle v_T\rangle\rangle)$ behaves quite differently in this regard. The values at E_{lab} = 10 A GeV are consistently higher than those at E_{lab} = 40 A GeV. We may recall that the mean radial velocity has been defined in a way such that the multiplicity effects are removed. Therefore, we conclude that the particle multiplicity plays a dominant role to determine the total transverse flow, and a higher energy input results in a lower amount of azimuthally integrated transverse flow.

4.2. Transverse Momentum Dependence of v_2 and v_0. It is well known that the anisotropy coefficient v_2 depends on p_T of charged hadrons. Hydrodynamics as well as resonance decay are expected to dominate at low p_T, whereas high p_T particles are expected to stem out from the fragmentation of jets modified in the hot and dense medium of the intermediate "fireball" [15]. At FAIR energies the production of high p_T hadrons would be rare, and owing to statistical reasons we restrict our analysis up to p_T = 2.0 GeV/c. v_2 arising from multiplicity distributions of the produced hadrons has been studied widely as a function of p_T using the data available from the experiments held at RHIC [39] and LHC [40]. Simulation results under FAIR-CBM conditions utilizing the UrQMD, AMPT (default), and AMPT (string melting) models can be found in [19, 31]. Figure 7 depicts that the anisotropies present in $\langle N_{\text{ch}}\rangle$, $\langle V_T\rangle$, and $\langle\langle v_T\rangle\rangle$ distributions rise monotonically with increasing p_T. At E_{lab} = 40 A GeV, beyond p_T = 1.5 GeV/c, there is a trend of saturation in

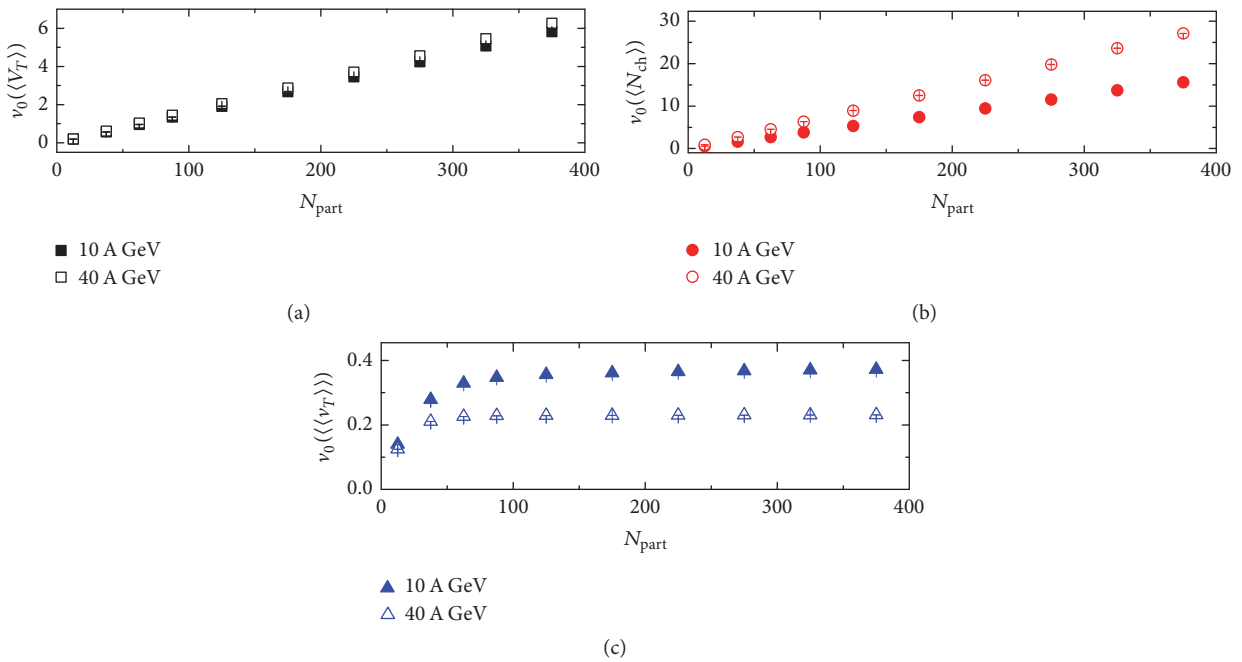

FIGURE 6: Centrality dependence of isotropic flow coefficient v_0 obtained from the azimuthal distributions of total radial velocity, multiplicity, and mean radial velocity in Au + Au collision at E_{lab} = 10 A and 40 A GeV.

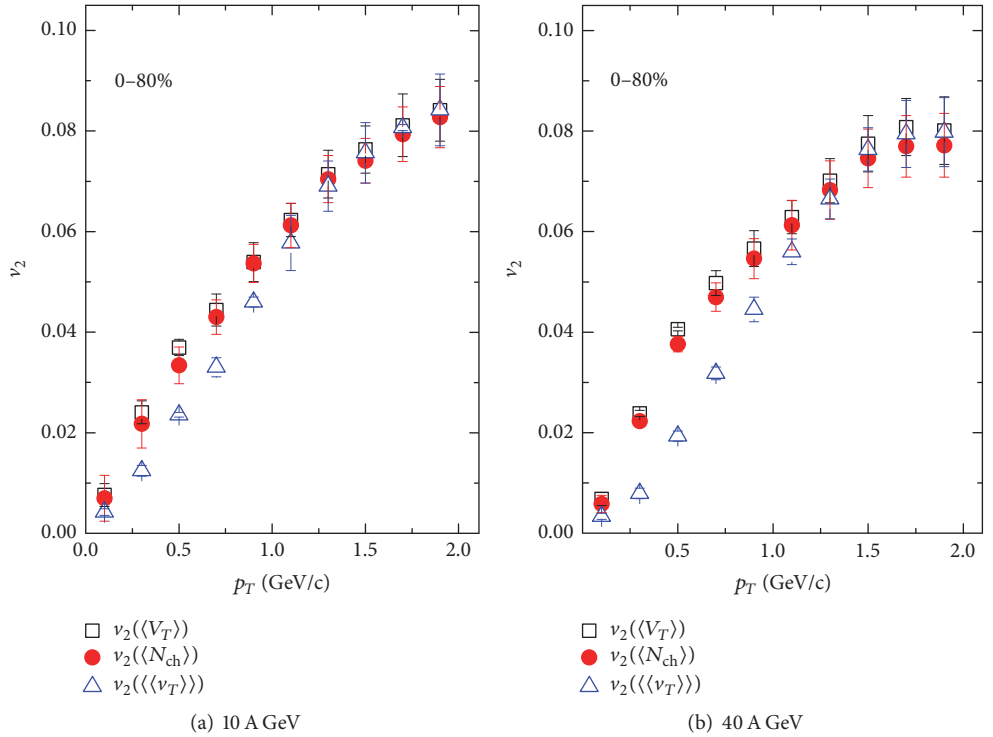

FIGURE 7: Transverse momentum dependence of anisotropy parameter v_2 obtained from the azimuthal distributions of total radial velocity, multiplicity, and mean radial velocity in Au + Au collision at E_{lab} = 10 A and 40 A GeV.

the v_2 values extracted from all three variables. Once again we conclude that the multiplicity dominates over the radial velocity at a particular p_T bin, and $v_2(\langle N_{\text{ch}} \rangle)$ and $v_2(\langle V_T \rangle)$ are found to be almost equal in the $0 \leqslant p_T \leqslant 2.0$ GeV/c range. Once we get rid of the multiplicity effects, the actual anisotropy present in the radial velocity comes out, which we can see in the plot of $v_2(\langle\langle v_T \rangle\rangle)$ against p_T shown in the same diagram. As a result, within $0.25 \leq p_T \leq 1.25$ GeV/c the

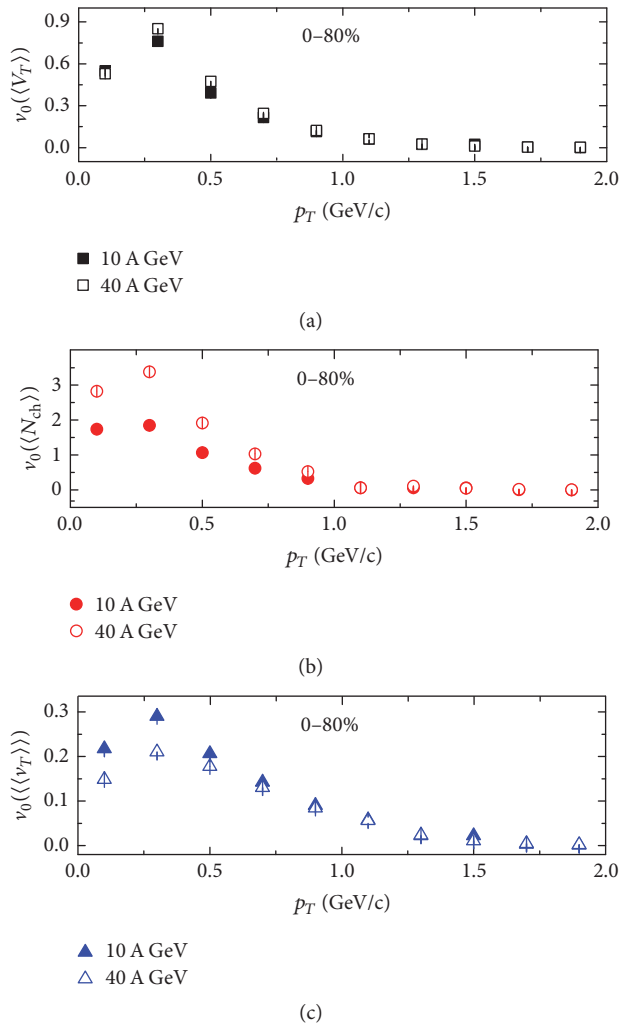

FIGURE 8: Transverse momentum dependence of isotropic coefficient v_0 obtained from the azimuthal distributions of total radial velocity, multiplicity, and mean radial velocity in Au + Au collision at E_{lab} = 10 A and 40 A GeV.

$v_2(\langle\langle v_T \rangle\rangle)$ values are slightly lower at higher E_{lab}. At FAIR energies, however, we do not find any noticeable deviation in the trend of this p_T dependence of v_2 from its nature observed at RHIC energies [24]. Comparing Figure 7(a) with Figure 7(b), we see a very weak (almost insignificant) energy dependence of v_2 in terms of all three variables concerned. We may reckon that FAIR-CBM energy range may not provide us with a proper platform to study the energy dependence of anisotropy, but it may be suitable for studying the issues related to the isotropy measure v_0. The p_T dependence of v_0 has been shown in Figure 8. It is observed that the v_0 coefficients associated with $\langle N_{ch} \rangle$, $\langle V_T \rangle$, and $\langle\langle v_T \rangle\rangle$ while being plotted against p_T exhibit similar nature. In the low p_T region, the v_0 values extracted from each variable rise with increasing p_T, attain a maximum, and then fall off to a very small saturation value (almost zero) at both incident energies beyond p_T = 1.25 GeV/c. Once again, while $v_0(\langle V_T \rangle)$ values at E_{lab} = 10 A and 40 A GeV are almost identical, the $v_0(\langle N_{ch} \rangle)$ values at E_{lab} = 40 A GeV are higher in the low p_T region ($p_T \lesssim 0.7$ GeV/c) than those at 10 A GeV. On the contrary, the $v_0(\langle\langle v_T \rangle\rangle)$ values obtained at E_{lab} = 40 A GeV are lower in the low p_T region ($p_T \lesssim 0.5$ GeV/c) than those at 10 A GeV. At FAIR energy the random thermal motion of particles perhaps dominates over their collective behavior, which at high p_T leads to a very small amount of azimuthally integrated magnitude of net flow.

5. Conclusion

In this paper we present some basic results on the elliptic and radial flow of charged hadrons. The study is based on the azimuthal distributions of total transverse velocity, mean transverse velocity, and multiplicity of charged hadrons produced in Au + Au collisions at E_{lab} = 10 A GeV and 40 A GeV. We have used the AMPT model (string melting version) to generate the events. We observe that azimuthal asymmetries are indeed present in all three distributions. However, we also note that in our simulation results the azimuthal anisotropy of the final state particles is predominantly due to the asymmetry of particle multiplicity distribution, and only a small fraction of this asymmetry is due to kinematic reasons. The overall nature of the dependence of the elliptic anisotropy parameter on the centrality of the collision and transverse momentum of produced particles are similar for the three variables considered in the present analysis. The elliptic flow parameter is highest in the mid-central collisions, and within the interval $0 \leqslant p_T \leqslant 2.0$ GeV/c it is highest at the highest p_T. From our simulated results in the FAIR energy range we find a very small energy dependence of the elliptic flow parameter. On the other hand, the azimuthally integrated magnitude of the radial flow is maximum for most central collisions and its values are high in the low p_T region. From this analysis we see that the contribution to v_0 from the asymmetry in multiplicity distribution and that coming from the asymmetry in kinematic variable v_T exhibit an opposite incident beam energy dependence. While the former is higher at higher E_{lab}, the latter is higher at lower E_{lab}. Our simulated results are consistent with those obtained from RHIC and LHC energies and do not require any new dynamics to interpret. However, in future there is enough scope to appropriately model these results in terms of relevant thermodynamic and hydrodynamic parameters associated with the intermediate "fireball" produced in AB collisions.

Conflicts of Interest

The authors declare that they have no conflicts of interest.

References

[1] S. Nagamiya and M. Gyulassy, "High-energy nuclear collisions," *Adv. Nucl. Phys*, vol. 13, p. 201, 1984.

[2] H.-T. Ding, F. Karsch, and S. Mukherjee, *Quark-Gluon Plasma V*, X.-N. Wang, Ed., pp. 1-65, World Scientific, Singapore, 2016.

[3] J. Y. Ollitrault, "Anisotropy as a signature of transverse collective flow," *Physical Review D: Particles, Fields, Gravitation and Cosmology*, vol. 46, p. 229, 1992.

[4] S. Voloshin and Y. Zhang, "Flow study in relativistic nuclear collisions by Fourier expansion of azimuthal particle distributions," *Zeitschrift für Physik C*, vol. 70, no. 4, pp. 665–671, 1996.

[5] S. A. Voloshin, A. M. Poskanzer, and R. Snellings, "Collective phenomena in non-central nuclear collisions," https://arxiv.org/abs/0809.2949, 2008.

[6] H. Sorge, "Elliptical flow: a signature for early pressure in ultra-relativistic nucleus-nucleus collisions," *Physical Review Letters*, vol. 78, pp. 2309–2312, 1997.

[7] P. Huovinen, P. F. Kolb, and U. Heinz, "Radial and elliptic flow at RHIC: further predictions," *Physics Letters B*, vol. 503, pp. 58–64, 2001.

[8] M. Luzum and P. Romatschke, "Conformal relativistic viscous hydrodynamics: Applications to RHIC results at $\sqrt{s_{NN}}$ = 200 GeV," *Physical Review C: covering nuclear physics*, vol. 78, no. 3, Article ID 034915, 2008.

[9] C. Adler et al., "Identified Particle Elliptic Flow in Au + Au Collisions at $\sqrt{s_{NN}}$ = 130 GeV," *Physical Review Letters*, vol. 87, no. 18, Article ID 182301, 2001.

[10] B. Abelev et al., "Mass, quark-number, and $\sqrt{s_{NN}}$ dependence of the second and fourth flow harmonics in ultrarelativistic nucleus-nucleus collisions," *Physical Review C: covering nuclear physics*, vol. 75, no. 5, Article ID 054906, 2007.

[11] L. Adamczyk et al., "Observation of an Energy-Dependent Difference in Elliptic Flow between Particles and Antiparticles in Relativistic Heavy Ion Collisions," *Physical Review Letters*, vol. 110, no. 14, Article ID 142301, 2013.

[12] A. Adare et al., "[PHENIX Collaboration]," *Physical Review Letters*, vol. 91, Article ID 182301, 2003.

[13] B. B. Back, M. D. Baker, and M. Ballintijn, "The PHOBOS perspective on discoveries at RHIC," *Nuclear Physics A*, vol. 757, no. 1-2, pp. 28–101, 2005.

[14] S. Chatrchyan et al., "Azimuthal anisotropy of charged particles at high transverse momenta in Pb-Pb collisions at $\sqrt{s_{NN}}$ = 2.76 TeV," *Physical Review Letters*, vol. 109, Article ID 022301, 2012.

[15] G. Aad et al., "Measurement of the pseudorapidity and transverse momentum dependence of the elliptic flow of charged particles in lead–lead collisions at $\sqrt{s_{NN}}$ = 2.76 TeV with the ATLAS detector," *Physics Letters B*, vol. 707, no. 3-4, p. 330, 2012.

[16] K. Aamodt et al., "Higher harmonic anisotropic flow measurements of charged particles in Pb-Pb collisions at $\sqrt{s_{NN}}$ = 2.76 TeV," *Physical Review Letters*, vol. 107, no. 3, Article ID 032301, 2011.

[17] B. Abelev, J. Adam, D. Adamová et al., "lliptic flow of identified hadrons in Pb-Pb collisions at $\sqrt{s_{NN}}$ = 2.76 TeV," *Journal of High Energy Physics*, vol. 190, 2015.

[18] L. Li, N. Li, and Y. Wu, "Measurement of anisotropic radial flow in relativistic heavy ion collisions," *Journal of Physics G: Nuclear and Particle Physics*, vol. 40, Article ID 075104, 2013.

[19] S. Sarkar, P. Mali, and A. Mukhopadhyay, "Simulation study of elliptic flow of charged hadrons produced in Au + Au collisions at energies available at the facility for antiproton and ion research," *Physical Review C: Covering Nuclear Physics*, vol. 95, no. 1, Article ID 014908, 2017.

[20] H. Stöcker and W. Greiner, "High energy heavy ion collisions—probing the equation of state of highly excited hardronic matter," *Physics Reports*, vol. 137, no. 5-6, pp. 277–392, 1986.

[21] C. Alt et al., "Directed and elliptic flow of charged pions and protons in Pb + Pb collisions at 40*A* and 158*A* GeV," *Physical Review C: Covering Nuclear Physics*, vol. 68, no. 3, pp. 661–670, 2003.

[22] B. Zhang, C. M. Ko, B.-A. Li, and Z.-W. Lin, "Multiphase transport model for relativistic nuclear collisions," *Physical Review C: Covering Nuclear Physics*, vol. 61, no. 6, Article ID 067901, 2000.

[23] Z.-W. Lin, C. M. Ko, B.-A. Li, B. Zhang, and S. Pal, "Multiphase transport model for relativistic heavy ion collisions," *Physical Review C: covering nuclear physics*, vol. 72, no. 6, Article ID 064901, 2005.

[24] L. Li, N. Li, and Y. Wu, "Azimuthal distributions of radial momentum and velocity in relativistic heavy ion collisions," *Chinese Physics C*, vol. 36, no. 5, p. 423, 2012.

[25] Y. B. Ivanov, I. N. Mishustin, V. N. Russkikh, and L. M. Satarov, "Elliptic flow and dissipation in heavy-ion collisions at $E_{lab} \simeq$ (1–160)*A* GeV," *Physical Review C nuclear physics*, vol. 80, no. 6, Article ID 064904, 2009.

[26] Z.-W. Lin and C. M. Ko, "Partonic effects on the elliptic flow at relativistic heavy ion collisions," *Physical Review C: Covering Nuclear Physics*, vol. 65, no. 3, Article ID 034904, 2002.

[27] L.-W. Chen, V. Greco, C. M. Ko, and P. F. Kolb, "Pseudorapidity dependence of anisotropic flows in relativistic heavy-ion collisions," *Physics Letters B*, vol. 605, no. 1-2, pp. 95–100, 2005.

[28] B. Zhang, L.-W. Chen, and C.-M. Ko, "Charm elliptic flow in Au+Au collisions at RHIC," *Nuclear Physics A*, vol. 774, pp. 665–668, 2006.

[29] L.-W. Chen and C. M. Ko, "System size dependence of elliptic flows in relativistic heavy-ion collisions," *Physics Letters B*, vol. 634, no. 2-3, pp. 205–209, 2006.

[30] J. Xu and C. M. Ko, "Pb-Pb collisions at $\sqrt{s_{NN}}$ = 2.76 TeV in a multiphase transport model," *Physical Review C nuclear physics*, vol. 83, no. 3, 2011.

[31] P. P. Bhaduri and S. Chattopadhyay, "Differential elliptic flow of identified hadrons and constituent quark number scaling at the GSI Facility for Antiproton and Ion Research (FAIR)," *Physical Review C: Nuclear Physics*, vol. 81, no. 3, Article ID 034906, 2010.

[32] M. Nasim, L. Kumar, P. K. Netrakanti, and B. Mohanty, "Energy dependence of elliptic flow from heavy-ion collision models," *Physical Review C nuclear physics*, vol. 82, no. 5, Article ID 054908, 2010.

[33] X.-N. Wang and M. Gyulassy, "Hijing: a Monte Carlo model for multiple jet production in pp, pA, and AA collisions," *Physical Review D: Particles, Fields, Gravitation and Cosmology*, vol. 44, no. 11, pp. 3501–3516, 1991.

[34] G. P. Zhang, "Modified explicitly restarted Lanczos algorithm," *Computer Physics Communications*, vol. 109, no. 1, pp. 27–33, 1998.

[35] S. Sarkar, P. Mali, and A. Mukhopadhyay, "Azimuthal anisotropy in particle distribution in a multiphase transport model," *Physical Review C: Nuclear Physics*, vol. 96, no. 2, Article ID 024913, 2017.

[36] M. L. Miller, K. Reygers, S. J. Sanders, and P. Steinberg, "Glauber modeling in high-energy nuclear collisions," *Annual Review of Nuclear and Particle Science*, vol. 57, pp. 205–243, 2007.

[37] B. Alver et al., "System size, energy, pseudorapidity, and centrality dependence of elliptic flow," *Physical Review Letters*, vol. 98, no. 24, Article ID 242302, 2007.

[38] S. Voloshin and A. Poskanzer, "The physics of the centrality dependence of elliptic flow," *Physics Letters B*, vol. 474, no. 1-2, pp. 27–32, 2000.

[39] K. Adcox, S. S. Adler, and S. Afanasiev, "Formation of dense partonic matter in relativistic nucleus–nucleus collisions at RHIC: experimental evaluation by the PHENIX collaboration," *Nuclear Physics A*, vol. 757, no. 1-2, pp. 184–283, 2005.

[40] K. Aamodt et al., "Elliptic Flow of Charged Particles in Pb-Pb Collisions at $\sqrt{s_{NN}} = 2.76$ TeV," *Physical Review Letters*, vol. 105, no. 25, Article ID 252302, 2010.

Hindawi
Advances in High Energy Physics
Volume 2018, Article ID 2136908, 11 pages
https://doi.org/10.1155/2018/2136908

Research Article

Entropy and Multifractality in Relativistic Ion-Ion Collisions

Shaista Khan and Shakeel Ahmad

Department of Physics, Aligarh Muslim University, Aligarh 202002, India

Correspondence should be addressed to Shakeel Ahmad; shakeel.ahmad@cern.ch

Received 31 August 2017; Revised 5 January 2018; Accepted 11 March 2018; Published 11 April 2018

Academic Editor: Raghunath Sahoo

Entropy production in multiparticle systems is investigated by analyzing the experimental data on ion-ion collisions at AGS and SPS energies and comparing the findings with those reported earlier for hadron-hadron, hadron-nucleus, and nucleus-nucleus collisions. It is observed that the entropy produced in limited and full phase space, when normalized to maximum rapidity, exhibits a kind of scaling which is nicely supported by Monte Carlo model HIJING. Using Rényi's order q information entropy, multifractal characteristics of particle production are examined in terms of generalized dimensions, D_q. Nearly the same values of multifractal specific heat, c, observed in hadronic and ion-ion collisions over a wide range of incident energies suggest that the quantity c might be used as a universal characteristic of multiparticle production in hadron-hadron, hadron-nucleus, and nucleus-nucleus collisions. The analysis is extended to the study of spectrum of scaling indices. The findings reveal that Rényi's order q information entropy could be another way to investigate the fluctuations in multiplicity distributions in terms of spectral function $f(\alpha)$, which has been argued to be a convenient function for comparison sake not only among different experiments but also between the data and theoretical models.

1. Introduction

The main objective of investigating the collisions of heavy nuclei at relativistic energies is to understand the nature of phase transition from normal hadronic matter to quark-gluon plasma (QGP) [1]. Dedicated experiments have been carried out at AGS and RHIC at BNL and SPS and LHC at CERN to search for the QGP phase and explore the QCD phase diagram. Heavy-ion collision experiments provide a unique opportunity to test the predictions of QCD and at the same time to understand the soft processes involved, which dominate even at LHC energies, as well as the hard scattering or the small cross-sectional physics [2–4]. Relativistic nucleus-nucleus (AA) collisions serve as a mean to study the novel regime of QCD where parton densities are high enough while the strong coupling constant between the partons is small and decreases further with decreasing interpartonic distances [2]. The parton densities in the early stage of the collision can be related to the density of the produced charged hadrons in the final state. Dominance of hard process (jets and minijets) in the hadron production increases with increasing collision energy and hence provides a unique opportunity to study the interplay between effects. In this scenario, the perturbative QCD (pQCD) lends a good basis for high energy dynamics and has achieved significant success in describing the hard processes involved in high energy collisions [2, 5]. Hadronic-jet production in e^+e^- annihilations [6, 7] and large p_t jet production in hadron-hadron (hh) collisions [8, 9] are the examples of these hard processes. However, in soft processes like hadron production with sufficiently low p_t in hadronic and heavy-ion collisions, the interactions become so strong that the pQCD is not applicable anymore [2]. Due to incapability of pQCD in this regime, phenomenological models based on experimental inputs have been proven to be an alternative tool to understand the dynamics of particle production in AA collisions.

Relativistic charged particle multiplicity is the simplest observable and by studying its distribution for a given data sample, information on soft QCD processes as well as on hard scattering can be extracted [3]. Furthermore, the charged hadron multiplicity of an event is taken as a direct measure of its inelasticity and can describe important features of particle production [3]. Investigations involving

multiparticle production in hh, hA, and AA collisions at relativistic energies have been carried out by numerous groups during the last four decades [10–15]. However, a complete understanding of particle production mechanism still remains elusive. Multiplicity distributions (MD) of relativistic charged particles produced in hh collisions have been observed to deviate from a Poisson distribution and are expected to provide information regarding the underlying production mechanism [13, 16]. Asymptotic scaling of MD in hh collisions referred to as the KNO scaling [17], predicted in 1972, was regarded as a useful phenomenological framework for comparing the MD at different energies ranging from $\sqrt{s} \sim 10$ GeV to ISR energies [18]. It was, however, pointed out [19, 20] that KNO scaling is not strictly followed for inelastic hh collisions. This scaling law was observed to breakdown when collision energy reached SPS range [13, 16, 18, 21]. After the observations of KNO scaling violation in $\overline{p}p$ collisions at $\sqrt{s} = 540$ GeV, it was remarked that the observed scaling up to ISR energies was approximate and accidental [21]. A new empirical regularity, in place of KNO scaling, was then proposed [21] to predict the multiplicity distributions at different energies. It was shown that MD at different energies in full and limited rapidity (η) windows may be nicely reproduced by negative binomial distributions (NBD) [18, 21, 22]. These observations lead to revival of interest in investigations involving MD and new scaling laws. Simak et al. [23], by introducing a new variable, the information entropy, showed that MD of charged particles produced in full and limited phase space in hh collisions exhibits a new type of scaling law in the energy range, $\sqrt{s} \sim 19$ to 900 GeV.

Sinyukov and Akkelin [24] have proposed a method to estimate entropy of thermal pions in AA collisions and have studied the average phase space densities and entropy of such pions against their multiplicities and beam energies. Their findings apparently suggest the presence of deconfinement and chiral phase transition in relativistic AA collisions. Moreover at RHIC energies, entropy per unit rapidity at freeze-out has been extracted with minimal model dependence from the available measurements of particle yields, spectra, and source sizes, determined from two-particle interferometry [25]. The extracted entropy per unit rapidity was observed to be consistent with the lattice gauge theory for thermalized QGP with an energy density calculated from the transverse energy production at RHIC energies.

Analyses of the experimental data on pp, $\overline{p}p$, and k^+p collisions over a wide energy range (up to $\sqrt{s} = 900$ GeV) carried out by several workers [23, 26, 27] indicate that entropy increases with beam energy while the entropy per unit rapidity appears to be an energy independent quantity. These results indicate the presence of entropy scaling up to a few TeV energy. Presence of a similar scaling behaviour in pp collisions at LHC energies has also been reported by Mizoguchi and Biyajima [28] and Das et al. [11, 13]. Analyses of AA collision data at AGS and SPS energies carried out by other workers [10, 15, 29, 30] too suggest that entropy produced in limited pseudorapidity (η) windows when normalized to the maximum rapidity is, essentially, independent of projectile and target mass as well as the beam energy, indicating the presence of entropy scaling.

The occurrence of unusual large particle density fluctuations in narrow phase space bins, observed in cosmic ray JACEE events [31] and in accelerator experiments [32, 33], have generated considerable interest in the study of nonlinear phenomena in hadronic and heavy-ion collisions. Such fluctuations may be taken as an indication of a phase transition from ordinary hadronic matter to QGP, predicted by QCD to occur in relativistic AA collisions. These fluctuations are also envisaged to arise either due to minijets produced at very high energies or (and) because of some other collective phenomena [34]. Such rare fluctuations of dynamical origin are to be identified and extracted from the statistical ones. Various methods for the identification of these fluctuations have been proposed which estimate the total deviation of the measured rapidity distribution from an idealized smooth distribution [34]. The analysis is based on the estimation of corresponding statistical probability through Monte Carlo (MC) simulations. The method of scaled factorial moments (SFMs), proposed by Bialas and Peschanski [35], has been proven to be well suited for not only to search for the dynamical fluctuations in narrow phase space bins but also to investigate the pattern of fluctuations which could lead to a physical interpretation of their origin [35]. The concept of SFMs was put forward in analogy with the phenomenon referred to as the "intermittency" in hydrodynamics of turbulent fluid flow [34]. This phenomenon is characterized by the presence of fluctuations in a small part of the available phase space. The method of SFMs was first applied to the pseudorapidity distribution of a single high multiplicity JACEE event [31] and the findings indicated the presence of intermittent pattern (large particle density fluctuations in narrow pseudorapidity bins) [35]. SFMs analysis, since its introduction, has been widely used to search for the nonlinear phenomena in hadronic and ion-ion collisions. It has been observed [36–39] that the presence of such a nonlinear phenomena might be rare but not impossible [40]. Such fluctuations, if not arising due to the statistical reasons, are envisaged to occur due to the dynamical correlations among the produced particles. These correlations might arise due to the phase transition from QGP to normal hadronic matter. As pointed out by Bialas and Peschanski [35], if the intermittency exists, the SFMs of multiplicity distributions should exhibit a power law dependence of the rapidity-bin width, as $\delta y \to 0$. Such a study would help understand the chaotic behaviour of rapidity distribution on event-by-event (ebe) basis instead of investigating the average phenomena [41].

The observations of intermittency in e^+e^- annihilation [42], hh [43], hA [34], and AA collisions [41] attracted a great deal of attention towards the investigations involving the power law behaviour of SFMs of the form

$$F_q \propto (\delta y)^{\alpha(q)}, \quad \delta y \longrightarrow 0, \tag{1}$$

where the exponent $\alpha(q)$ increases with order q of the moment [41].

Although the intermittency analysis in terms of SFMs has been successfully applied to the hadronic and heavy-ion collisions, yet the dynamical explanation of its origin in

some cases is not clear [44]. The concept of self-similarity is closely related to the fractal theory [45, 46] which is a natural consequence of the cascading mechanism prevailing in the multiparticle production. A formalism for treating the fractal dimensions and its generalization has been developed and applied to the study of turbulent fluids and other transitions to chaos [41, 47]. However, in the case of multiparticle production, the dynamics is not well known and one has to discover the proper dynamics that gives rise to the chaotic structure. The fractal dimensions, in multiparticle production, were first studied by Carruthers and Duong-Van [48]. Later on Dermin [49] suggested the study of correlation dimensions, while Lipa and Buschbeck [50] considered other generalized dimensions. However, in none of these investigations a formalism for systematic studies of fractal properties has been presented. Considering inelastic collisions as purely geometrical objects with noninteger dimensions, a formalism for treating the fractal dimensions and its generalization was developed and successfully applied to the study of intermittent behaviour and other transitions to chaos [44, 47, 51–53]. In order to reveal the multifractal nature of multiparticle production, Hwa [41], Chiu and Hwa [54], and Florkowski and Hwa [55] introduced G_q moments, which can be estimated from the particle multiplicities in limited rapidity windows that might lead to inferences on the nature of the dimensions, D_q, that are the generalizations of the fractal dimensions for multifractal sets. Using the G_q moments properties of scaling indices spectrum may be investigated which, in turn, would indicate as to how it can provide effective means to describe a highly nonuniform rapidity distribution.

As the studies involving AA collisions at relativistic energies are concerned, the main goal is to study the properties of strongly interacting matter under extreme conditions of nuclear density and temperature, where formation of quark-gluon plasma (QGP) is predicted to take place [10, 15, 56, 57]. Fluctuations in physical observables in AA collisions are regarded as one of the important signals, for QGP formation because of the idea that, in many body systems, phase transition may result in significant changes in the quantum fluctuations of an observable from its average behaviour [15, 29, 56]. For example, when a system undergoes a phase-transition, heat capacity changes abruptly, whereas the energy density remains the smooth function of temperature [10, 15, 25, 58, 59]. Entropy is regarded yet another important characteristics of a system with many degrees of freedom [15, 60–63]. Processes in which particles are produced may be considered as the so-called *dynamical systems* [60–64] in which entropy is generally produced. Systematic measurements of local entropy produced in AA collisions may provide direct information about the internal degrees of freedom of the QGP medium and its evolution [10, 15, 27]. It has been pointed out [65] that in high energy collisions particle production occurs on the maximum stochasticity; that is, they should follow the maximum entropy principle. This type of stochasticity may also be quantified in terms of information entropy which may be regarded as a natural and more general parameter to measure the chaoticity in branching processes [66].

Table 1: Number of events selected for the analysis.

Energy (GeV/c)	Type of interactions	Number of events
10.6A	^{197}Au-AgBr	577
14.5A	^{16}O-AgBr	379
14.5A	^{28}Si-AgBr	561
60A	^{16}O-AgBr	422
200A	^{16}O-AgBr	223
200A	^{32}S-AgBr	452

Bialas et al. [60, 61, 67] proposed that Rényi entropies may also be used as a tool for studying the dynamical systems and are closely related to the thermodynamic entropy of the system, the Shannon entropy. Bialas et al. [68] have also suggested that Rényi's entropies may serve as a useful tool for examining the correlation among the particles produced in high energy collisions. Furthermore, the generalization of Rényi's order-q information entropy contains information on the multiplicity moments that can be used to investigate the multifractal characteristics of particle production [14, 69, 70]. It should be mentioned that this method of multifractal studies is not related to the phase space bin-width or the detector resolution but to the collision energy [69]. It is, therefore, considered worthwhile to carry out a well focused study of entropy production and subsequent scaling in AA collisions by analyzing the several sets of experimental data on AA collisions at AGS and SPS energies. Rényi's information entropies are also estimated to investigate the multifractal characteristics of multiparticle production. Moreover, the analysis is further extended to study the fractal dimensions, multifractal spectrum, and their dependence on the energy and mass of the projectile.

2. Details of Data

Six sets of events produced in collisions of ^{16}O, ^{28}Si, ^{32}S, and ^{197}Au beams with AgBr group of nuclei in emulsion at AGS and SPS energies, available in the laboratory, are used in the present study. Details of these samples are presented in Table 1. These events are taken from the emulsion experiments performed by EMU01 Collaboration [71–74]. The other relevant details of the data, like selection criteria of events, classification of tracks, extraction of AgBr group of interactions, method of measuring the emission angle, θ of relativistic charged particles, and so on, may be found elsewhere [10, 15, 71, 75–77].

From the measured values of the emission angle θ, the pseudorapidity variable, η, was calculated using the relation, $\eta = -\ln\tan(\theta/2)$. It is worthwhile to mention that the conventional emulsion technique has two main advantages over the other detectors: (i) its 4π solid angle coverage and (ii) emulsion data being free from biases due to full phase space acceptance. In the case of other detectors, only a fraction of charged particles is recorded due to the limited acceptance cone. This not only reduces the multiplicity but also may distort some of the event characteristics like particle density fluctuations [15, 75, 78]. In order to compare the findings of the present work with the predictions of Monte Carlo

model HIJING [79, 80], event samples corresponding to the experimental ones are simulated using the code HIJING-1.35; the number of events in each simulated sample is equal to that in the corresponding real event sample. The events are simulated by taking into account the percentage of interactions which occur in the collision of projectile with various targets in emulsion which constitute the AgBr group of nuclei [71, 74, 75]. The value of impact parameter for each data sample was so set that the mean multiplicity of the relativistic charged particles becomes nearly equal to those obtained for the real data sets.

3. Formalism

For entropy of the charged particle multiplicity distribution, *Shannon's information entropy* is calculated using [10, 23]

$$S = -\sum_n P_n \ln P_n \tag{2}$$

and its generalization, Rényi's order q information entropy, is estimated as [14, 26, 70]

$$I_q = \frac{1}{q-1} \ln \sum_n P_n^q \quad \text{for } q \neq 1, \tag{3}$$

where for $q = 1$ $\lim_{q\to 1} I_q = I_1 = S$, and P_n is the probability of production of n charged particles. The generalized dimensions of order q may be estimated as [14, 69, 70]

$$D_q = \frac{I_q}{Y_m}, \qquad \text{where } Y_m = \ln\left[\frac{\left(\sqrt{s} - 2m_n \left\langle n_p \right\rangle\right)}{m_\pi}\right] = \ln n_{\max}. \tag{4}$$

Y_m denotes the maximum rapidity in the centre-of-mass frame, $\sqrt{s}$ represents the center-of-mass energy, m_π is the pion rest mass, $\langle n_p \rangle$ denotes the average number of participating nucleons, and $n_{\max}$ is maximum multiplicity of relativistic charged particles produced for a given pair of colliding nuclei at a given energy.

For the particle production process to follow self-similar behaviour, the G moments of order q, defined as [81]

$$G_q = \sum P_n^q; \quad q \text{ is any real number}, \tag{5}$$

should follow the power law of the form

$$G_q \propto (\partial\eta)^{\tau(q)}, \tag{6}$$

where $\partial\eta$ is the pseudorapidity bin-width. The parameter $\tau(q)$ is related to the dimension D_q, for all q, by

$$\tau(q) = (q-1) D_q, \tag{7}$$

where D_0, D_1, and D_2 are usually referred to as the fractal dimensions, information dimension, and correlation dimension, respectively [41]. It has been pointed out by Hwa [41] that values of G_q moments obtained from various experiments can not be compared as they depend on the number of events in the data samples and on $\partial\eta$, that is, on detector resolution. It is the $\partial\eta$ dependence of G_q that is the aim of studying G_q; in particular data analysis should aim to extract the generalized dimensions D_q, where

$$D_q = (q-1)^{-1} \lim_{\partial\eta\to 0} \left(\frac{\ln G_q}{\ln \partial\eta}\right). \tag{8}$$

The meaning of function $\tau(q)$ becomes rather more obvious after performing the Legendre transformation from independent variables τ and q to the variables α and f:

$$\alpha_q = \frac{d\tau(q)}{dq}, \qquad f(\alpha_q) = q\alpha_q - \tau(q). \tag{9}$$

$f(\alpha)$ is fractal dimension of a subset composed from bins whose occupancy probability lies in the interval ($P - dP$ to $P + dP$). Thus by estimating the G_q moments, the continuous scaling function $f(\alpha_q)$ can be constructed [44].

The thermodynamical interpretation of these relationships means that q can be interpreted with an inverse temperature $q = T^{-1}$ whereas the spectrum $f(\alpha)$ and α play the role of entropy and energy (per unit volume), respectively [81–84].

4. Results and Discussion

Probability $P_n(\Delta\eta)$ of production of n charged particles in a pseudorapidity window of fixed width is calculated by selecting a window of width $\Delta\eta = 0.5$. This window is so chosen that its midposition coincides with the center of symmetry of η distribution, η_c. Thus, all the relativistic charged particles having their η values lying in the range $(\eta_c - \Delta\eta/2) \leq \eta \leq (\eta_c + \Delta\eta/2)$ are counted to evaluate P_n. The window size is then increased in steps of 0.5 until the region, $\eta_c \pm 3.0$, is covered. Values of entropy, S, for different η-windows are calculated by using (2), while the value of maximum rapidity is estimated from (4). Variations of entropy normalized to maximum rapidity, S/Y_m, with η-window width, also normalized to maximum rapidity, $\Delta\eta/Y_m$, for the experimental and HIJING data sets are plotted in Figure 1. It is observed in the figure that S/Y_m first increases up to $\Delta\eta/Y_m \sim 0.5$ and thereafter acquires nearly a constant value. It is interesting to note that the data points for various samples of events overlap to form a single curve. This indicates the presence of entropy scaling in AA collisions at AGS and SPS energies. Results from HIJING simulated events also support the presence of entropy scaling.

Similar entropy scaling in AA collisions has been reported by us [10, 15] and also by the other workers [29, 70] for central and minimum bias events. In our earlier work, attempt was made to look for whether the observed entropy scaling is of dynamical nature. For this purpose the correlation free Monte Carlo events samples (Mixed events) corresponding to each of the real data samples were generated and analyzed. These

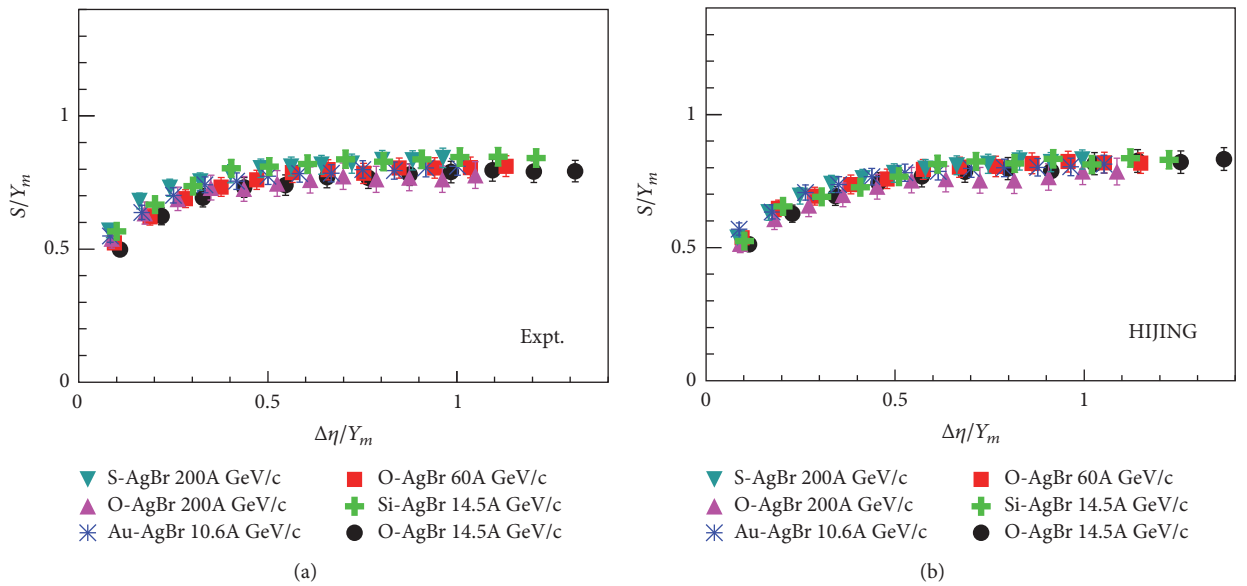

FIGURE 1: Variations of entropy normalized to maximum rapidity, S/Y_m, with η-window width normalized to maximum rapidity, $\Delta\eta/Y_m$, for the Experimental (a) and HIJING events (b).

findings revealed that the entropy scaling observed was the distinct feature of the data and was of dynamical origin [10, 15].

According to (4) the quantity, $(\sqrt{s} - 2m_n\langle n_p\rangle)/m_\pi$, is equal to the maximum charged particle multiplicity at a given center of mass energy. It would, therefore, be convenient to examine the mean multiplicity $\langle n_s\rangle$ versus entropy in limited η windows as well as in full η range; the entropy in the entire η range, $S_{\max}$, is calculated using (2). Variations of $S_{\max}$ with $\ln E_{\text{total}}$ for the experimental and HIJING events are exhibited in Figure 2: E_{total} denotes the total energy of the beam nucleus. It may be noticed in the figure that $S_{\max}$ increases linearly with $\ln E_{\text{total}}$ for both real and simulated event samples. HIJING, however, predicts somewhat smaller values of $S_{\max}$ as compared to the corresponding $S_{\max}$ values estimated from the real data. These findings are, thus, in agreement with those reported for ^{16}O-nucleus collision at 60A and 200A GeV/c and ^{32}S-nucleus interaction at 200 GeV/c [70]. Shown in Figure 3 are the variations of $S/S_{\max}$ with $\langle n\rangle/\langle n\rangle_{\max}$ for the six data sets considered. It is evident from the figure that the data points corresponding to various types of collisions almost overlap to form a single curve. It may also be noted that $S/S_{\max} \to 1.0$ as $\langle n\rangle/\langle n\rangle_{\max} \to 1.0$. These observations too support the presence of entropy scaling in AA collisions at AGS and SPS energies.

It has been reported [14, 81, 85, 86] that the constant specific heat (CSH) approximation widely used in standard thermodynamics is applicable to the multifractal data too. Nearly constant value of multifractal specific heat has been observed [87–90] from the analysis of the experimental data on hadronic and heavy-ion collisions at different energies. These investigations have been carried out by following the methods proposed by Hwa [41] and Takagi [88], where the multiplicities of particles in narrow η-bins, $\delta\eta$, are involved. This introduces a limit to analysis because $\delta\eta$ would depend

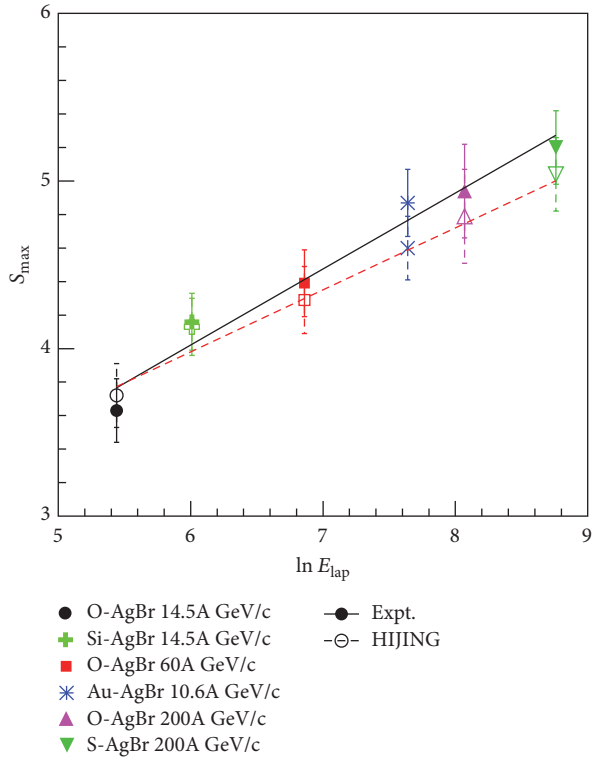

FIGURE 2: Variations of $S_{\max}$ with $\ln E_{\text{total}}$ for the experimental and HIJING events.

on the detector resolution (see (6)). However, since the quantity $\sum(P_n)^q$ scales with improving relative resolution $\delta\eta$ [70] like $G_q \approx (\delta\eta)^{\tau(q)} = \sum(P_n)^q$, the Rényi's order-$q$ information entropy may also be used to understand the multifractal nature of particle production and estimation

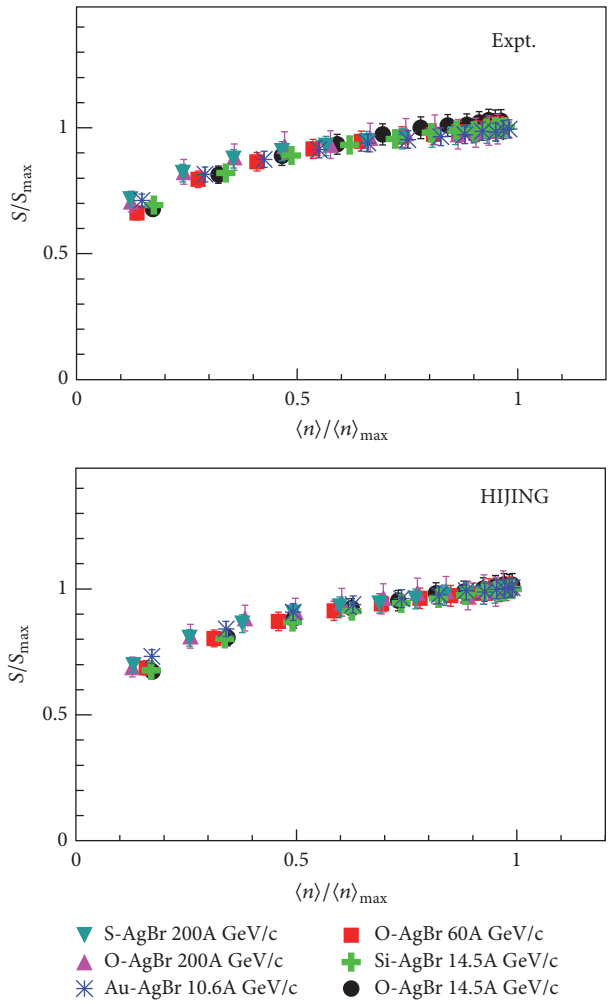

FIGURE 3: Variations of S/S_{max} with $\langle n\rangle/\langle n\rangle_{max}$ for the experimental and HIJING event samples.

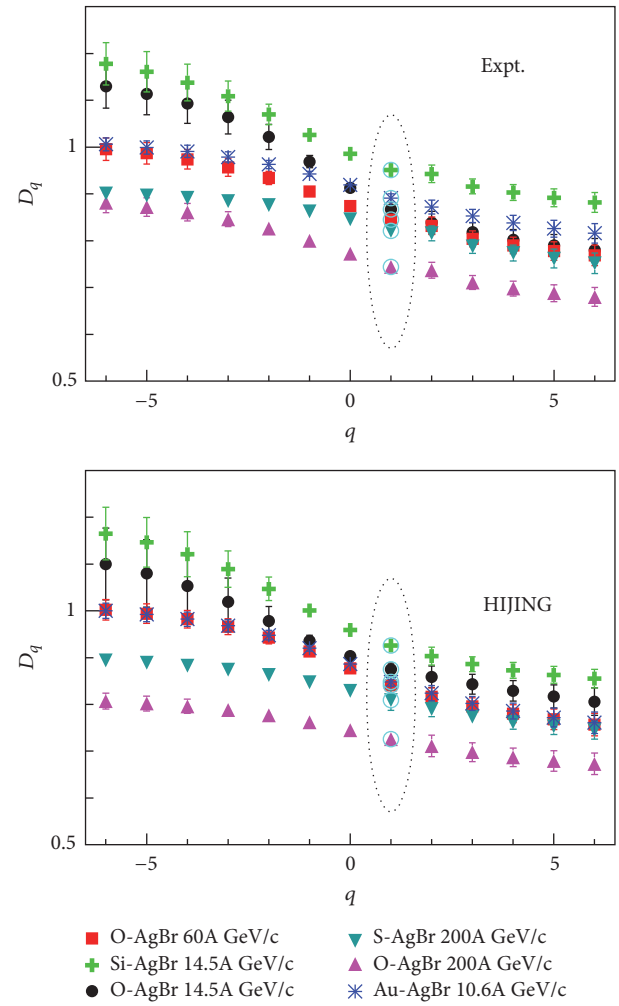

FIGURE 4: Dependence of D_q on q for experimental and HIJING events. The values of D_1 (encircled) are obtained from $f(\alpha(q))$ spectrum.

of multifractal specific heat. The advantage of this method is that it does not depend on the phase space bin width and hence on detector resolution; rather it accounts for the fractal resolution, which is related to the collision energy [14]. From the definitions of Rényi's information entropy, I, and generalized dimensions, D_q (see (3) and (4)), it is evident that, for a given q, $(I_q)_{max} = \ln n_{max}$. The highest entropy is achieved for the greatest "chaos" of a uniformly distributed probability function $P_n = 1/n_{max}$ [71] and (4) gives $D_q = I_q/(I_q)_{max}$.

Variations of D_q with q for various event samples are shown in Figure 4. The values of D_1 have been obtained from the $f(\alpha_q)$ spectrum (Figure 6) and discussed in the coming part of the text. It is observed that D_q monotonously decreases with increasing order q and the trend of decrease for the real and HIJING events is nearly the same except that HIJING predicts somewhat smaller values of D_q as compared to that for experimental data. The D_q spectrum for order $q \geq 2$, which for multifractals is decreasing function of q, can be related to the scaling behaviour of q point correlation integrals [14, 47]. Thus, the trend of variations of D_q against q observed in the present study indicates the multifractal nature of multiplicity distributions in full phase space in ion-ion collisions at the energies considered. Similar variations of D_q with q have also been reported earlier [70] in collisions of protons (800 GeV) and heavy ions (^{4}He at 11A, ^{28}Si at 14.5A, ^{16}O at 60A and 200A, and ^{32}S at 200A GeV/c) collisions. Although the presence of multifractality predicts the decrease of D_q with q, yet no further useful information about the q-dependence of D_q spectrum can be extracted which may lead to making remarks on the scaling properties of q-correlation integrals [14]. It has been suggested [81, 85, 90] that in constant heat approximation, D_q, dependence on q acquires the following simple form:

$$D_q \simeq (a - c) + c\frac{\ln q}{q - 1}, \tag{10}$$

where a is the information dimension, D_1, while c denotes the multifractal specific heat. The linear trend of variation D_q with $\ln q/q - 1$, given by (10), is expected to be observed for multifractals. On the basis of classical analogy with specific

Table 2: Values of parameters a and c, occurring in (4) for the various event samples.

Type of interactions	Energy (GeV/c)	Expt.		HIJING	
		a	c	a	c
^{197}Au-AgBr	10.6A	0.746 ± 0.003	0.195 ± 0.006	0.684 ± 0.002	0.213 ± 0.004
^{16}O-AgBr	14.5A	0.708 ± 0.001	0.200 ± 0.003	0.738 ± 0.003	0.189 ± 0.006
^{28}Si-AgBr	14.5A	0.815 ± 0.002	0.185 ± 0.005	0.795 ± 0.002	0.167 ± 0.004
^{16}O-AgBr	60A	0.700 ± 0.002	0.191 ± 0.004	0.682 ± 0.002	0.209 ± 0.005
^{16}O-AgBr	200A	0.613 ± 0.001	0.190 ± 0.003	0.614 ± 0.001	0.158 ± 0.004
^{32}S-AgBr	200A	0.681 ± 0.002	0.196 ± 0.005	0.685 ± 0.001	0.165 ± 0.003

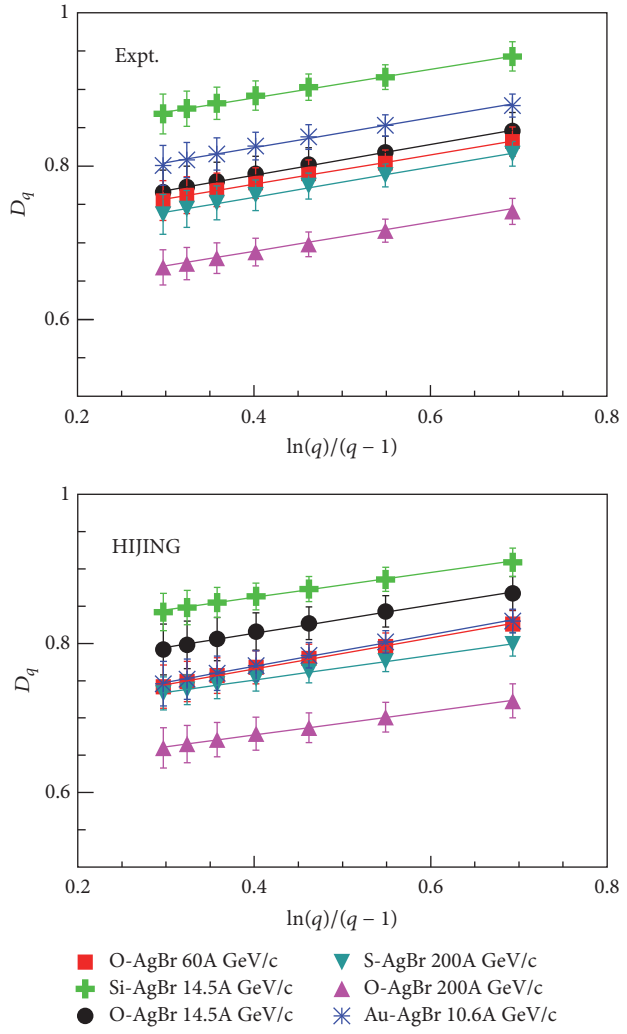

Figure 5: D_q versus $\ln(q)/(q-1)$ plots for the experimental and HIJING data at various energies.

heat of gases and solids, the value of c is predicted [89] to remain independent of temperature in a wide range of q. In order to test the validity of (10), D_q values are plotted against $\ln q/q-1$ in Figure 5. It is evident from the figure that D_q increases linearly with $\ln q/q-1$. The lines in the figure are due to the best fits to the data obtained using (10). The values of the parameters "a" and "c," thus, obtained are listed in Table 2. It is interesting to note from the table that the values of multifractal specific heat, c, for all the data sets, are nearly the same, ~0.2 there by indicating its independence of the beam energy and projectile mass. It may also be noticed from the table that the experimental values of c are quite close to those predicted by HIJING. It is worthwhile to mention that the values of multifractal specific heat obtained in the present study are close to those obtained by us [87] by analysing some of these data sets using Takagi's approach [88]. Incidentally similar values of c have been reported by Du et al. [90] for 10.6A GeV/c ^{197}Au-nucleus collisions. In p-nucleus interactions too, the value of multifractal specific heat has been observed to be ~0.25 in the energy range, 200–800 GeV [70, 85, 90]. However, in the case of $pp/\overline{p}p$ collisions the values of this parameter have been found to be ~0.08 in the wide energy range 25–1800 GeV [14].

These findings, thus, indicate that the constant-specific heat approximation is applicable to the multiparticle production in relativistic hadronic and ion-ion collisions. Moreover, nearly the same values of multifractal specific heat, c, observed in the present study as well as other workers using the data on hh, hA, and AA collisions involving various projectiles/targets at widely different energies do indicate that the parameter c may be regarded as a universal characteristics of hadronic and heavy-ion collisions.

In order to construct the multifractal spectrum, values of τ_q, α_q, and $f(\alpha_q)$ are evaluated using (7) and (9) for $q = -6$ to 6. $f(\alpha_q)$ spectra for various data sets are displayed in Figure 6. It is evidently clear from the figure that these spectra are represented by continuous curves, thus, characterising a qualitative manifestation of the multiplicity fluctuations. Spectra for all the data sets (real and HIJING) are noticed to follow the general characteristics of occurrence of peaks at α_0 and a common target at an angle of 45° at $f(\alpha_1) = \alpha_1$. The spectrum is noticed to have a peak at α_0 and is concave downwards everywhere. As expected the values of α_q decrease with increasing q as D_q decreases with increasing q. The region $\alpha_q < \alpha_0$ corresponds to positive q and the curves in this region have positive slope, whereas the region $\alpha_q > \alpha_0$ would correspond to negative q and the slope of the curves in this region is negative.

The values of $f(\alpha_q)$ for $q = 0, 1, 2$ would give the fractal dimensions ($D_0 = f(\alpha_0)$), the information dimension ($D_1 = f(\alpha_1) = \alpha_1$), and the correlation dimension ($D_2 = 2\alpha_2 - f(\alpha_2)$). The values of information dimension are shown in Figure 4 to distinguish these points in the figure; the

Table 3: Values of width ($\alpha_{max} - \alpha_{min}$) of $f(\alpha(q))$ spectrum for the various event samples.

Type of interactions	Energy (GeV/c)	Expt.			HIJING		
		α_{max}	α_{min}	$(\alpha_{max} - \alpha_{min})$	α_{max}	α_{min}	$(\alpha_{max} - \alpha_{min})$
^{197}Au-AgBr	10.6A	1.045	0.776	0.269	1.045	0.716	0.329
^{16}O-AgBr	14.5A	1.224	0.742	0.482	1.220	0.764	0.456
^{28}Si-AgBr	14.5A	1.279	0.845	0.434	1.278	0.821	0.457
^{16}O-AgBr	60A	1.054	0.732	0.322	1.055	0.717	0.338
^{16}O-AgBr	200A	0.932	0.647	0.285	0.834	0.647	0.187
^{32}S-AgBr	200A	0.924	0.712	0.212	0.923	0.713	0.210

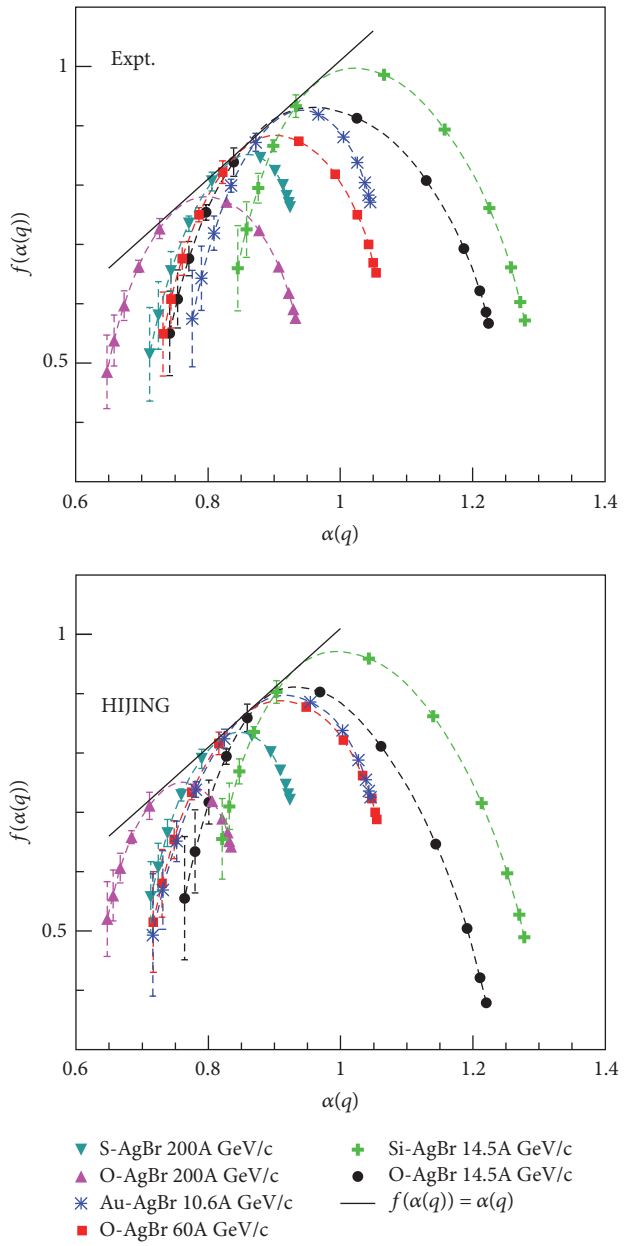

Figure 6: $f(\alpha(q))$ spectra for the experimental and HIJING event samples.

data points are encircled. The widths of the $f(\alpha_q)$ spectrum ($\alpha_{max} - \alpha_{min}$) for various data sets (real and HIJING) are also calculated and presented in Table 3. The width of the spectrum has been suggested as a measure of the degree of multifractality [91–93]. The broader the spectrum, the higher the multifractality [93, 94].

It may be observed from Figure 6 that the spectrum becomes wider with increasing beam energy (^{16}O-AgBr data at 14.5A, 60A, and 200A GeV/c) as well as with increasing projectile mass (^{16}O-AgBr and ^{28}Si-AgBr data at 14.5A GeV/c and ^{16}O-AgBr and ^{32}S-AgBr data at 200A GeV/c). Similar dependence of $f(\alpha_q)$ spectrum has also been observed in ^{12}C-, ^{24}Mg-, ^{16}O-, and ^{32}S-AgBr collisions at 2.1A, 4.5A, 60A, and 200A GeV/c [93].

These observations, thus, tend to suggest that multifractality is more pronounced if the beam energy or mass of the colliding nuclei increases. However, it has been pointed out that at higher energies influence of energy is more prominent as compared to the mass [93]. Hwa [41] has also pointed out that since D_q increases with energy for all q values, α_0 and $f(\alpha_0)$ will increase with energy too and hence the entire spectrum ($f(\alpha_q)$) would be a broader once. This, in turn, implies that the rapidity distribution will become more jagged and irregular with prominent sharp peaks and deep valleys. As the analysis method suggested by Hwa [41] is based on the multiplicity fluctuations in limited rapidity bins, the remark made in [41] that the highly chaotic behaviour of MD in narrow rapidity bins, $n(y)$, can be observed by a smooth function $f(\alpha)$ is quite interesting. It has also been remarked that averaging $n(y)$ over all events would be devoid of any information about fluctuation and intermittency and also that if the experimental/detector resolution is not good enough to capture the sharp peaks and deep valleys, the $f(\alpha_q)$ spectrum would appear narrower than it should otherwise be [41]. In contrast to the standard intermittency and multifractal analysis which are based on the multiplicities in phase space bins, the present analysis, as mentioned earlier, does not depend on the experimental resolution. It rather considers fractal resolution related to the total energy available [14]. Assuming that, during collisions with many particles produced, energy dissipates into N discrete sites. The site labeled by n is occupied by the probability P_n. Since most of the sites are unoccupied, the overlay of many inelastic

events can be visualized as a fractal with overall extent $\sqrt{s}$. The sufficient condition to produce self-similar structure is that P_n would exhibit some type of scaled invariant behaviour. At sufficiently high energies, which correspond to high enough resolution $\delta = 1/N$, P_n acquires a power law dependence on the resolution δ and hence the quantity $\sum(P_n)^q$ will scale with δ as [14]

$$\sum (P_n)^q \sim (\delta)^{-(1-q)D}. \tag{11}$$

The independence of generalized dimension

$$D_q = -\frac{I_q}{n\delta} \tag{12}$$

on energy (resolution δ) would refer the presence of multifractality in MD of relativistic charged particles produced in high energy collisions [14, 95].

5. Conclusions

On the basis of the findings of the present work the following conclusions may be reached:

(1) The entropy normalized to maximum rapidity exhibits a saturation beyond $\Delta\eta/Y_m \sim 0.5$ indicating thereby the presence of large amount of entropy around midrapidity region.

(2) Overlapping data points for various sets of events in S/Y_m vs $\Delta\eta/Y_m$ plots exhibit entropy scaling in AA collisions at AGS and SPS energies.

(3) The scaling observed with the experimental data is nicely supported by HIJING model.

(4) The decreasing values of D_q with increasing order number q may be taken as a signal of multifractal nature of multiplicity distributions of relativistic charged particle produced in hadronic and heavy-ion collisions.

(5) Besides the information dimension, D_1, there is yet another parameter, c, which may be used as a universal parameter for multiparticle production in high energy hadronic and heavy-ion collisions.

(6) Rényi's order q-information entropy may also be used to construct the multifractal spectrum, which in turn would help study the multiplicity fluctuations and scaling in high energy hadronic and heavy-ion collisions.

Conflicts of Interest

The authors declare that there are no conflicts of interest.

References

[1] M. Mukherjee, S. Basu, S. Choudhury, and T. K. Nayak, "Fluctuations in charged particle multiplicities in relativistic heavy-ion collisions," *Journal of Physics G*, vol. 43, no. 8, Article ID 085102, 2016.

[2] A. Kumar, P. K. Srivastava, B. K. Singh, and C. P. Singh, "Charged hadron multiplicity distribution at relativistic heavy-ion colliders," *Advances in High Energy Physics*, vol. 2013, pp. 1–27, 2013.

[3] A. Alkin, "Phenomenology of charged-particle multiplicity distributions," *Ukrainian Journal of Physics*, vol. 62, pp. 743–756, 2017.

[4] I. M. Dremin and J. W. Gary, "Hadron multiplicities," *Physics Reports*, vol. 349, p. 301, 2001.

[5] P. Castorina, G. Nardulli, and G. Preparata, "Are quantum-chromodynamic scaling violations in deep-inelastic lepton-hadron scattering really observed?" *Physical Review Letters*, vol. 47, no. 7, pp. 468–471, 1981.

[6] G. Hanson, "Evidence for jet structure in hadron production by e^+e^- annihilation," *Physical Review Letters*, vol. 35, no. 24, pp. 1607–1609, 1975.

[7] C. Berger, "A study of jets in electron positron annihilation into hadrons in the energy range 3.1 to 9.5 GeV," *Physics Letters B*, vol. 78B, no. 1, pp. 176–182, 1978.

[8] G. Aad et al., "Measurement of multi-jet cross sections in proton–proton collisions at a 7 TeV center-of-mass energy," *The European Physical Journal C*, vol. 71, p. 1763, 2011.

[9] Z. Bern, "Two "New" categories of papers welcomed in corrosion," *Corrosion*, vol. 68, no. 4, 2012.

[10] S. Ahmad, A. Chandra, M. Zafar, M. Irfan, and A. Ahmad, "Entropy scaling in ion–ion collisions at ags and sps energies," *International Journal of Modern Physics E*, vol. 22, no. 8, Article ID 1330019, 2013.

[11] S. Das, S. K. Ghosh, S. Raha, and R. Ray, "Entropy scaling from chaotically produced particles in p-p collisions at LHC energies," *Nuclear Physical A*, vol. 438, pp. 862-863, 2011.

[12] R. M. Weiner, "Primordial nucleosynthesis: successes and challenges," *International Journal of Modern Physics E*, vol. 15, no. 1, p. 37, 2006.

[13] S. Das, S. K. Ghosh, S. Raha, and R. Ray, "Entropy scaling and thermalization in hadron-hadron collisions at LHC," *High Energy Physics - Phenomenology*, p. 4, 2011.

[14] M. K. Suleymanov, M. Sumbera, and I. Zborovsky, "hep-ph/0304206".

[15] S. Ahmad, A. Ahmad, A. Chandra, M. Zafar, and M. Irfan, "Entropy analysis in relativistic heavy-ion collisions," *Advances in High Energy Physics*, vol. 2013, Article ID 836071, 10 pages, 2013.

[16] G. J. Alner, "Scaling violation favouring high multiplicity events at 540 GeV CMS energy," *Physics Letters B*, vol. 138B, pp. 304–310, 1984.

[17] Z. Koba, H. B. Nielsen, and P. Olesen, "Scaling of multiplicity distributions in high energy hadron collisions," *Nuclear Physics B*, vol. 40, pp. 317–334, 1972.

[18] G. J. Alner, "Scaling violations in multiplicity distributions at 200 and 900 GeV," *Physics Letters B*, vol. 167B, pp. 476–480, 1986.

[19] A. Wroblewski, "Multiplicity distributions in proton proton collisions," *Acta Physica Polonica B*, vol. 4, p. 857, 1973.

[20] W. Thome, K. Eggert, and K. Giboni, "Charged particle multiplicity distributions in pp collisions at ISR energies," *Nuclear Physics B*, vol. 129, no. 3, pp. 365–389, 1977.

[21] G. J. Alner, "A new empirical regularity for multiplicity distributions in place of KNO scaling," *Physics Letters B*, pp. 199–206, 1985.

[22] G. J. Alner, "Multiplicity distributions in different pseudorapidity intervals at a CMS energy of 540 GeV," *Physics Letters B*, vol. 160B, pp. 193–198, 1985.

[23] V. Simak, M. Sumbera, and I. Zborovsky, "Entropy in multiparticle production and ultimate multiplicity scaling," *Physics Letters B*, vol. 206, no. 1, pp. 159–162, 1988.

[24] Y. M. Sinyukov and S. V. Akkelin, "Pion entropy and phase-space densities in $A + A$ collisions," *Acta Physica Hungarica Series A*, vol. 22, no. 1-2, pp. 171–178, 2005.

[25] S. Pal and S. Pratt, "Entropy production at RHIC," *Physics Letters B*, vol. 578, no. 3-4, pp. 310–317, 2004.

[26] P. Carruthers, M. Plümer, S. Raha, and R. Weiner, "Entropy scaling in high energy collisions. Chaos and coherence," *Physics Letters B*, vol. 212, no. 3, pp. 369–374, 1988.

[27] M. R. Ataian, "EHS/NA22 collaboration," *Acta Physica Polonica B*, vol. 36, p. 2969, 2005.

[28] T. Mizoguchi and M. Biyajima, "Analyses of multiplicity distributions with η_c and Bose–Einstein correlations at LHC by means of generalized Glauber–Lachs formula," *The European Physical Journal C*, vol. 70, no. 4, pp. 1061–1069, 2010.

[29] D. Ghosh et al., "Entropy scaling in high-energy nucleus-nucleus interactions," *Journal of Physics G*, vol. 38, no. 065105, 2011.

[30] D. Ghosh, A. Deb, P. K. Haldar, S. R. Sahoo, and D. Maity, "Validity of the negative binomial multiplicity distribution in case of ultra-relativistic nucleus-nucleus interaction in different azimuthal bins," *Europhysics Letters*, vol. 65, p. 311, 2004.

[31] T. H. Burnett, S. Dake, M. Fuki et al., "Extremely high multiplicities in high-energy nucleus-nucleus collisions," *Physical Review Letters*, vol. 50, no. 26, 2062 pages, 1983.

[32] G. J. Alner, R. E. Ansorge, and B. Åsman, "Scaling of pseudorapidity distributions at c.m. energies up to 0.9 TeV," *Zeitschrift für Physik C: Particles and Fields*, vol. 33, no. 1, pp. 1–6, 1986.

[33] M. Adamus, "Maximum particle densities in rapidity space of $\pi + p$, $K + p$ and pp collisions at 250 GeV/c," *Physics Letters B*, vol. 185, no. 3-4, p. 446, 1987.

[34] R. Holynski et al., "Evidence for intermittent patterns of fluctuations in particle production in high-energy interactions in nuclear emulsion," *Physical Review Letters*, vol. 62, p. 733, 1989.

[35] A. Bialas and R. Peschanski, "Moments of rapidity distributions as a measure of short-range fluctuations in high-energy collisions," *Nuclear Physics B*, vol. 273, no. 3-4, pp. 703–718, 1986.

[36] D. Ghosh, "Evidence of non-statistical fluctuation in medium-energy protons emitted in the fragmentation process of ultra-relativistic nuclear interaction," *Europhysics Physical Letters*, vol. 48, p. 508, 1999.

[37] D. Ghosh, "Multifractality and intermittency study of ultrarelativistic ^{32}S–AgBr AND ^{16}O–AgBr interactions: further evidence of a nonthermal phase transition," *International Journal of Modern Physics A*, vol. 14, p. 2091, 1999.

[38] M. I. Adamovich, "Scaled-factorial-moment analysis of 200A-GeV sulfur+gold interactions," *Physical Review Letters*, vol. 65, no. 6, p. 412, 1990.

[39] M. M. Khan, A. Shakeel, N. Ahmad et al., "Dynamical fluctuations and Levy stability in 14.5-A-GeV/c Si-28 nucleus interactions," *Acta Physica Polonica B*, vol. 38, p. 2653, 2007.

[40] A. Bialas and R. B. Peschanski, "Intermittency in multiparticle production at high energy," *Nuclear Physics B*, vol. 308, p. 857, 1988.

[41] R. C. Hwa, "Fractal measures in multiparticle production," *Physical Review D: Particles, Fields, Gravitation and Cosmology*, vol. 41, no. 5, pp. 1456–1462, 1990.

[42] B. Buschbeck, P. Lipa, and R. Peschanski, "Signal for intermittency in e+e− reactions obtained from negative binomial fits," *Physics Letters B*, vol. 215, no. 4, pp. 788–791, 1988.

[43] I. V. Ajinenko, "Results and future prospects for muon $(g - 2)$," *Physics Letters B*, vol. 222, no. 306, 1989.

[44] P. L. Jain, G. Singh, and A. Mukhopadhyay, "Multifractals at relativistic energies," *Physical Review C: Nuclear Physics*, vol. 46, no. 2, pp. 721–726, 1992.

[45] B. B. Mandelbrot, *The Fractal Geometry of Nature*, Freeman, New York, NY, USA, 1982.

[46] R. Saha, A. Deb, D. Ghosh, and J. Phys, "Study of phase transition and its dependence on target excitation using fractal properties of pionization process," *Canadian Journal of Physics*, vol. 95, no. 8, p. 699, 2017.

[47] G. Paladin and A. Vulpiani, "Anomalous scaling laws in multifractal objects," *Physics Reports*, vol. 156, no. 4, pp. 147–225, 1987.

[48] P. Carruthers and M. Duong-Van, "Evidence for a common fractal dimension in turbulence, galaxy distributions and hadronic multiparticle production," *Los alamos preprint LA-UR-83-2419*, 1983.

[49] I. M. Dermin, "The fractal correlation measure for multiple production," *Modern Physics Letters A*, vol. 3, no. 14, p. 1333, 1988.

[50] P. Lipa and B. Buschbeck, "From strong to weak intermittency," *Physics Letters B*, vol. 223, no. 3-4, pp. 465–469, 1989.

[51] H. G. E. Hentschel and I. Procaccia, "The infinite number of generalized dimensions of fractals and strange attractors," *Physica D: Nonlinear Phenomena*, vol. 8, no. 3, pp. 435–444, 1983.

[52] P. Grassberger and I. Procaccia, "Dimensions and entropies of strange attractors from a fluctuating dynamics approach," *Physica D: Nonlinear Phenomena*, vol. 13, no. 1-2, pp. 34–54, 1984.

[53] M. H. Jensen, L. P. Kadanoff, A. Libchaber, I. Procaccia, and J. Stavans, "Global universality at the onset of chaos: results of a forced rayleigh-bénard experiment," *Physical Review Letters*, vol. 55, no. 25, pp. 2798–2801, 1985.

[54] C. B. Chiu and R. C. Hwa, "Multifractal structure of multiparticle production in branching models," *Physical Review D: Particles, Fields, Gravitation and Cosmology*, vol. 43, no. 1, pp. 100–103, 1991.

[55] W. Florkowski and R. C. Hwa, "Universal multifractality in multiparticle production," *Physical Review D: Particles, Fields, Gravitation and Cosmology*, vol. 43, no. 5, pp. 1548–1554, 1991.

[56] M. Rybczynski, "Energy dependence of fluctuations in central Pb+Pb collisions from NA49 at the CERN SPS," *Journal of Physics G*, vol. 35, Article ID 104091, 2008.

[57] E. V. Shuryak, "Quantum chromodynamics and the theory of superdense matter," *Physics Reports A Review Section of Physics Letters*, vol. 61, no. 2, pp. 71–158, 1980.

[58] F. Karsch, E. Laermann, and A. Peikert, "Quark mass and flavour dependence of the QCD phase transition," *Nuclear Physics B*, vol. 605, p. 579, 2001.

[59] F. Karsch, "Lattice results on QCD thermodynamics," *Nuclear Physics A*, vol. 698, no. 4, pp. 199–208, 2002.

[60] A. Bialas and W. Czyz, "Measurement of entropy of a multiparticle system: a do list," *Acta Physica Polonica B*, vol. 31, p. 687, 2000.

[61] A. Bialas and W. Czyz, "Renyi entropies in multiparticle production," *Acta Physica Polonica B*, vol. 31, p. 2803, 2000.

[62] A. Bialas and W. Czyz, "Renyi Entropies for Bernoulli Distributions," *Acta Physica Polonica B*, vol. 32, p. 2793, 2001.

[63] A. Bialas and W. Czyz, "Event by event analysis and entropy of multiparticle systems," *Physical Review D: Particles, Fields, Gravitation and Cosmology*, vol. 61, no. 7, 2000.

[64] P. A. Muller et al., "Quantum chaos: entropy signatures," *Acta Physica Polonica B*, vol. 29, p. 3643, 1998.

[65] Y. G. Ma, "Application of Information Theory in Nuclear Liquid Gas Phase Transition," *Physical Review Letters*, vol. 83, no. 18, pp. 3617–3620, 1999.

[66] P. Brogueira, J. Dias de Deus, and I. P. da Silva, "Information entropy and particle production in branching processes," *Physical Review D: Particles, Fields, Gravitation and Cosmology*, vol. 53, no. 9, pp. 5283–5285, 1996.

[67] A. Bialas, W. Czyz, and J. Wosiek, "Studying thermodynamics in heavy ion collisions," *Acta Physica Polonica B*, vol. 30, p. 107, 1999.

[68] A. Bialas, W. Czyz, and A. Ostruszka, "Renyi entropies in particle cascades," *Acta Physica Polonica B*, vol. 34, p. 69, 2003.

[69] M. Pachr, V. Simak, M. Sumbera, and I. Zborovsky, "Entropy, dimensions and other multifractal characteristics of multiplicity distributions," *Modern Physics Letters A*, vol. 07, no. 25, pp. 2333–2339, 1992.

[70] A. Mukhopadhyay, P. L. Jain, and G. Singh, "Entropy and fractal characteristics of multiparticle production at relativistic heavy ion interactions," *Physical Review C: Nuclear Physics*, vol. 47, no. 1, pp. 410–412, 1993.

[71] M. I. Adamovich, M. M. Aggarwal, and Y. A. Alexandrov, "Produced particle multiplicity dependence on centrality in nucleus-nucleus collisions," *Journal of Physics G: Nuclear and Particle Physics*, vol. 22, no. 10, p. 1469, 1996.

[72] M. I. Adamovich, "Erratum: stochastic emission of particles in ultra-relativistic heavy-ion collisions," *Modern Physics Letters A*, vol. 06, no. 17, pp. 1629-1629, 1989.

[73] F. Glück, I. Joób, and J. Lastc, "Measurable parameters of neutron decay," *Nuclear Physics A*, vol. 593, no. 2, pp. 125–150, 1995.

[74] M. I. Adamovich, "EMU-01 Collaboration," *Physics Letters B*, vol. 201, no. 1, pp. 95–100, 1988.

[75] S. Ahmad, A. Ahmad, and A. Chandra, "Forward-backward multiplicity fluctuations in 200A GeV/c 16O-AgBr and 32S-AgBr collisions," *Physica Scripta*, vol. 87, no. 4, Article ID 045201, 2013.

[76] S. Ahmad, M. M. Khan, N. Ahmad, and A. Ahmad, "Erraticity behaviour in relativistic nucleus-nucleus collisions," *Journal of Physics G: Nuclear and Particle Physics*, vol. 30, no. 9, pp. 1145–1152, 2004.

[77] S. Ahmad, M. M. Khan, S. Khan, A. Khatun, and M. Irfan, "A study of fluctuations of voids in relativistic ion–ion collisions," *International Journal of Modern Physics E*, vol. 24, no. 10, p. 15, 2015.

[78] M. L. Cherry et al., "KLM Collaboration," *Acta Physica Polonica B*, vol. 29, p. 2129, 1998.

[79] X. N. Wang, "A pQCD-based approach to parton production and equilibration in high-energy nuclear collisions," *Physics Reports*, vol. 287, no. 5-6, pp. 287–371, 1997.

[80] M. Gyulassy and X. N. Wang, "HIJING 1.0: A Monte Carlo program for parton and particle production in high energy hadronic and nuclear collisions," *Computer Physics Communications*, vol. 83, pp. 307–331, 1994.

[81] A. Bershadsky, "Multifractal thermodynamics of hadron-hadron and hadron-nucleus interactions," *The European Physical Journal A*, vol. 2, p. 223, 1998.

[82] A. Arneodo, E. Bacry, and J. F. Muzy, "The thermodynamics of fractals revisited with wavelets," *Physica A: Statistical Mechanics and its Applications*, vol. 213, no. 1-2, pp. 232–275, 1995.

[83] E. A. De Wolf, I. M. Dremin, and W. Kittel, "Scaling laws for density correlations and fluctuations in multiparticle dynamics," *Physics Reports*, vol. 270, pp. 1–141, 1996.

[84] R. B. Peschanski, "Intermittency in particle collisions," *International Journal of Modern Physics A*, vol. 6, p. 3681, 1991.

[85] A. Bershadskii, "Multifractal specific heat," *Physica A: Statistical Mechanics and its Applications*, vol. 253, no. 1-4, pp. 23–37, 1998.

[86] D. Ghosh, A. Deb, P. Bandyopadhyay et al., "Evidence of multifractality and constant specific heat in hadronic collisions at high energies," *Physical Review C: Nuclear Physics*, vol. 65, no. 6, 2002.

[87] S. Ahmad, A. R. Khan, M. Zafar, and M. Irfan, "On multifractality and multifractal specific heat in ion-ion collisions," *Chaos, Solitons & Fractals*, vol. 42, no. 1, pp. 538–547, 2009.

[88] F. Takagi, "Multifractal structure of multiplicity distributions in particle collisions at high energies," *Physical Review Letters*, vol. 72, no. 1, pp. 32–35, 1994.

[89] L. D. Landau and E. M. Lifshitz, *Statistical Physics, Part I*, Pergamon Press, Oxford, USA, 1980.

[90] D.-S. Du, X.-Q. Li, Z.-T. Wei, and B.-S. Zou, "Inelastic final-state interactions in $B \to VV \to \pi K$ processes," *The European Physical Journal A*, vol. 4, no. 1, pp. 91–96, 1999.

[91] Y. Ashkenazy, D. R. Baker, H. Gildor, and S. Havlin, "Nonlinearity and multifractality of climate change in the past 420,000 years," *Geophysical Research Letters*, vol. 30, no. 22, p. 2146, 2003.

[92] Y. U. Shimizu, S. Thurner, and K. Ehrenberger, "Multifractal spectra as a measure of complexity in human posture," *Fractals*, vol. 10, no. 1, pp. 103–116, 2002.

[93] G. Bhoumik, A. Deb, S. Bhattacharyya, and D. Ghosh, "Comparative multifractal detrended fluctuation analysis of heavy ion interactions at a few GeV to a few hundred GeV," *Advances in High Energy Physics*, vol. 2016, pp. 1–9, 2016.

[94] L. Telesca, "Investigating the multifractal properties of geoelectrical signals measured in southern Italy," *Physics and Chemistry of the Earth*, vol. 29, p. 295, 2004.

[95] J. Feder, *Fractals*, Plenum Press, New York, NY, USA, 1989.

Hindawi
Advances in High Energy Physics
Volume 2018, Article ID 6914627, 11 pages
https://doi.org/10.1155/2018/6914627

Research Article

Correlations and Event-by-Event Fluctuations in High Multiplicity Events Produced in ^{208}Pb-^{208}Pb Collisions

Shakeel Ahmad,[1] **Shaista Khan**,[1] **Ashwini Kumar**,[2] **Arpit Singh**,[3] **A. Ahmad**,[4] **and B. K. Singh**[3]

[1]*Department of Physics, Aligarh Muslim University, Aligarh 202002, India*
[2]*Department of Physics and Electronics, Dr. Ram Manohar Lohia Avadh University, Faizabad 224001, India*
[3]*Department of Physics, Banaras Hindu University, Varanasi 221005, India*
[4]*Department of Applied Physics, Aligarh Muslim University, Aligarh 202002, India*

Correspondence should be addressed to Shakeel Ahmad; shakeel.ahmad@cern.ch

Received 27 October 2017; Accepted 7 March 2018; Published 8 April 2018

Academic Editor: Andrea Coccaro

Analysis of high multiplicity events produced in 158A GeV/c ^{208}Pb-^{208}Pb collisions is carried out to study the event-by-event fluctuations. The findings reveal that the method of scaled factorial moments can be used to identify the events having densely populated narrow phase space bins. A few events sorted out by adopting this approach are individually analyzed. It is observed that these events do exhibit large fluctuations in their pseudorapidity, η, and azimuthal angle, ϕ, distributions arising due to some dynamical reasons. Two-particle $\Delta\eta$-$\Delta\phi$ correlation study applied to these events too indicates that some complex two-dimensional structure of significantly high magnitude is present in these events which might have some dynamical origin. The findings reveal that the method of scaled factorial moments may be used as an effective triggering for events with large dynamical fluctuations.

1. Introduction

Investigations involving fluctuations in collisions of heavy nuclei at relativistic energies might serve as a useful tool to identify the existence of the state of partonic matter in early life of the fireball because of the idea that the fluctuations in a thermal system are directly related to various susceptibilities and would be a good indication for the possible phase changes [1–4]. Furthermore, large event-by-event (ebe) fluctuations of the suitably chosen observables in ion-ion (AA) collisions would help in identifying events of distinct classes, for example, one with and another without quark-gluon plasma (QGP) [2], as, under extreme conditions of temperature and energy density, a novel phase of matter, the QGP, is expected to be produced. The search for the occurrence of phase transition from hadronic matter to QGP still remains a favorite topic for high energy physicists [1, 5, 6]. It is commonly believed that even if the extreme conditions of QGP formation are achieved in relativistic AA collisions, not all the events would be produced via QGP as the cross section for the QGP formation [1] is still not known. Therefore, a chosen subsample of events exhibiting large fluctuations in certain observables should be studied in detail [7, 8]. A significant contribution to the observed fluctuations in a variable comes due to finite number of particles produced in an event and is referred to as the statistical fluctuations. Its magnitude could be evaluated by considering the independent emission of particles or by using the event mixing technique [1, 2, 7, 8]. All other fluctuations are of dynamical origin and are divided into two groups: (a) fluctuations which do not change on ebe basis, for example, two-particle correlation due to Bose-Einstein statistics or due to decay of resonances and (b) fluctuations which change on ebe basis and are termed as ebe fluctuations. Examples are fluctuations in charged to neutral particle multiplicity ratio due to creation of disoriented chiral condensate (DCC) region or creation of jets which contribute to the high p_t tail of transverse momentum distributions [1, 2]. Several attempts

[1–3, 9–14] have been made to investigate ebe fluctuations in heavy-ion collisions at relativistic energies. The findings do indicate the presence of dynamical fluctuations. The main aim of the present study is to search for the rare events exhibiting some unusual behaviour from a data sample with large number of events. The analyses of individual collision events at SPS and RHIC energies have been argued to statistically reliable as the multiplicities of these events would be high enough and the statistical fluctuations may be treated as under control [15–22]. Moreover, from the study of such events with strong fluctuations, information about the dominance of dynamical components of fluctuations over the statistical ones can be extracted, which, in turn, would provide more insight into the underlying dynamics of high multiplicity events [23, 24]. Analyses of one "hadron-rich" event [25] in the context of Centauro event, single event p_t distributions [26], single event k/π ratio [27], intermittency in individual events, entropy and cluster analysis in single events [21, 22], and so on are some of the investigations carried out so far.

An attempt, therefore, has been made to carry out the analysis of a few high multiplicity individual events produced in 158A GeV/c Pb-Pb collisions. These events are taken from the emulsion experiment performed by EMU01 Collaboration [28–31]. It should be emphasized that the conventional emulsion technique has an advantage over the other detectors due to its 4π solid angle coverage and the data are free from biases due to full phase space acceptance whereas other detectors have limited acceptance cone. This not only reduces the charged particle multiplicity but might also distort some of the event characteristics, like particle density fluctuations. Furthermore, to test whether the fluctuations are arising due to nonstatistical reasons, the findings are compared with the reference distributions obtained by event mixing technique [15, 16, 32].

2. Results and Discussion

2.1. Single Event Factorial Moments. Method of scaled factorial moments (SFMs) [33–35] has been extensively used [1, 15, 36] to search for the nonlinear phenomena in hadronic and ion-ion collisions at widely different energies. The power law behaviour of the type $F_q \sim M_q^{\psi}$ has been investigated by studying [37, 38] the horizontally averaged vertical moments F_q^v and (or) the vertically averaged horizontal moments, F_q^h. The results suggest the presence of large particle density fluctuations in narrow phase space bins to be rare that cannot be ignored. It has, however, been pointed out [37, 39] that because of the averaging procedure adopted, studies involving F_q^v or F_q^h may not fully account for all the fluctuations a system might exhibit. Moreover, the values of the factorial moments F_q^e, estimated on ebe basis, have been observed to exhibit large fluctuations and hence a distinct distribution of F_q^e for a given order q and bin width, δ, may be obtained for a given data sample [18, 37, 39]. This result suggests that the method of SFMs may be applied to individual events [15, 40, 41] to search for the nonlinear phenomena in "hot" and "cold" events; the "hot" and "cold" events refer to the events, respectively, with and without large particle densities in narrow phase space bins. Method of SFMs applied to individual high multiplicity cosmic ray events [41] does indicate the presence of dynamical fluctuations. Such analysis, if carried out on ebe basis would help selecting in the events with large dynamical fluctuations, if this property is not a typical one for each single event. These suppositions have, therefore, been tested in the present study by applying the SFMs analysis to the individual events.

The event factorial moments of order q are defined as

$$F_q^e = \frac{\langle n(n-1)\cdots(n-q+1)\rangle_e}{\langle n\rangle_e^q}, \tag{1}$$

where n denotes the multiplicity in a particular η or ϕ bin.

Values of F_q^e for $q = 2$ are calculated for each of 47 events considered by varying the number of cells, M. Since the number of events are limited, instead of plotting the F_2^e distributions; we have plotted event-wise $\ln F_2$ values for $M = 10$ and 30 (in the pseudorapidity ($\eta = -\ln\tan\theta/2$) and the azimuthal angle (ϕ) spaces), with θ being the emission angle of a charged particle with respect to the mean beam direction. For the values $M = 25$ and 100, we have shown the plot in two-dimensional η-ϕ space. These plots are shown in Figure 1. Values of $\ln F_2$ for the corresponding mixed events are also displayed in the same figure for comparison sake. It may be noted from the figure that $\ln F_2$ values of mixed events are nearly the same ~0.3 whereas these values for the real data vary from event to event such that one would get a distinct distribution of $\ln F_2$ for a significant number of events. It is quite interesting to notice that the values of $\ln F_2$ for few of the real events are much higher as compared to the average values taken over all the events or the values from the mixed events. These observations, thus, help in identifying a few events exhibiting significantly large F_2 values in η-, ϕ-, or η-ϕ space for further analysis. Four such events picked-up are labeled as Evt# 5, 16, 21, and 27. These events henceforth, would be termed as "hot" events. The multiplicities of these events are, respectively, 932, 852, 1433, and 974. Yet another event, Evt# 22, having F_2 values close to the mixed events values has also been taken for comparison sake. This event henceforth will be referred to as the "cold" event. The multiplicity of this event is 1480. Variations of $\ln F_2$ with $\ln M$ for these five real and corresponding mixed events in η-, ϕ-, or η-ϕ spaces are displayed in Figure 2. Event averaged values, $\langle \ln F_2\rangle$ against $\ln M$ for the entire event sample are also plotted in the same figure. It is evidently clear from Figure 2 that F_2 values for the four "hot" events are significantly larger than that of the "cold" event or the event averaged values. These findings, therefore, tend to suggest a few events with high density phase region or strong fluctuations are present in the real data and that these fluctuations might have some dynamical origin. These dynamical fluctuations are the reflection of the dynamics and response of the system and are indicative of phase transition like phenomenon occurring under extreme conditions of heavy-ion collision such as the conditions achieved here at 158A GeV/c. This result, in turn, leads us to conclude that the method of SFMs, if applied to the single event, may be useful for selecting the preliminary

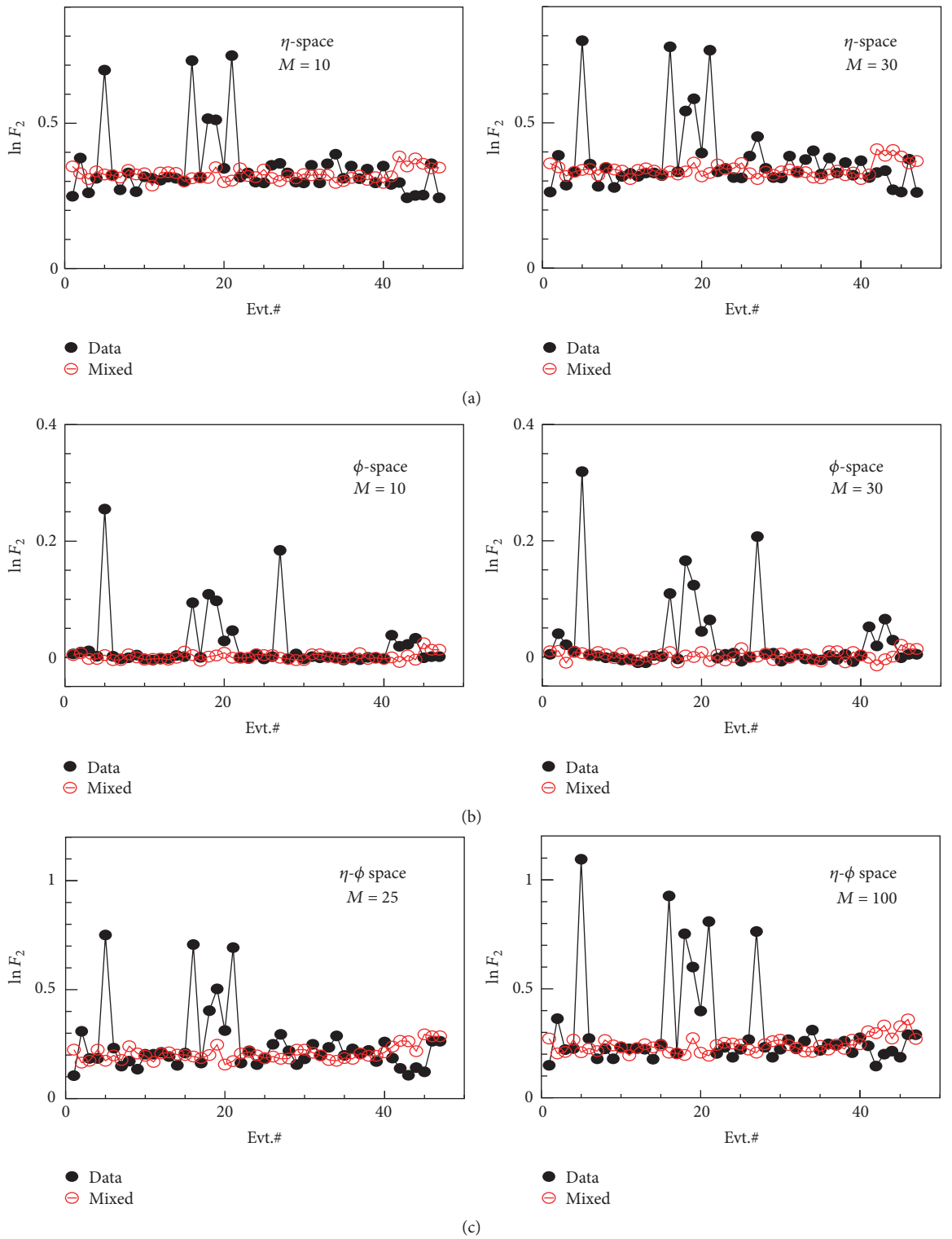

FIGURE 1: Event-wise variations of $\ln F_2$ in η-space (a), ϕ-space (b), and η-ϕ space (c) for the data and mixed events produced in ^{208}Pb-^{208}Pb collisions at 158A GeV/c.

events where strong dynamical fluctuations might be present and thereafter more advanced triggering might occur; for example, particle ratios and enhanced particle multiplicities in certain kinematical regions may be applied.

2.2. η and ϕ Distribution of Single Event. By examining the F_2 values on ebe basis it might be possible to identify the rare events having high density phase space regions. Therefore, to check further that the four "hot" events identified as above

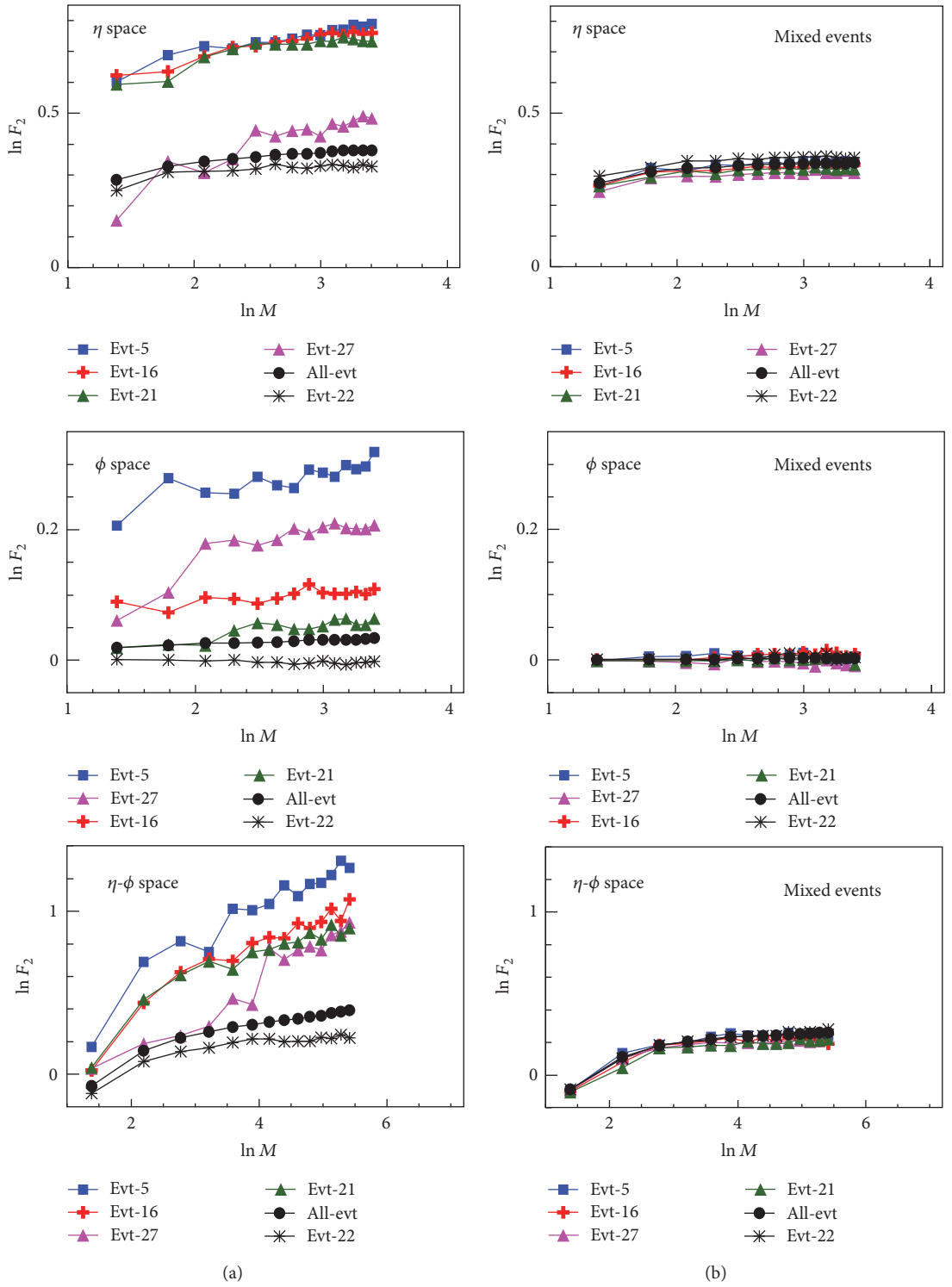

FIGURE 2: Variations of $\ln F_2$ with $\ln M$ in η-, ϕ-, and η-ϕ spaces for all and five individual events produced in 158A GeV/c ^{208}Pb-^{208}Pb interactions. Results from the mixed events are shown (b).

on the basis of their F_2 values do have the densely populated phase space regions, η and ϕ distributions of these events along with the "cold" event are plotted in Figure 3, whereas two-dimensional η-ϕ distributions for these events are exhibited in Figures 4 and 5. Moreover in order to ensure that the observed spikes and valleys are the event characteristics and are not due to statistical reasons η and ϕ distributions of the corresponding five mixed events are also plotted in the same figures. It is interesting to note in these figures that one-dimensional η and ϕ distributions and two-dimensional η-ϕ

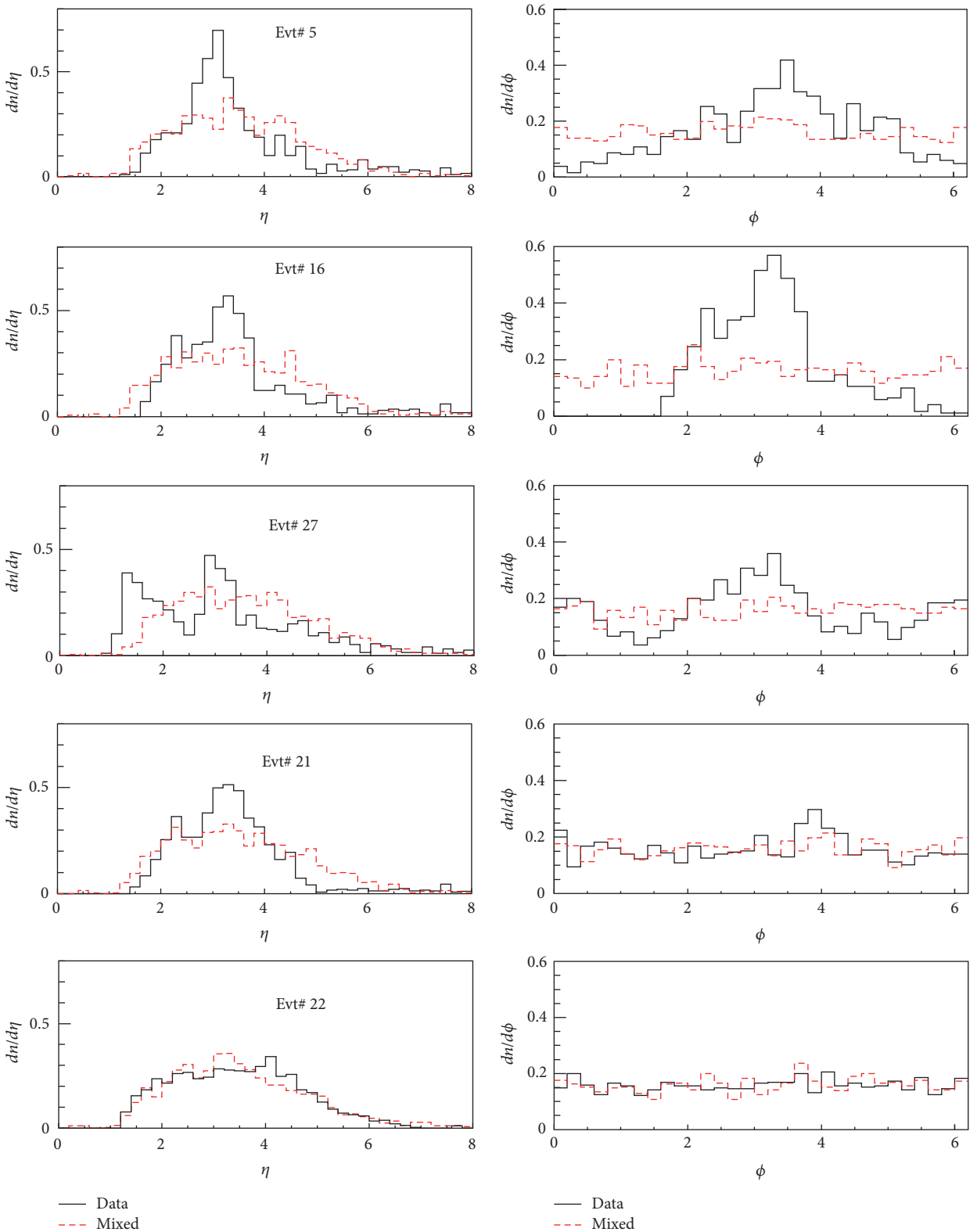

FIGURE 3: η and ϕ distributions for the four "hot" and one "cold" 158A GeV/c ^{208}Pb-^{208}Pb collision events (solid lines) and corresponding mixed events (broken lines).

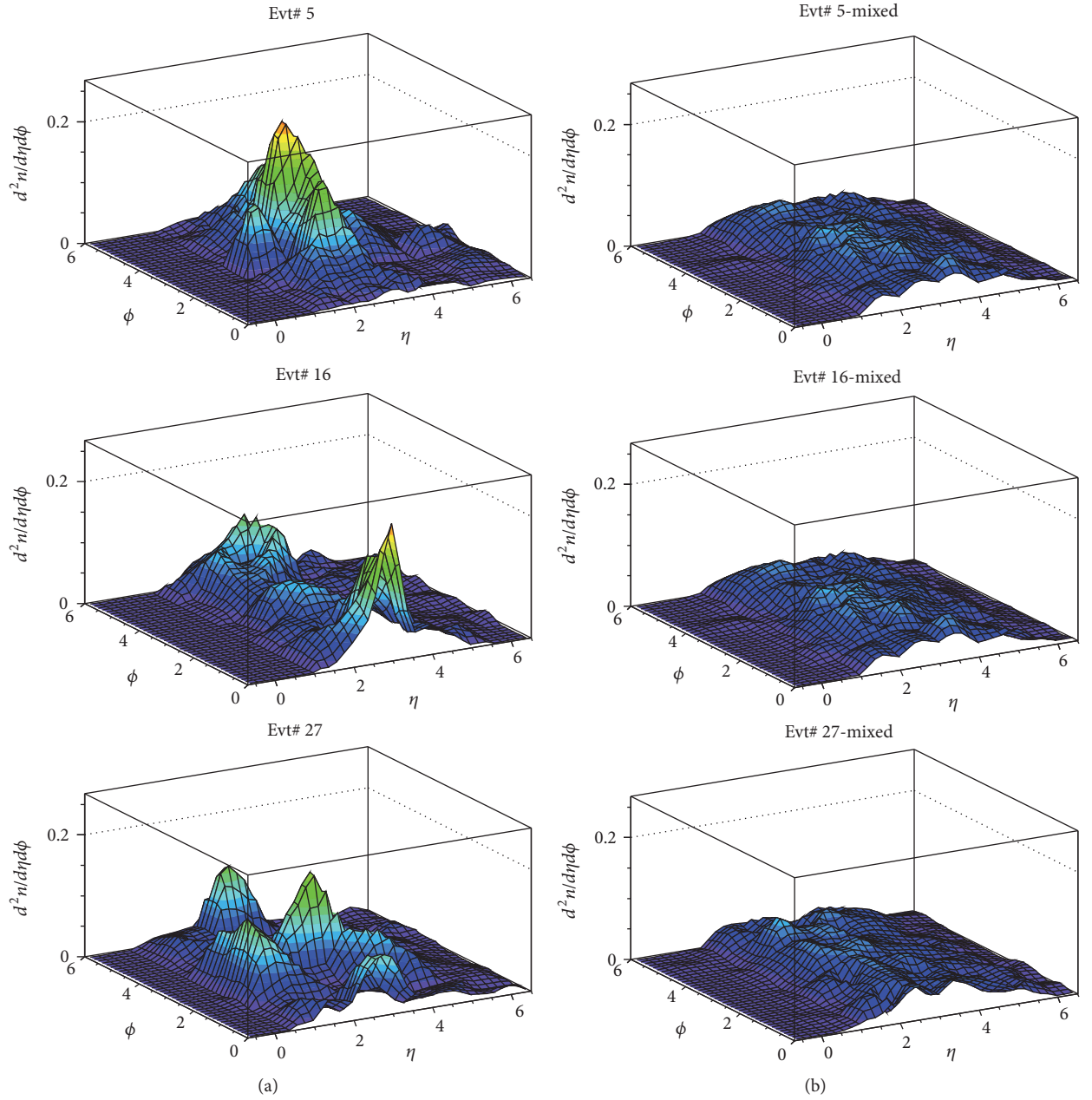

FIGURE 4: Two-dimensional η-ϕ distributions for events # 5, 16, and 27 produced in 158A GeV/c ^{208}Pb-^{208}Pb collisions (a) and corresponding mixed events (b).

distributions of the four "hot" events do exhibit distinct peaks and valleys while the fifth event (the "cold" event) shows no such spikes and the distributions of these events match with those obtained from the corresponding mixed events. It may also be noted from the figure that the particle densities in the spiky regions are larger than the expected average values by a factor of ~2.

2.3. Two-Particle Correlations. Studies involving multiparticle correlations are widely accepted as a tool to search for the occurrence of phase transition in relativistic AA collisions [42, 43]. The presence of the correlations among emitted particles guides us towards the fluctuation occurring in the observables during the phase transition. It has been reported [43, 44] that the inclusive two-particle correlations have two components: the direct two-particle correlations conventionally referred to as the short-range correlations (SRC) and the effective long-range correlations (LRC). The strong SRC have been reported to be present in several investigations [42–44]. These correlations have been reported to remain confined to a region, $\eta \pm 1$ units around mid-rapidity. Their properties have been explored by the concept of clustering

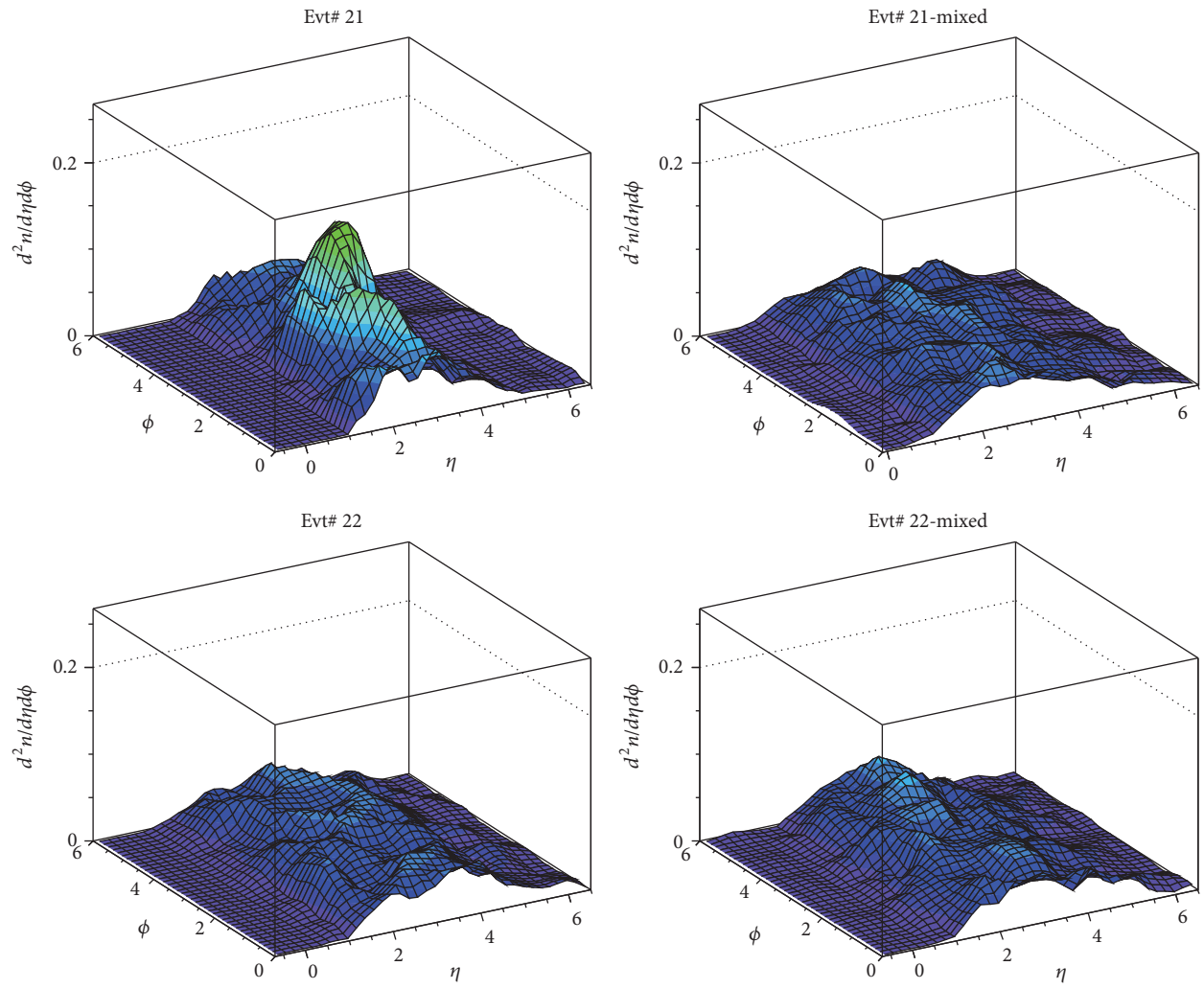

FIGURE 5: The same plots as in Figure 4 but for Evts# 21 and 22.

[44]. LRC, on the other hand, arise due to ebe fluctuations of overall multiplicity and are expected [43, 44] to extend over a relatively longer range (>2 units of η). The idea of particle production through the formation of clusters, rather than the independent emission, has been widely adopted in describing the various features of particle production [44, 45]. It is widely accepted that the SRC arise due to the tendency of hadrons to be grouped in clusters, which are formed during the intermediate stage of the collision. The clusters formed are independently emitted according to a dynamically generated distribution in η and ϕ and then decay isotropically in their own rest frame into the real physical particles [43, 44] finally measured in the detectors. The observed two-particle correlations would permit disentangling different correlation sources which can be directly connected to the phenomena like collective flow, jets, resonance decays, and so forth [46].

Two-particle angular correlations in η and ϕ spaces were first studied by ACM Collaboration at ISR energies [47]. It was observed that the dominant contribution to the correlation comes from the two- and three-body decay of resonances (η, ρ^0, ω). Two structures were discovered: (i) an enhancement near $\Delta\phi = \pi$ (away-side) explained by the two-body decay scenario and (ii) the enhancement at $\Delta\phi \simeq 0$ together with an azimuthal ridge (centred at $\Delta\eta = 0$) consistent with three-body decays. These features were, later on, confirmed by PHOBOS Collaboration [44]. Fluctuations observed in the physically measurable quantities provide us indirect measure of the width of the two particle densities. Thus, these are quite useful in providing us with additional information in comparison to those obtained by studying their averages. Besides this, a significant contribution to the two-particle correlations comes from the collective effects. They appear as a modulation in $\Delta\phi$ and are usually searched for in high multiplicity events [46, 48]. An attempt is, therefore, made to study the two-particle correlations in individual events exhibiting large fluctuations in their η and ϕ distributions which have been sorted out as discussed in the previous sections. The findings are compared with the corresponding mixed events which would help in extracting the contributions present due to the dynamical reasons.

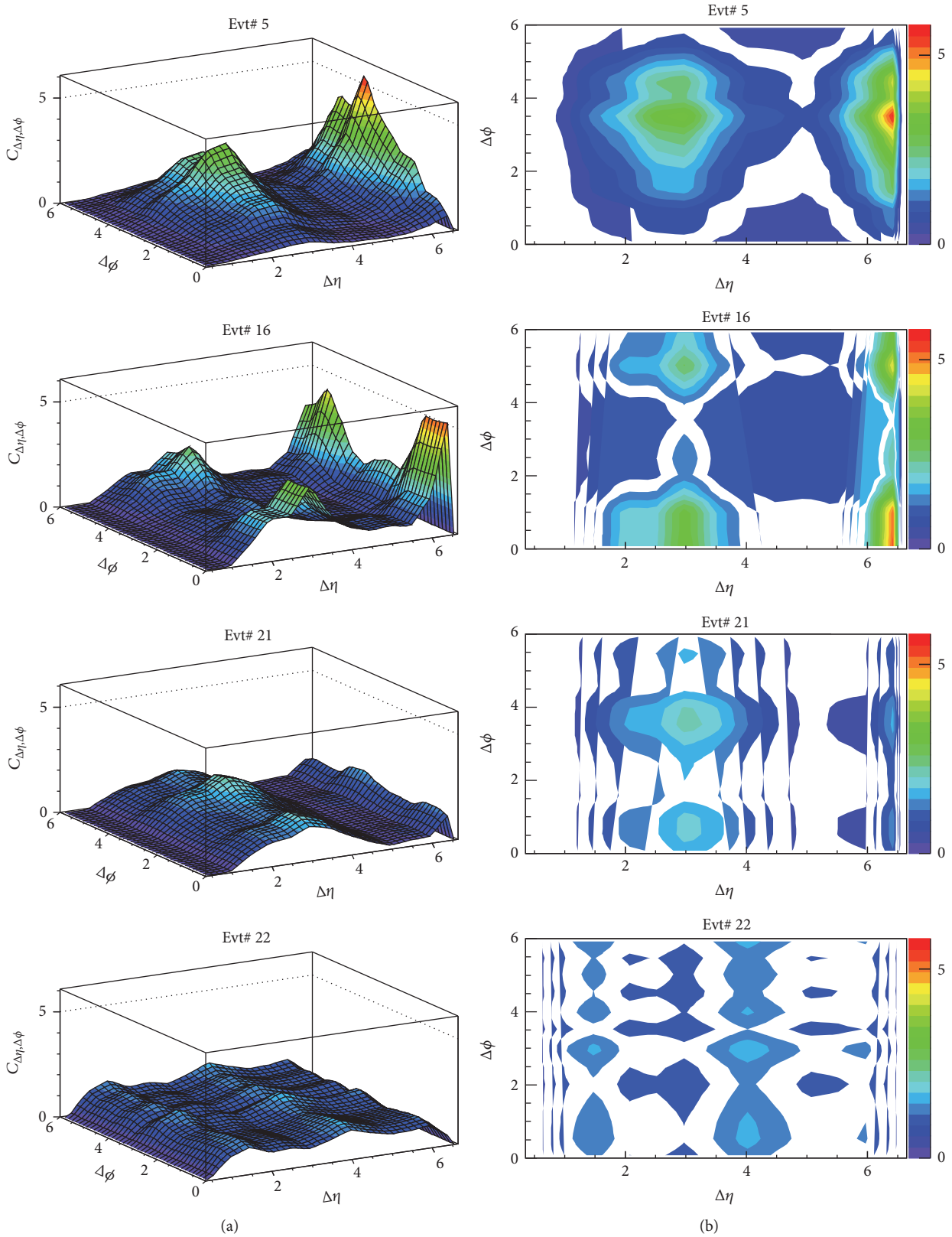

FIGURE 6: Correlation function $C(\Delta\eta, \Delta\phi)$ for Evts# 5, 16, 21, and 22 produced in ^{208}Pb-^{208}Pb collisions at 158A GeV/c. The plots shown in (b) are the contour plots corresponding to those shown in (a).

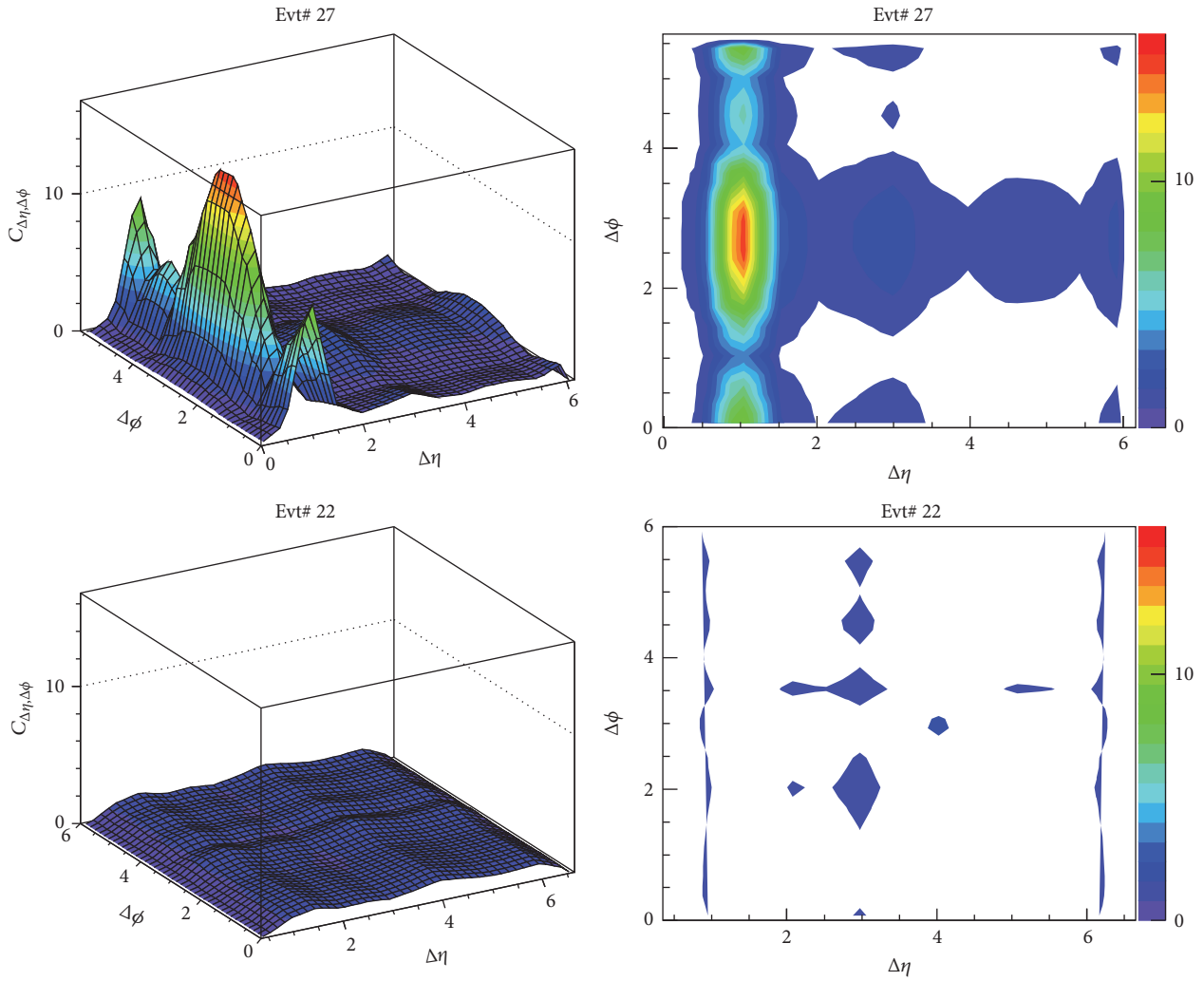

FIGURE 7: Same plot as in Figure 6 but for Evts# 22 and 27: results from Evt# 22, shown in Figure 6, are replotted here but on z-scale, different from that in Figure 6, for comparison with Evts# 27.

Two-particle correlations are generally studied in terms of the differences in η and ϕ values between the two particles produced in the same event [46].

$$\Delta\eta = |\eta_1 - \eta_2|, \qquad \Delta\phi = |\phi_1 - \phi_2|. \tag{2}$$

The correlation function $C(\Delta\eta, \Delta\phi)$ is defined and calculated as follows:

$$C(\Delta\eta, \Delta\phi) = \frac{N^{\text{pair}}_{\text{mixed}} \rho^{\text{II}}_d(\Delta\eta, \Delta\phi)}{N^{\text{pair}}_{\text{data}} \rho^{\text{II}}_m(\Delta\eta, \Delta\phi)} \tag{3}$$

$$\text{where, } \rho^{\text{II}}_d(\Delta\eta, \Delta\phi) = \frac{d^2 N_{\text{data}}}{d\Delta\eta d\Delta\phi}, \ \rho^{\text{II}}_m = \frac{d^2 N_{\text{mixed}}}{d\Delta\eta d\Delta\phi}$$

being the distributions of pairs of particles from the data and mixed events, respectively. $\rho^{\text{II}}(\Delta\eta, \Delta\phi)$ distributions for the data and mixed event were generated by counting the number of pairs in the intervals $\Delta\eta$ and $\Delta\phi$. For evaluating $C(\Delta\eta, \Delta\phi)$, the distributions for the data/mixed events were normalized to the number of pairs ($N^{\text{pair}}_{\text{data}}$ or $N^{\text{pair}}_{\text{mixed}}$). The calculations are performed considering the charged particles of each event having ϕ values lying in the interval $0 < \phi < 2\pi$ and η values lying in the range $|\eta| \leq \eta_c \pm 3.0$, η_c being the centre of symmetry of the η distribution.

The correlation function $C(\Delta\eta, \Delta\phi)$ is estimated for the five events selected on the basis of the criteria discussed in the previous section and are plotted in Figures 6 and 7; the different scales of z-axis be noted for the plots for Evts# 5, 16, 21, and 22 shown in Figure 6 and that for Evts# 27 and 22, displayed in Figure 7. The correlation function for Evt# 22 (the "cold" event) is plotted in both the figures on different Z-scales of "hot" events for comparison's sake. The difference is noticeable due to the different z-scales chosen in the two figures. The z-scales in the two figures are kept the same as that for the other events in the figure so that the fluctuations in

the hot and cold events can be clearly reflected. The following references may be drawn from Figures 6 and 7:

(1) In the "cold" event (Evt# 22), shown in the bottom panel of the figures, presence of two-particle correlations is noticed in the region of $\Delta\eta$ ($\eta_c \pm 2$) and throughout the ϕ region considered. This indicates the presence of two-particle correlations in ^{208}Pb-^{208}Pb collisions at 158A GeV/c.

(2) Evt# 21 shows few distinct peaks around η_c (~3.5) which spreads in considerable range of ϕ. It is interesting to mention that the F_2 values of this event are significantly large in the η-space while in the ϕ-space its F_2 values are not so large and compare well with the event averaged values (Figure 2).

(3) Evts# 5 and 16 exhibit some distinct peaks at $\Delta\eta \sim$ 1.5 and 3.5 and 6.0. The magnitude of correlation, $C(\Delta\eta, \Delta\phi)$, in these regions is as large as ~6.

(4) Evt# 27 at $\Delta\eta \sim 1.0$ gives very prominent peaks where the magnitude of correlations function is as high as ~16.

(5) The F_2 values of the Evts# 5, 16, and 27 which exhibit strong two-particle correlations may also be noted to be quite large in η, ϕ, and η-ϕ spaces. These events have been noticed to show dominant peaks and valleys in their η and ϕ distributions too.

3. Summary

In the present article, we have studied the fluctuation observables relevant to investigation of ^{208}Pb-^{208}Pb collisions at 158A GeV/c. Intermittency or factorial moment analysis applied to individual high multiplicity events may be used to identify events with densely populated narrow phase space regions. The four events selected on the basis of their F_2 values are found to exhibit large fluctuations in η and ϕ distributions and exhibit strong two-particle correlations. The magnitude of the correlation function in few of the events appears to be as high as ~16. These observations give clear indication that if the system created during the collision has undergone phase transition, the associated fluctuation observables can be reliably analyzed on the basis of SFMs value. The result of the present analysis thus suggests that if the system formed during the collision has undergone the phase transition, the associated events identified on the basis of their SFMs values can be analyzed individually in detail which may lead to drawing some interesting conclusions.

Conflicts of Interest

The authors declare that there are no conflicts of interest.

References

[1] S. Shakeel Ahmad, M. M. Khan, S. Khan, A. Khatun, and M. Irfan, "A study of event-by-event fluctuations in relativistic heavy-ion collisions," *International Journal of Modern Physics E*, vol. 23, no. 11, Article ID 1450065, 18 pages, 2014.

[2] S. A. Voloshin, V. Koch, and H. G. Ritter, "Event-by-event fluctuations in collective quantities," *Physical Review C: Nuclear Physics*, vol. 60, no. 2, Article ID 024901, 1999.

[3] M. Döring and V. Koch, "Event-by-event fluctuations in heavy ion collisions," *Acta Physica Polonica B*, vol. 33, no. 6, pp. 1495–1504, 2002.

[4] L. D. Landau and E. M. Lifshitz, *Statistical Physics*, Pergamon Press, 1958.

[5] E. Shuryak, "Quark–gluon plasma—new frontiers," *Journal of Physics G: Nuclear and Particle Physics*, vol. 35, no. 10, Article ID 104044, 2008.

[6] H. van Hees, V. Greco, and R. Rapp, "Heavy-quark probes of the quark-gluon plasma and interpretation of recent data taken at the BNL Relativistic Heavy Ion Collider," *Physical Review C: Nuclear Physics*, vol. 73, no. 3, Article ID 034913, 2006.

[7] K. Adcox and PHENIX Collaboration, "Event-by-event fluctuations in mean p_T and mean e_T in $\sqrt{s_{NN}}$ = 130 GeV Au + Au collisions," *Physical Review C: Nuclear Physics*, vol. 66, no. 2, Article ID 024901, 2002.

[8] S. Ahmad, A. Ahmad, A. Chandra, M. Zafar, and M. Irfan, "Forward–backward multiplicity fluctuations in 200A GeV/c ^{16}O–AgBr and ^{32}S–AgBr collisions," *Physica Scripta*, vol. 87, no. 4, Article ID 045201, 2013.

[9] S. S. Adler and PHENIX Collaboration, "Measurement of nonrandom event-by-event fluctuations of average transverse momentum in $\sqrt{s_{NN}}$ = 200 GeV Au+Au and $p + p$ collisions," *Physical Review Letters*, vol. 93, no. 9, Article ID 092301, pp. 22–29, 2004.

[10] D. Adamová, G. Agakichiev, H. Appelshäuser, V. Belaga, P. Braun-Munzinger et al., "Event-by-event fluctuations of the mean transverse momentum in 40, 80, and 158 A GeV/c Pb Au collisions," *Nuclear Physics A*, vol. 727, no. 1-2, pp. 97–119, 2003.

[11] F. Jinghua and L. Lianshou, "Extracting event dynamics from event-by-event analysis," *Physical Review C*, vol. 68, no. 6, Article ID 064904, 2003.

[12] L. Lianshou and F. Jinghua, "A Comparison of different measures for dynamical event-mean transverse momentum fluctuation," 2004, https://arxiv.org/abs/hep-ph/0401129.

[13] C. Alt, T. Anticic, and B. Baatar, "Energy dependence of ϕ meson production in central Pb + Pb collisions at $\sqrt{s_{NN}}$ = 6 to 17 GeV," *Physical Review C: Nuclear Physics*, vol. 78, no. 4, Article ID 044907, 2008.

[14] S. Bhattacharyya, *Phys. Rev. Lett. B*, vol. 726, Article ID 1350066, 2013.

[15] M. L. Cherry, A. Dabrowska, P. Deines-Jones et al., "Event-by-event analysis of high multiplicity Pb (158-GeV/nucleon) Ag/Br collisions," *Acta Physica Polonica B*, vol. 29, no. 8, pp. 2129–2146, 1998.

[16] S. Ahmad, A. Chandra, A. Kumar et al., "Event-by-event analysis of high-multiplicity events produced in 158 A GeV/c ^{208}Pb-^{208}Pb collisions," *Europhysics Letters*, vol. 112, no. 4, Article ID 42001, 2015.

[17] T. Anticic and NA49 Collaboration, "Search for the QCD critical point in nuclear collisions at 158A GeV at the CERN Super Proton Synchrotron (SPS)," *Physical Review C*, vol. 81, no. 6, 2010.

[18] A. Bialas and B. Ziaja, "Intermittency in a single event," *Physics Letters B*, vol. 378, no. 1-4, pp. 319–322, 1996.

[19] S. Mrowczynski, "Overview of event-by-event fluctuations," *Acta Physica Polonica B*, vol. 40, pp. 1053–1074, 2009.

[20] L. Lianshou, "Single event 2-dimensional factorial moment analysis of ^{197}Au-emulsion data from EMU01 experiment," *Nuclear Physics B - Proceedings Supplements*, vol. 71, no. 1-3, pp. 341–345, 1999.

[21] K. Fialkowski and R. Wit, "Entropy in cluster analysis of single events in heavy ion collisions," *Acta Physica Polonica B*, vol. 31, pp. 681–686, 2000.

[22] K. Fialkowski and R. Wit, "Event-by-event cluster analysis of final states from heavy ion collisions," *Acta Physica Polonica B*, vol. 30, pp. 2759–2765, 1999.

[23] M. Hauer, V. V. Begun, M. Gaździcki, M. I. Gorenstein, V. P. Konchakovski, and B. Lungwitz, "Multiplicity fluctuations in relativistic nuclear collisions: statistical model versus experimental data," *Journal of Physics G: Nuclear and Particle Physics*, vol. 35, no. 4, Article ID 044064, 2008.

[24] D. Ghosh, A. Deb, P. Mandal, S. Biswas, K. Chattopadhyay et al., "Non-statistical fluctuation of compound multiplicity in nucleus-nucleus interactions: evidence of strong intermittency," *Chinese Physics Letters*, vol. 19, no. 10, pp. 1436–1438, 2002.

[25] S. L. C. Barroso, A. O. deCarvalho, J. A. Chinellato et al., "Analysis of one hadron rich event," in *Proceedings of the XVI International Symposium on Very High Energy Cosmic Ray Interactions*, Batavia, Ill, USA, July 2010.

[26] Y. F. Wu and L. S. Liu, "Low average-transverse-momentum intermittency," *Physics Letters B*, vol. 269, p. 28, 1999.

[27] L. S. Liu, "Single event 2-dimensional factorial moment analysis of ^{197}Au-emulsion data from EMU01 experiment," *Nuclear Physics B - Proceedings Supplements*, vol. 71, no. 1-3, pp. 341–345, 1999.

[28] M. I. Adamovich, M. M. Aggarwal, Y. A. Alexandrov et al., "Produced particle multiplicity dependence on centrality in nucleus - nucleus collisions," *Journal of Physics G: Nuclear and Particle Physics*, vol. 22, no. 10, p. 1469, 1996.

[29] M. I. Adamovich, M. M. Aggarwal, N. P. Andreeva et al., "Rapidity densities and their fluctuations in central 200 *A* GeV ^{32}S interactions with Au and Ag, Br nuclei EMU01 collaboration," *Physical Letters B*, vol. 227, no. 2, pp. 285–290, 1989.

[30] M. I. Adamovich, M. M. Aggarwal, Y. A. Alexandrov et al., "Scaled-factorial-moment analysis of 200A-GeV sulfur + gold interactions," *Physical Review Letters*, vol. 65, article 412, 1990.

[31] M. I. Adamovich, Y. A. Alexandrov, and S. A. Asimov, "Multiplicities and rapidity densities in 200 AGeV^{16}O interactions with emulsion nuclei," *Physics Letters B*, vol. 201, no. 3, pp. 397–402, 1988.

[32] M. I. Adamovich, M. M. Aggarwal, Y. A. Alexandrov et al., "On the systematic behaviour of the intermittency-indices in nuclear interactions," *Physics Letters B*, vol. 263, no. 3-4, pp. 539–543, 1991.

[33] A. Bialas and R. Peschanski, "Moments of rapidity distributions as a measure of short-range fluctuations in high-energy collisions," *Nuclear Physics B*, vol. 273, no. 3-4, pp. 703–718, 1986.

[34] V. Azhinenko, Y. A. Belokopytov, H. Böttcher et al., "Intermittency patterns in $\pi^+ p$ and $K^+ p$ collisions at 250 GeV/c," *Physics Letters B*, vol. 222, no. 2, pp. 306-210, 1989.

[35] R. Holynski, A. Jurak, A. Olszewski, and B. Wilczynska, "Evidence for intermittent patterns of fluctuations in particle production in high-energy interactions in nuclear emulsion," *Physical Review Letters*, vol. 62, article 733, 1989.

[36] E. A. De Wolf, I. M. Dremin, and W. Kittel, "Scaling laws for density correlations and fluctuations in multiparticle dynamics," *Physics Reports*, vol. 270, no. 1-2, pp. 1–141, 1996.

[37] S. Ahmad, M. M. Khan, N. Ahmad, and A. Ahmad, "Erraticity behaviour in relativistic nucleus-nucleus collisions," *Journal of Physics G: Nuclear and Particle Physics*, vol. 30, no. 9, pp. 1145–1152, 2004.

[38] S. Ahmad, M. M. Khan, N. Ahmad, A. R. Khan, M. Zafar, and M. Irfan, "Erratic fluctuations in 14.5A GeV/c ^{28}Si–AgBr Collisions," *Acta Physica Hungarica Series A, Heavy Ion Physics*, vol. 25, no. 1, pp. 105–115, 2006.

[39] R. C. Hwa, "Beyond intermittency: erraticity," *Acta Phys. Pol B*, vol. 27, p. 1789, 1996.

[40] B. Wosiek, "Review of experimental results on intermittency," *Acta Phys. Slov*, vol. 46, no. 4, p. 531, 1996.

[41] A. Bialas and R. Peschanski, "Intermittency in multiparticle production at high energy," *Nuclear Physics B*, vol. 308, no. 4, pp. 857–867, 1988.

[42] B. I. Abelev, M. M. Aggarwal, Z. Ahammed et al., "Growth of long range forward-backward multiplicity correlations with centrality in Au + Au Collisions at $\sqrt{s_{NN}}$ = 200 GeV," *Physical Review Letters*, vol. 103, Article ID 172301, 2009.

[43] S. Ahmad, A. Chandra, M. Zafar et al., "Short- and long-range multiplicity correlations in relativistic heavy-ion collisions," *International Journal of Modern Physics E*, vol. 22, no. 9, Article ID 1350066, 2013.

[44] B. Alver, B. B. Back, M. D. Baker et al., "Cluster properties from two-particle angular correlations in $p+p$ collisions at $\sqrt{s}$ = 200 and 410 GeV," *Physical Review C*, vol. 75, Article ID 054913, 2007.

[45] UA5 Collaboration, R. E. Ansorge, B. Åsman, C. N. Booth, L. Burow et al., "Charged particle correlations in $\overline{p}p$ collisions at c.m. energies of 200, 546 and 900 GeV," *Zeitschrift für Physik C Particles and Fields*, vol. 37, no. 2, pp. 191–213, 1988.

[46] A. Aduszkiewicz, Y. Ali, E. Andronov, T. Antićić, N. Antoniou et al., "Two-particle correlations in azimuthal angle and pseudorapidity in inelastic p + p interactions at the CERN Super Proton Synchrotron," *The European Physical Journal C*, vol. 77, article 59, 2017.

[47] K. Eggert, H. Frenzel, W. Thomé et al., "Angular correlations between the charged particles produced in pp collisions at ISR energies," *Nuclear Physics B*, vol. 86, no. 2, pp. 201–215, 1975.

[48] G. Agakishiev, M. M. Aggarwal, Z. Ahammed et al., "Anomalous centrality evolution of two-particle angular correlations from Au-Au collisions at $\sqrt{s_{NN}}$ = 62 and 200 GeV," *Physical Review C: Nuclear Physics*, vol. 86, Article ID 064902, 2012.

Hindawi
Advances in High Energy Physics
Volume 2018, Article ID 7682325, 9 pages
https://doi.org/10.1155/2018/7682325

Research Article

A Description of the Transverse Momentum Distributions of Charged Particles Produced in Heavy Ion Collisions at RHIC and LHC Energies

Jia-Qi Hui, Zhi-Jin Jiang, and Dong-Fang Xu

College of Science, University of Shanghai for Science and Technology, Shanghai 200093, China

Correspondence should be addressed to Zhi-Jin Jiang; jzj265@163.com

Received 5 November 2017; Revised 27 January 2018; Accepted 6 March 2018; Published 8 April 2018

Academic Editor: Bhartendu K. Singh

By assuming the existence of memory effects and long-range interactions, nonextensive statistics together with relativistic hydrodynamics including phase transition are used to discuss the transverse momentum distributions of charged particles produced in heavy ion collisions. It is shown that the combined contributions from nonextensive statistics and hydrodynamics can give a good description of the experimental data in Au+Au collisions at $\sqrt{s_{NN}} = 200$ GeV and in Pb+Pb collisions at $\sqrt{s_{NN}} = 2.76$ TeV for $\pi^{\pm}$ and $K^{\pm}$ in the whole measured transverse momentum region and for $p(\overline{p})$ in the region of $p_T \leq 2.0$ GeV/c. This is different from our previous work using the conventional statistics plus hydrodynamics, where the describable region is only limited in $p_T \leq 1.1$ GeV/c.

1. Introduction

The primary goals of the experimental programs performed in high energy heavy ion collisions are to find the deconfined nuclear matter, namely, the quark-gluon plasma (QGP), which is believed to have filled in the early universe several microseconds after the Big Bang. Therefore, studying the properties of QGP is important for both particle physics and cosmology. In the past decade, a number of bulk observables about charged particles, such as the Fourier coefficients v_n of azimuth-angle distributions [1, 2], transverse momentum spectra [3–8], and pseudorapidity distributions [9–12], have been extensively studied in nuclear collisions at both RHIC and LHC energies. These investigations have shown that the matter created in these collisions is in the state of strongly coupled quark-gluon plasma (sQGP), exhibiting a clear collective behavior nearly like a perfect fluid with very low viscosity [13–31]. Therefore, the space-time evolution of sQGP can be described in the scope of relativistic hydrodynamics, which connects the static aspects of sQGP properties and the dynamical aspects of heavy ion collisions [32].

In our previous work [33], by considering the effects of thermalization, we once used a hydrodynamic model incorporating phase transition in analyzing the transverse momentum distributions of identified charged particles produced in heavy ion collisions. In that model, the quanta of hot and dense matter are supposed to obey the standard statistical distributions and the experimental measurements in Au+Au collisions at $\sqrt{s_{NN}} = 200$ and 130 GeV can be well matched up in the region of $p_T \leq 1.1$ GeV/c. Known from the investigations in [34, 35], the memory effects and long-range interactions might appear in the hot and dense matter. This guarantees the reasonableness of nonextensive statistics in describing the thermal motions of quanta of hot and dense matter, since this new statistics is just suitable for the thermodynamic system including memory effects and long-range interactions. Hence, in this paper, on the basis of hydrodynamics taking phase transition into consideration, we will use nonextensive statistics instead of conventional statistics to simulate the transverse collective flow of the matter created in collisions.

The nonextensive statistics are also known as Tsallis nonextensive thermostatistics, which were first proposed by Tsallis in 1988 in his pioneering work [36]. This statistical theory overcomes the shortcomings of the conventional statistics in many physical problems with long-range interactions, memory effects, or fractal space-time constrains [34]. It has a wide range of applications in high energy physics [37–39], astrophysical self-gravitating systems [40], cosmology [41], the solar neutrino problem [42], many-body theory, dynamical linear response theory, and variational methods [43].

In Section 2, a brief description is given on the employed hydrodynamics, presenting its analytical solutions. The solutions are then used in Section 3 to formulate the transverse momentum distributions of charged particles produced in heavy ion collisions in the light of nonextensive statistics and Cooper-Frye prescription. The last section is about conclusions.

2. A Brief Introduction to the Hydrodynamic Model

The key points of the hydrodynamic model [18] used in the present paper are as follows.

The expansions of fluid follow the continuity equation

$$\frac{\partial T^{\mu\nu}}{\partial x^{\nu}} = 0, \quad \mu, \nu = 0, 1, \tag{1}$$

where $x^{\nu} = (x^0, x^1) = (t, z)$ and

$$T^{\mu\nu} = (\varepsilon + p)\, u^{\mu} u^{\nu} - p g^{\mu\nu} \tag{2}$$

is the energy-momentum tensor of perfect fluid, where $g^{\mu\nu} = \mathrm{diag}(1, -1)$ is the metric tensor and $u^{\mu} = (u^0, u^1) = (\cosh y_F, \sinh y_F)$ is the four-velocity of fluid with rapidity y_F. The energy density ε and the pressure p of fluid are related by the sound speed c_s via the equation of state

$$\frac{dp}{d\varepsilon} = \frac{s dT}{T ds} = c_s^2, \tag{3}$$

where T is the temperature and s is the entropy density of fluid.

Projecting (1) to the direction of u_{μ} gives

$$\frac{\partial (s u^{\nu})}{\partial x^{\nu}} = 0, \tag{4}$$

which is the continuity equation for entropy conservation. Projecting (1) to the direction Lorentz perpendicular to u_{μ} leads to the following equation:

$$\frac{\partial (T \sinh y_F)}{\partial t} + \frac{\partial (T \cosh y_F)}{\partial z} = 0, \tag{5}$$

which means the existence of scalar function ϕ satisfying

$$\begin{aligned} \frac{\partial \phi}{\partial t} &= T \cosh y_F, \\ \frac{\partial \phi}{\partial z} &= -T \sinh y_F. \end{aligned} \tag{6}$$

From ϕ and Legendre transformation, Khalatnikov potential χ is introduced by

$$\chi = \phi - tT \cosh y_F + zT \sinh y_F, \tag{7}$$

which makes the coordinates of (t, z) transform to

$$\begin{aligned} t &= \frac{e^{\omega}}{T_0} \left(\frac{\partial \chi}{\partial \omega} \cosh y_F + \frac{\partial \chi}{\partial y_F} \sinh y_F \right), \\ z &= \frac{e^{\omega}}{T_0} \left(\frac{\partial \chi}{\partial \omega} \sinh y_F + \frac{\partial \chi}{\partial y_F} \cosh y_F \right), \end{aligned} \tag{8}$$

where T_0 is the initial temperature of fluid and $\omega = \ln(T_0/T)$. In terms of χ, (4) can be rewritten as the so-called telegraphy equation:

$$\frac{\partial^2 \chi}{\partial \omega^2} - 2\beta \frac{\partial \chi}{\partial \omega} - \frac{1}{c_s^2} \frac{\partial^2 \chi}{\partial y_F^2} = 0, \quad \beta = \frac{1 - c_s^2}{2c_s^2}. \tag{9}$$

With the expansions of created matter, its temperature becomes lower and lower. When the temperature reduces from initial temperature T_0 to the critical temperature T_c, the matter transforms from the sQGP state to the hadronic state. The produced hadrons are initially in the violent and frequent collisions, which are mainly inelastic. Hence, the abundance of identified hadrons is constantly changing. Furthermore, the mean free paths of these primary hadrons are very short. In sQGP, $c_s = c_0 = 1/\sqrt{3}$. The evolution of them still satisfies (9) with only difference being the values of c_s. In the hadronic state, $0 < c_s = c_h \leq c_0$. At the point of phase transition, c_s is discontinuous.

The solutions of (9) for the sQGP and hadronic state are, respectively [18],

$$\chi_0(\omega, y_F) = \frac{Q_0 c_0}{2} e^{\beta_0 \omega} I_0 \left(\beta_0 \sqrt{\omega^2 - c_0^2 y_F^2} \right), \tag{10}$$

$$\begin{aligned} &\chi_h(\omega, y_F) \\ &\quad = \frac{Q_0 c_0}{2} e^{\beta_h (\omega - \omega_c) + \beta_0 \omega_c} I_0 \left(\beta_h c_h \sqrt{y_h^2(\omega) - y_F^2} \right), \end{aligned} \tag{11}$$

where Q_0 is a constant determined by fitting the theoretical results with experimental data, I_0 is the 0th-order modified Bessel function, and

$$\begin{aligned} \beta_0 &= \frac{\left(1 - c_0^2\right)}{2c_0^2} = 1, \\ \beta_h &= \frac{\left(1 - c_h^2\right)}{2c_h^2}, \\ \omega_c &= \ln\left(\frac{T_0}{T_c}\right), \\ y_h(\omega) &= \left[\frac{(\omega - \omega_c)}{c_h} \right] + \left(\frac{\omega_c}{c_0} \right). \end{aligned} \tag{12}$$

3. The Transverse Momentum Distributions of Charged Particles Produced in Heavy Ion Collisions

3.1. The Energy of Quantum of Produced Matter. In the nonextensive statistics, there are two basic postulations [36, 40].

(a) The entropy of a statistical system possesses the form of

$$s_q = \frac{1}{q-1}\sum_{i=1}^{\Omega} p_i\left(1 - p_i^{q-1}\right), \tag{13}$$

where p_i is the probability of a given microstate among Ω different ones and q is a real parameter.

(b) The mean value of an observable O is given by

$$\overline{O}_q = \sum_{i=1}^{\Omega} p_i^q O_i, \tag{14}$$

where O_i is the value of an observable O in the microstate i.

From the above two postulations, the average occupational number of the quantum in the state with temperature T can be written in a simple analytical form [44]:

$$\overline{n}_q = \frac{1}{\left[1 + (q-1)(E-\mu_B)/T\right]^{1/(q-1)} + \delta}, \tag{15}$$

where E is the energy of quantum and μ_B is its baryochemical potential. $\delta = 1$ for fermions, and $\delta = -1$ for bosons. In the limit of $q \to 1$, it reduces to the conventional Fermi-Dirac or Bose-Einstein distributions. Hence, the value of q reflects the discrepancies of nonextensive statistics from the conventional ones. Known from (15), the average energy of quantum in the state with temperature T reads

$$\overline{E}_q = \frac{m_T \cosh(y - y_F)}{\left[1 + (q-1)(m_T \cosh(y - y_F) - \mu_B)/T\right]^{1/(q-1)} + \delta}, \tag{16}$$

where y is the rapidity of quantum and $m_T = \sqrt{p_T^2 + m^2}$ is its transverse mass with rest mass m and transverse momentum p_T.

3.2. The Rapidity Distributions of Charged Particles in the State of Fluid. In terms of Khalatnikov potential χ, the rapidity distributions of charged particles in the state of fluid can be written as [45]

$$\frac{dN}{dy_F} = \frac{Q_0 c_0}{2} A(b)\left(\cosh y \frac{dz}{dy_F} - \sinh y \frac{dt}{dy_F}\right), \tag{17}$$

where

$$A(b) = 2r^2 \arccos\frac{b}{2r} - b\sqrt{r^2 - \left(\frac{b}{2}\right)^2} \tag{18}$$

is the area of overlap region of collisions, b is impact parameter, and r is the radius of colliding nucleus. From (8), the expression in the round brackets in (17) becomes

$$\begin{aligned}\cosh y \frac{dz}{dy_F} - \sinh y \frac{dt}{dy_F} &= \frac{1}{T} c_s^2 \frac{\partial}{\partial \omega}\left(\chi + \frac{\partial \chi}{\partial \omega}\right)\cosh(y - y_F) \\ &\quad - \frac{1}{T}\frac{\partial}{\partial y_F}\left(\chi + \frac{\partial \chi}{\partial \omega}\right)\sinh(y - y_F).\end{aligned} \tag{19}$$

3.3. The Transverse Momentum Distributions of Charged Particles Produced in Heavy Ion Collisions. Along with the expansions of hadronic matter, its temperature becomes even lower. As the temperature drops to kinetic freeze-out temperature T_f, the inelastic collisions among hadronic matter stop. The yields of identified hadrons remain unchanged, becoming the measured results. According to Cooper-Frye scheme [45], the invariant multiplicity distributions of charged particles take the form [18, 45, 46]

$$\frac{d^2N}{2\pi p_T dy dp_T} = \frac{1}{(2\pi)^3}\int_{-y_h(\omega_f)}^{y_h(\omega_f)}\left(\frac{dN}{dy_F}\overline{E}_q\right)\Big|_{T=T_f} dy_F, \tag{20}$$

where $\omega_f = \ln(T_0/T_f)$ and the integrand takes values at the moment of $T = T_f$.

Substituting χ in (19) by χ_h of (11), it becomes

$$\begin{aligned}\left(\cosh y \frac{dz}{dy_F} - \sinh y \frac{dt}{dy_F}\right)\Big|_{T=T_f} &= \frac{1}{T_f}(\beta_h c_h)^2 \\ &\cdot e^{\beta_h(\omega-\omega_c)+\beta_0\omega_c}\left[B(\omega_f, y_F)\sinh(y - y_F)\right. \\ &\left. + C(\omega_f, y_F)\cosh(y - y_F)\right],\end{aligned} \tag{21}$$

where

$$\begin{aligned}B(\omega_f, y_F) &= \frac{\beta_h y_F}{\lambda(\omega_f, y_F)}\left\{\frac{\beta_h c_h y_h(\omega_f)}{\lambda(\omega_f, y_F)} I_0\left[\lambda(\omega_f, y_F)\right]\right. \\ &\left. + \left[\frac{\beta_h + 1}{\beta_h} - \frac{2\beta_h c_h y_h(\omega_f)}{\lambda^2(\omega_f, y_F)}\right] I_1\left[\lambda(\omega_f, y_F)\right]\right\}, \\ C(\omega_f, y_F) &= \left\{\frac{\beta_h + 1}{\beta_h} + \frac{\left[\beta_h c_h y_h(\omega_f)\right]^2}{\lambda^2(\omega_f, y_F)}\right\} \\ &\cdot I_0\left[\lambda(\omega_f, y_F)\right] + \frac{1}{\lambda(\omega_f, y_F)}\left\{\frac{y_h(\omega_f)}{c_h} + 1\right. \\ &\left. - \frac{2\left[\beta_h c_h y_h(\omega_f)\right]^2}{\lambda^2(\omega_f, y_F)}\right\} I_1\left[\lambda(\omega_f, y_F)\right],\end{aligned} \tag{22}$$

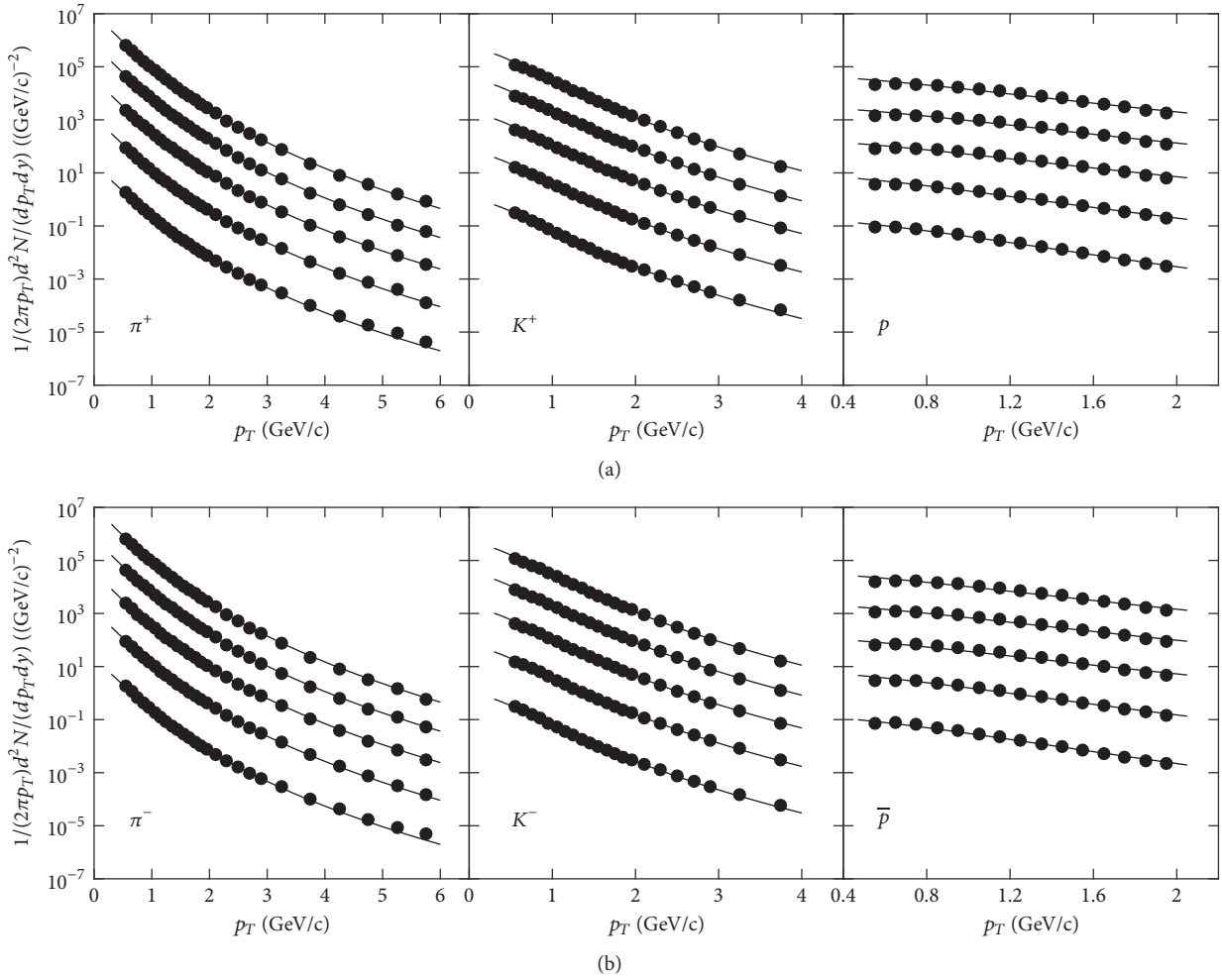

Figure 1: The invariant yields of $\pi^{\pm}$, $K^{\pm}$, and $p(\overline{p})$ as a function of p_T in Au+Au collisions at $\sqrt{s_{NN}} = 200$ GeV. The solid dots represent the experimental data of the PHENIX Collaboration [3]. The solid curves are the results calculated from (20). The centrality cuts counted from top to bottom in each panel are 0–10% ($\times 10^4$), 10–20% ($\times 10^3$), 20–40% ($\times 10^2$), 40–60% ($\times 10^1$), and 60–92% ($\times 10^0$), respectively.

where $\lambda(\omega_f, y_F) = \beta_h c_h \sqrt{y_h^2(\omega_f) - y_F^2}$ and I_1 is the 1st-order modified Bessel function.

By using (17) and (20)–(22), we can obtain the transverse momentum distributions of identified charged particles as shown in Figures 1 and 2.

Figure 1 shows the invariant yields of $\pi^{\pm}$, $K^{\pm}$, and $p(\overline{p})$ as a function of p_T in Au+Au collisions at $\sqrt{s_{NN}} = 200$ GeV. Figure 2 shows the same distributions in Pb+Pb collisions at $\sqrt{s_{NN}} = 2.76$ TeV. The solid dots represent the experimental data [3, 4]. The solid curves are the results calculated from (20). It can be seen that the theoretical results are in good agreement with the experimental data for $\pi^{\pm}$ and $K^{\pm}$ in the whole measured p_T region. For $p(\overline{p})$, the theoretical model works well in the region of $p_T \leq 2.0$ GeV/c. Beyond this region, the deviation appears as shown in Figure 3, which presents the fittings for $p(\overline{p})$ in the most peripheral collisions for p_T up to about 4 GeV/c.

In analyses, the sound speed in hadronic state takes the value of $c_h = 0.35$ [46–49]. The critical temperature takes the value of $T_c = 0.16$ GeV [50]. The kinetic freeze-out temperature T_f takes the values of 0.12 GeV for pions and kaons and 0.13 GeV for protons, respectively, from the investigations of [8], which also shows that the average value of baryochemical potential μ_B is about 0.019 GeV in Au+Au collisions. For Pb+Pb collisions, μ_B takes the value of $\mu_B = 0$ [8]. The initial temperature in central Au+Au and Pb+Pb collisions takes the values of $T_0 = 0.35$ GeV and $T_0 = 0.6$ GeV, respectively [51].

Tables 1 and 2 list the values of T_0, q, Q_0, and χ^2/NDF in different centrality cuts. It can be seen that T_0 decreases with increasing centrality cuts. The value of q, affecting the slopes of curves, is slightly larger than 1 for different kinds of charged particles. It is almost irrelevant to centrality cuts, while it increases with increasing beam energies and the masses of charged particles.

The parameter Q_0 has the same effects as T_0 on curves. They all affect the heights of the curves. The fitted Q_0 in Tables 1 and 2 gives the ratios

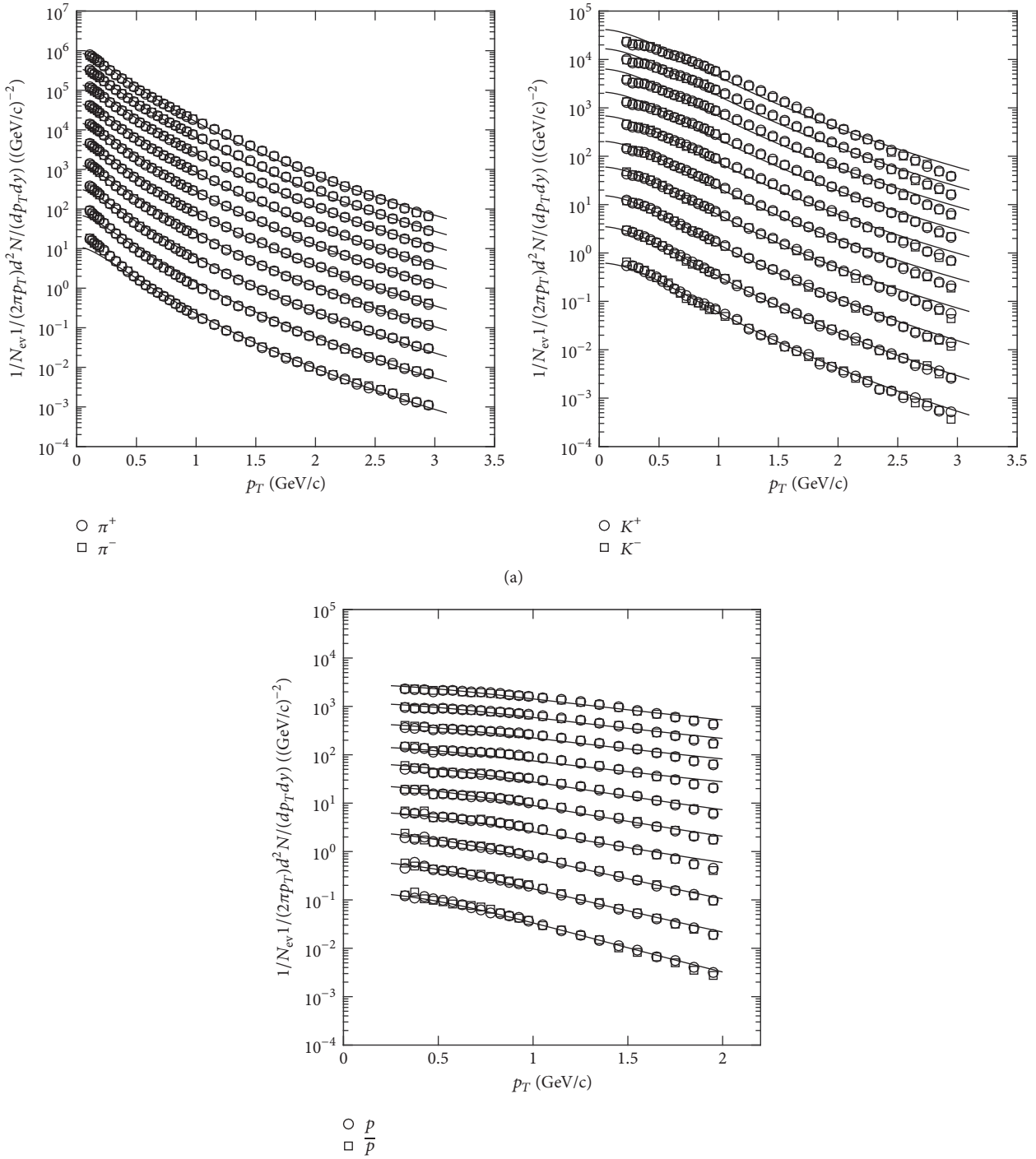

FIGURE 2: The invariant yields of $\pi^{\pm}$, $K^{\pm}$, and $p(\overline{p})$ as a function of p_T in Pb+Pb collisions at $\sqrt{s_{NN}} = 2.76$ TeV. The circles and squares represent the experimental data of the ALICE Collaboration [4]. The solid curves are the results calculated from (20). The centrality cuts counted from top to bottom in each panel are 0–5% ($\times 2^9$), 5–10% ($\times 2^8$), 10–20% ($\times 2^7$), 20–30% ($\times 2^6$), 30–40% ($\times 2^5$), 40–50% ($\times 2^4$), 50–60% ($\times 2^3$), 60–70% ($\times 2^2$), 70–80% ($\times 2^1$), and 80–90% ($\times 2^0$), respectively.

Table 1: The values of T_0, q, and Q_0 in different centrality Au+Au collisions at $\sqrt{s_{NN}} = 200$ GeV.

Centrality cuts	T_0 (GeV)	$q(\pi/K/p)$	$Q_0(\pi^+/\pi^-)$	$Q_0(K^+/K^-)$	$Q_0(p/\overline{p})$	χ^2/NDF
0–10%	0.350 ± 0.001	1.0808 ± 0.00001	0.7953 ± 0.0081	0.3552 ± 0.0043	0.4490 ± 0.0050	25/23
	0.350 ± 0.001	1.0880 ± 0.00004	0.7952 ± 0.0078	0.3315 ± 0.0040	0.3228 ± 0.0040	27/33
	0.350 ± 0.001	1.1012 ± 0.0004				18/14
10–20%	0.349 ± 0.002	1.0822 ± 0.0002	0.7953 ± 0.0112	0.3545 ± 0.0043	0.4494 ± 0.0052	20/17
	0.349 ± 0.001	1.0892 ± 0.0002	0.7965 ± 0.0110	0.3307 ± 0.0041	0.3259 ± 0.0040	21/21
	0.349 ± 0.001	1.1012 ± 0.0004				17/13
20–40%	0.320 ± 0.001	1.0838 ± 0.0002	0.7953 ± 0.0098	0.3514 ± 0.0030	0.4470 ± 0.0036	24/17
	0.320 ± 0.001	1.0904 ± 0.0003	0.8010 ± 0.0060	0.3276 ± 0.0030	0.3274 ± 0.0029	21/18
	0.320 ± 0.001	1.1012 ± 0.0002				31/32
40–60%	0.278 ± 0.001	1.0838 ± 0.0005	0.7953 ± 0.0067	0.3260 ± 0.0031	0.5494 ± 0.0048	19/14
	0.278 ± 0.001	1.0905 ± 0.0005	0.7985 ± 0.0062	0.3053 ± 0.0031	0.4093 ± 0.0038	22/10
	0.278 ± 0.001	1.0912 ± 0.0002				19/27
60–92%	0.210 ± 0.001	1.0854 ± 0.0002	0.7953 ± 0.0100	0.3134 ± 0.0033	0.9299 ± 0.0090	26/32
	0.210 ± 0.001	1.0908 ± 0.0005	0.8040 ± 0.0067	0.2943 ± 0.0032	0.7029 ± 0.0066	28/25
	0.210 ± 0.001	1.0744 ± 0.0002				3.6/9.2

Table 2: The values of T_0, q, and Q_0 in different centrality Pb+Pb collisions at $\sqrt{s_{NN}} = 2.76$ TeV.

Centrality cuts	T_0 (GeV)	$q(\pi/K/p)$	$Q_0(\pi^+/\pi^-)$	$Q_0(K^+/K^-)$	$Q_0(p/\overline{p})$	χ^2/NDF
0–5%	0.60 ± 0.02	1.104 ± 0.001	0.20 ± 0.02	0.050 ± 0.003	0.0069 ± 0.0005	1.88/2.00
	0.60 ± 0.01	1.130 ± 0.003				6.50/5.42
	0.60 ± 0.01	1.260 ± 0.005				2.35/1.50
5–10%	0.59 ± 0.02	1.104 ± 0.001	0.20 ± 0.03	0.051 ± 0.004	0.0073 ± 0.0005	2.46/2.56
	0.59 ± 0.02	1.130 ± 0.005				6.15/5.22
	0.59 ± 0.01	1.260 ± 0.004				2.75/2.15
10–20%	0.58 ± 0.02	1.104 ± 0.001	0.20 ± 0.02	0.048 ± 0.003	0.0068 ± 0.0005	2.21/2.14
	0.58 ± 0.01	1.130 ± 0.004				5.65/4.85
	0.58 ± 0.01	1.260 ± 0.004				3.43/2.79
20–30%	0.54 ± 0.01	1.104 ± 0.001	0.20 ± 0.02	0.048 ± 0.004	0.0069 ± 0.0005	2.19/2.00
	0.54 ± 0.01	1.130 ± 0.004				4.55/3.46
	0.54 ± 0.01	1.260 ± 0.004				4.60/4.08
30–40%	0.50 ± 0.02	1.104 ± 0.002	0.20 ± 0.02	0.047 ± 0.004	0.0156 ± 0.0011	2.69/2.41
	0.50 ± 0.01	1.130 ± 0.003				3.29/2.54
	0.50 ± 0.01	1.200 ± 0.004				2.27/1.87
40–50%	0.45 ± 0.01	1.103 ± 0.001	0.20 ± 0.02	0.046 ± 0.004	0.0221 ± 0.0015	2.68/2.49
	0.45 ± 0.01	1.130 ± 0.003				2.35/1.91
	0.45 ± 0.01	1.180 ± 0.003				1.89/2.00
50–60%	0.40 ± 0.01	1.103 ± 0.001	0.20 ± 0.01	0.048 ± 0.004	0.0215 ± 0.0016	5.66/5.12
	0.40 ± 0.01	1.125 ± 0.003				1.31/1.22
	0.40 ± 0.01	1.180 ± 0.002				3.97/4.86
60–70%	0.34 ± 0.01	1.100 ± 0.001	0.20 ± 0.02	0.050 ± 0.005	0.0560 ± 0.0043	5.20/4.66
	0.34 ± 0.01	1.120 ± 0.003				0.58/1.05
	0.34 ± 0.01	1.130 ± 0.003				0.91/1.25
70–80%	0.28 ± 0.01	1.100 ± 0.001	0.20 ± 0.02	0.052 ± 0.005	0.0686 ± 0.0054	8.21/7.86
	0.28 ± 0.01	1.115 ± 0.004				0.22/0.27
	0.28 ± 0.01	1.120 ± 0.002				1.01/1.43
80–90%	0.21 ± 0.01	1.099 ± 0.001	0.20 ± 0.02	0.056 ± 0.006	0.1250 ± 0.0117	6.42/5.98
	0.21 ± 0.01	1.115 ± 0.002				0.86/1.19
	0.21 ± 0.01	1.100 ± 0.003				0.40/1.42

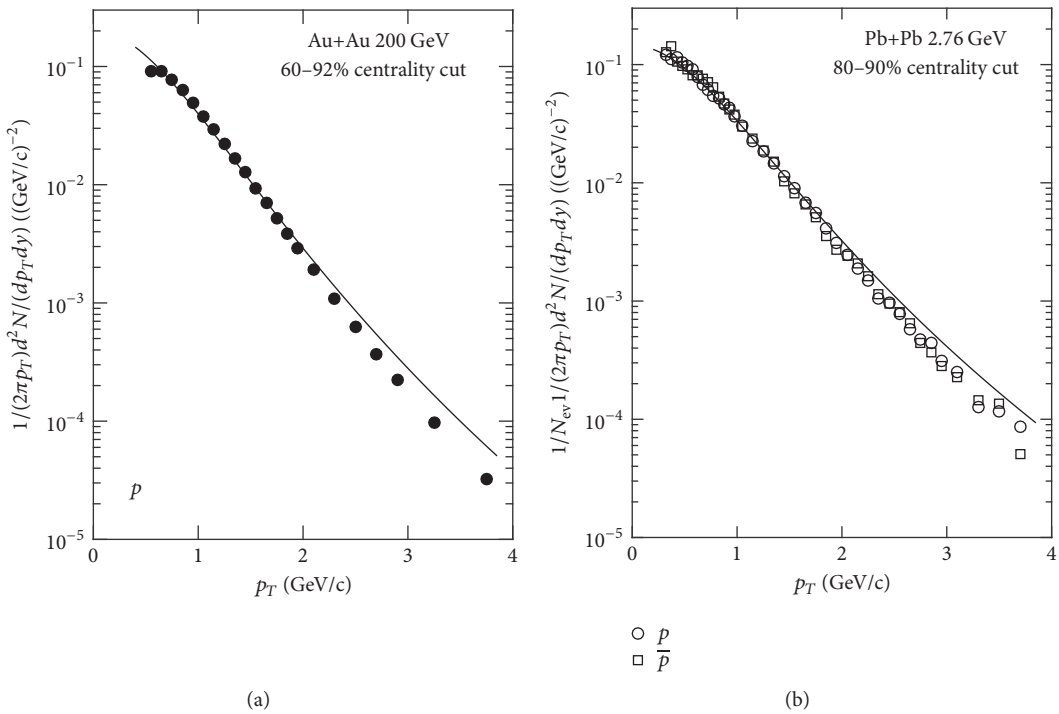

FIGURE 3: The invariant yields of $p(\overline{p})$ as a function of p_T in 60–92% Au+Au collisions at $\sqrt{s_{NN}}$ = 200 GeV (a) and in 80–90% Pb+Pb collisions at $\sqrt{s_{NN}}$ = 2.76 TeV (b). The meanings of solid dots, circles, squares, and solid curves are the same as those in Figures 1 and 2.

$$\frac{Q_0(\pi^-)}{Q_0(\pi^+)} = 1,$$

$$\frac{Q_0(K^-)}{Q_0(K^+)} = 0.93,$$

$$\frac{Q_0(\overline{p})}{Q_0(p)} = 0.72 \quad \text{(Au+Au 200 GeV)}, \tag{23}$$

$$\frac{Q_0(\pi^-)}{Q_0(\pi^+)} = \frac{Q_0(K^-)}{Q_0(K^+)} = \frac{Q_0(\overline{p})}{Q_0(p)} = 1 \quad \text{(Pb+Pb 2.76 TeV)}.$$

These ratios are in good agreement with the relative abundance of particles and antiparticles given in [3, 4]. This agreement may be due to the fact that the integrand of (20) is the same for particles and antiparticles in case that T_f takes a common constant for these two kinds of particles. Hence, Q_0 might be proportional to the abundance of corresponding particles.

4. Conclusions

By introducing the nonextensive statistics, we employ the relativistic hydrodynamics including phase transition to discuss the transverse momentum distributions of charged particles produced in heavy ion collisions. The model contains rich information about the transport coefficients of fluid, such as the initial temperature T_0, the critical temperature T_c, the kinetic freeze-out temperature T_f, the baryochemical potential μ_B, the sound speed in sQGP state c_0, and the sound speed in hadronic state c_h. Except for T_0, the other five parameters take the values either from widely accepted theoretical results or from experimental measurements. As for T_0, there are no widely acknowledged values so far. In this paper, T_0 takes the values referring to other studies for the most central collisions, and, for the rest of centrality cuts, T_0 is determined by tuning the theoretical results to experimental data. The present investigations show the conclusions as follows:

(1) The theoretical model can give a good description of the experimental data in Au+Au collisions at $\sqrt{s_{NN}}$ = 200 GeV and in Pb+Pb collisions at $\sqrt{s_{NN}}$ = 2.76 TeV for $\pi^{\pm}$ and $K^{\pm}$ in the whole measured transverse momentum region and for $p(\overline{p})$ in the region of $p_T \leq 2.0$ GeV/c.

(2) The fitted q is close to 1. This might mean that the difference between nonextensive statistics and conventional statistics is small. However, it is this small difference that plays an essential role in extending the fitting region of p_T.

(3) The fitted q increases with beam energies and the masses of charged particles. This might mean that the nonextensive statistics are more suitable for these conditions.

(4) The model cannot describe the experimental measurements for $p(\overline{p})$ in the region of $p_T \geq 2.0$ GeV/c for the both kinds of collisions. This might be caused by the hard scattering process [52]. To improve the fitting conditions, the results from perturbative QCD should be taken into account.

Conflicts of Interest

The authors declare that there are no conflicts of interest regarding the publication of this paper.

Acknowledgments

This work is supported by the Shanghai Key Lab of Modern Optical System.

References

[1] L. Adamczyk, J. K. Adkins, G. Agakishiev et al., "Centrality dependence of identified particle elliptic flow in relativistic heavy ion collisions at $\sqrt{s_{NN}}$ = 7.7–62.4 GeV," *Physical Review C*, vol. 93, Article ID 014907, 2016.

[2] J. Adam, D. Adamova, M. M. Aggarwal et al., "Anisotropic Flow of Charged Particles in Pb-Pb Collisions at $\sqrt{s_{NN}}$ = 5.02 TeV," *Physical Review Letters*, vol. 116, Article ID 132302, 2016.

[3] A. Adare, S. Afanasiev, C. Aidala et al., "Spectra and ratios of identified particles in Au+Au and d+Au collisions at $\sqrt{s_{NN}}$ = 200 GeV," *Physical Review C*, vol. 88, Article ID 024906, 2013.

[4] B. Abelev, J. Adam, D. Adamova et al., "Centrality dependence of π, K, and p production in Pb-Pb collisions at $\sqrt{s_{NN}}$ = 2.76 TeV," *Physical Review C*, vol. 88, Article ID 044910, 2013.

[5] K. Adcox, S. S. Adler, N. N. Ajitanand et al., "Single identified hadron spectra from $\sqrt{s_{NN}}$ = 130 GeV Au + Au collisions," *Physical Review C*, vol. 69, Article ID 024904, 2004.

[6] C. Adler, Z. Ahammed, C. Allgower et al., "Measurement of Inclusive Antiprotons from Au+Au Collisions at $\sqrt{s_{NN}}$ = 130 GeV," *Physical Review Letters*, vol. 87, Article ID 262302, 2001.

[7] K. Adcox, S. Belikov, J. C. Hill et al., "Centrality Dependence of $\pi\pm$, K±, p, and p Production from $\sqrt{s_{NN}}$ = 130 GeV Au+Au Collisions at RHIC," *Physical Review Letters*, vol. 88, Article ID 242301, 2002.

[8] B. I. Abelev, M. Aggarwal, Z. Ahammed et al., "Systematic measurements of identified particle spectra in pp, d+Au, and Au+Au collisions at the STAR detector," *Physical Review C*, vol. 79, Article ID 034909, 2009.

[9] B. Alver, B. Back, M. D. Baker et al., "Charged-particle multiplicity and pseudorapidity distributions measured with the PHOBOS detector in Au+Au, Cu+Cu, d+Au, and p+p collisions at ultrarelativistic energies," *Physical Review C*, vol. 83, Article ID 024913, 2011.

[10] M. Murray, "Scanning the phases of QCD with BRAHMS," *Journal of Physics G: Nuclear and Particle Physics*, vol. 30, no. 8, pp. S667–S674, 2004.

[11] M. Murray, J. Natowitz, B. S. Nielsen et al., "Flavor dynamics," *Journal of Physics G: Nuclear and Particle Physics*, vol. 35, no. 4, Article ID 044015, 2008.

[12] I. G. Bearden, D. Beavis, C. Besliu et al., "Charged Meson Rapidity Distributions in Central Au+Au Collisions at $\sqrt{s_{NN}}$ = 200 GeV," *Physical Review Letters*, vol. 94, Article ID 162301, 2005.

[13] A. Bialas, R. A. Janik, and R. Peschanski, "Unified description of Bjorken and Landau 1+1 hydrodynamics," *Physical Review C nuclear physics*, vol. 76, no. 5, Article ID 054901, 2007.

[14] C.-Y. Wong, "Landau hydrodynamics reexamined," *Physical Review C: Nuclear Physics*, vol. 78, no. 5, Article ID 054902, 2008.

[15] G. Beuf, R. Peschanski, and E. N. Saridakis, "Entropy flow of a perfect fluid in (1+1) hydrodynamics," *Physical Review C: Nuclear Physics*, vol. 78, no. 6, Article ID 064909, 2008.

[16] T. Csörgo, M. I. Nagy, and M. Csanád, "New family of simple solutions of relativistic perfect fluid hydrodynamics," *Physics Letters B*, vol. 663, no. 4, pp. 306–311, 2008.

[17] Z. W. Wang, Z. J. Jiang, and Y. S. Zhang, "The investigations of pseudorapidity distributions of final multiplicity in Au+Au collisions at high energy," *Journal of university of Shanghai for science andtechnology*, vol. 31, pp. 322–326, 2009.

[18] N. Suzuki, "One-dimensional hydrodynamical model including phase transition," *Physical Review C nuclear physics*, vol. 81, no. 4, Article ID 044911, 2010.

[19] E. K. G. Sarkisyan and A. S. Sakharov, "Relating multihadron production in hadronic and nuclear collisions," *The European Physical Journal C*, vol. 70, no. 3, pp. 533–541, 2010.

[20] A. Bialas and R. Peschanski, "Asymmetric (1+1)-dimensional hydrodynamics in high-energy collisions," *Physical Review C: Nuclear Physics*, vol. 83, no. 5, Article ID 054905, 2011.

[21] M. Csanád, M. I. Nagy, and S. Lökös, "Exact solutions of relativistic perfect fluid hydrodynamics for a QCD Equation of State," *The European Physical Journal A*, vol. 48, no. 11, pp. 173–178, 2012.

[22] Z. J. Jiang, Q. G. Li, and H. L. Zhang, "Revised Landau hydrodynamic model and the pseudorapidity distributions of charged particles produced in nucleus-nucleus collisions at maximum energy at the BNL Relativistic Heavy Ion Collider," *Physical Review C: Nuclear Physics*, vol. 87, no. 4, Article ID 044902, 2013.

[23] C. Gale, S. Jeon, and B. Schenke, "Hydrodynamic modeling of heavy-ion collisions," *International Journal of Modern Physics A*, vol. 28, no. 11, Article ID 1340011, 2013.

[24] U. Heinz and R. Snellings, "Collective flow and viscosity in relativistic heavy-ion collisions," *Annual Review of Nuclear and Particle Science*, vol. 63, pp. 123–151, 2013.

[25] A. N. Mishra, R. Sahoo, E. K. G. Sarkisyan, and A. S. Sakharov, "Effective-energy budget in multiparticle production in nuclear collisions," *The European Physical Journal C*, vol. 74, article 3147, 2014.

[26] Z. J. Jiang, Y. Zhang, H. L. Zhang, and H. P. Deng, "A description of the pseudorapidity distributions in heavy ion collisions at RHIC and LHC energies," *Nuclear Physics A*, vol. 941, pp. 188–200, 2015.

[27] H. Niemi, K. J. Eskola, and R. Paatelainen, "Event-by-event fluctuations in a perturbative QCD + saturation + hydrodynamics model: Determining QCD matter shear viscosity in ultrarelativistic heavy-ion collisions," *Physical Review C: Nuclear Physics*, vol. 93, no. 2, Article ID 024907, 2016.

[28] J. Noronha-Hostler, M. Luzum, and J.-Y. Ollitrault, "Hydrodynamic predictions for 5.02 TeV Pb-Pb collisions," *Physical Review C nuclear physics*, vol. 93, no. 3, Article ID 034912, 2016.

[29] J. S. Moreland and R. A. Soltz, "Hydrodynamic simulations of relativistic heavy-ion collisions with different lattice quantum chromodynamics calculations of the equation of state," *Physical Review C: Nuclear Physics*, vol. 93, no. 4, Article ID 044913, 2016.

[30] E. K. G. Sarkisyan, A. N. Mishra, R. Sahoo, and A. S. Sakharov, "Erratum: Multihadron production dynamics exploring the energy balance in hadronic and nuclear collisions (Physical Review D - Particles, Fields, Gravitation and Cosmology (2016) D93 (054046))," *Physical Review D: Particles, Fields, Gravitation and Cosmology*, vol. 93, no. 7, Article ID 079904, 2016.

[31] E. K. G. Sarkisyan, A. N. Mishra, R. Sahoo, and A. S. Sakharov, "Centrality dependence of midrapidity density from GeV to TeV heavy-ion collisions in the effective-energy universality picture of hadroproduction," *Physical Review D: Particles, Fields, Gravitation and Cosmology*, vol. 94, no. 1, Article ID 011501, 2016.

[32] T. Hirano, N. Van Der Kolk, and A. Bilandzic, "Hydrodynamics and flow," *Lecture Notes in Physics*, vol. 785, pp. 139–178, 2008.

[33] Z.-J. Jiang, J.-Q. Hui, and Y. Zhang, "The Rapidity Distributions and the Thermalization Induced Transverse Momentum Distributions in Au-Au Collisions at RHIC Energies," *Advances in High Energy Physics*, vol. 2017, Article ID 6896524, 8 pages, 2017.

[34] W. M. Alberico, A. Lavagno, and P. Quarati, "Nonextensive statistics, fluctuations and correlations in high energy nuclear collisions," *The European Physical Journal C*, vol. 13, pp. 499–506, 2000.

[35] M. Biyajima, T. Mizoguchi, N. Nakajima, N. Suzuki, and G. Wilk, "Modified Hagedorn formula including temperature fluctuation: Estimation of temperatures at RHIC experiments," *The European Physical Journal C*, vol. 48, no. 2, pp. 597–603, 2006.

[36] C. Tsallis, "Possible generalization of Boltzmann-Gibbs statistics," *Journal of Statistical Physics*, vol. 52, no. 1-2, pp. 479–487, 1988.

[37] T. S. Biro and G. Purcsel, "Non-extensive Boltzmann equation and hadronization," *Physical Review Letters*, vol. 95, Article ID 162302, 2005.

[38] A. S. Parvan and T. S. Biró, "Equilibrium statistical mechanics for incomplete nonextensive statistics," *Physics Letters A*, vol. 375, no. 3, pp. 372–378, 2011.

[39] T. S. Biró, G. G. Barnaföldi, and P. Ván, "Thermodynamic derivation of the tsallis and rényi entropy formulas and the temperature of quark-gluon plasma," *The European Physical Journal A*, vol. 49, no. 9, p. 110, 2013.

[40] A. R. Plastino and A. Plastino, "Information theory, approximate time dependent solutions of Boltzmann's equation and Tsallis' entropy," *Physics Letters A*, vol. 193, no. 3, pp. 251–258, 1994.

[41] D. F. Torres, H. Vucetich, and A. Plastino, "Early universe test of nonextensive statistics," *Physical Review Letters*, vol. 79, no. 9, pp. 1588–1590, 1997.

[42] G. Kaniadakis, A. Lavagno, M. Lissia, and P. Quarati, "Nonextensive statistical effects in nuclear physics problems," *Physica A: Statistical Mechanics and its Applications*, vol. 261, no. 3-4, pp. 359–373, 1998.

[43] A. K. Rajagopal, R. S. Mendes, and E. K. Lenzi, "Quantum statistical mechanics for nonextensive systems: Prediction for possible experimental tests," *Physical Review Letters*, vol. 80, no. 18, pp. 3907–3910, 1998.

[44] U. Tirnakli, F. Büyükkiliç, and D. Demirhan, "Some bounds upon the nonextensivity parameter using the approximate generalized distribution functions," *Physics Letters A*, vol. 245, no. 1-2, pp. 62–66, 1998.

[45] F. Cooper and G. Frye, "Landau's hydrodynamic model of particle production and electron-positron annihilation into hadrons," *Physical Review D: Particles, Fields, Gravitation and Cosmology*, vol. 11, pp. 192–213, 1975.

[46] T. Mizoguchi, H. Miyazawa, and M. Biyajima, "A potential including the Heaviside function in the 1 + 1 dimensional hydrodynamics by Landau : IIts basic properties and application to data at RHIC energies," *The European Physical Journal A*, vol. 40, no. 1, pp. 99–108, 2009.

[47] A. Adare, S. Afanasiev, C. Aidala et al., "Scaling properties of azimuthal anisotropy in Au+Au and Cu+Cu collisions at $\sqrt{s_{NN}}$ = 200 GeV," *Physical Review Letters*, vol. 98, Article ID 162301, 2007.

[48] L. N. Gao, Y. H. Chen, H. R. Wei, and F. H. Liu, "Speed of sound parameter from RHIC and LHC heavy-ion data," *Advances in High Energy Physics*, vol. 2013, Article ID 450247, 8 pages, 2013.

[49] S. Borsányi, G. Endrodi, Z. Fodor et al., "The QCD equation of state with dynamical quarks," *Journal of High Energy Physics*, vol. 2010, no. 11, article 77, pp. 1–31, 2010.

[50] D. Teaney, J. Lauret, and E. V. Shuryak, "A hydrodynamic description of heavy ion collisions at the SPS and RHIC," *Physical*, 2001.

[51] M. Strickland, "Thermal Y(1s) and χb1 suppression at $\sqrt{s_{NN}}$ = 2.76 TeV Pb-Pb collisions at the LHC," *Physical Review Letters*, vol. 107, no. 13, Article ID 132301, 2011.

[52] H. Lao, F. Liu, and R. A. Lacey, "Erratum to: Extracting kinetic freeze-out temperature and radial flow velocity from an improved Tsallis distribution," *The European Physical Journal A*, vol. 53, no. 6, pp. 44–64, 2017.

Hindawi
Advances in High Energy Physics
Volume 2018, Article ID 9141249, 4 pages
https://doi.org/10.1155/2018/9141249

Research Article

Renormalization Group Equation for Tsallis Statistics

Airton Deppman

Instituto de Física, Universidade de São Paulo, Rua do Matão Travessa R Nr. 187, Cidade Universitária, 05508-090 São Paulo, SP, Brazil

Correspondence should be addressed to Airton Deppman; deppman@if.usp.br

Received 22 November 2017; Revised 22 January 2018; Accepted 6 March 2018; Published 3 April 2018

Academic Editor: Edward Sarkisyan-Grinbaum

The nonextensive statistics proposed by Tsallis has found wide applicability, being present even in the description of experimental data from high energy collisions. A system with a fractal structure in its energy-momentum space, named thermofractal, was shown to be described thermodynamically by the nonextensive statistics. Due to the many common features between thermofractals and Hagedorn's fireballs, this system offers the possibility of investigating the origins of nonextensivity in hadronic physics and in QCD. In this regard, the investigation of the scaling properties of thermofractals through the renormalization group equation, known as Callan–Symanzik equation, can be an interesting approach.

In the present work Tsallis statistics is analyzed in the context of renormalization theory. The relations between such nonextensive statistics and scaling properties are expressed in terms of a Callan–Symanzik equation [1–3], which represents the fundamental properties of a scale-free system.

The generalization of Boltzmann-Gibbs-Shannon (BGS) statistics by violation of entropy additivity mediated by the entropic index q leads to Tsallis statistics [4], which will lead to nonextensive thermodynamical quantities that were expected to be extensive in the context of BGS. Tsallis statistics is known to apply to a large number of systems in physics and in other fields, and one of its most distinguished features is the power-law distribution in contrast to the exponential behavior common to BGS distributions. One of the most interesting applications of the generalized thermodynamics lies in the description of distributions found in high energy collisions experiments [5–8]. A generalized version of Hagedorn's self-consistent thermodynamics [9] has allowed the prediction of a limiting temperature and a common entropic index, q, and a new hadron mass spectrum formula. The results found fair agreement with experiments [10–15].

The Callan–Symanzik equation was formulated in the context of renormalization theory of quantum gauge fields with scale invariance. The Yang–Mills theory, in particular, is scale-free and may satisfy that equation. In this regard, the Callan–Symanzik equation was fundamental to determine the asymptotic freedom of QCD [16–19].

In [20–22] it was shown that a system with a particular fractal structure in the energy-momentum space should be described by the nonextensive statistics proposed by Tsallis. Such system, named thermofractal, presents three fundamental properties:

(1) It has an internal structure formed by N' thermofractals.

(2) The total energy of the thermofractal is the sum of the total kinetic energy, F, and the total internal energy, E, of the compound thermofractals. These energies are such that the ratio $E/F = \varepsilon/k\tau$ fluctuates according to the probability density $P(\varepsilon)$.

(3) The internal energy decreases as deeper levels of the thermofractals are considered.

It is possible to show [20] that the probability density for such system is given by

$$P(\varepsilon) = \left[1 + (q-1)\frac{\varepsilon}{k\tau}\right]^{-1/(q-1)}, \quad (1)$$

where $\tau = (q-1)T$, with T being the temperature of the thermofractal. A consequence of such properties is that the

temperature of thermofractals at level n scales, on average, is as

$$\frac{T^{(n)}}{T} = \frac{E^{(n)}}{E}. \tag{2}$$

This system can be shown to have a fractal dimension in the energy-momentum space, so from now on it will be referred to as fractal. They are scale-free systems and present several characteristics that are interesting to investigate the origin of nonextensivity in hadron systems, as the similarities with Hagedorn's fireballs. With the introduction of this kind of fractal it was possible to understand that Hagedorn's theory, which is based on a self-referenced definition of fireballs or hadrons, should necessarily be described by Tsallis statistics. In the circumstances of hadron physics, it allows a new understanding on the intermittency effect [23–28] observed in high energy data, determines the related fractal dimension, and connects this effect to other features of high energy experimental data, such as self-similarity [29–31], long-tail distributions [8], and mass spectrum [12].

Intermittency effects, in particular, have been associated with fractal-like properties of the multiparticle production process [32–34] (see [35, 36] for a more complete account on the subject), and it was associated with gluon emission of high energy jets [37–39] that results from the QCD evolution equations [40]. These equations arise from the properties of the renormalization group for non-Abelian Yang–Mills gauge field theory [16–19].

A detailed analysis of thermofractals and their properties allows one to show that the density in (1) can be written in terms of F and E for a fractal at an arbitrary level n as

$$P(F,E) = N'^{n} \left(\frac{F^{(n)}}{kT^{(n)}}\right)^{3/2} \cdot e^{-U^{(n)}/(kT^{(n)})} \left[1 - (q-1)\frac{\varepsilon}{k\tau}\right]^{-1/(q-1)}, \tag{3}$$

with $U = E + F$. Introducing $M = kT$ for convenience and taking into account the fact that

$$\left(\frac{1}{N}\right)^{n/(1-D)} = \frac{T^{(n)}}{T} \tag{4}$$

results in the following:

$$P(F,E) = \left(\frac{M^{(n)}}{M}\right)^{-(1-D)} \left(\frac{F^{(n)}}{M^{(n)}}\right)^{3/2} \cdot e^{-U^{(n)}/M^{(n)}} \left[1 - (q-1)\frac{\varepsilon}{k\tau}\right]^{-1/(q-1)}, \tag{5}$$

where D is the Hausdorff fractal dimension [20].

Notice that for a fixed value of the scale M, at a fixed level n of the fractal structure, the equation above is a well-defined continuous function and a simple analysis would lead one to conclude that dimension D is not fractal but reflects the topology of the phase-space where the system is embedded. This is due to the fact that the anomalous dimension arises from the fractal structure itself and not from the underlying distribution. In other words, it is necessary to take into account the fractal evolution with the scale variation, which leads to a tree-like diagram, to obtain the fractal dimension. A nice account on the subject, in general, can be found in [27, 41], and for a specific description of the system analyzed here, see [42].

In the present work, the scaling properties of the fractal structure will be investigated in the light of renormalization theory. In this sense, the scaling properties can be analyzed in two ways: (a) by varying E and F while keeping M fixed; (b) by varying M while keeping E and F constant. Both transformations are equivalent according to scaling properties and are related through the fundamental equation of renormalization theory, the Callan–Symanzik equation. The main objective here is to obtain such equation in the context of fractals. Before doing that, observe that since E and F are transformed by the same scale factor, ration E/F remains constant and so remains the parameter $\varepsilon/(k\tau)$. In addition, the exponential factor in (5) amounts to the Boltzmann factor for thermal equilibrium and bears no relation to the fractal structure itself, so it must be dropped for the analysis. With these considerations, the invariance of the fractal structure by scale transformation can be expressed by the identity

$$\Gamma(F,M) = \left(\frac{M}{\Lambda}\right)^{-(1-D)} \left(\frac{F}{M}\right)^{3/2}, \tag{6}$$

with Λ being some reference scale.

The equation above is suitable for the scaling analysis in both ways described above. From method (a), where M is fixed and F varies, one gets

$$F\frac{\partial \Gamma}{\partial F} = \frac{3}{2}\Gamma. \tag{7}$$

From method (b), where F remains constant while scale M varies, one gets from (6)

$$M\frac{\partial \Gamma}{\partial M} = \left(-\frac{3}{2} - (1-D)\right)\Gamma. \tag{8}$$

The results above allow one to obtain the Callan–Symanzik equation for the fractals considered here; that is,

$$\left[M\frac{\partial}{\partial M} + F\frac{\partial}{\partial F} + d\right]\Gamma = 0, \tag{9}$$

where $d = 1 - D$ is the anomalous fractal dimension.

The fractal dimension D was determined in terms of the parameters that characterize thermofractals [20] and is given by

$$D = 1 + \frac{\log N'}{\log R}, \tag{10}$$

where

$$R = \frac{(q-1)N/N'}{3 - 2q + (q-1)N}, \tag{11}$$

with $N = N' + 2/3$.

Equation (9) represents the fundamental properties of the fractal structure under scale transformation. Since it is related to a system whose scaling properties are the main ingredient to obtain Tsallis statistics, one can recognize the equation above as the Callan–Symanzik equation for Tsallis statistics.

This result sets the ground for an interpretation of Tsallis statistics in association with renormalization group theory. In addition, it opens new possibilities of exploring the potential applicability of nonextensive statistics in the domain of hadronic physics and, hopefully, allows for a deeper understanding of the properties of QCD that make self-similarity and fractal structures emerge from the strong interaction in complex system. It can be also be associated with the nonthermal phase transition of hadronic matter associated with Quark–Gluon Plasma [35, 43].

In a thermodynamical approach, the application of the nonextensive self-consistent thermodynamics that arises from the fractal structure when applied to hadronic systems has gone already beyond the usual description of high energy distributions and has been extended to systems with finite chemical potential [44, 45], to extend the MIT Bag model by including a fractal structure [46] and to describe neutron star equilibrium [47].

In conclusion, the Callan–Symanzik equation associated with Tsallis statistics was derived here in association with the thermofractal scale-free structure, setting new grounds for the interpretation of nonextensive thermodynamics in terms of renormalization group theory and opening new possibilities of its application in QCD related problems.

Conflicts of Interest

The author declare that there are no conflicts of interest regarding the publication of this paper.

Acknowledgments

This work is supported by Conselho Nacional de Desenvolvimento Cietífico e Tecnológico, CNPq.

References

[1] C. G. Callan, "Broken scale invariance in scalar field theory," *Physical Review D: Particles, Fields, Gravitation and Cosmology*, vol. 2, no. 8, pp. 1541–1547, 1970.

[2] K. Symanzik, "Small distance behaviour in field theory and power counting," *Communications in Mathematical Physics*, vol. 18, no. 3, pp. 227–246, 1970.

[3] K. Symanzik, "Small-distance-behaviour analysis and Wilson expansions," *Communications in Mathematical Physics*, vol. 23, no. 1, pp. 49–86, 1971.

[4] C. Tsallis, "Possible generalization of Boltzmann-Gibbs statistics," *Journal of Statistical Physics*, vol. 52, no. 1-2, pp. 479–487, 1988.

[5] I. Bediaga, E. M. F. Curado, and J. M. De Miranda, "Nonextensive thermodynamical equilibrium approach in $e^+e^- \rightarrow hadrons$," *Physica A: Statistical Mechanics and its Applications*, vol. 286, no. 1-2, pp. 156–163, 2000.

[6] C. Beck, "Non-extensive statistical mechanics and particle spectra in elementary interactions," *Physica A: Statistical Mechanics and its Applications*, vol. 286, no. 1, pp. 164–180, 2000.

[7] C. Wong, G. Wilk, L. J. Cirto, C. Tsallis, F. Fabbri, and P. Giacomelli, "From QCD-based hard-scattering to nonextensive statistical mechanical descriptions of transverse momentum spectra in high-energy pp and $p\overline{p}$ collisions," *Physical Review D: Particles, Fields, Gravitation and Cosmology*, vol. 91, Article ID 114027, 2015.

[8] C. Y. Wong and G. Wilk, "Tsallis fits to p_T spectra and multiple hard scattering in pp collisions at the LHC," *Physical Review D: Particles, Fields, Gravitation and Cosmology*, vol. 87, Article ID 114007, 2013.

[9] A. Deppman, "Self-consistency in non-extensive thermodynamics of highly excited hadronic states," *Physica A: Statistical Mechanics and its Applications*, vol. 391, no. 24, pp. 6380–6385, 2012.

[10] I. Sena and A. Deppman, "Systematic analysis of p_T-distributions in p + p collisions," *The European Physical Journal A*, vol. 49, article 17, 2013.

[11] J. Cleymans and D. Worku, "The Tsallis distribution in proton–proton collisions at $\sqrt{s} = 0.9$ TeV at the LHC," *Journal of Physics G: Nuclear and Particle Physics*, vol. 39, no. 2, Article ID 025006, 2012.

[12] L. Marques, E. Andrade-II, and A. Deppman, "Nonextensivity of hadronic systems," *Physical Review D: Particles, Fields, Gravitation and Cosmology*, vol. 87, no. 11, 2013.

[13] L. Marques, J. Cleymans, and A. Deppman, "Description of high-energy pp collisions using Tsallis thermodynamics: transverse momentum and rapidity distributions," *Physical Review D: Particles, Fields, Gravitation and Cosmology*, vol. 91, no. 5, Article ID 054025, 2015.

[14] M. D. Azmi and J. Cleymans, "The Tsallis distribution at large transverse momenta," *The European Physical Journal C*, vol. 75, article 430, 2015.

[15] B. De, "Non-extensive statistics and understanding particle production and kinetic freeze-out process from p_T-spectra at 2.76 TeV," *The European Physical Journal A*, vol. 50, article 138, 2014.

[16] H. D. Politzer, "Asymptotic freedom: an approach to strong interactions," *Physics Reports*, vol. 14, no. 4, pp. 129–180, 1974.

[17] H. Georgi and H. D. Politzer, "Electroproduction scaling in an asymptotically free theory of strong interactions," *Physical Review D: Particles, Fields, Gravitation and Cosmology*, vol. 9, no. 2, pp. 416–420, 1974.

[18] D. J. Gross and F. Wilczek, "Asymptotically free gauge theories. I," *Physical Review D: Particles, Fields, Gravitation and Cosmology*, vol. 8, no. 10, pp. 3633–3652, 1973.

[19] D. J. Gross and F. Wilczek, "Asymptotically free gauge theories. II," *Physical Review D: Particles, Fields, Gravitation and Cosmology*, vol. 9, no. 4, pp. 980–993, 1974.

[20] A. Deppman, "Thermodynamics with fractal structure, Tsallis statistics, and hadrons," *Physical Review D: Particles, Fields, Gravitation and Cosmology*, vol. 93, no. 5, Article ID 054001, 2016.

[21] A. Deppman, E. Megías, and D. P. Menezes, "Nonextensive thermodynamics with finite chemical potential, hadronic matter and protoneutron stars," *Journal of Physics: Conference Series*, vol. 607, no. 1, Article ID 012007, 2015.

[22] A. Deppman and E. Megías, "Fractal aspects of hadrons," *EPJ Web of Conferences*, vol. 141, Article ID 01011, 2017.

[23] A. Bialas and R. Peschanski, "Moments of rapidity distributions as a measure of short-range fluctuations in high-energy collisions," *Nuclear Physics B*, vol. 273, no. 3-4, pp. 703–718, 1986.

[24] A. Bialas and R. Peschanki, "Intermittency in multiparticle production at high energy," *Nuclear Physics B*, vol. 308, no. 4, pp. 857–867, 1988.

[25] R. C. Hwa, "Fractal measures in multiparticle production," *Physical Review D: Particles, Fields, Gravitation and Cosmology*, vol. 41, no. 5, pp. 1456–1462, 1990.

[26] R. C. Hwa and J. Pan, "Fractal behavior of multiplicity fluctuations in high-energy collisions," *Physical Review D: Particles, Fields, Gravitation and Cosmology*, vol. 45, no. 5, pp. 1476–1483, 1992.

[27] E. K. G. Sarkisyan, "Description of local multiplicity fluctuations and genuine multiparticle correlations," *Physics Letters B*, vol. 477, no. 1-3, pp. 1–12, 2000.

[28] E. K. Sarkisyan, L. K. Gelovani, G. G. Taran, and G. I. Sakharov, "Fractal analysis of pseudorapidity fluctuations in 4.5 A GeV/c C-(Ne, Cu) central collisions," *Physics Letters B*, vol. 318, no. 3, pp. 568–574, 1993.

[29] G. Wilk and Z. Włodarczyk, "Self-similarity in jet events following from *pp* collisions at LHC," *Physics Letters B*, vol. 727, no. 1-3, pp. 163–167, 2013.

[30] M. Tokarev and I. Zborovsky, "Top-Quark p_T-Spectra at LHC and Flavor Independence of z-scaling," *EPJ Web of Conferences*, vol. 141, Article ID 02006, 2017.

[31] I. Zborovsk and M. V. Tokarev, "Generalized z-scaling in proton-proton collisions at high energies," *Physical Review D: Particles, Fields, Gravitation and Cosmology*, vol. 75, no. 9, Article ID 094008, 2007.

[32] P. Brax and R. Peschanski, "Multifractal analysis of intermittency and phase transitions in multiparticle dynamics," *Nuclear Physics B*, vol. 346, no. 1, pp. 65–83, 1990.

[33] J.-L. Meunier and R. Peschanski, "Intermittency, fragmentation, and the Smoluchowski equation," *Nuclear Physics B*, vol. 374, no. 2, pp. 327–339, 1992.

[34] A. Bialas and K. Zalewski, "Phase structure of self-similar multiparticle systems and experimental determination of intermittency parameters," *Physics Letters B*, vol. 238, no. 2-4, pp. 413–416, 1990.

[35] W. Kittel and E. A. de Wolf, *Soft Multihadron Dynamics*, World Scientific Publishers, Singapore, Singapore, 2005.

[36] E. A. De Wolf, I. M. Dremin, and W. Kittel, "Scaling laws for density correlations and fluctuations in multiparticle dynamics," *Physics Reports*, vol. 270, no. 1-2, pp. 1–141, 1996.

[37] G. Veneziano, "Momentum and Colour Structure of Jets in QCD," in *Proceedings of the 3rd Workshop on Current Problems in High Energy Particle Theory*, Florence, Italy, 1979.

[38] K. Konishi, A. Ukawa, and G. Veneziano, "A simple algorithm for QCD jets," *Physics Letters B*, vol. 78, no. 2-3, pp. 243–248, 1978.

[39] K. Konishi, A. Ukawa, and G. Veneziano, "On the transverse spread of QCD jets," *Physics Letters B*, vol. 80, no. 3, pp. 259–264, 1979.

[40] G. Altarelli and G. Parisi, "Asymptotic freedom in parton language," *Nuclear Physics B*, vol. 126, no. 2, pp. 298–318, 1977.

[41] R. K. Nayak, S. Dash, E. K. Sarkisyan-Grinbaum, and M. Tasevsky, "Describing dynamical fluctuations and genuine correlations by Weibull regularity," 2017, https://arxiv.org/abs/1704.08377.

[42] A. Deppman, E. Megias, D. P. Menezes, and T. Frederico, "Fractal structure and non extensive statistics," 2017, https://arxiv.org/abs/1801.01160.

[43] R. Peschanski, "On the existence of a non-thermal phase transition in multi-particle production," *Nuclear Physics B*, vol. 327, no. 1, pp. 144–156, 1989.

[44] E. Megías, D. P. Menezes, and A. Deppman, "Non extensive thermodynamics for hadronic matter with finite chemical potentials," *Physica A: Statistical Mechanics and its Applications*, vol. 421, pp. 15–24, 2015.

[45] E. Megías, D. P. Menezes, and A. Deppman, "Nonextensive thermodynamics with finite chemical potentials and protoneutron starss," *EPJ Web of Conferences*, vol. 80, Article ID 00040, 2014.

[46] P. H. G. Cardoso, T. Nunes da Silva, A. Deppman, and D. P. Menezes, "Quark matter revisited with non-extensive MIT bag model," *The European Physical Journal A*, vol. 53, no. 10, article no. 191, 2017.

[47] D. P. Menezes, A. Deppman, E. Megias, and L. B. Castro, "Non-extensive thermodynamics and neutron star properties," *The European Physical Journal A*, vol. 51, article 155, 2015.

Hindawi
Advances in High Energy Physics
Volume 2018, Article ID 7895967, 12 pages
https://doi.org/10.1155/2018/7895967

Research Article

Comparing Standard Distribution and Its Tsallis Form of Transverse Momenta in High Energy Collisions

Rui-Fang Si,[1,2] **Hui-Ling Li**,[3] **and Fu-Hu Liu**[1]

[1]*Institute of Theoretical Physics and State Key Laboratory of Quantum Optics and Quantum Optics Devices, Shanxi University, Taiyuan, Shanxi 030006, China*
[2]*Department of Mathematics and Science, Fenyang Normal Campus Lvliang College, Fenyang, Shanxi 032300, China*
[3]*Institute of Modern Physics, Shanxi Normal University, Linfen, Shanxi 041004, China*

Correspondence should be addressed to Hui-Ling Li; lihuilingxyx@sina.com and Fu-Hu Liu; fuhuliu@163.com

Received 26 October 2017; Accepted 2 January 2018; Published 19 March 2018

Academic Editor: Lorenzo Bianchini

The experimental (simulated) transverse momentum spectra of negatively charged pions produced at midrapidity in central nucleus-nucleus collisions at the Heavy-Ion Synchrotron (SIS), Relativistic Heavy-Ion Collider (RHIC), and Large Hadron Collider (LHC) energies obtained by different collaborations are selected by us to investigate, where a few simulated data are taken from the results of FOPI Collaboration which uses the IQMD transport code based on Quantum Molecular Dynamics. A two-component standard distribution and the Tsallis form of standard distribution are used to fit these data in the framework of a multisource thermal model. The excitation functions of main parameters in the two distributions are analyzed. In particular, the effective temperatures extracted from the two-component standard distribution and the Tsallis form of standard distribution are obtained, and the relation between the two types of effective temperatures is studied.

1. Introduction

High energy heavy-ion (nucleus-nucleus) collisions are an important method to simulate and study the big bang in the early universe, properties of new matter created in extreme conditions, accompanying phenomena in the creation, and physics mechanisms of the creation. Some models based on the quantum chromodynamics (QCD) and/or thermal and statistical methods can be used to analyze the equation of state (EoS) at finite temperature and density, properties of chemical and kinetic freeze-outs in collision process, distribution laws of different particles in final state, and universality of hadroproduction in different systems [1–5]. The properties of nuclear matter and its phase transition to quark-gluon plasma (QGP) at high temperature and density can be obtained. With the developments in the methodologies of experimental techniques and theoretical studies, the collision energy per nucleon pair in the center-of-mass system increases from high energy range which has a few to several hundred GeV to ultrahigh energy range which has presently a few to over ten TeV.

The temperature and density described the EoS showing that the new matter created in high and ultrahigh energy ranges is not similar to the ideal gas-like state of quarks and gluons expected by early theoretical models. Instead, the effects of strong dynamical coupling, long-range interactions, local memory, and others appear in the interior of interacting system. The rapid evolution of interacting system and the indirect measurements of some observable quantities result in that one can use the statistical method to study the distribution properties of some observable quantities such as (pseudo) rapidity, (transverse) momentum, (transverse) energy, azimuthal angle, elliptic flow, multiplicity, and others of final-state fragments and particles [1–5]. Thus, some quantitative or qualitative results related to the properties of interacting system and particle production can be observed.

As the quantities which can be early measured in experiments, that is, the so-called "the first day" measureable quantities, the rapidity and transverse momentum distributions attract wide attentions due to their carryovers on the information of longitudinal extension and transverse expansion of the

emission source in interacting system. With the increasing collision energy, the rapidity distribution range extends from a few rapidity units to over ten rapidity units, and the transverse momentum distribution range increases from 0 until a few GeV/c to 0 until over hundred GeV/c. Different functions and methods are used by different researchers to describe rapidity and transverse momentum distributions as well as other distributions which can be measured in experiments [1–5]. Based on a multisource thermal model [6–9], the rapidity and transverse momentum distributions obtained in experiments at different collision energies are studied by us in terms of two-cylinder, Rayleigh, Boltzmann, Tsallis, and other distributions. In particular, comparing with rapidity distribution, transverse momentum distribution contains more abundant information and attracts wider attentions. Although one has Monte Carlo and other indirect methods to describe transverse momentum distributions, analytical functions are more expected to use.

Because of the same transverse momentum distribution being described by different functions to obtain values of different parameters, possible relations existing among different parameters can be studied. In this paper, based on the multisource thermal model [6–9], the standard distribution (Boltzmann, Fermi-Dirac, and Bose-Einstein distributions) and its Tsallis form are used to describe the transverse momentum distribution of final-state particles produced in high energy nucleus-nucleus collisions. The excitation functions of effective temperatures obtained by the two distributions are extracted and the relation between the two effective temperatures is studied.

The rest part of this paper is structured as follows. A brief description of the model and method is presented in Section 2. Results on comparisons with experimental (simulated) data and discussion are given in Section 3. Finally, we summarize our main observations and conclusions in Section 4.

2. The Model and Method

According to the multisource model [6–9], a few emission sources of produced particles are assumed to form in interacting system due to different reaction mechanisms and/or data examples. For each emission source, the thermal model or other similar models and distributions can be used to perform calculation on the production of particles. The potential models include [10], but are not limited to, ideal gas-like model, ideal hydrodynamic model, and viscous hydrodynamic model. In these models, the relativistic effect has to be particularly considered, and the quantum effect can be usually neglected. If we study in detail the interacting system and final-state particles, both the relativistic and quantum effects have to be considered.

In the middle stage of collision process, the interacting system and emission sources in it can be regarded as to stay at the hydrodynamic state. After the stage of chemical freeze-out, in particular after the stage of kinetic freeze-out, the interacting system and emission sources in it should stay at the gas-like state. Otherwise, it is difficult to understand the kinetic information of singular particle measured in experiments. What had happened during the phase transition from the liquid-like state at the middle stage to the gas-like state at the final stage and why is beyond the focus of the present work. We shall not discuss this issue here.

According to the ideal gas model with the relativistic and quantum effects, the particle spectra can be described by the standard distribution. The number of particles is [11]

$$N = \frac{gV}{(2\pi)^3} \int d^3p \left[\exp\left(\pm \frac{E-\mu}{T_S} \right) + S \right]^{-1}, \quad (1)$$

where g is the degeneracy factor, V is the volume, p is the momentum, $E = \sqrt{p^2 + m_0^2}$ is the energy, m_0 is the rest mass, μ is the chemical potential, and T_S is the effective temperature; $S = 0$, $+1$, and -1 correspond to the Boltzmann, Fermi-Dirac, and Bose-Einstein statistics, respectively; $E - \mu > 0$ corresponds to plus +, and $E - \mu \leq 0$ corresponds to minus −. The invariant momentum distribution of particles is

$$E\frac{d^3N}{dp^3} = \frac{gV}{(2\pi)^3} E \left[\exp\left(\pm \frac{E-\mu}{T_S} \right) + S \right]^{-1}. \quad (2)$$

The normalized probability density distribution of particle momenta can be written as

$$f_p(p) = \frac{1}{N}\frac{dN}{dp} = C_S p^2 \left[\exp\left(\pm \frac{\sqrt{p^2 + m_0^2} - \mu}{T_S} \right) + S \right]^{-1}, \quad (3)$$

where C_S is the normalized constant in the standard probability density distribution of momenta. It is related to the selection of parameters.

The normalized joint probability density distribution of particle rapidities and transverse momenta is

$$f_{y,p_T}(y, p_T) = \frac{1}{N}\frac{d^2N}{dy\, dp_T} = C_S p_T \sqrt{p_T^2 + m_0^2} \cosh y \cdot \left[\exp\left(\pm \frac{\sqrt{p_T^2 + m_0^2}\cosh y - \mu}{T_S} \right) + S \right]^{-1}, \quad (4)$$

where $\sqrt{p_T^2 + m_0^2}\cosh y - \mu > 0$ corresponds to plus + and $\sqrt{p_T^2 + m_0^2}\cosh y - \mu \leq 0$ corresponds to minus −. The normalized probability density distribution of particle rapidities is then written to be

$$f_y(y) = \frac{1}{N}\frac{dN}{dy} = C_S \cosh y \cdot \int_0^{p_{T\max}} p_T \sqrt{p_T^2 + m_0^2} \left[\exp\left(\pm \frac{\sqrt{p_T^2 + m_0^2}\cosh y - \mu}{T_S} \right) + S \right]^{-1} dp_T, \quad (5)$$

where $p_{T\max}$ denotes the maximum transverse momentum. This rapidity distribution is only for an emission source. In the case of considering multiple sources, we have to consider sources distribution in the rapidity space [2–4, 12–16]. This issue is beyond the focus of the present work, and we shall not discuss it anymore. The normalized probability density distribution of particle transverse momenta is written to be

$$f_{p_T}(p_T) = \frac{1}{N}\frac{dN}{dp_T} = C_S p_T \sqrt{p_T^2 + m_0^2} \int_{y_{\min}}^{y_{\max}} \cosh y \cdot \left[\exp\left(\pm \frac{\sqrt{p_T^2 + m_0^2}\cosh y - \mu}{T_S} \right) + S \right]^{-1} dy, \quad (6)$$

where $y_{\max}$ and $y_{\min}$ denote the maximum and minimum rapidities, respectively.

It should be noted that, in the above formulas, although the same symbol C_S is used to represent the normalized constants in different formulas, these constants may be different from each other. In the case of considering multisource emission, we have to use the multicomponent distribution to describe the transverse momentum distribution of final-state particles. If n_0 emission sources are considered, we have

$$f_{p_T}(p_T) = \frac{1}{N}\frac{dN}{dp_T} = \sum_{i=1}^{n_0} k_{Si} \cdot C_{Si} p_T \sqrt{p_T^2 + m_0^2} \int_{y_{\min}}^{y_{\max}} \cosh y \cdot \left[\exp\left(\pm \frac{\sqrt{p_T^2 + m_0^2}\cosh y - \mu}{T_{Si}} \right) + S \right]^{-1} dy, \quad (7)$$

where C_{Si} denotes the normalized constant for the ith component in n_0 components, k_{Si} denotes the contribution fraction of the ith component in final-state distribution, and T_{Si} denotes the effective temperature corresponding to the ith component. There are temperature fluctuations among different components. In the case of considering multisource emission, we have the effective temperature of interacting system as $T_S = \sum_i k_{Si} T_{Si}$. Generally, two or three emission sources are enough to describe the experimental data obtained in soft excitation process. That is, $i = 2$ or 3 in most cases.

If we consider the Tsallis form of standard distribution, the number of particles is [11, 17]

$$N = \frac{gV}{(2\pi)^3} \int d^3p \left\{ \left[1 \pm \frac{q-1}{T_T}(E-\mu) \right]^{\pm 1/(q-1)} + S \right\}^{-1}, \quad (8)$$

where q is an entropy index which characterizes the departing degree of the interacting system from the equilibrium state. Generally, we have $q > 1$; if $q = 1$, the system stays in the equilibrium state. T_T is the effective temperature. Other symbols have the same meanings as (1). The invariant momentum distribution of particles is

$$E\frac{d^3N}{dp^3} = \frac{gV}{(2\pi)^3} E \left\{ \left[1 \pm \frac{q-1}{T_T}(E-\mu) \right]^{\pm 1/(q-1)} + S \right\}^{-1}. \quad (9)$$

The normalized probability density distribution of particle momenta is

$$f_p(p) = \frac{1}{N}\frac{dN}{dp} = C_T p^2 \left\{ \left[1 \pm \frac{q-1}{T_T}\left(\sqrt{p^2 + m_0^2} - \mu \right) \right]^{\pm 1/(q-1)} + S \right\}^{-1}. \quad (10)$$

The normalized joint probability density distribution of particle rapidities and transverse momenta is

$$f_{y,p_T}(y, p_T) = \frac{1}{N}\frac{d^2N}{dy\,dp_T} = C_T p_T \sqrt{p_T^2 + m_0^2}\cosh y \cdot \left\{ \left[1 \pm \frac{q-1}{T_T}\left(\sqrt{p_T^2 + m_0^2}\cosh y - \mu \right) \right]^{\pm 1/(q-1)} + S \right\}^{-1}. \quad (11)$$

Then, the normalized probability density distribution of particle rapidities is

$$f_y(y) = \frac{1}{N}\frac{dN}{dy} = C_T \cosh y \int_0^{p_{T\max}} p_T \sqrt{p_T^2 + m_0^2} \left\{ \left[1 \pm \frac{q-1}{T_T}\left(\sqrt{p_T^2 + m_0^2}\cosh y - \mu \right) \right]^{\pm 1/(q-1)} + S \right\}^{-1} dp_T. \quad (12)$$

The normalized probability density distribution of particle transverse momenta is

$$f_{p_T}(p_T) = \frac{1}{N}\frac{dN}{dp_T} = C_T p_T \sqrt{p_T^2 + m_0^2} \int_{y_{\min}}^{y_{\max}} \cosh y \cdot \left\{ \left[1 \pm \frac{q-1}{T_T} \left(\sqrt{p_T^2 + m_0^2} \cosh y - \mu \right) \right]^{\pm 1/(q-1)} + S \right\}^{-1} dy. \quad (13)$$

In the above formulas, although the same symbol C_T is used to represent the normalized constants in different formulas, these constants may be different from each other. As discussed in [17], the Tsallis form has at least four types of function representations, though we choose only one that contains p_T after C_T and the index $1/(q-1)$. We do not need to consider a multisource for the Tsallis form due to it covering a two- or three-component standard distribution, and the two- or three-component standard distribution describes well the transverse momentum spectrum of particles produced in soft excitation process.

It should be noted again that the above multicomponent (two- or three-component) standard distribution and the Tsallis form of standard distribution can describe only the transverse momentum spectrum of particles produced in soft excitation process. The transverse momentum spectrum produced in soft excitation process covers a narrow range. For the transverse momentum spectrum covering a wide range, we have to consider the contribution of hard scattering process. According to the QCD calculus [18–20], we have an inverse power-law

$$f_H(p_T) = \frac{1}{N}\frac{dN}{dp_T} = A p_T \left(1 + \frac{p_T}{p_0} \right)^{-n} \quad (14)$$

to describe the transverse momentum spectrum produced in hard scattering process, where p_0 and n are free parameters and A is the normalized constant which is related to the free parameters. It is obvious that a two-component function is needed for a wide transverse momentum spectrum. The first component is the multicomponent (two- or three-component) standard distribution or Tsallis form which describes the soft process, and the second component is the inverse power-law which describes the hard process. The application of the inverse power-law is beyond the focus of the present work. We shall not discuss it anymore.

In the above discussions, to obtain chemical potential of a given particle, the chemical freeze-out temperature $T_{\rm ch}$ of the emission source is needed to know first of all. In the case of assuming the same chemical freeze-out moment, the emission source has the sole $T_{\rm ch}$. According to [21, 22], there is a relation among $T_{\rm ch}$, the yield n_1 and mass m_1 of the first particle, the yield n_2 and mass m_2 of the second particle, and the ratio $n_{12} = n_1/n_2$. We have

$$n_{12} = \frac{n_1}{n_2} = \frac{\exp(m_2/T_{\rm ch}) + S_2}{\exp(m_1/T_{\rm ch}) + S_1}, \quad (15)$$

where $S_1(S_2) = \pm 1$ denote fermion and boson, respectively. If the fermion and boson are not needed to distinguish each other, we have $S = 0$. This results in a simple expression for (15); that is, $n_{12} = n_1/n_2 \approx \exp(-m_1/T_{\rm ch})/\exp(-m_2/T_{\rm ch})$.

In the framework of a statistical thermal model of noninteracting gas particles with the assumption of standard Maxwell-Boltzmann statistics, there is an empirical expression for the chemical freeze-out temperature [23–26],

$$T_{\rm ch} = \frac{0.164}{1 + \exp\left[2.60 - \ln\left(\sqrt{s_{NN}}\right)/0.45\right]}, \quad (16)$$

where $\sqrt{s_{NN}}$ denotes the energy per nucleon pair in the center-of-mass system. Both the units of $T_{\rm ch}$ and $\sqrt{s_{NN}}$ are in GeV. The limiting value of $T_{\rm ch}$ is 0.164 GeV.

In the framework of a thermal model with standard distribution, the chemical potentials of some particles can be obtained from the ratios of negatively to positively charged particles. According to [27], we have

$$\frac{\overline{p}}{p} = \exp\left(-\frac{2\mu_p}{T_{\rm ch}}\right) \equiv k_p, \quad (17)$$

$$\frac{K^-}{K^+} = \exp\left(-\frac{2\mu_K}{T_{\rm ch}}\right) \equiv k_K, \quad (18)$$

$$\frac{\pi^-}{\pi^+} = \exp\left(-\frac{2\mu_\pi}{T_{\rm ch}}\right) \equiv k_\pi, \quad (19)$$

where the symbol of a given particle is used for its yield for the purpose of simplicity. Further, the chemical potentials of the mentioned particles are

$$\mu_p = -\frac{1}{2} T_{\rm ch} \cdot \ln\left(k_p\right), \quad (20)$$

$$\mu_K = -\frac{1}{2} T_{\rm ch} \cdot \ln\left(k_K\right), \quad (21)$$

$$\mu_\pi = -\frac{1}{2} T_{\rm ch} \cdot \ln\left(k_\pi\right). \quad (22)$$

Empirically, the chemical potential for baryon is [23–26]

$$\mu_B = \frac{1.303}{1 + 0.286\sqrt{s_{NN}}} \quad (23)$$

which is also obtained in the framework of a statistical thermal model of noninteracting gas particles with the assumption of standard Maxwell-Boltzmann statistics, where both the units of μ_B and $\sqrt{s_{NN}}$ are in GeV.

We would like to point out that (16) and (23) should be modified in the framework of generalized nonextensive statistics when we use the Tsallis form of standard distribution. At the same time, (17)–(22) should be generalized within an analysis with the Tsallis form. To modify (16)–(23) is beyond our focus and ability. We shall not discuss these modifications here. Instead, as an approximate treatment, we use $T_{\rm ch}$ and μ_π obtained within an analysis with the standard distribution as those within the Tsallis form. In fact, the absolute value of μ_π is very small, and its effect on the

transverse momentum spectra can be neglected. Therefore, this approximate treatment is acceptable.

It should be noted once more that, as mentioned in the above discussions, what we extract from the multicomponent standard distribution or the Tsallis form of standard distribution is the effective temperature, but not the real temperature of emission source. Generally, the transverse momentum spectrum contains both the contributions of thermal motion and flow effect. The real temperature is only a reflection of purely thermal motion, and the flow effect should not be included in it. As for the methods to obtain the real temperature by disengaging the contributions of thermal motion and flow effect, we can use the blast-wave model based on the Boltzmann distribution [28–30], the blast-wave model based on the Tsallis distribution [31], the improved Tsallis distribution [32, 33], some alternative methods [21, 29, 34–36], and others [37–40]. These methods themselves are beyond the focus of the present work. We shall not discuss them anymore.

3. Results and Discussion

The transverse momentum spectra of negatively charged pions produced in midrapidity range in $\sqrt{s_{NN}}$ = 2.24 and 2.52 GeV central gold-gold (Au-Au) collisions [41] measured (simulated) by the FOPI Collaboration at the Heavy-Ion Synchrotron (SIS), 11.5 [42], 62.4, 130, and 200 GeV central Au-Au collisions [29] measured by the STAR Collaboration at the Relativistic Heavy-Ion Collider (RHIC), 22.5 GeV central copper-copper (Cu-Cu) [43] and 200 GeV central Au-Au collisions [27] measured by the PHENIX Collaboration at the RHIC, and 2.76 TeV central lead-lead (Pb-Pb) collisions [44] measured by the ALICE Collaboration at the Large Hadron Collider (LHC) are selected to investigate. Among them, the results of FOPI Collaboration are given in Figure 1 with the simulated data (the last eight circles) of the IQMD transport code [45] which is based on Quantum Molecular Dynamics [46]. To avoid confusion, most results of the STAR Collaboration are given in Figure 2, and the results corresponding to 11.5 GeV are given in Figure 3. The results of PHENIX and ALICE Collaborations are given in Figures 3 and 4, respectively. In each figure, the symbols represent the experimental (simulated) data scaled by different amounts in some cases. The collision energy and type, centrality and midrapidity ranges, and scaled amount if not 1 are marked in the panel. The dashed and solid curves denote the results fitted by the two-component standard distribution and the Tsallis form of standard distribution. The values of parameters, χ^2, and degree of freedom (dof) are listed in Table 1 ordered by the energy from low to high. In particular, $T_S = k_{S1}T_{S1} + (1 - k_{S1})T_{S2}$ is the average weighted by the fractions of different components, μ_π is obtained by (16) and (22), and the values of k_π in (22) at different energies are obtained from [47]. As a preliminary result, the values of μ_π for the first and second standard distributions and the Tsallis form are assumed to be the same. In the fitting, the method of least square is used to obtain the best parameter values. One can see that the two-component standard distribution and the Tsallis form of standard distribution describe approximately

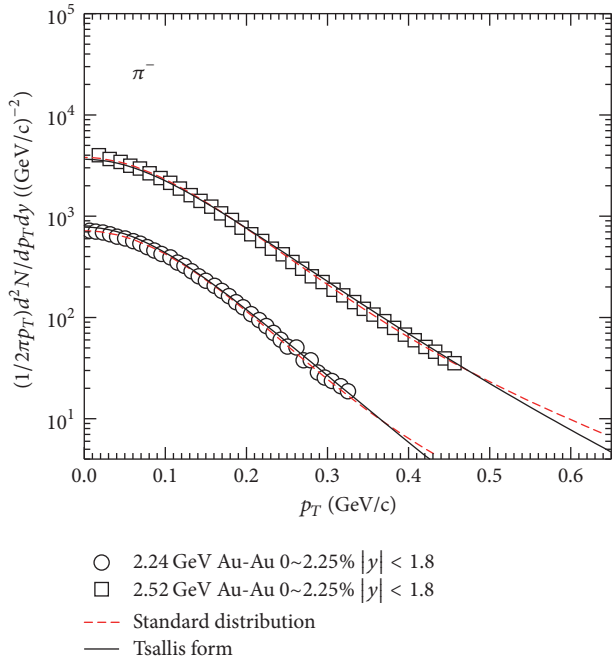

FIGURE 1: Transverse momentum spectra of π^- produced in central Au-Au collisions at $\sqrt{s_{NN}}$ = 2.24 (circles) and 2.52 GeV (squares). The symbols represent the experimental data of the FOPI Collaboration [41] measured in midrapidity range and the last eight circles represent the simulated data of the IQMD transport code [45] which is based on Quantum Molecular Dynamics [46]. The statistical errors are smaller than the size of symbols. The dashed and solid curves are the results fitted by the two-component standard distribution and the Tsallis form of standard distribution, respectively.

the transverse momentum spectra of negatively charged pions produced in central nucleus-nucleus collisions in the energy range from SIS to LHC.

To study the excitation functions of free parameters, that is, the dependence of free parameters on collision energy, the relations $T_{S1} - \ln\sqrt{s_{NN}}$ ($T_{S2} - \ln\sqrt{s_{NN}}$), $T_S - \ln\sqrt{s_{NN}}$ ($T_T - \ln\sqrt{s_{NN}}$), $k_{S1} - \ln\sqrt{s_{NN}}$, and $q - \ln\sqrt{s_{NN}}$ are presented in Figures 5–8, respectively. The symbols and error bars in the figures denote the values of free parameters and their errors. Both the values of free parameters and their errors are taken from Table 1. The lines in Figures 5 and 6 are obtained by the method of least square. These lines can be described by linear functions $T_{S1,S2,S,T} = a\ln\sqrt{s_{NN}} + b$, where the slope a and intercept b are listed in Table 1 and the unit of $\sqrt{s_{NN}}$ is in GeV. One can see that the four effective temperatures T_{S1}, T_{S2}, T_S, and T_T increase linearly with increase of $\ln\sqrt{s_{NN}}$. In particular, the relation between T_S and T_T can be obtained to be $T_S = (2.500 \pm 0.170)T_T + (-0.040 \pm 0.013)$ due to Table 1, which shows a linear relation between T_S and T_T. With increase of $\sqrt{s_{NN}}$, k_{S1} has a minimum at about 10 GeV, and q increases primitively and saturates at about 10 GeV.

Our results show some interesting features. Actually, one could as well say that there is no difference in the particle production in central nucleus-nucleus collisions from a few GeV to a few TeV. This in some sense echoes recent studies of

Table 1: Values of free parameters (T_{S1}, T_{S2}, and k_{S1}) for the two-component standard distribution, free parameters (T_T and q) for the Tsallis form of standard distribution, derivative parameters (T_S and μ_π), χ^2, and dof corresponding to the fits in Figures 1–4, as well as values of slope a and intercept b corresponding to the fits of linear functions $T_{S1,S2,S,T} = a \ln \sqrt{s_{NN}} + b$ in Figures 5 and 6. As a preliminary result, the values of μ_π for the first and second standard distribution and the Tsallis form are assumed to be the same. The units of effective temperatures and chemical potential are in GeV.

	T_{S1}	T_{S2}	k_{S1}	T_S	μ_π	χ^2/dof	T_T	q	χ^2/dof
2.24 GeV Au-Au (FOPI Collab.)	0.038 ± 0.004	0.100 ± 0.050	0.825 ± 0.100	0.049 ± 0.012	−(0.021 ± 0.002)	14.880/31	0.039 ± 0.005	1.042 ± 0.010	24.043/32
2.52 GeV Au-Au (FOPI Collab.)	0.054 ± 0.007	0.126 ± 0.012	0.810 ± 0.050	0.068 ± 0.008	−(0.019 ± 0.003)	11.004/42	0.040 ± 0.003	1.072 ± 0.008	16.856/43
11.5 GeV Au-Au (STAR Collab.)	0.076 ± 0.010	0.175 ± 0.009	0.432 ± 0.070	0.132 ± 0.009	−(0.005 ± 0.007)	1.350/18	0.067 ± 0.008	1.106 ± 0.008	2.850/19
22.5 GeV Cu-Cu (PHENIX Collab.)	0.088 ± 0.025	0.219 ± 0.008	0.620 ± 0.085	0.138 ± 0.019	−(0.003 ± 0.011)	4.123/19	0.075 ± 0.005	1.089 ± 0.004	1.360/20
62.4 GeV Au-Au (STAR Collab.)	0.106 ± 0.012	0.242 ± 0.029	0.620 ± 0.009	0.158 ± 0.019	−(0.002 ± 0.014)	2.130/6	0.070 ± 0.005	1.131 ± 0.011	1.561/7
130 GeV Au-Au (STAR Collab.)	0.102 ± 0.012	0.250 ± 0.060	0.600 ± 0.085	0.161 ± 0.031	−(0.001 ± 0.015)	6.246/6	0.076 ± 0.005	1.117 ± 0.016	42.448/7
200 GeV Au-Au (STAR Collab.)	0.112 ± 0.010	0.310 ± 0.085	0.671 ± 0.080	0.177 ± 0.035	−(0.002 ± 0.018)	10.241/7	0.078 ± 0.006	1.120 ± 0.015	10.736/8
200 GeV Au-Au (PHENIX Collab.)	0.134 ± 0.020	0.270 ± 0.010	0.761 ± 0.092	0.167 ± 0.018	−(0.002 ± 0.018)	3.048/24	0.089 ± 0.004	1.096 ± 0.005	7.650/25
2.76 TeV Pb-Pb (ALICE Collab.)	0.145 ± 0.010	0.345 ± 0.011	0.761 ± 0.040	0.193 ± 0.010	−(0.001 ± 0.011)	6.475/37	0.097 ± 0.005	1.112 ± 0.005	9.766/38
a	0.015 ± 0.012	0.034 ± 0.022		0.020 ± 0.023			0.008 ± 0.008		
b	0.035 ± 0.004	0.088 ± 0.007		0.067 ± 0.008			0.039 ± 0.003		

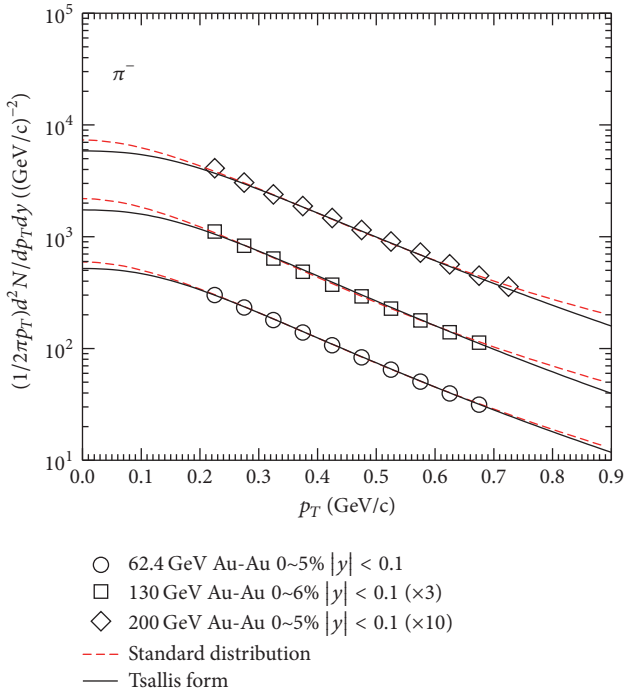

FIGURE 2: Same as Figure 1, but for $\sqrt{s_{NN}}$ = 62.4 (circles), 130 (squares), and 200 GeV (rhombuses). The symbols represent the experimental data of the STAR Collaboration with errors being the root quadratic sum of statistical and systematic errors [29].

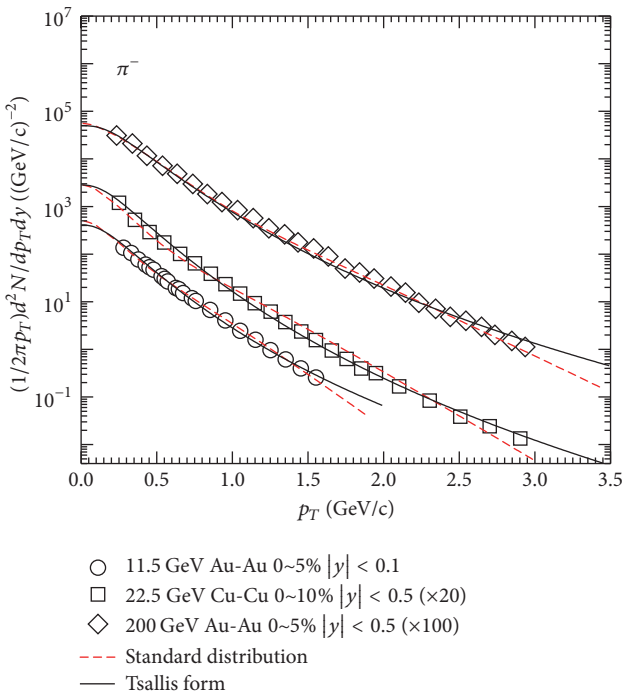

FIGURE 3: Same as Figure 1, but for central Au-Au collisions at $\sqrt{s_{NN}}$ = 11.5 GeV (circles), central Cu-Cu collisions at $\sqrt{s_{NN}}$ = 22.5 GeV (squares), and central Au-Au collisions at $\sqrt{s_{NN}}$ = 200 GeV (rhombuses). The symbols represent the experimental data of the STAR Collaboration with the statistical and systematic errors added in quadrature (circles) [42], and the PHENIX Collaborations with statistical errors only (squares [43] and rhombuses [27]).

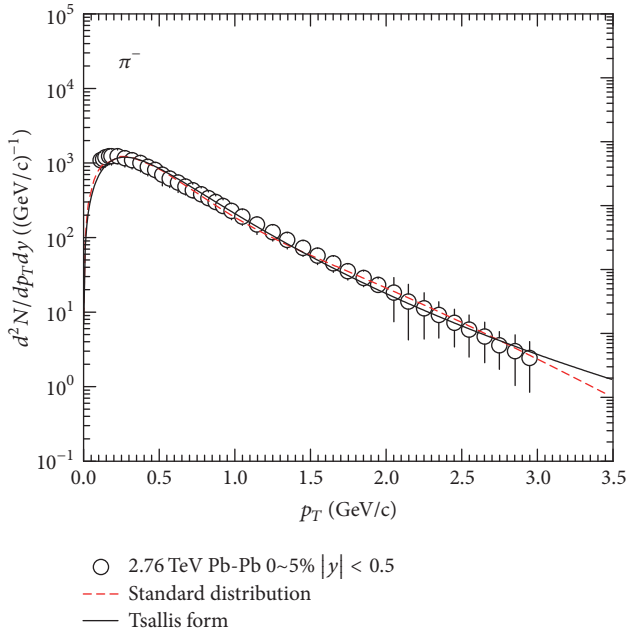

FIGURE 4: Same as Figure 1, but for central Pb-Pb collisions at $\sqrt{s_{NN}}$ = 2.76 TeV. The symbols represent the experimental data of the ALICE Collaborations and errors are the root quadratic sum of statistical and systematic errors [44].

Sarkisyan et al. [1, 48]. In addition, our recent study shows that the same or similar fits to be good for proton-proton collisions [40], though the parameter values in proton-proton collisions are closer to those in peripheral nucleus-nucleus collisions when comparing with central nucleus-nucleus collisions. This suggests universality in particle production, as it is obtained in recent and previous studies of Sarkisyan et al. [1, 12, 48–50], but now for transverse momentum distribution as well. On the other hand, the multiplicity and transverse momentum distributions observed in different data samples can be uniformly fitted by multicomponent Erlang distribution [8, 51, 52], which also show the universality in particle production. Indeed, the universality in particle production exists not only in mean multiplicity and pseudorapidity density but also in multiplicity and transverse momentum distributions in some conditions.

Our observation that k_{S1} has a minimum at about 10 GeV and q increases primitively and saturates at about 10 GeV is in agreement with recent work of Cleymans [53] in which the energy region $\sqrt{s_{NN}} \approx 10$ GeV for heavy-ion collisions is indicated to be an interesting one. In fact, in this energy region, the final state has the highest net baryon density, and a transition from a baryon dominated to a meson dominated final state takes place. At the same time, ratios of strange particles to mesons show obviously maxima in this energy region [53]. At a slightly smaller energy (about 6~8 GeV), other works show some extremes or saturation in excitation functions of parameters. These parameters include, but are not limited to, the specific reduced curvature of net-proton rapidity distribution [54–56], chemical freeze-out temperature [57, 58], mean transverse mass minus rest mass [57], yield ratios

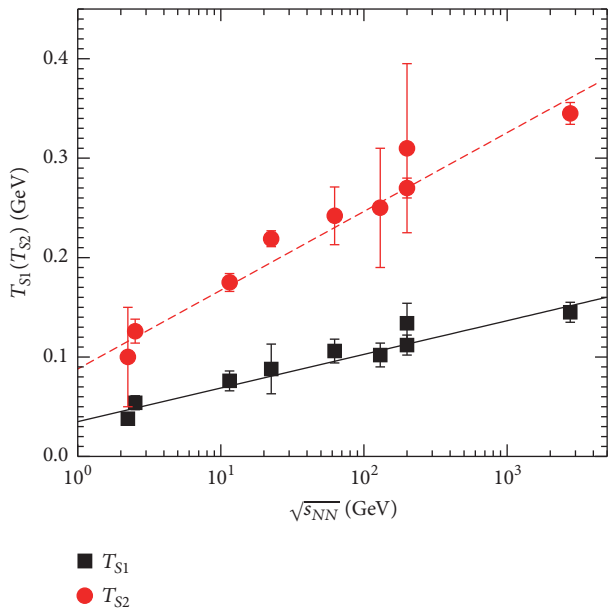

FIGURE 5: Dependence of T_{S1} (squares) and T_{S2} (circles) on $\sqrt{s_{NN}}$. The symbols represent the values of parameters taken from Table 1, and the error bars represent the statistical errors. The lines are the results fitted by the linear functions $T_{S1,S2} = a \ln \sqrt{s_{NN}} + b$.

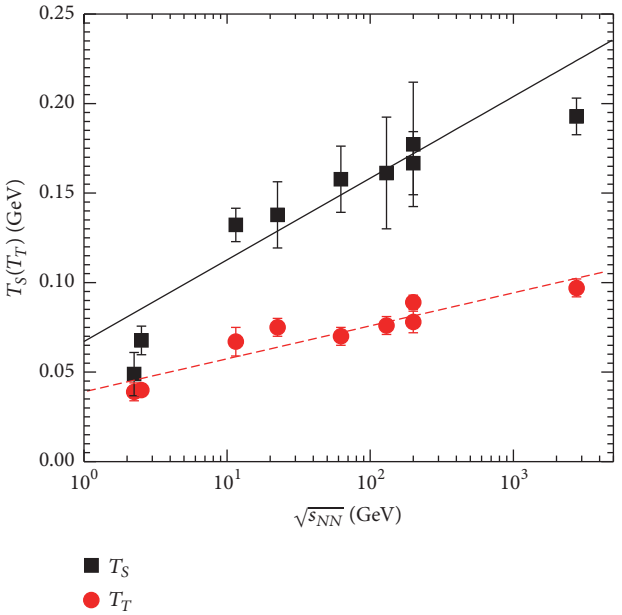

FIGURE 6: Same as Figure 5, but for the dependence of T_S (squares) and T_T (circles) on $\sqrt{s_{NN}}$ and the linear functions are $T_{S,T} = a \ln \sqrt{s_{NN}} + b$.

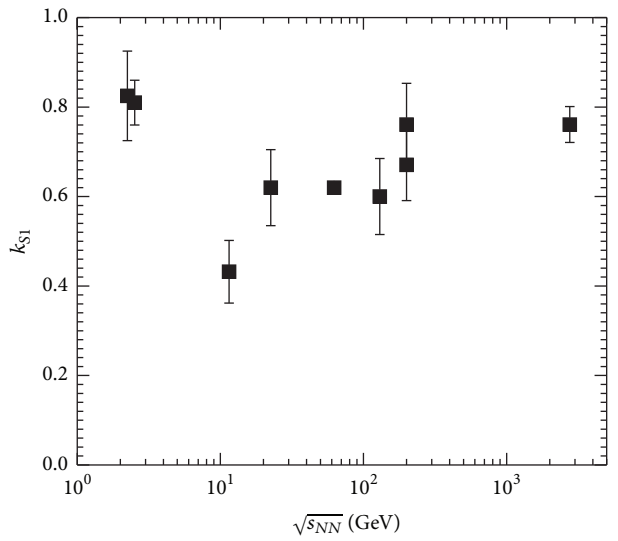

FIGURE 7: Dependence of k_{S1} on $\sqrt{s_{NN}}$. The symbols represent the values of parameter taken from Table 1 and the error bars represent the statistical errors.

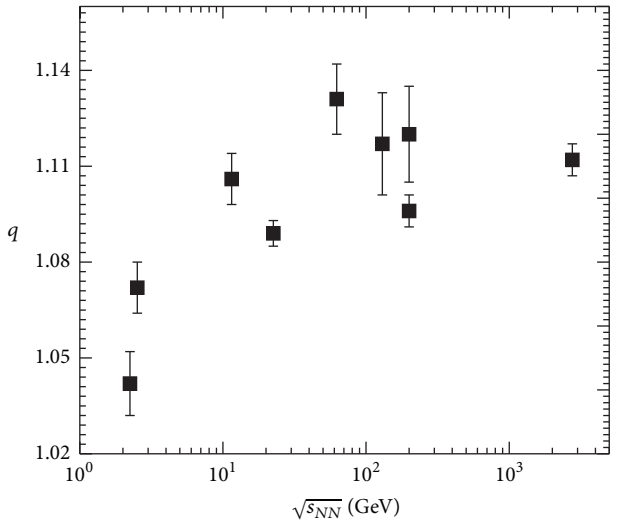

FIGURE 8: Dependence of q on $\sqrt{s_{NN}}$. The symbols represent the values of parameter taken from Table 1 and the error bars represent the statistical errors.

of positive kaons to pions [57–59], squared speed-of-sound [60], string tension in Schwinger mechanism [61], width and fraction of fragmentation source [62], and width ratios of experimental negative pion rapidity distribution to Landau hydrodynamic model prediction [58].

In the above analyses, for a not too wide transverse momentum spectrum, a standard distribution is usually not enough to describe the spectrum. Generally, we need a two-component standard distribution to describe the not too wide spectrum. It is expected that, in the case of studying a wider transverse momentum spectrum, we need a three-component standard distribution to describe the wider spectrum. If a set of experimental data is described by the two- or three-component standard distribution, it is also described by the Tsallis form of standard distribution [11]. If the two- or three-component standard distribution describes a temperature fluctuation between two or among three emission sources, the Tsallis form of standard distribution describes a degree of nonequilibrium. The degree of nonequilibrium is characterized by the entropy index q. A larger q corresponds to a farther nonequilibrium among different emission

sources. One can see from Table 1 that $q < 1.13$ in most cases, which renders an approximate equilibrium among different emission sources or the whole interacting system stays in an approximate equilibrium state.

Both the two- or three-component standard distribution and the Tsallis form of standard distribution describe only the results of soft excitation process. For the soft process, the particle spectrum appears with the characteristics of thermal emission phenomenon. Although the standard distribution describes the characteristics of thermal emission, some nonthermal emissions also obey the standard distribution. Even if the Tsallis form has less connection with thermal emission, they are relative due to the standard distribution. In the case of studying a very wide transverse momentum spectrum, for example, for a width of more than 5 GeV/c, to consider only the contribution of soft process is not enough in description of experimental data. To describe a wider transverse momentum spectrum, we have to consider simultaneously the contribution of hard scattering process. As mentioned in Section 2, according to the QCD calculus [18–20], the hard process can be described by the inverse power-law. Because of the hard process having no connection with the thermal emission, it does not affect the extraction of temperature parameter. In the case of extracting only temperature parameter, a too wide transverse momentum spectrum is not needed.

In the above analyses, the temperature extracted by us is in fact the effective temperature T. It is neither the temperature T_0 at the kinetic freeze-out nor the temperature $T_{\rm ch}$ at the chemical freeze-out of the emission source or interacting system. Generally, T_0 can be extracted from the transverse momentum spectra, and $T_{\rm ch}$ can be extracted from the ratios of different types of particles. However, the temperature extracted from the transverse momentum spectra is not surely T_0 due to the contribution of flow effect. How to get rid of the contribution of flow effect is a question that is worth discussing. In the blast-wave model [28–31], the mean transverse flow velocity $\langle\beta_T\rangle$ is introduced. Thus, T_0 and $\langle\beta_T\rangle$ can be simultaneously obtained based on the analysis of transverse momentum spectrum by the model. In addition, by using the standard distribution and its Tsallis form to analyze the transverse momentum spectra of different particles, we can obtain the linear relation between T and m_0. The intercept in the linear relation is regarded as T_0 [21, 29, 34–36]. We can also obtain the linear relation between $\langle p_T\rangle$ and mean moving mass $\overline{m}$ (mean energy). The slope in the linear relation is regarded as $\langle\beta_T\rangle$ [37–40].

Generally speaking, the two-component standard distribution and the Tsallis form of standard distribution are the same in essentials while differing in minor points in the behaviors in the figures. The standard distribution corresponds to the classical statistical system which has short-range interactions in interior and non-multifractal structure in boundary. Some extensive thermodynamic quantities such as energy, momentum, internal energy, and entropy are linearly related to the system size and particle number. These quantities obey simply additive property. The statistical method and the microscopic description of system are adaptive. The entropy function is a power tool to study the microscopic dynamics of system under the macroscopic condition by describing the occupation number of phase spaces of the system. The Tsallis form breaks through the limitation of classical statistics by using the entropy index q. The complex system with long-range interactions, local memory effect, strong dynamic correlation, fractal or multifractal occupation in phase space, and others can be described by the Tsallis form. The Tsallis form also causes the classical extensive quantities not to obey the simple additive property. Instead, the coupled item appears in the quantities and the nonextensive statistical effects are formed in the transverse and longitudinal dynamics [63–73].

In the above discussions, one can see that the two- or three-component standard distribution can be described by the Tsallis form of the standard distribution. It does not mean that the single standard distribution cannot be described by the Tsallis form. In fact, by using a lower temperature and an entropy index that is closer to 1, the Tsallis form describes well the single standard distribution. The standard distribution is successfully replaced by the Tsallis form due to q changing from 1 to a value that is greater than 1. This means that the interacting system changes from the classical and extensive statistical system to the nonextensive system, which is an essential change of the system properties. However, in some cases, the same set of experimental data can be described by both the (two- or three-component) standard distribution obeying the extensive statistics and the Tsallis form obeying the nonextensive statistics. This means that in these cases there is no obvious boundary to distinguish extensive system and nonextensive system for a given interacting system. We have to examine which property is the main factor. Or, the interacting system in the present energy range stays in a transition gradation from extensive system to nonextensive system.

4. Conclusions

We summarize here our main observations and conclusions.

(a) The transverse momentum spectra of negatively charged pions produced in central nucleus-nucleus collisions measured (simulated) in midrapidity range by different collaborations at the SIS, RHIC, and LHC are studied by the two-component standard distribution and the Tsallis form of standard distribution which are fitted into the frame of multisource thermal model. The two distributions describe approximately the experimental (simulated) data.

(b) The excitation functions of related parameters are analyzed. The four effective temperatures T_{S1}, T_{S2}, T_S, and T_T increase linearly with increase of $\ln\sqrt{s_{NN}}$. In particular, the relation between T_S and T_T can be obtained to be $T_S = (2.500 \pm 0.170)T_T + (-0.040 \pm 0.013)$ which shows a linear relation between T_S and T_T. With increase of $\sqrt{s_{NN}}$, k_{S1} has a minimum at about 10 GeV, and q increases primitively and saturates at about 10 GeV.

(c) There is no difference in the particle production in central nucleus-nucleus collisions from a few GeV to a few TeV. Combining with other works, one can say that the same or similar fits are good for proton-proton collisions. This suggests universality in particle production, as it is already

obtained in mean multiplicity, pseudorapidity density, and multiplicity distribution, but now for transverse momentum distribution as well.

(d) The energy of $\sqrt{s_{NN}} \approx 10$ GeV for heavy-ion collisions is indicated to have the highest net baryon density and the maximum ratios of strange particles to mesons and to take place a transition from the final state which has mainly baryons to the final state which has mainly mesons [53]. At a slightly smaller energy (about 6~8 GeV), other works show some extremes or saturation in excitation functions of some parameters [54–62]. These extremes and saturation are related to the search of soft point of equation of state.

(e) To be closer to the classical situation, the two- or three-component standard distribution has an advantage over the Tsallis form of standard distribution due to similar statistics for the classical situation and standard distribution. However, the Tsallis form of standard distribution uses less parameter than the two- or three-component standard distribution. If the two- or three-component standard distribution describes a temperature fluctuation between two or among three sources, the Tsallis form of standard distribution describes a degree of nonequilibrium.

(f) In the considered energy range, different emission sources stay in an approximate equilibrium state or the whole interacting system stays in an approximate equilibrium state. There is no obvious boundary to distinguish extensive system and nonextensive system for a given interacting system. The interacting system stays in a transition gradation from extensive system to nonextensive system. To obtain only the kinetic freeze-out temperature, we would rather use the two- or three-component standard distribution due to it being closer to the classical situation.

Conflicts of Interest

The authors declare that they have no conflicts of interest.

Acknowledgments

Comments on the manuscript and relevant communications from Edward K. G. Sarkisyan and Ya-Hui Chen are highly acknowledged. This work was supported by the National Natural Science Foundation of China under Grants nos. 11575103 and 11747319, the Shanxi Provincial Natural Science Foundation under Grant no. 201701D121005, and the Fund for Shanxi "1331 Project" Key Subjects Construction.

References

[1] E. K. G. Sarkisyan, A. N. Mishra, R. Sahoo, and A. S. Sakharov, "Multihadron production dynamics exploring the energy balance in hadronic and nuclear collisions," *Physical Review D*, vol. 93, no. 5, Article ID 054046, 2016.

[2] I. Bautista, J. G. Milhano, C. Pajares, and J. D. de Deus, "Multiplicity in pp and AA collisions: The same power law from energy-momentum constraints in string production," *Physics Letters B*, vol. 715, no. 1-3, pp. 230–233, 2012.

[3] Z. J. Jiang, Y. Zhang, H. L. Zhang, and H. P. Deng, "A description of the pseudorapidity distributions in heavy ion collisions at RHIC and LHC energies," *Nuclear Physics A*, vol. 941, pp. 188–200, 2015.

[4] G. Wolschin, "Ultraviolet energy dependence of particle production sources in relativistic heavy-ion collisions," *Physical Review C*, vol. 91, no. 1, Article ID 014905, 2015.

[5] M. Sanchis-Lozano and E. Sarkisyan-Grinbaum, "Ridge effect and three-particle correlations," *Physical Review D*, vol. 96, no. 7, Article ID 074012, 2017.

[6] F.-H. Liu, "Particle production in Au-Au collisions at RHIC energies," *Physics Letters B*, vol. 583, no. 1-2, pp. 68–72, 2004.

[7] F.-H. Liu, "Dependence of charged particle pseudorapidity distributions on centrality and energy in p(d)A collisions at high energies," *Physical Review C*, vol. 78, no. 1, Article ID 014902, 2008.

[8] F.-H. Liu, "Unified description of multiplicity distributions of final-state particles produced in collisions at high energies," *Nuclear Physics A*, vol. 810, no. 1–4, pp. 159–172, 2008.

[9] F.-H. Liu, "Charged particle production in d+Au collisions at $\sqrt{s_{NN}}$ = 200 GeV," *Physical Review C*, vol. 69, no. 6, Article ID 067901, 2004.

[10] S. Abreu, S. V. Akkelin, J. Alam et al., "Heavy-ion collisions at the LHC Last call for predictions," *Journal of Physics G*, vol. 35, no. 5, Article ID 054001, 2008.

[11] J. Cleymans and D. Worku, "Relativistic thermodynamics: transverse momentum distributions in high-energy physics," *The European Physical Journal A*, vol. 48, Article ID 160, 2012.

[12] A. N. Mishra, R. Sahoo, E. K. G. Sarkisyan, and A. S. Sakharov, "Effective-energy budget in multiparticle production in nuclear collisions," *The European Physical Journal C*, vol. 74, Article ID 3147, 2014.

[13] G. Wolschin, "Particle production sources at LHC energies," *Journal of Physics G: Nuclear and Particle Physics*, vol. 40, no. 4, Article ID 045104, 2013.

[14] I. Bautista, C. Pajares, J. G. Milhano, and J. D. De Deus, "Rapidity dependence of particle densities in pp and AA collisions," *Physical Review C*, vol. 86, no. 3, Article ID 034909, 2012.

[15] Z. J. Jiang and H. L. Zhang, "Pseudorapidity distributions of charged particles produced in p-p collisions at center-of-mass energies from 23.6 GeV to 900 GeV," *Modern Physics Letters A*, vol. 29, no. 27, Article ID 1450130, 2014.

[16] Z. J. Jiang, H. L. Zhang, J. Wang, and K. Ma, "The evolution-dominated hydrodynamic model and the pseudorapidity distributions in high energy physics," *Advances in High Energy Physics*, vol. 2014, Article ID 248360, 10 pages, 2014.

[17] H. Zheng and L. Zhu, "Comparing the Tsallis distribution with and without thermodynamical description in p+p collisions," *Advances in High Energy Physics*, vol. 2016, Article ID 9632126, 10 pages, 2016.

[18] R. Odorico, "Does a transverse energy trigger actually trigger on large-P_T jets?" *Physics Letters B*, vol. 118, no. 1-3, pp. 151–154, 1982.

[19] G. Arnison, A. Astbury, B. Aubert (UA1 Collaboration) et al., "Transverse momentum spectra for charged particles at the CERN proton-antiproton collider," *Physics Letters B*, vol. 118, no. 1-3, pp. 167–172, 1982.

[20] T. Mizoguchi, M. Biyajima, and N. Suzuki, "Analyses of whole transverse momentum distributions in $p\overline{p}$ and pp collisions by using a modified version of Hagedorn's formula," *International Journal of Modern Physics A*, vol. 32, no. 11, Article ID 1750057, 2017.

[21] S. Takeuchi, K. Murase, T. Hirano, P. Huovinen, and Y. Nara, "Effects of hadronic rescattering on multistrange hadrons in high-energy nuclear collisions," *Physical Review C*, vol. 92, no. 4, Article ID 044907, 2015.

[22] C. Gale, Y. Hidaka, S. Jeon et al., "Production and elliptic flow of dileptons and photons in a matrix model of the quark-gluon plasma," *Physical Review Letters*, vol. 114, no. 7, Article ID 072301, 2015.

[23] A. Andronic, P. Braun-Munzinger, and J. Stachel, "Thermal hadron production in relativistic nuclear collisions," *Acta Physica Polonica B*, vol. 40, pp. 1005–1012, 2009.

[24] A. Andronic, P. Braun-Munzinger, and J. Stachel, "The Horn, the hadron mass spectrum and the QCD phase diagram: the statistical model of hadron production in central nucleus-nucleus collisions," *Nuclear Physics A*, vol. 834, pp. 237c–240c, 2010.

[25] A. Andronic, P. Braun-Munzinger, and J. Stachel, "Hadron production in central nucleus-nucleus collisions at chemical freeze-out," *Nuclear Physics A*, vol. 772, no. 3-4, pp. 167–199, 2006.

[26] J. Cleymans, H. Oeschler, K. Redlich, and S. Wheaton, "Comparison of chemical freeze-out criteria in heavy-ion collisions," *Physical Review C*, vol. 73, no. 3, Article ID 034905, 2006.

[27] S. S. Adler, S. Afanasiev, C. Aidala (PHENIX Collaboration) et al., "Identified charged particles spectra and yields in Au+Au collisions at $\sqrt{s_{NN}}$ = 200 GeV," *Physical Review C*, vol. 69, Article ID 034909, 2004.

[28] E. Schnedermann, J. Sollfrank, and U. Heinz, "Thermal phenomenology of hadrons from 200A GeV S+S collisions," *Physical Review C*, vol. 48, no. 5, pp. 2462–2475, 1993.

[29] B. I. Abelev, M. M. Aggarwal, Z. Ahammed (STAR Collaboration) et al., "Systematic measurements of identified particles spectra in pp, d+Au, and Au+Au collisions at the STAR detector," *Physical Review C*, vol. 79, no. 3, Article ID 034909, 2009.

[30] B. I. Abelev, M. M. Aggarwal, Z. Ahammed (STAR Collaboration) et al., "Identified particle production, azimuthal anisotropy, and interferometry measurements in Au+Au collisions at $\sqrt{s_{NN}}$ = 9.2 GeV," *Physical Review C*, vol. 81, no. 2, Article ID 024911, 2010.

[31] Z. Tang, Y. Xu, L. Ruan, G. van Buren, F. Wang, and Z. Xu, "Spectra and radial flow in relativistic heavy ion collisions with Tsallis statistics in a blast-wave description," *Physical Review C*, vol. 79, no. 5, Article ID 051901, 2009.

[32] D. Thakur, S. Tripathy, P. Garg, R. Sahoo, and J. Cleymans, "Indication of a differential freeze-out in proton-proton and heavy-ion collisions at RHIC and LHC energies," *Advances in High Energy Physics*, vol. 2016, Article ID 4149352, 13 pages, 2016.

[33] T. Bhattacharyya, J. Cleymans, A. Khuntia, P. Pareek, and R. Sahoo, "Radial flow in non-extensive thermodynamics and study of particle spectra at LHC in the limit of small (q-1)," *The European Physical Journal A*, vol. 52, Article ID 30, 2016.

[34] H. Heiselberg and A.-M. Levy, "Elliptic flow and Hanbury-Brown-Twiss correlations in noncentral nuclear collisions," *Physical Review C*, vol. 59, no. 5, pp. 2716–2727, 1999.

[35] U. W. Heinz, Concepts of heavy-ion physics, Lecture Notes for Lectures Presented at the 2nd CERN-Latin-American School of High-Energy Physics, 1-14 June 2003, San Miguel Regla, Mexico, arXiv:hep-ph/0407360, 2004.

[36] R. Russo, *Measurement of D^+ meson production in p-Pb collisions with the ALICE detector [Ph.D. thesis]*, Universita degli Studi di Torino, Torino, Italy, 2015.

[37] H.-R. Wei, F.-H. Liu, and R. A. Lacey, "Kinetic freeze-out temperature and flow velocity extracted from transverse momentum spectra of final-state light flavor particles produced in collisions at RHIC and LHC," *The European Physical Journal A*, vol. 52, Article ID 102, 2016.

[38] H.-R. Wei, F.-H. Liu, and R. A. Lacey, "Disentangling random thermal motion of particles and collective expansion of source from transverse momentum spectra in high energy collisions," *Journal of Physics G: Nuclear and Particle Physics*, vol. 43, no. 12, Article ID 125102, 2016.

[39] H.-L. Lao, H.-R. Wei, F.-H. Liu, and R. A. Lacey, "An evidence of mass-dependent differential kinetic freeze-out scenario observed in Pb-Pb collisions at 2.76 TeV," *The European Physical Journal A*, vol. 52, Article ID 203, 2016.

[40] H.-L. Lao, F.-H. Liu, B.-C. Li, M.-Y. Duan, and R. A. Lacey, Examining the model dependence of extracting the kinetic freeze-out temperature and transverse flow velocity in small collision system, arXiv:1708.07749, 2017.

[41] W. Reisdorf, M. Stockmeier, A. Andronic (FOPI Collaboration) et al., "Systematics of pion emission in heavy ion collisions in the 1*A* GeV regime," *Nuclear Physics A*, vol. 781, no. 3-4, pp. 459–508, 2007.

[42] S. Das (for the STAR Collaboration), "Centrality dependence of freeze-out parameters from the beam energy scan at STAR," *Nuclear Physics A*, vol. 904–905, pp. 891c–894c, 2013.

[43] J. T. Mitchell (for the PHENIX Collaboration), "The PHENIX potential in the search for the QCD critical point, Talk given at the 3rd International Workshop on the Critical Point and Onset of Deconfinement, Florence, Italy, July 2006, arXiv:nucl-ex/0701079, 2006".

[44] M. Floris (for the ALICE Collaboration), "Identified particles in pp and Pb-Pb collisions at LHC energies with the ALICE detector," *Journal of Physics G: Nuclear and Particle Physics*, vol. 38, no. 12, Article ID 124025, 2011.

[45] C. Hartnack, R. K. Puri, J. Aichelin et al., "Modelling the many-body dynamics of heavy ion collisions: Present status and future perspective," *The European Physical Journal A*, vol. 1, pp. 151–169, 1998.

[46] J. Aichelin, "'Quantum' molecular dynamics–a dynamical microscopic n-body approach to investigate fragment formation and the nuclear equation of state in heavy ion collisions," *Physics Reports*, vol. 202, pp. 233–360, 1991.

[47] S. Das (for the STAR Collaboration), "Identified particle production and freeze-out properties in heavy-ion collisions at RHIC beam energy scan program," in *Proceedings of the EPJ Web of Conference*, vol. 90, Article ID 08007, 2015.

[48] E. K. G. Sarkisyan, A. N. Mishra, R. Sahoo, and A. S. Sakharov, "Centrality dependence of midrapidity density from GeV to TeV heavy-ion collisions in the effective-energy universality picture of hadroproduction," *Physical Review D*, vol. 94, no. 1, Article ID 011501, 2016.

[49] E. K. G. Sarkisyan and A. S. Sakharov, "Relating multihadron production in hadronic and nuclear collisions," *The European Physical Journal C*, vol. 70, no. 3, pp. 533–541, 2010.

[50] E. K. G. Sarkisyan and A. S. Sakharov, "On similarities of bulk observables in nuclear and particle collisions," in *Proceedings of the AIP Conference*, vol. 828, pp. 35–41, 2006.

[51] F.-H. Liu, Q.-W. Lü, B.-C. Li, and R. Bekmirzaev, "A description of the multiplicity distributions of nuclear fragments in hA and AA collisions at intermediate and high energies," *Chinese Journal of Physics*, vol. 49, pp. 601–620, 2011.

[52] F.-H. Liu, Y.-Q. Gao, T. Tian, and B.-C. Li, "Unified description of transverse momentum spectrums contributed by soft and hard processes in high-energy nuclear collisions," *The European Physical Journal A*, vol. 50, Article ID 94, 2014.

[53] J. Cleymans, The physics case for the $\sqrt{s_{NN}} \approx 10$ GeV energy region, arXiv:1711.02882 [hep-ph], 2017.

[54] Y. B. Ivanov and D. Blaschke, "Robustness of the baryon-stopping signal for the onset of deconfinement in relativistic heavy-ion collisions," *Physical Review C*, vol. 92, no. 2, Article ID 024916, 2015.

[55] Y. B. Ivanov, "Baryon stopping as a probe of deconfinement onset in relativistic heavy-ion collisions," *Physics Letters B*, vol. 721, no. 1-3, pp. 123–130, 2013.

[56] Y. B. Ivanov, "Alternative scenarios of relativistic heavy-ion collisions. I. Baryon stopping," *Physical Review C*, vol. 87, no. 6, Article ID 064904, 2013.

[57] L. Kumar (for the STAR Collaboration), "Identified hadron production from the RHIC beam energy scan," *Journal of Physics G: Nuclear and Particle Physics*, vol. 38, no. 12, Article ID 124145, 2011.

[58] A. Rustamov, "The horn, kink and step, dale: from few GeV to few TeV," *Central European Journal of Physics*, vol. 10, pp. 1267–1270, 2012.

[59] D. T. Larsen, "Energy dependence of hadron spectra and yields in p+p and ^{7}Be+^{9}Be collisions from the NA61/SHINE experiment at the CERN SPS," *Journal of Physics: Conference Series*, vol. 668, no. 1, Article ID 012020, 2016.

[60] F.-H. Liu, L.-N. Gao, and R. A. Lacey, "Searching for Minimum in Dependence of Squared Speed-of-Sound on Collision Energy," *Advances in High Energy Physics*, vol. 2016, Article ID 9467194, 9 pages, 2016.

[61] L.-N. Gao, F.-H. Liu, and R. A. Lacey, "Excitation functions of parameters in Erlang distribution, Schwinger mechanism, and Tsallis statistics in RHIC BES program," *The European Physical Journal A*, vol. 52, Article ID 137, 2016.

[62] L.-N. Gao, F.-H. Liu, Y. Sun, Z. Sun, and R. A. Lacey, "Excitation functions of parameters extracted from three-source (net-)proton rapidity distributions in Au-Au and Pb-Pb collisions over an energy range from AGS to RHIC," *The European Physical Journal A*, vol. 53, Article ID 61, 2017.

[63] C. Tsallis, "Possible generalization of Boltzmann-Gibbs statistics," *Journal of Statistical Physics*, vol. 52, no. 1-2, pp. 479–487, 1988.

[64] C. Tsallis and E. P. Borges, "Nonextensive statistical mechanics Applications to nuclear and high energy physics," in *Proceedings of the 10th International Workshop on Multiparticle Production*, N. Antoniou, Ed., 2003.

[65] W. M. Alberico, P. Czerski, A. Lavagno, M. Nardi, and V. Somá, "Signals of non-extensive statistical mechanics in high energy nuclear collisions," *Physica A: Statistical Mechanics and its Applications*, vol. 387, no. 2-3, pp. 467–475, 2008.

[66] C. Tsallis, "Nonadditive entropy: the concept and its use," *The European Physical Journal A*, vol. 40, pp. 257–266, 2009.

[67] G. Wilk and Z. Włodarczyk, "Power laws in elementary and heavy-ion collisions : a story of fluctuations and nonextensivity?" *The European Physical Journal A*, vol. 40, pp. 299–312, 2009.

[68] W. M. Alberico and A. Lavagno, "Non-extensive statistical effects in high-energy collisions," *The European Physical Journal A*, vol. 40, pp. 313–323, 2009.

[69] C. Tsallis, "An introduction to nonadditive entropies and a thermostatistical approach to inanimate and living matter," *Contemporary Physiscs*, vol. 55, no. 3, pp. 179–197, 2014.

[70] L. Marques, J. Cleymans, and A. Deppman, "Description of high-energy pp collisions using Tsallis thermodynamics: transverse momentum and rapidity distributions," *Physical Review D*, vol. 91, no. 5, Article ID 054025, 2015.

[71] C.-Y. Wong, G. Wilk, L. J. L. Cirto, and C. Tsallis, "From QCD-based hard-scattering to nonextensive statistical mechanical descriptions of transverse momentum spectra in high-energy pp and $p\overline{p}$ collisions," *Physical Review D*, vol. 91, no. 11, Article ID 114027, 2015.

[72] M. Rybczyński, G. Wilk, and Z. Włodarczyk, "System size dependence of the log-periodic oscillations of transverse momentum spectra," in *Proceedings of the EPJ Web of Conference*, vol. 90, 6 pages, 2015.

[73] H. Shababi and P. Pedram, "The minimal length uncertainty and the nonextensive thermodynamics," *International Journal of Theoretical Physics*, vol. 55, no. 6, pp. 2813–2823, 2016.

Hindawi
Advances in High Energy Physics
Volume 2018, Article ID 8347408, 9 pages
https://doi.org/10.1155/2018/8347408

Research Article

Azimuthal Anisotropy in High-Energy Nuclear Collision: An Approach Based on Complex Network Analysis

Susmita Bhaduri and Dipak Ghosh

Deepa Ghosh Research Foundation, Kolkata 700031, India

Correspondence should be addressed to Susmita Bhaduri; susmita.sbhaduri@dgfoundation.in

Received 25 October 2017; Revised 19 December 2017; Accepted 15 January 2018; Published 11 February 2018

Academic Editor: Edward Sarkisyan-Grinbaum

Recently, a complex network based method of visibility graph has been applied to confirm the scale-freeness and presence of fractal properties in the process of multiplicity fluctuation. Analysis of data obtained from experiments on hadron-nucleus and nucleus-nucleus interactions results in values of *Power of Scale-Freeness of Visibility Graph (PSVG)* parameter extracted from the visibility graphs. Here, the relativistic nucleus-nucleus interaction data have been analysed to detect *azimuthal anisotropy* by extending the visibility graph method and extracting the average clustering coefficient, one of the important topological parameters, from the graph. Azimuthal-distributions corresponding to different pseudorapidity regions around the central pseudorapidity value are analysed utilising the parameter. Here we attempt to correlate the conventional physical significance of this coefficient with respect to complex network systems, with some basic notions of particle production phenomenology, like clustering and correlation. Earlier methods for detecting anisotropy in azimuthal distribution were mostly based on the analysis of statistical fluctuation. In this work, we have attempted to find deterministic information on the anisotropy in azimuthal distribution by means of precise determination of topological parameter from a complex network perspective.

1. Introduction

Many authors have probed the azimuthal anisotropy of the produced particles in ultrarelativistic heavy-ion collisions as a function of transverse momentum and it has been used as one of the major observables to study the *collective properties* of nuclear matter [Ex. [1]]. The initial volume enclosing the interacting nucleons is essentially anisotropic in coordinate space, because of the geometry of noncentral heavy-ion collisions. The initial coordinate space anisotropy of the overlapping zone of the colliding nuclei, in which the produced nuclear matter thermalization transforms via reciprocal interactions into the final state anisotropy in the momentum space. This area has been a field of immense interest in the recent past.

The azimuthal anisotropic distribution in momentum space has been analysed using Fourier series [2], where the first few harmonicas have been referred to as directed flow, elliptical flow, and so on, and in general different harmonics will have different symmetry planes. In case of an idealized initial geometry of heavy-ion interactions, all symmetry planes coincide to the reaction plane of the collision, which is constituted by the impact parameter and the beam axis. If one uses just the orthogonality properties of trigonometric functions, the Fourier series can produce some nonvanishing flow harmonics which can not confirm whether the azimuthal anisotropic distribution in momentum space has originated from a collective anisotropic flow or from some other fully unrelated physical process capable of yielding event-by-event anisotropies (as, for example, minijets) [3]. Hence, more rigorous attempts were made to analyse collective behaviour from different perspectives which could disentangle it from the processes which normally involve only a smaller subset of the produced particles termed as *nonflow* [3]. The use of correlation-based techniques by including two or more particles has eventually led to multiparticle correlation techniques. Recently, Bilandzic et al. have suggested that if all produced particles are independently emitted and correlated only to a few common reference planes, then the presence of *azimuthal anisotropy* can be confirmed [3]. This has already

been confirmed mathematically in [4]. Sarkisyan [5] has analysed the parametrization of multiplicity distributions of the produced hadrons in high-energy interaction to describe higher order genuine correlations [6] and established the necessity of incorporating the multiparticle correlations with the property of self-similarity to achieve a good description of the measurements. Wang et al. [7] and Jiang et al. [8] were the first to go beyond two-particle azimuthal correlations, in terms of experimental analysis. However, it did not work for increased number of particles in such multiplets. The joint probability distribution of M number of particles with an M-multiplicity event has been applied theoretically, for the first time, in flow analysis of global event shapes [4] and then in other studies [1]. Borghini et al. have further reported a series of analysis on multiparticle correlations and cumulants [9]. Two- and multiparticle cumulants had drawbacks stemming from trivial and nonnegligible contributions from autocorrelations, which generates interference among various harmonics. Then Lee-Yang Zero (LYZ) method [10, 11] filters out the authentic multiparticle estimate for flow harmonics, equivalent to the asymptotic behaviour of the cumulant series. But this approach has its own integral systematic biases. Most recently, Bilandzic et al. have proposed the Q-cumulants by implementing Voloshin's fundamental idea of manifesting multiparticle azimuthal correlations in terms of Q-vectors assessed for different harmonics [12]. Though previous drawbacks are partially removed the method is very monotonous as calculation and hence could be accomplished only for a small subset of multiparticle azimuthal correlations. Bilandzic et al. have provided a generic framework which allows all multiparticle azimuthal correlations to be evaluated analytically, with a fast single pass over the data [3]. It removed previous limitations and new multiparticle azimuthal observables could be obtained experimentally. But in this method a systematic bias has been found, when all particles got divided into two groups, one of reference particles and the other particles of interest.

The evidences of self-similar characteristics in high-energy interactions have connections to the idea of fractality. In view of these, study of *azimuthal anisotropy* can also be attempted using different methods that are based on fractality of a complex system. It started from the introduction of intermittency by Bialas and Peschanski [13], for the analysis of large fluctuations, where the power-law behaviour (indicating self-similarity) of the factorial moments with decreasing size of phase-space intervals was confirmed. A relationship between the anomalous fractal dimension and intermittency indices has been established by Paladin and Vulpiani [14]. The evolution of scaling-law (thereby self-similarity) in small phase-space domains has been reviewed in terms of particle correlations and fluctuations in different high-energy multiparticle collisions by De Wolf et al. [15], and eventually a relationship between fractality and intermittency in multiparticle final states has been established. The built-in cascading mechanism in the multiparticle production process [16], naturally gives rise to a fractal structure to form the spectrum of fractal dimensions, and hence the presence of scale invariance in the hadronization process is evident. Further, various methods based on the fractal theory have been utilised to examine the multiparticle emission data [14, 17–20], and two of them, the Gq moment and Tq moment methods, were developed, respectively, by Ghosh et al. and implemented extensively to similar systems [21]. Then techniques like the Detrended Fluctuation Analysis (DFA) method [22] and Multifractal-DFA (MF-DFA) method [23] were introduced for analysing fractal and multifractal behaviour of fluctuations in high-energy interactions.

Recently, novel approaches to analyse complex networks have been proposed. Various natural systems can be termed as complex, and heterogeneous systems consisting of various kinds of fundamental units which communicate among themselves through varied interactions (namely, long-range and short-range interactions). Complex network based systems present us with a quantitative model for large-scale natural systems (in the various fields like physics, biology, and social sciences). The topological parameters extracted from these complex networks provide us with important information about the nature of the real system. The latest advances in the field of complex networks have been reviewed and the analytical models for random graphs, small-world, and scale-free networks have been analysed in the recent past [24, 25]. Havlin et al. have reported the relevance of network sciences to the analysis, perception, design, and repair of multilevel complex systems which are found in man-made and human social systems, in organic and inorganic matter, in various scales (from nano to macro), in natural and in anthropogenic systems [26]. Zhao et al. have investigated the dynamics of stock market, using correlation-based network, and identified global expansion and local clustering market behaviours during crises, using the heterogeneous time scales [27].

Lacasa et al. have introduced a very interesting method of visibility graph analysis [28, 29] that has gained importance because of its completely different, rigorous approach to estimate fractality. They have started applying the classical method of complex network analysis to measure long-range dependence and fractality of a time series [29]. Using fractional Brownian motion (fBm) and fractional Gaussian noises (fGn) series as a theoretical framework, they have experimented over real time series in various scientific fields. They have converted fractional Brownian motion (fBm) and fractional Gaussian noises (fGn) series into a scale-free visibility graph having degree distribution as a function of the Hurst parameter associated with the fractal dimension which is the degree of fractality of the time series and can be deduced from the Detrended Fluctuation Analysis (DFA) of the time series [23]. Recently, multiplicity fluctuation in π^--AgBr interaction at an incident energy of 350 GeV and ^{32}S-AgBr interaction at an incident energy of 200A GeV have been analysed using visibility graph method [30] and the fractality of void probability distribution in ^{32}S-Ag/Br interaction at an incident energy of 200 GeV per nucleon has also been analysed, using the same method (see [31] and reference there in).

Motivated by the findings obtained from the previous studies in this work the *azimuthal anisotropy* was studied

using the ^{32}S-AgBr interaction at 200A GeV by extending the complex network based visibility graph method. The average clustering coefficient [32], one of the important topological parameters, is extracted from the visibility graph constructed from the azimuthal distribution data corresponding to several pseudorapidity regions around the central pseudorapidity. The scale-freeness and fractal and multifractal properties of the process of multiparticle production have already been confirmed in [33–36], by using the DFA and MF-DFA methods. Recently, complex network based visibility graph method has been applied over data collected from π^--AgBr interaction at 350 GeV and ^{32}S-AgBr interaction at 200A GeV, and then by analysing the *Power of Scale-Freeness of Visibility Graph (PSVG)* [28, 29, 37] parameter extracted from the graphs, the scale-freeness and fractal properties of the process of particle production have been established [30, 31]. Mali et al. have applied visibility, horizontal visibility graphs, and the sandbox algorithm to analyse multiparticle emission data in high-energy nucleus-nucleus collisions in [38, 39]. The topological parameters of the visibility graphs have their usual significance with respect to the complex network systems. Here we attempted to correlate the physical significance of average clustering coefficient with some fundamental notions of particle production phenomenology, like clustering and correlation. Earlier methods for detecting anisotropy in azimuthal distribution were mostly based on the analysis of statistical fluctuation. So, in this work, we have attempted to analyse the azimuthal distribution using the approach of complex network which gives more deterministic information about the anisotropy in azimuthal distribution by means of precise topological parameters.

The rest of the paper is organized as follows. The method of visibility graph algorithm and the significance of complex network parameters like scale-freeness and average clustering coefficient are presented in Section 2. The data description and related terminologies are elaborated in Section 3.1. The details of our analysis are given in Section 3.2. The physical significance of the network parameter and its prospective correlation with the traditional concepts of *azimuthal anisotropy* in heavy-ion collisions is elaborated in Section 3.3, and the paper is concluded in Section 4.

2. Method of Analysis

As per the visibility graph method, a graph can be formed for a time or data series according to the visibility of each node from the rest of the nodes [29]. In this way the visibility graph preserves the dynamics of the fluctuation of the data present within it. Hence periodic series is transformed to a regular graph, random series to a random graph, and naturally fractal series to a scale-free network in which the graph's degree distribution conforms to the power-law with respect to its degree. Thus a fractal series can be mapped into a scale-free visibility graph [29], which is also from a series with finite number of data points [40]. However, other nonstationary and nonlinear methods like DFA and MF-DFA require an infinite number of data points as input for yielding accurate result

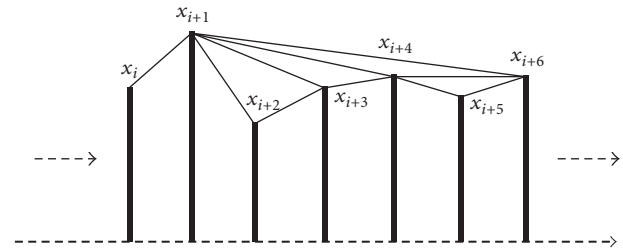

Figure 1: Visibility graph for time series X.

2.1. Visibility Graph Method. Let us suppose that the value of the ith (in the sequence of the input data series) point of time series is X_i. In this way all the input data points are mapped to their corresponding nodes or vertices (according to their value or magnitude). In this node-series, two nodes, say X_m and X_n, corresponding to the mth and nth points in the time series are said to be visible to each other or in other words joined by a two-way edge, if and only if the following equation is satisfied. In this way, a visibility graph is constructed out of a time series X:

$$X_{m+j} < X_n + \left(\frac{n-(m+j)}{n-m}\right)\cdot\left(X_m - X_n\right), \tag{1}$$

where $\forall j \in Z^+$ and $j < (n-m)$. The nodes X_m and X_n with $m = i$ and $n = i + 6$ are shown in Figure 1 where the nodes X_m and X_n are visible to each other and connected with a bidirectional edge as they satisfy (1). It is evident that the sequential nodes are always connected as two sequential points of the time or data series can always see each other.

The degree of a node of the graph, here visibility graph, is the number of connections/edges a node has with the rest of the nodes in the graph. Hence, the degree distribution of a network, say $P(k)$, is defined as the fraction of nodes in the network having degree k. Let us assume that there are n_k number of nodes with degree k and n is the total number of nodes present in a network; then $P(k) = n_k/n$ for all probable k-s.

According to Lacasa et al. [28, 29] and Ahmadlou et al. [37], the degree of scale-freeness of visibility graph corresponds to the degree of fractality and complexity of the input time or data series. The manifestation of the scale-freeness property of a visibility graph is reflected in its degree distribution, which must obey a power-law. It means that, for a visibility graph, $P(k) \sim k^{-\lambda_P}$ is satisfied, where λ_p, a constant, is called the *Power of the Scale-Freeness in Visibility Graph or PSVG*. PSVG, thus, signifies the degree of self-similarity and fractality and is, therefore, a measurement of complexity of the input time series and is linearly related to the fractal dimension of the time series [28, 29, 37]. Also, there is an inverse linear relationship between PSVG and the Hurst exponent of the time series [29].

2.2. Average Clustering Coefficient. We know that by definition a cluster in a network is a set of nodes with similar features. In this experiment, we have extracted clusters of particles based on a density-based algorithm proposed by

Ester et al. [41] from the visibility networks constructed from various experimental data sets. The algorithm followed is underlined below.

For a given set of points in some space, the points that are closely packed together or points with numerous nearby neighbours are grouped together to form clusters. Here, the density of nodes has been measured in terms of number of nodes (which has a threshold value; let's denote it by δ in our experiment) between each pair of visible nodes in the visibility graph, to form clusters. That means the closeness of the nodes to be included in a particular cluster is measured in terms of proximity as well as in terms of the visibility with respect to each other. For each node (let's denote by n_a), among all nodes that are visible from n_a, (let's denote them by $\{n_{b1}, n_{b2}, \ldots, n_{bn}\}$) those having a count less than δ, between each node $\in \{n_{b1}, n_{b2}, \ldots, n_{bn}\}$ and the source node n_a, remain in the same cluster. Naturally, these nodes are both visible from and close to the source node n_a. In this way the cluster data sets are formed for each visibility graph. Then for each of the data sets corresponding to a particular cluster, again visibility graphs are constructed and the average clustering coefficient is extracted from each of these graphs.

Clustering coefficient is the calculation of the extent to which nodes in a graph have the tendency to cluster together. Average clustering coefficient has been defined by Watts and Strogatz [32] as the overall clustering coefficient of a network, which is estimated as the mean local clustering coefficient of all the nodes in the network. For each node present in a visibility graph, the more visible its neighbouring nodes are, the more correlated and clustered these neighbours will be. In this way for each node the correlation between its neighbouring nodes is calculated and finally the average clustering coefficient of the particular visibility graph is measured. High value of this coefficient indicates the robustness of a network.

3. Experimental Details

3.1. Data Description. The experimental data has been collected by exposing Illford G5 emulsion plates to a ^{32}S-beam of 200 GeV per nucleon incident energy, from CERN. A Leitz Metaloplan microscope having 10x ocular lens and equipped with a semiautomatic scanning stage was used to examine the plate. Each plate was examined by two observers to increase the accuracy in detection, counting, and measurement. For the angle measurement of tracks, an oil immersion-100x objective was used. The measuring system has 1 μm resolution along X- and Y-axes, and 0.5 μm resolution along Z-axis.

In the previous works [31, 42] the basis for event selection is already explained. In the context of nuclear emulsion [43], after interactions the emitted particles of different categories result in shower, grey, and black tracks.

3.2. Method of Analysis. In [30] the pseudorapidity space for 10 overlapping intervals around the central pseudorapidity value (denoted by c_r) of the ^{32}S-AgBr interaction has been analysed using the visibility graph method. There, it has been established that the multiplicity fluctuation in high- energy interaction follows scaling laws in pseudorapidity space.

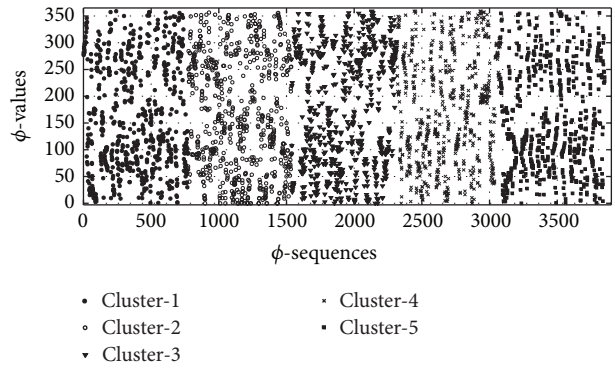

Figure 2: 5 clusters extracted from the azimuthal space corresponding to a sample pseudorapidity data set around c_r for ^{32}S-AgBr (200A GeV) interaction.

In this experiment, we have considered the azimuthal angles of the shower tracks belonging to four overlapping pseudorapidity intervals centered around c_r, from the same interaction to analyse the fluctuation and to identify the clustering pattern from a complex network perspective, and attempted to detect whether the azimuthal fluctuation is also self-similar in nature and follows scaling laws. Further the presence of *azimuthal anisotropy* has been probed by extracting the clusters and calculating the average clustering coefficient, for each of the four ϕ-data sets, in the light of conventional concept of multiparticle correlations.

The detailed steps for the analysis are described below.

(1) For each of the 4 overlapping pseudorapidity intervals centered around c_r (the range of the η-values is indicated by $c_r - \Delta\eta$ to $c_r + \Delta\eta$, where $\Delta\eta$ varies from 1 to 4), the ϕ-values of the shower tracks are considered, and this way the 4 input data sets for the experiment are formed. Four visibility graphs are constructed according to the method described in Section 2.1.

(2) Then clusters are extracted following the density-based algorithm proposed by Ester et al. [41] from each of the 4 visibility graphs and one set of data points corresponding to each of the clusters is obtained. Figure 2 shows a specimen of 5 clusters taken out from the data set of ϕ-values in the pseudorapidity region closest to c_r for ^{32}S-AgBr (at 200A GeV) interaction.

(3) Once again visibility graphs are constructed from all the cluster data extracted from the four visibility graphs constructed in the step (1). For each graph the values of $P(k)$ for all possible values of k-s are computed and the power-law fitting is done by following the method suggested by Clauset et al. [44].

In Figure 3(a) the $P(k)$ versus k plot for a sample cluster is shown, where the power-law relationship is evident from the value of $R^2(0.96)$ of the power-law fitting. As explained in Section 2.1, once the power-law has been confirmed for the $P(k)$ versus k variation, the power-law exponent PSVG of the corresponding cluster is obtained.

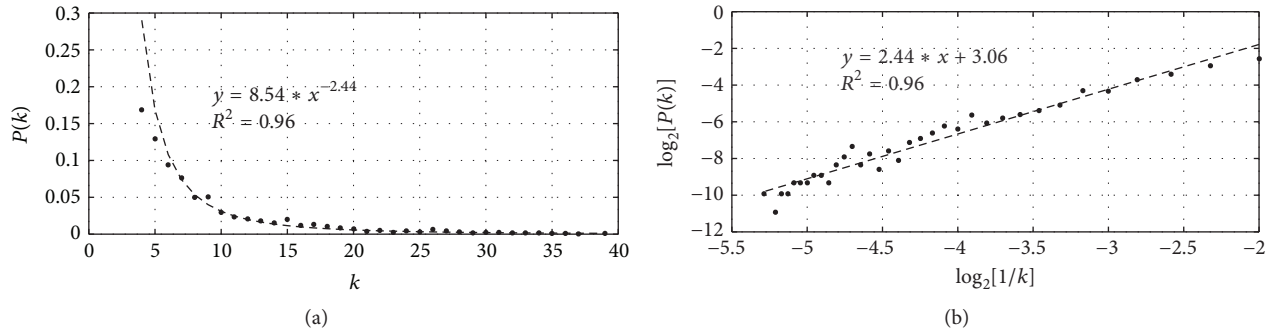

FIGURE 3: (a) $P(k)$ versus k plot for a cluster (b) $\log_2[P(k)]$ versus $\log_2[1/k]$ plot for the same cluster.

The same values of PSVG parameter are also obtained from the gradient of $\log_2[P(k)]$ versus $\log_2[1/k]$ plot for the same cluster data. Again goodness of fit for straight line fitting can be confirmed from the corresponding value of R^2. Figure 3(b) shows such a plot for the same specimen cluster data that is plotted in Figure 3(a) and the PSVG is 2.44 ± 0.1, while $R^2 = 0.96$.

Table 1 shows a list of PSVG values calculated for the visibility graphs constructed from a sample set of 30 cluster data sets extracted from the visibility graph corresponding to one of the four data set of ϕ-values for ^{32}S-AgBr (200A GeV) interaction data (constructed in step (1)). The table also shows the corresponding χ^2/DOF values, and the values of R^2 calculated for both power-law fitting for $P(k)$ versus k data set and straight line fitting for $\log_2[P(k)]$ versus $\log_2[1/k]$ plot of the same data set. The power-law relationship and good scaling behaviour can be confirmed from the corresponding χ^2/DOF values and the values of R^2 for all the cluster data sets in Table 1.

(4) Similar analysis for all the clusters extracted from the visibility graphs constructed for all four ϕ-data sets around the c_r value of the experimental data (constructed in step (1)) is carried out. As PSVG correlates the amount of complexity with fractality of the data series, and eventually with the fractal dimension of the experimental data series [28, 29, 37], it can be confirmed that all these clusters are scale-free and also are of fractal structure.

(5) Then Monte-Carlo simulated data set is generated for each of the cluster data sets, assuming independent emission of pions in ^{32}S-Ag/Br interaction at 200A GeV. The data for Monte-Carlo simulated data sets have been chosen in such a way that $dn/d\phi$ distribution of the Monte-Carlo simulated data resembles the corresponding $dn/d\phi$ of the experimental ensembles. Then for all these Monte-Carlo simulated data sets, first visibility graphs are constructed and then PSVG-s are calculated. Table 2 shows the list of PSVG values along with values of χ^2/DOF and R^2, calculated for the visibility graphs constructed from the Monte-Carlo simulated version of the same sample set of

TABLE 1: List of PSVG values calculated for the visibility graphs constructed from a sample set of 30 cluster data sets extracted from the visibility graph corresponding to one of the four data sets of ϕ-values for ^{32}S-AgBr (200A GeV) interaction data (constructed in step (1)).

$\text{Cluster}_{\text{seq}}$	PSVG	χ^2/DOF	R^2
Cluster_1	2.2 ± 0.14	0.92	0.03
Cluster_2	2.03 ± 0.18	0.86	0.03
Cluster_3	2.12 ± 0.17	0.88	0.02
Cluster_4	2.1 ± 0.14	0.92	0.02
Cluster_5	2.02 ± 0.19	0.85	0.02
Cluster_6	2.15 ± 0.18	0.89	0.05
Cluster_7	2.33 ± 0.17	0.92	0.02
Cluster_8	2.25 ± 0.2	0.88	0.02
Cluster_9	2.61 ± 0.26	0.86	0.03
Cluster_{10}	2.3 ± 0.13	0.94	0.02
Cluster_{11}	2.11 ± 0.1	0.95	0.02
Cluster_{12}	2.16 ± 0.14	0.91	0.03
Cluster_{13}	2 ± 0.18	0.87	0.01
Cluster_{14}	1.83 ± 0.16	0.84	0.04
Cluster_{15}	2.34 ± 0.15	0.93	0.03
Cluster_{16}	2.51 ± 0.13	0.96	0.03
Cluster_{17}	2.32 ± 0.15	0.93	0.03
Cluster_{18}	2.23 ± 0.15	0.92	0.02
Cluster_{19}	2.02 ± 0.13	0.91	0.03
Cluster_{20}	2.14 ± 0.18	0.88	0.02
Cluster_{21}	2.31 ± 0.11	0.95	0.04
Cluster_{22}	2.06 ± 0.18	0.87	0.04
Cluster_{23}	1.98 ± 0.23	0.79	0.02
Cluster_{24}	2.21 ± 0.19	0.87	0.02
Cluster_{25}	1.88 ± 0.18	0.82	0.02
Cluster_{26}	2.03 ± 0.21	0.83	0.04
Cluster_{27}	2 ± 0.12	0.91	0.02
Cluster_{28}	2.15 ± 0.17	0.87	0.04
Cluster_{29}	1.93 ± 0.15	0.86	0.03
Cluster_{30}	2.16 ± 0.19	0.86	0.04

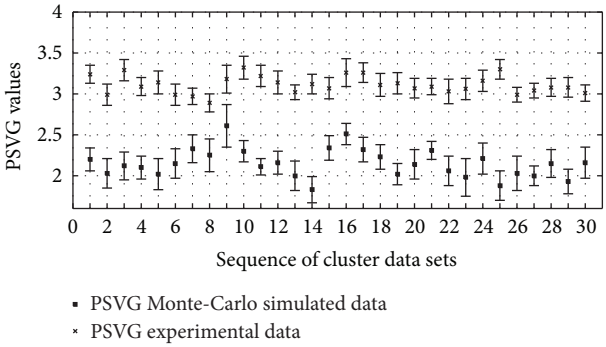

Figure 4: Trend of PSVG values calculated for a specimen set of 30 cluster data sets (both experimental and their MC simulated ones as shown in Tables 1 and 2) extracted from the visibility graph corresponding to one of the four data sets of ϕ-values for ^{32}S-AgBr (200A GeV) interaction data (constructed in step (1)).

30 cluster data sets as shown in Table 1 for the same particular ϕ-data set for ^{32}S-AgBr (200A GeV) interaction (constructed in step (1)) data.

Figure 4 also shows the trend of PSVG values calculated for the same specimen set of 30 cluster-datasets (both experimental and the MC simulated results) as shown in Tables 1 and 2. The PSVG values calculated for the experimental data sets significantly differ from their Monte-Carlo simulated counterpart. This finding establishes that the degree of complexity for any cluster is not the result of the Monte-Carlo simulated fluctuation pattern, but of some dynamics present in the cluster data sets.

(6) The statistical errors shown in Tables 1 and 2 and Figure 4 are obtained from the corresponding fit processes. The details of error calculation have already been discussed in a previous work [45]. The values of χ^2/DOF and R^2 for the straight line fitting (for $\log_2[1/k]$ versus $\log_2[P(k)]$ plots) and power-law fitting (for k versus $P(k)$ plots) in these figures and tables reflect the goodness of fit. We have followed Pearson's chi-squared test [46] to calculate the χ^2/DOF values, after considering the statistical errors. These errors are calculated individually for every point and the diagonal elements of the full covariance matrix are obtained thereof [47]. The off-diagonal elements of the covariance matrix are produced because of the correlation between the data points and this correlation must be considered to have a detailed picture of the full covariance matrix. The diagonal elements of the full covariance matrix mainly contribute to χ^2/DOF values, as per the analysis done in various other works [48]. If the off-diagonal elements are considered, the changes contributing to the χ^2/DOF values are trivial and hence do not affect the final conclusion.

(7) In the next step the average clustering coefficients are extracted from the visibility graphs for all the cluster data sets corresponding to the four ϕ-data sets (constructed in step (1)), as per the method explained in Section 2.2. Then from the visibility graphs constructed from all the corresponding Monte-Carlo simulated data sets, the average clustering coefficients are calculated.

(i) In this way we obtain 4 sets containing pairs of average clustering coefficients (calculated for experimental and MC simulated cluster-datasets) for the four ϕ-data sets.

(ii) Each pair of average clustering coefficients corresponds to the average clustering coefficient of the visibility graph created for a particular cluster data set, and the average clustering coefficient of the visibility graph constructed also for its Monte-Carlo simulated version.

Table 2: List of PSVG values calculated for the visibility graphs constructed from the Monte-Carlo simulated version of the same sample set of 30 cluster data sets (as shown in Table 1) extracted from the visibility graph corresponding to one of the four data sets of ϕ-values for ^{32}S-AgBr (200A GeV) interaction data (constructed in step (1)).

$\text{Cluster}_{\text{seq}}$	PSVG	χ^2/DOF	R^2
Cluster_1	3.24 ± 0.11	0.96	0.02
Cluster_2	2.99 ± 0.13	0.94	0.02
Cluster_3	3.29 ± 0.13	0.95	0.02
Cluster_4	3.09 ± 0.11	0.96	0.03
Cluster_5	3.14 ± 0.14	0.94	0.02
Cluster_6	2.99 ± 0.13	0.94	0.03
Cluster_7	2.97 ± 0.1	0.96	0.02
Cluster_8	2.89 ± 0.11	0.95	0.03
Cluster_9	3.18 ± 0.17	0.91	0.02
Cluster_{10}	3.32 ± 0.14	0.94	0.02
Cluster_{11}	3.22 ± 0.13	0.95	0.01
Cluster_{12}	3.14 ± 0.14	0.94	0.02
Cluster_{13}	3.02 ± 0.09	0.97	0.02
Cluster_{14}	3.12 ± 0.12	0.95	0.02
Cluster_{15}	3.07 ± 0.13	0.94	0.02
Cluster_{16}	3.26 ± 0.17	0.93	0.02
Cluster_{17}	3.26 ± 0.12	0.95	0.03
Cluster_{18}	3.11 ± 0.14	0.94	0.02
Cluster_{19}	3.13 ± 0.13	0.95	0.03
Cluster_{20}	3.07 ± 0.12	0.95	0.03
Cluster_{21}	3.09 ± 0.1	0.97	0.02
Cluster_{22}	3.03 ± 0.15	0.93	0.03
Cluster_{23}	3.06 ± 0.13	0.94	0.02
Cluster_{24}	3.16 ± 0.13	0.95	0.03
Cluster_{25}	3.3 ± 0.12	0.95	0.02
Cluster_{26}	2.99 ± 0.09	0.97	0.01
Cluster_{27}	3.04 ± 0.09	0.97	0.02
Cluster_{28}	3.08 ± 0.11	0.95	0.02
Cluster_{29}	3.08 ± 0.12	0.95	0.02
Cluster_{30}	3.01 ± 0.1	0.96	0.02

Table 3: Trend of number of clusters is selected from each of the four ϕ-data sets [corresponding to the pseudorapidity regions around c_r for ^{32}S-AgBr (200A GeV) interaction] which have almost similar average clustering coefficient to their Monte-Carlo simulated counterparts.

$\Delta\eta$	Number of clusters
1.0	7
2.0	5
3.0	5
4.0	2

(iii) Then from each these four sets, the cluster data sets which have almost similar average clustering coefficient as their Monte-Carlo simulated counterparts are selected.

(iv) The count of such clusters for each of the four ϕ-data sets is calculated and listed in Table 3. The trend of this count across the ϕ-data sets (corresponding to the pseudorapidity regions with $\Delta\eta = 1.0$ to $\Delta\eta = 4.0$ around c_r) is shown in Table 3. The trend is evidently *decreasing* from the azimuthal distribution in the pseudorapidity region closest to c_r to the farthest one.

3.3. Results and Discussions. As already mentioned in the Section 1, several analyses have shown that the power-law spectra arising even from nonextensive statistics can rightly identify the general properties of particle production in high-energy interactions. Recently, Deppman and Megías [49] have shown that the fractal dimensions of the thermofractal obtained from values of temperature and *entropic* index resulting from the analysis of p_T distributions in high-energy interactions are similar to those found in analyses of intermittency in experimental data in high-energy collisions.

Experimental data from ^{32}S-AgBr at 200A GeV interaction has been analysed using the complex network based visibility graph method and the PSVG values obtained thereof have been compared for all the overlapping η-regions centered around c_r, and it has been shown that the multiplicity fluctuation in high-energy interaction is self-similar and scale-free [30]. The present work provides another evidence of fractal structure in multiparticle emission data.

In this work we have constructed visibility graphs from their corresponding azimuthal space or ϕ-data sets. From each visibility graph, a number of cluster data sets are extracted, and then again visibility graphs are constructed for each cluster data set and its Monte-Carlo simulated counterpart. Finally it is shown that each of these clusters is self-similar and scale-free and hence is of fractal structure.

(i) For each cluster and its Monte-Carlo simulated counterpart, average clustering coefficients are calculated, and it has been found that the count of clusters having almost similar average clustering coefficient to their Monte-Carlo simulated counterparts is decreasing from the ϕ-region closest to the farthest from c_r. Clustering coefficient is essentially generalised as signed correlation between the nodes of the networks [50]. In this experiment the correlation is measured in terms of the visibility between the nodes of the cluster data sets.

(ii) Hence this decreasing count of clusters shown in Table 3 from pseudorapidity regions with $\Delta\eta = 1.0$ to $\Delta\eta = 4.0$ around c_r signifies that the particle-to-particle correlation in the azimuthal distribution is *least* in the pseudorapidity region that is closest to c_r (with $\Delta\eta = 1.0$). Therefore, this region has the maximum number of clusters having similar average clustering coefficient to their Monte-Carlo simulated versions. However, the particle-to-particle correlation is gradually increasing as the count of clusters having similar average clustering coefficient compared to their Monte-Carlo simulated counterparts decreases in the regions that are farther from c_r and finally this count is least in the farthest pseudorapidity region from c_r.

(iii) Particle-to-particle correlation in the azimuthal distribution is *least* in the most central pseudorapidity space, which gradually increases towards the region farthest from c_r and becomes *highest* in the pseudorapidity region with $\Delta\eta = 4.0$.

4. Conclusion

Bilandzic et al. have discussed that azimuthal anisotropic distribution might be the underlying cause of collective anisotropic flow of the produced particles in ultrarelativistic heavy-ion collisions [3]. The dynamics of *azimuthal anisotropy* in multiparticle production process is yet to come out with accurate parameters. Detailed and latest methods to analyse collective anisotropic flow using multiparticle azimuthal correlations are not free from systematic bias in conventional differential flow analyses. Hence, this is still an open area of research. In view of this, we have attempted to analyse *azimuthal anisotropy* by analysing the azimuthal distribution from a complex network perspective, which gives more deterministic information about the anisotropy in azimuthal distribution in terms of precise topological parameter.

It is observed that particle-to-particle correlation in the azimuthal distribution is least in the region closest to the central pseudorapidity, because in this region the pattern of clusters formed by the particles is mostly similar to their Monte-Carlo simulated counterparts. But, this correlation increases monotonically towards the region farthest from the central pseudorapidity. This in effect establishes the anisotropic nature of the azimuthal distribution closest to the central pseudorapidity region. This interesting observation might have a far reaching consequence to confirm the *collective anisotropic flow* in that region.

Conflicts of Interest

There are no conflicts of interest related to this paper.

Acknowledgments

The authors thank the *Department of Higher Education, Govt. of West Bengal, India,* for financial support.

References

[1] J. Y. Ollitrault, "Anisotropy as a signature of transverse collective flow," *Physical Review D: Particles, Fields, Gravitation and Cosmology*, vol. 46, p. 229, 1992.

[2] S. Voloshin and Y. Zhang, "Flow study in relativistic nuclear collisions by Fourier expansion of azimuthal particle distributions," *Zeitschrift für Physik C Particles and Fields*, vol. 70, no. 4, pp. 665–671, 1996.

[3] A. Bilandzic, C. H. Christensen, K. Gulbrandsen, A. Hansen, and Y. Zhou, "Generic framework for anisotropic flow analyses with multiparticle azimuthal correlations," *Physical Review C: Nuclear Physics*, vol. 89, no. 6, Article ID 064904, 2014.

[4] P. Danielewicz and M. Gyulassy, "Jacobian free global event analysis," *Physics Letters B*, vol. 129, no. 5, pp. 283–288, 1983.

[5] E. K. G. Sarkisyan, "Description of local multiplicity fluctuations and genuine multiparticle correlations," *Physics Letters B*, vol. 477, no. 1–3, pp. 1–12, 2000.

[6] G. Abbiendi, K. Ackerstaff, and G. Alexander, "Intermittency and correlations in hadronic Z0 decays," *The European Physical Journal C*, vol. 11, no. 2, pp. 239–250, 1999.

[7] S. Wang, Y. Z. Jiang, Y. M. Liu et al., "Measurement of collective flow in heavy-ion collisions using particle-pair correlations," *Physical Review C: Nuclear Physics*, vol. 44, no. 3, pp. 1091–1095, 1991.

[8] J. Jiang, D. Beavis, S. Y. Chu et al., "High-order collective-flow correlations in heavy-ion collisions," *Physical Review Letters*, vol. 68, no. 18, pp. 2739–2742, 1992.

[9] N. Borghini, P. M. Dinh, and J.-Y. Ollitrault, "Flow analysis from multiparticle azimuthal correlations," *Physical Review C: Nuclear Physics*, vol. 64, no. 5, Article ID 054901, 2001.

[10] R. S. Bhalerao, N. Borghini, and J.-Y. Ollitrault, "Analysis of anisotropic flow with Lee-Yang zeroes," *Nuclear Physics A*, vol. 727, no. 3-4, pp. 373–426, 2003.

[11] R. S. Bhalerao, N. Borghini, and J.-Y. Ollitrault, "Genuine collective flow from Lee-Yang zeroes," *Physics Letters B*, vol. 580, no. 3-4, pp. 157–162, 2004.

[12] A. Bilandzic, R. Snellings, and S. Voloshin, "Flow analysis with cumulants: direct calculations," *Physical Review C: Nuclear Physics*, vol. 83, no. 4, Article ID 044913, 11 pages, 2011.

[13] A. Bialas and R. Peschanski, "Moments of rapidity distributions as a measure of short-range fluctuations in high-energy collisions," *Nuclear Physics B*, vol. 273, no. 3-4, pp. 703–718, 1986.

[14] G. Paladin and A. Vulpiani, "Anomalous scaling laws in multifractal objects," *Physics Reports*, vol. 156, no. 4, pp. 147–225, 1987.

[15] E. A. De Wolf, I. M. Dremin, and W. Kittel, "Scaling laws for density correlations and fluctuations in multiparticle dynamics," *Physics Reports*, vol. 270, no. 3, pp. 1–141, 1996.

[16] A. Bialas and R. Peschanski, "Intermittency in multiparticle production at high energy," *Nuclear Physics B*, vol. 308, no. 4, pp. 857–867, 1988.

[17] R. C. Hwa, "Fractal measures in multiparticle production," *Physical Review D: Particles, Fields, Gravitation and Cosmology*, vol. 41, no. 5, pp. 1456–1462, 1990.

[18] P. Grassberger and I. Procaccia, "Dimensions and entropies of strange attractors from a fluctuating dynamics approach," *Physica D: Nonlinear Phenomena*, vol. 13, no. 1-2, pp. 34–54, 1984.

[19] T. C. Halsey, M. H. Jensen, L. P. Kadanoff, I. Procaccia, and B. I. Shraiman, "Fractal measures and their singularities: the characterization of strange sets," *Physical Review A: Atomic, Molecular and Optical Physics*, vol. 33, no. 2, pp. 1141–1151, 1986.

[20] F. Takagi, "Multifractal structure of multiplicity distributions in particle collisions at high energies," *Physical Review Letters*, vol. 72, no. 1, pp. 32–35, 1994.

[21] D. Ghosh, A. Deb, S. Bhattacharyya, and U. Datta, "Multiplicity scaling of target protons in high-energy nucleusnucleus and hadronnucleus interactions," *Journal of Physics G: Nuclear and Particle Physics*, vol. 39, no. 3, Article ID 035101, 2012.

[22] C.-K. Peng, S. V. Buldyrev, S. Havlin, M. Simons, H. E. Stanley, and A. L. Goldberger, "Mosaic organization of DNA nucleotides," *Physical Review E: Statistical, Nonlinear, and Soft Matter Physics*, vol. 49, no. 2, pp. 1685–1689, 1994.

[23] J. W. Kantelhardt, E. Koscielny-Bunde, H. H. A. Rego, S. Havlin, and A. Bunde, "Detecting long-range correlations with detrended fluctuation analysis," *Physica A: Statistical Mechanics and its Applications*, vol. 295, no. 3-4, pp. 441–454, 2001.

[24] R. Albert and A.-L. Barabási, "Statistical mechanics of complex networks," *Reviews of Modern Physics*, vol. 74, no. 1, pp. 47–97, 2002.

[25] A.-L. Barabási, "The network takeover," *Nature Physics*, vol. 8, no. 1, pp. 14–16, 2012.

[26] S. Havlin, D. Y. Kenett, E. Ben-Jacob et al., "Challenges in network science: Applications to infrastructures, climate, social systems and economics," *The European Physical Journal Special Topics*, vol. 214, no. 1, pp. 273–293, 2012.

[27] L. Zhao, W. Li, and X. Cai, "Structure and dynamics of stock market in times of crisis," *Physics Letters A*, vol. 380, no. 5-6, pp. 654–666, 2016.

[28] L. Lacasa, B. Luque, F. Ballesteros, J. Luque, and J. C. Nuno, "From time series to complex networks: the visibility graph," *Proceedings of the National Acadamy of Sciences of the United States of America*, vol. 105, no. 13, pp. 4972–4975, 2008.

[29] L. Lacasa, B. Luque, J. Luque, and J. C. Nũo, "The visibility graph: A new method for estimating the Hurst exponent of fractional Brownian motion," *EPL (Europhysics Letters)*, vol. 86, no. 3, Article ID 30001, 2009.

[30] S. Bhaduri and D. Ghosh, "Multiplicity fluctuation and phase transition in high-energy collision-A chaos-based study with complex network perspective," *International Journal of Modern Physics A*, vol. 31, no. 35, Article ID 1650185, 2016.

[31] S. Bhaduri, A. Bhaduri, and D. Ghosh, "A new approach of chaos and complex network method to study fluctuation and phase transition in nuclear collision at high energy," *The European Physical Journal A*, vol. 53, no. 6, article no. 135, 2017.

[32] D. J. Watts and S. H. Strogatz, "Collective dynamics of 'small-world' networks," *Nature*, vol. 393, no. 6684, pp. 440–442, 1998.

[33] C. Albajar, O. C. Allkofer, R. J. Apsimon et al., "Multifractal analysis of minimum bias events in s**(1/2) = 630-GeV anti-p p collisions," *Zeitschrift für Physik C Particles and Fields*, vol. 56, no. 1, pp. 37–46, 1992.

[34] M. K. Suleymanov, M. Sumbera, and I. Zborovsky, *Entropy and multifractal analysis of multiplicity distributions from pp simulated events up to LHC energies*, 2003.

[35] Y. X. Zhang, W. Y. Qian, and C. B. Yang, "Multifractal structure of pseudorapidity and azimuthal distributions of the shower particles in Au + Au collisions at 200 A GeV," *International Journal of Modern Physics A*, vol. 23, no. 18, p. 2809, 2008.

[36] E. G. Ferreiro and C. Pajares, *High multiplicity pp events and J/Ψ production at LHC*, 2012.

[37] M. Ahmadlou, H. Adeli, and A. Adeli, "Improved visibility graph fractality with application for the diagnosis of Autism Spectrum Disorder," *Physica A: Statistical Mechanics and its Applications*, vol. 391, no. 20, pp. 4720–4726, 2012.

[38] P. Mali, A. Mukhopadhyay, S. K. Manna, P. K. Haldar, and G. Singh, "Multifractal analysis of charged particle distributions using horizontal visibility graph and sandbox algorithm," *Modern Physics Letters A*, vol. 32, no. 8, Article ID 1750024, 2017.

[39] P. Mali, S. K. Manna, A. Mukhopadhyay, P. Haldar, and G. Singh, "Multifractal analysis of multiparticle emission data in the framework of visibility graph and sandbox algorithm," *Physica A: Statistical Mechanics and its Applications*, vol. 493, pp. 253–266, 2018.

[40] S. Jiang, C. Bian, X. Ning, and Q. D. Y. Ma, "Visibility graph analysis on heartbeat dynamics of meditation training," *Applied Physics Letters*, vol. 102, no. 25, Article ID 253702, 2013.

[41] M. Ester, H. P. Kriegel, J. Sander, and X. Xu, "A Density-Based Algorithm for Discovering Clusters in Large Spatial Databases with Noise," in *Proceedings of the 2nd International Conference on Knowledge Discovery and Data Mining*, pp. 226–231, 1996.

[42] S. Bhaduri and D. Ghosh, "Study of Void Probability Scaling of Singly Charged Particles Produced in Ultrarelativistic Nuclear Collision in Fractal Scenario," *Advances in High Energy Physics*, vol. 2016, Article ID 6848197, 2016.

[43] C. F. Powell and H. d. Perkins, *The Study of Elementary Particles by the Photographic Method*, Pergamon Press, Oxford, 1959.

[44] A. Clauset, C. R. Shalizi, and M. E. Newman, "Power-law distributions in empirical data," *SIAM Review*, vol. 51, no. 4, pp. 661–703, 2009.

[45] D. Ghosh, A. Deb, S. Bhattacharyya, and U. Datta, "Multiplicity dependence of entropy in different rapidity bins in high-energy nucleusnucleus interactions," *Physica Scripta*, vol. 85, no. 6, Article ID 065205, 2012.

[46] K. X. Pearson, "On the criterion that a given system of deviations from the probable in the case of a correlated system of variables is such that it can be reasonably supposed to have arisen from random sampling," *Philosophical Magazine*, vol. 50, no. 302, pp. 157–175, 2009.

[47] R. L. Plackett, "Karl Pearson and the chi-squared test," *International Statistical Review*, vol. 51, no. 1, pp. 59–72, 1983.

[48] N. M. Agababyan, M. R. Atayan, M. Charlet et al., "Self-affine fractality in π+p and K+p collisions at 250 GeV/c," *Physics Letters B*, vol. 382, no. 3, pp. 305–311, 1996.

[49] A. Deppman and E. Megías, "Fractal aspects of hadrons," in *Proceedings of the 46th International Symposium on Multiparticle Dynamics, ISMD 2016*, Republic of Korea, September 2016.

[50] G. Costantini and M. Perugini, "Generalization of clustering coefficients to signed correlation networks," *PLoS ONE*, vol. 9, no. 2, Article ID e88669, 2014.

Hindawi
Advances in High Energy Physics
Volume 2018, Article ID 1369098, 8 pages
https://doi.org/10.1155/2018/1369098

Research Article

A Description of Pseudorapidity Distributions of Charged Particles Produced in Au+Au Collisions at RHIC Energies

Z. J. Jiang, Dongfang Xu, and Yan Huang

College of Science, University of Shanghai for Science and Technology, Shanghai 200093, China

Correspondence should be addressed to Z. J. Jiang; jzj265@163.com

Received 15 October 2017; Revised 10 December 2017; Accepted 27 December 2017; Published 24 January 2018

Academic Editor: Fu-Hu Liu

In heavy ion collisions, charged particles come from two parts: the hot and dense matter and the leading particles. In this paper, the hot and dense matter is assumed to expand according to the hydrodynamic model including phase transition and decouples into particles via the prescription of Cooper-Frye. The leading particles are as usual supposed to have Gaussian rapidity distributions with the number equaling that of participants. The investigations of this paper show that, unlike low energy situations, the leading particles are essential in describing the pseudorapidity distributions of charged particles produced in high energy heavy ion collisions. This might be due to the different transparencies of nuclei at different energies.

1. Introduction

The BNL Relativistic Heavy Ion Collider (RHIC) accelerates nuclei up to the center-of-mass energies from a dozen GeV to 200 GeV per nucleon. In the past decade, the measurements from such collisions have triggered an extensive research for the properties of matter at extreme conditions of very high temperature and energy densities [1–33]. One of the most important achievements from such research is the discovery that the matter created in nucleus-nucleus collisions at RHIC energies is in the state of strongly coupled quark-gluon plasma (sQGP) exhibiting a clear collective behavior nearly like a perfect fluid with very low viscosity [10–33].

The best approach for describing the space-time evolution of fluid-like sQGP is the relativistic hydrodynamics. However, owing to the formidable complexities of hydrodynamic equations, the most analytical work so far is mainly limited to 1+1 expansion for a perfect fluid with simple equation of state, which can be found as an important application in the analysis of the pseudorapidity distributions of charged particles in high energy physics. In this paper, combining the effects of leading particles, we will discuss such distributions in the framework of 1+1 hydrodynamic model including phase transition [10].

2. A Brief Introduction to the Model

Here, for the purpose of completeness and applications, we will list the key ingredients of the hydrodynamic model [10].

(1) The expansion of fluid is subject to the conservation of energy and momentum. This is reflected in continuity equation

$$\frac{\partial T^{\mu\nu}}{\partial x^{\nu}} = 0, \quad \mu, \nu = 0, 1, \tag{1}$$

where $T^{\mu\nu}$ is the energy-momentum tensor. For a perfect fluid

$$T^{\mu\nu} = (\varepsilon + p) u^{\mu} u^{\nu} - p g^{\mu\nu}, \tag{2}$$

where

$$u^{\mu} = \left(u^0, u^1\right) = \left(\cosh y_F, \sinh y_F\right), \quad u^{\mu} u_{\mu} = 1, \tag{3}$$

is the 4-velocity of fluid and y_F is its rapidity. ε and p in (2) are the energy density and pressure of fluid, which meet the thermodynamical relations

$$\begin{aligned} \varepsilon + p &= Ts, \\ \mathrm{d}\varepsilon &= T\mathrm{d}s, \\ \mathrm{d}p &= s\mathrm{d}T, \end{aligned} \tag{4}$$

where T and s are the temperature and entropy density of fluid, respectively. To close (1), another relation, namely, the equation of state

$$\frac{\mathrm{d}p}{\mathrm{d}\varepsilon} = \frac{s\mathrm{d}T}{T\mathrm{d}s} = c_s^2, \tag{5}$$

is needed, where c_s is the sound speed of fluid, which takes different values in sQGP and in hadronic phase.

(2) Project (1) to the direction of u_μ and the direction perpendicular to u_μ, respectively. This leads to equations

$$\frac{\partial (su^\nu)}{\partial x^\nu} = 0, \tag{6}$$

$$\frac{\partial (T\sinh y_F)}{\partial t} + \frac{\partial (T\cosh y_F)}{\partial z} = 0. \tag{7}$$

Equation (6) is the continuity equation for entropy conservation. Equation (7) means the existence of a scalar function ϕ satisfying relations

$$\begin{aligned} \frac{\partial \phi}{\partial t} &= T\cosh y_F, \\ \frac{\partial \phi}{\partial z} &= -T\sinh y_F. \end{aligned} \tag{8}$$

From ϕ and Legendre transformation, Khalatnikov potential χ is introduced via relation

$$\chi = \phi - tT\cosh y_F + zT\sinh y_F. \tag{9}$$

In terms of χ, the variables t and z can be expressed as

$$\begin{aligned} t &= \frac{e^\theta}{T_0}\left(\frac{\partial \chi}{\partial \theta}\cosh y_F + \frac{\partial \chi}{\partial y_F}\sinh y_F\right), \\ z &= \frac{e^\theta}{T_0}\left(\frac{\partial \chi}{\partial \theta}\sinh y_F + \frac{\partial \chi}{\partial y_F}\cosh y_F\right), \end{aligned} \tag{10}$$

where T_0 is the initial temperature of fluid and $\theta = \ln(T_0/T)$. Through the above equations, the coordinate base of (t, z) is transformed to that of (θ, y_F), and (6) is translated into the so-called telegraphy equation

$$\frac{\partial^2 \chi}{\partial \theta^2} - 2\beta\frac{\partial \chi}{\partial \theta} - \frac{1}{c_s^2}\frac{\partial^2 \chi}{\partial y_F^2} = 0, \quad \beta = \frac{1 - c_s^2}{2c_s^2}. \tag{11}$$

(3) Along with the expansions of matter created in collisions, it becomes cooler and cooler. As its temperature drops from the initial T_0 to the critical T_c, phase transition occurs. The matter transforms from sQGP state to hadronic state. The produced hadrons are initially in the violent and frequent collisions. The major part of these collisions is inelastic. Hence, the abundances of identified hadrons are changing. Furthermore, the mean free paths of these primary hadrons are very short. The movement of them is still like that of a fluid meeting (11) with only difference being the value of c_s. In sQGP, $c_s = c_0 = 1/\sqrt{3}$, which is the sound speed of a massless perfect fluid, being the maximum of c_s. In the hadronic state, $c_s = c_h < c_0$. At the point of phase transition, that is, as $T = T_c$, c_s is discontinuous.

(4) The solution of (11) for the sector of sQGP is [10]

$$\chi_0(\theta, y_F) = \frac{q_0 c_0}{2} e^{\beta_0 \theta} I_0\left(\beta_0 c_0 \sqrt{y_0^2(\theta) - y_F^2}\right), \tag{12}$$

where q_0 is a constant determined by tuning the theoretical results to experimental data and I_0 is the 0th-order modified Bessel function of the first kind, and

$$\begin{aligned} \beta_0 &= \frac{1 - c_0^2}{2c_0^2} = 1, \\ y_0(\theta) &= \frac{\theta}{c_0}. \end{aligned} \tag{13}$$

In the sector of hadrons, the solution of (11) is [10]

$$\chi_h(\theta, y_F) = \frac{q_0 c_0}{2} B(\theta)\, I_0\left[\lambda(\theta, y_F)\right], \tag{14}$$

where

$$\begin{aligned} B(\theta) &= e^{\beta_h(\theta - \theta_c) + \beta_0 \theta_c}, \\ \lambda(\theta, y_F) &= \beta_h c_h \sqrt{y_h^2(\theta) - y_F^2}, \\ \beta_h &= \frac{1 - c_h^2}{2c_h^2}, \\ y_h(\theta) &= \frac{\theta - \theta_c}{c_h} + \frac{\theta_c}{c_0}, \\ \theta_c &= \ln\left(\frac{T_0}{T_c}\right). \end{aligned} \tag{15}$$

3. The Pseudorapidity Distributions of Charged Particles

(1) The Invariant Multiplicity Distributions of Charged Particles Frozen Out from sQGP. From Khalatnikov potential χ, the rapidity distributions of charged particles frozen out from fluid-like sQGP read [34]

$$\frac{\mathrm{d}N_{\mathrm{sQGP}}}{\mathrm{d}y_F} = \frac{q_0 c_0}{2} A(b)\left(\cosh y\frac{\mathrm{d}z}{\mathrm{d}y_F} - \sinh y\frac{\mathrm{d}t}{\mathrm{d}y_F}\right), \tag{16}$$

where $A(b)$ is the area of overlap region of collisions, being the function of impact parameter b or centrality cuts. Inserting (10) into the above equation, the part in the round brackets becomes

$$\begin{aligned} &\cosh y\frac{\mathrm{d}z}{\mathrm{d}y_F} - \sinh y\frac{\mathrm{d}t}{\mathrm{d}y_F} \\ &\quad = \frac{1}{T}c^2\frac{\partial}{\partial \theta}\left(\chi + \frac{\partial \chi}{\partial \theta}\right)\cosh(y - y_F) \\ &\qquad - \frac{1}{T}\frac{\partial}{\partial y_F}\left(\chi + \frac{\partial \chi}{\partial \theta}\right)\sinh(y - y_F). \end{aligned} \tag{17}$$

With the expansions of hadronic matter, it continues becoming cooler. According to the prescription of Cooper-Frye [34], as the temperature drops to the freeze-out temperature T_{FO}, the inelastic collisions among hadrons cease. The yields of identified hadrons remain unchanged becoming the measured results in experiments. The invariant multiplicity distributions of charged particles equal [10, 15, 34]

$$\frac{\mathrm{d}^2N_{\mathrm{sQGP}}}{2\pi p_T \mathrm{d}y\mathrm{d}p_T} = \frac{1}{(2\pi)^3}\int \frac{\mathrm{d}N_{\mathrm{sQGP}}}{\mathrm{d}y_F} \cdot \frac{m_T\cosh(y-y_F)}{\exp\{[m_T\cosh(y-y_F)-\mu_B]/T\}+\delta}\bigg|_{T=T_{\mathrm{FO}}} \mathrm{d}y_F, \tag{18}$$

where $m_T = \sqrt{m^2+p_T^2}$ is the transverse mass of produced charged particle with rest mass m. μ_B in (18) is the baryochemical potential. For Fermi charged particles, $\delta = 1$ in the denominator of (18), and for Bosons, $\delta = -1$. The meaning of (18) is evident. It is the convolution of $\mathrm{d}N_{\mathrm{sQGP}}/\mathrm{d}y_F$ with the energy of the charged particles in the state with temperature T.

The integral interval of y_F in (18) is $[-y_h(\theta_f), y_h(\theta_f)]$. The integrand is evaluated with $T = T_{\mathrm{FO}}$. At this moment, the fluid freezes out into the charged particles. Replacing χ in (17) by χ_h of (14), it becomes

$$\left(\cosh y\frac{\mathrm{d}z}{\mathrm{d}y_F} - \sinh y\frac{\mathrm{d}t}{\mathrm{d}y_F}\right)\bigg|_{T=T_{\mathrm{FO}}} = \frac{1}{T_{\mathrm{FO}}}(\beta_h c_h)^2 \cdot B(\theta_{\mathrm{FO}})\left[S(\theta_{\mathrm{FO}}, y_F)\sinh(y-y_F) + C(\theta_{\mathrm{FO}}, y_F)\cosh(y-y_F)\right], \tag{19}$$

where

$$S(\theta_{\mathrm{FO}}, y_F) = \frac{\beta_h y_F}{\lambda(\theta_{\mathrm{FO}}, y_F)}\left\{\frac{\beta_h c_h y_h(\theta_{\mathrm{FO}})}{\lambda(\theta_{\mathrm{FO}}, y_F)} I_0[\lambda(\theta_{\mathrm{FO}}, y_F)] + \left[\frac{\beta_h+1}{\beta_h} - \frac{2\beta_h c_h y_h(\theta_{\mathrm{FO}})}{\lambda^2(\theta_{\mathrm{FO}}, y_F)}\right] I_1[\lambda(\theta_{\mathrm{FO}}, y_F)]\right\},$$

$$C(\theta_{\mathrm{FO}}, y_F) = \left\{\frac{\beta_h+1}{\beta_h} + \frac{[\beta_h c_h y_h(\theta_{\mathrm{FO}})]^2}{\lambda^2(\theta_{\mathrm{FO}}, y_F)}\right\} \cdot I_0[\lambda(\theta_{\mathrm{FO}}, y_F)] + \frac{1}{\lambda(\theta_{\mathrm{FO}}, y_F)}\left\{\frac{y_h(\theta_{\mathrm{FO}})}{c_h}+1 - \frac{2[\beta_h c_h y_h(\theta_{\mathrm{FO}})]^2}{\lambda^2(\theta_{\mathrm{FO}}, y_F)}\right\} I_1[\lambda(\theta_{\mathrm{FO}}, y_F)], \tag{20}$$

where I_1 is the 1st-order modified Bessel function of the first kind.

(2) The Invariant Multiplicity Distributions of Leading Particles. Investigations have shown that the leading particles are formed outside the overlap region of collisions [35, 36]. The generation and movement of them are therefore beyond the scope of hydrodynamic description and should be treated separately.

In our previous work [24–26], we once argued that the rapidity distributions of leading particles take the Gaussian form

$$\frac{\mathrm{d}N_{\mathrm{Lead}}(b, \sqrt{s_{\mathrm{NN}}}, y)}{\mathrm{d}y} = \frac{N_{\mathrm{Lead}}(b, \sqrt{s_{\mathrm{NN}}})}{\sqrt{2\pi}\sigma}\exp\left\{-\frac{[|y| - y_0(b, \sqrt{s_{\mathrm{NN}}})]^2}{2\sigma^2}\right\}, \tag{21}$$

where $y_0(b, \sqrt{s_{\mathrm{NN}}})$ and σ are, respectively, the central position and width of distributions. It can be expected that $y_0(b, \sqrt{s_{\mathrm{NN}}})$ should increase with increasing energies and centrality cuts, while σ should not, at least not apparently, depend on the energies, centrality cuts, and even colliding systems. The specific values of them can be determined by comparing the theoretical results with experimental data. $N_{\mathrm{Lead}}(b, \sqrt{s_{\mathrm{NN}}})$ in (21) represents the number of leading particles, which, for an identical nucleus-nucleus collision, equals half of the number of participants.

The investigations have shown that [37], for certain rapidity, the invariant multiplicity distributions of leading particles possess the form

$$\frac{\mathrm{d}^2N_{\mathrm{Lead}}}{2\pi p_T \mathrm{d}y\mathrm{d}p_T} \propto \exp\left(-ap_T^2\right), \tag{22}$$

where a is a constant. Then, as a function of rapidity, the invariant multiplicity distributions of leading particles can be written as

$$\frac{\mathrm{d}^2N_{\mathrm{Lead}}}{2\pi p_T \mathrm{d}y\mathrm{d}p_T} = \frac{\mathrm{d}N_{\mathrm{Lead}}}{\mathrm{d}y}\frac{a}{\pi}\exp\left(-ap_T^2\right), \tag{23}$$

which is normalized to N_{Lead}.

(3) The Pseudorapidity Distributions of Charged Particles. Writing invariant multiplicity distributions in terms of pseudorapidity, we have

$$\frac{\mathrm{d}^2N}{2\pi p_T \mathrm{d}\eta\mathrm{d}p_T} = \sqrt{1-\frac{m^2}{m_T^2\cosh^2 y}}\,\frac{\mathrm{d}^2N}{2\pi p_T \mathrm{d}y\mathrm{d}p_T}, \tag{24}$$

where

$$\frac{\mathrm{d}^2N}{2\pi p_T \mathrm{d}y\mathrm{d}p_T} = \frac{\mathrm{d}^2N_{\mathrm{sQGP}}}{2\pi p_T \mathrm{d}y\mathrm{d}p_T} + \frac{\mathrm{d}^2N_{\mathrm{Lead}}}{2\pi p_T \mathrm{d}y\mathrm{d}p_T}. \tag{25}$$

To fulfill the transformation of (24), another relation

$$y = \frac{1}{2}\ln\left[\frac{\sqrt{p_T^2\cosh^2\eta + m^2} + p_T\sinh\eta}{\sqrt{p_T^2\cosh^2\eta + m^2} - p_T\sinh\eta}\right] \tag{26}$$

is in order.

Substituting (18) and (23) into (24) and carrying out the integration of p_T, we can get the pseudorapidity distributions

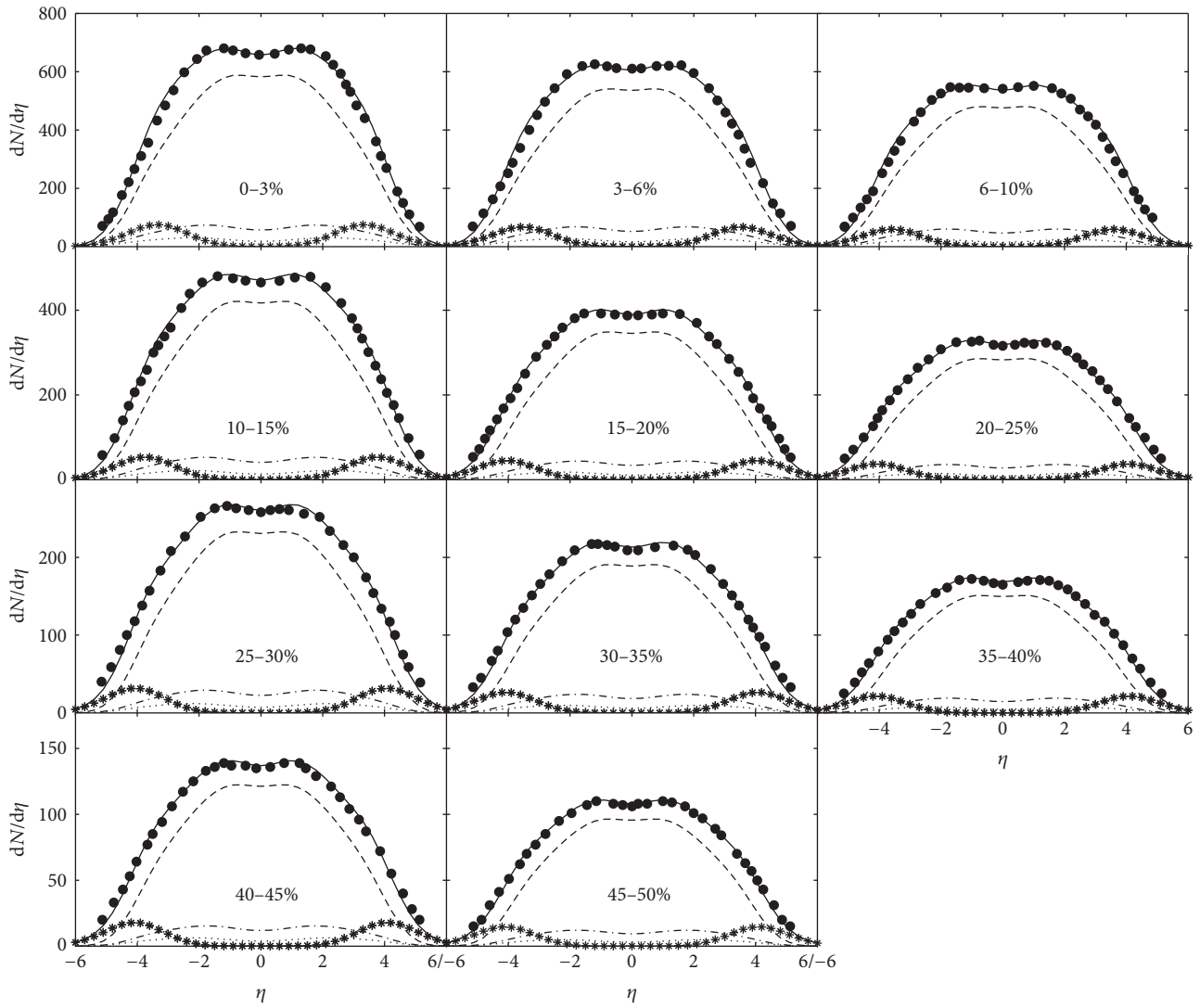

FIGURE 1: The pseudorapidity distributions of charged particles produced in different centrality Au+Au collisions at $\sqrt{s_{\mathrm{NN}}} = 200$ GeV. The solid dots are the experimental measurements [5]. The dashed, dashed-dotted, and dotted curves are, respectively, the contribution from pions, kaons, and protons got from the hydrodynamic result of (18). The dotted-star curves are the components of leading particles obtained from (23). The solid curves are the sums of the four types of curves.

of charged particles produced in high energy heavy ion collisions. Figures 1 and 2 show such distributions in Au+Au collisions at $\sqrt{s_{\mathrm{NN}}} = 200$ and 62.4 GeV, respectively. The solid dots in the figures are the experimental measurements [5]. The dashed, dashed-dotted, and dotted curves are, respectively, the contribution from pions, kaons, and protons got from the hydrodynamic result of (18). The dotted-star curves are the components of leading particles obtained from (23). The solid curves are the sums of the four types of curves. χ^2/NDF for each curve is listed in Table 1. It can be seen that the combined contribution from both hydrodynamics and leading particles matches up well with experimental data.

Experiments have shown that the overwhelming majority of charged particles produced in Au+Au collisions at $\sqrt{s_{\mathrm{NN}}} = 200$ GeV consists of pions, kaons, and protons with proportions of about 84%, 12%, and 4%, respectively [38], which are roughly independent of energies, centrality cuts, and colliding systems. In calculations, the ratios of these three kinds of particles take about the same as these values. c_h in (15) takes the values of $c_h = 0.45$ and 0.42 for $\sqrt{s_{\mathrm{NN}}} = 200$ and 62.4 GeV from the investigations of [15, 39–41]. T_c in (15) takes the well-recognized value of $T_c = 180$ MeV. The freeze-out temperature T_{FO} takes the values of $T_{\mathrm{FO}} = 120$ MeV from the studies of [6], which also shows that the baryochemical potential μ_B in (18) is about equal to 20 and 50 MeV for $\sqrt{s_{\mathrm{NN}}} = 200$ and 62.4 GeV, respectively. For the most central collisions at these two different energies, T_0 in (15) takes the values of $T_0 = 0.95$ and 0.68 GeV referring to those given in [15]. This allows us to determine the constant q_0 in (16) to be $q_0 = 7.38 \times 10^{-4}$, 6.01×10^{-4}, and 4.50×10^{-3} for pions, kaons, and protons, respectively. Keeping q_0 unchanged, T_0 is fixed for the rest centrality cuts by making theoretical results fit in with experimental data. The results are listed in Table 1. It can be seen that T_0 decreases slowly with increasing centralities

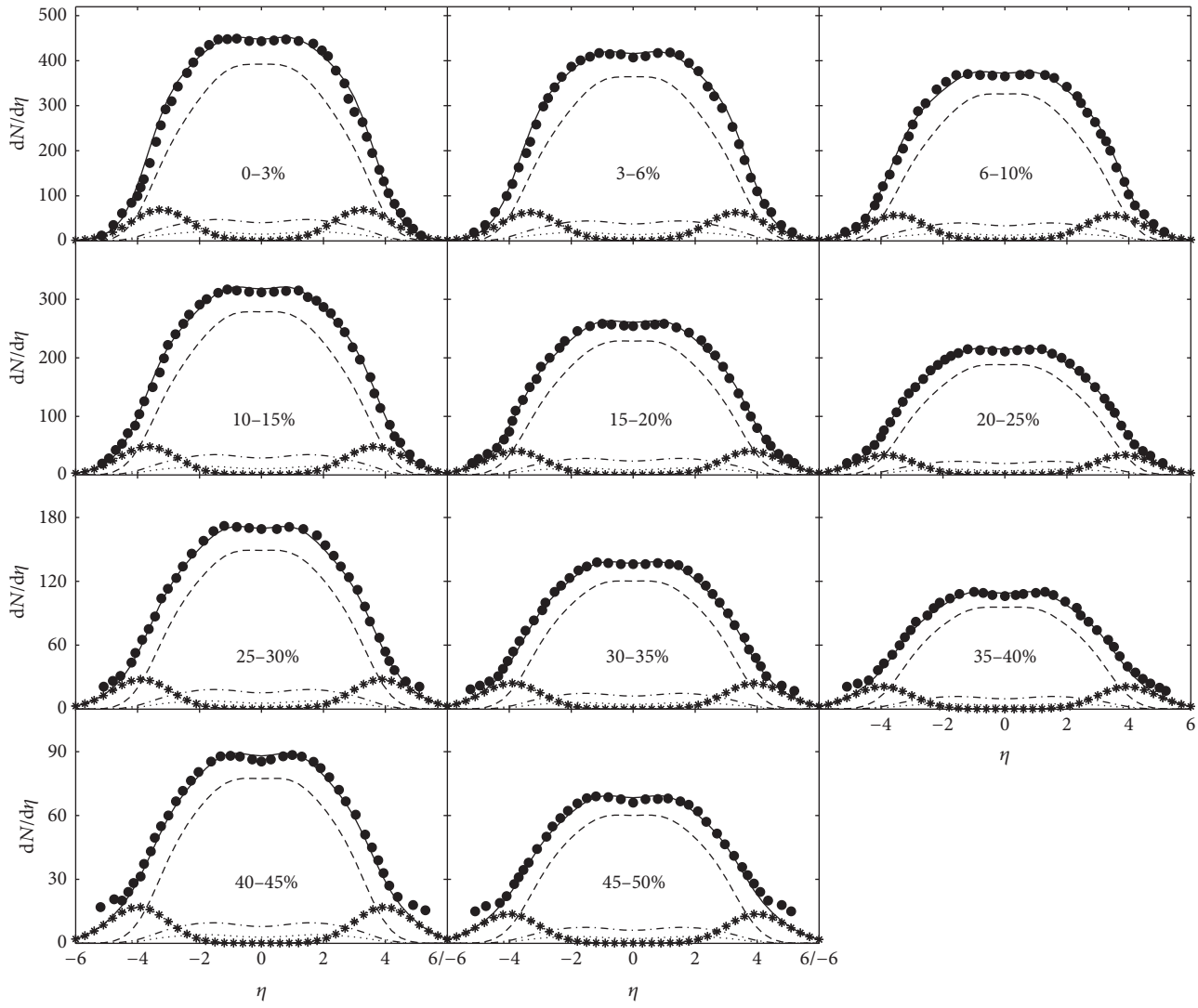

FIGURE 2: The pseudorapidity distributions of charged particles produced in different centrality Au+Au collisions at $\sqrt{s_{NN}}$ = 62.4 GeV. The solid dots are the experimental measurements [5]. The dashed, dashed-dotted, and dotted curves are, respectively, the contribution from pions, kaons, and protons got from the hydrodynamic result of (18). The dotted-star curves are the components of leading particles obtained from (23). The solid curves are the sums of the four types of curves.

TABLE 1: χ^2/NDF, initial temperature T_0, and central position y_0 in different centrality Au+Au collisions at $\sqrt{s_{NN}}$ = 200, 62.4, and 19.6 GeV, respectively.

Centrality cuts (%)	0–3	3–6	6–10	10–15	15–20	20–25	25–30	30–35	35–40	40–45	45–50
χ^2/NDF											
200 GeV	0.496	0.693	0.402	0.260	0.310	0.217	0.354	0.151	0.161	0.123	0.089
62.4 GeV	0.696	0.519	0.300	0.192	0.188	0.079	0.266	0.376	0.444	0.481	0.405
19.6 GeV	0.816	0.533	0.359	0.614	0.802	0.309	0.559	0.496	0.229	0.577	—
T_0 (GeV)											
200 GeV	0.950	0.949	0.948	0.947	0.945	0.941	0.922	0.909	0.885	0.874	0.860
62.4 GeV	0.680	0.676	0.675	0.671	0.660	0.650	0.623	0.607	0.599	0.593	0.585
19.6 GeV	0.551	0.549	0.547	0.543	0.539	0.533	0.529	0.518	0.510	0.493	—
y_0											
200 GeV	2.86	3.03	3.13	3.23	3.46	3.54	3.55	3.57	3.58	3.59	3.60
62.4 GeV	2.80	2.88	3.05	3.21	3.35	3.39	3.42	3.46	3.50	3.51	3.54

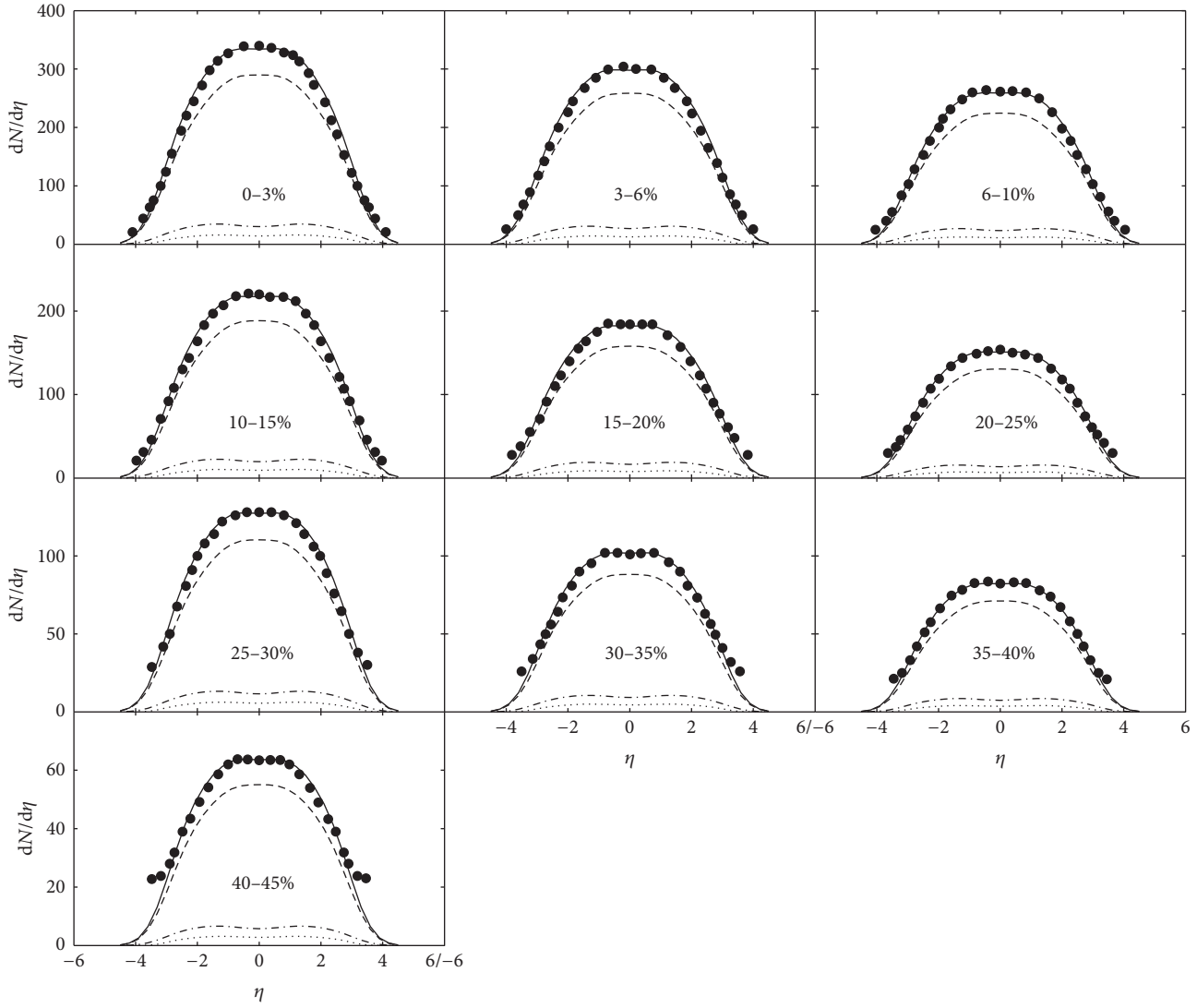

FIGURE 3: The pseudorapidity distributions of charged particles produced in different centrality Au+Au collisions at $\sqrt{s_{\mathrm{NN}}} = 19.6$ GeV. The solid dots are the experimental measurements [5]. The dashed, dashed-dotted, and dotted curves are, respectively, the contribution from pions, kaons, and protons got from the hydrodynamic results of (18). The solid curves are the sums of the three types of curves.

especially in the first four cuts. Table 1 also lists the central position y_0 in (21). As addressed above, it increases with increasing energies and centralities. The width parameter σ in (21) takes the value of a constant of $\sigma = 0.90$, being independent of energies and centrality cuts. The parameter a in (23) takes the value of $a = 0.92$ for the two different energies.

Figure 3 shows the pseudorapidity distributions of charged particles produced in Au+Au collisions at $\sqrt{s_{\mathrm{NN}}} = 19.6$ GeV. χ^2/NDF for each curve is listed in Table 1. The meanings of different types of curves are the same as those in Figures 1 and 2. It can be seen that, in the absence of leading particles, the hydrodynamics alone can give a good description to the experimental observations. This is different from Figures 1 and 2, where leading particles are essential in fitting experimental data. This difference might be caused by the different transparencies of nuclei in different energies. As the analyses given in [42], in central Au+Au collisions at $\sqrt{s_{\mathrm{NN}}} = 200$ GeV, the leading particles are located at about $y_0 = 2.91$. This position is far away from the mid-rapidity region, where, relative to the low yields of charged particles frozen out from sQGP, the effect of leading particles is evident which should be considered separately. On the contrary, in case of Au+Au collisions at $\sqrt{s_{\mathrm{NN}}} = 19.6$ GeV, $y_0 = 1.28$. This position is so close to the mid-rapidity region that the effect of leading particles is hidden by the large yields of charged particles generated from the freeze-out of sQGP. Therefore, there is no need to consider the contribution of leading particles separately.

In drawing Figure 3, T_0 takes the values as those listed in Table 1. $c_h = 0.40$ and $\mu_B = 210$ MeV. The other parameters,

such as T_c, T_{FO}, and q_0, are the same as those used in drawing Figures 1 and 2.

4. Conclusions

By taking into consideration the effect of leading particles, the hydrodynamic model incorporating the phase transition is used to analyze the pseudorapidity distributions of charged particles produced in Au+Au collisions at RHIC energies.

The hydrodynamic model contains rich information about transport coefficients of sQGP, such as the sound speed c_0 in sQGP, the sound speed c_h in hadronic phase, the phase transition temperature T_c, the chemical freeze-out temperature T_{FO}, the baryochemical potential μ_B, and the initial temperature T_0. With the exception of T_0, the other five coefficients take the values either from the well-known theoretical results or from experimental measurements. As for T_0, there are no widely accepted results so far. In our calculations, T_0 in the most central Au+Au collisions at $\sqrt{s_{NN}} = 200$ and 62.4 GeV takes the value referring to those given by other investigations, which enables us to ascertain the constant q_0 in (16). In the rest centrality cuts and in Au+Au collisions at $\sqrt{s_{NN}} = 19.6$ GeV, T_0 is determined by maintaining q_0 unchanged and comparing the theoretical results with experimental data.

The leading particles, by conventional definition, are the particles carrying on the quantum numbers of colliding nucleons and taking away the most part of incident energy. They are separately in projectile and target fragmentation region. The present investigations show that the importance of leading particles in describing the pseudorapidity distributions of charged particles produced in heavy ion collisions is related to the incident energy. At high energy, owing to the high transparency of nuclei, the contribution of leading particles is evident and indispensable, while, at low energy, as a result of poor transparency of nuclei the effect of leading particles is integrated with the results of freeze-out of sQCD. It does not need to be dealt with separately.

Conflicts of Interest

The authors declare that there are no conflicts of interest regarding the publication of this paper.

Acknowledgments

This work is supported by the Shanghai Key Lab of Modern Optical System.

References

[1] C. Adler and STAR Collaboration, "Measurement of inclusive antiprotons from Au+Au collisions at $\sqrt{s_{NN}} = 130$ GeV," *Physical Review Letters*, vol. 87, Article ID 262302, 2001.

[2] K. Adcox and PHENIX Collaboration, "Centrality dependence of $\pi^{+/-}$, $K^{+/-}$, p, and $\overline{p}$ production from $\sqrt{s_{NN}} = 130$ GeV Au+Au collisions at RHIC," *Physical Review Letters*, vol. 88, Article ID 242301, 2002.

[3] S. S. Adler and PHENIX collaboration, "Elliptic flow of identified hadrons in Au+Au collisions at $\sqrt{s_{NN}} = 200$ GeV," *Physical Review Letters*, vol. 91, Article ID 182301, 2003.

[4] K. Adcox and PHENIX Collaboration, "Single identified hadron spectra from $\sqrt{s_{NN}} = 130$ GeV Au+Au collisions," *Physical Review C*, vol. 69, Article ID 024904, 2004.

[5] B. Alver and PHOBOS Collaboration, "Charged-particle multiplicity and pseudorapidity distributions measured with the PHOBOS detector in Au+Au, Cu+Cu, d+Au, and p+p collisions at ultrarelativistic energies," *Physical Review C*, vol. 83, Article ID 024913, 2011.

[6] B. I. Abelev and STAR Collaboration, "Systematic measurements of identified particle spectra in $p + p$, d + Au, and Au+Au collisions at the STAR detector," *Physical Review C*, vol. 79, Article ID 034909, 2009.

[7] A. Adare and PHENIX Collaboration, "Spectra and ratios of identified particles in Au+Au and d+Au collisions at $\sqrt{s_{NN}} = 200$ GeV," *Physical Review C*, vol. 88, Article ID 024906, 2013.

[8] L. C. Arsene and BRAHMS collaboration, "Rapidity and centrality dependence of particle production for identified hadrons in Cu+Cu collisions at $\sqrt{s_{NN}} = 200$ GeV," *Physical Review C*, vol. 94, Article ID 014907, 2016.

[9] L. Adamczyk and STAR Collaboration, "Centrality dependence of identified particle elliptic flow in relativistic heavy ion collisions at $\sqrt{s_{NN}} = 7.7$–62.4 GeV," *Physical Review C*, vol. 93, Article ID 014907, 2016.

[10] N. Suzuki, "One-dimensional hydrodynamical model including phase transition," *Physical Review C nuclear physics*, vol. 81, no. 4, Article ID 044911, 2010.

[11] A. Bialas, R. A. Janik, and R. Peschanski, "Unified description of Bjorken and Landau 1+1 hydrodynamics," *Physical Review C nuclear physics*, vol. 76, no. 5, Article ID 054901, 2007.

[12] G. Beuf, R. Peschanski, and E. N. Saridakis, "Entropy flow of a perfect fluid in (1+1) hydrodynamics," *Physical Review C: Nuclear Physics*, vol. 78, no. 6, Article ID 064909, 2008.

[13] T. Csörgo, M. I. Nagy, and M. Csanád, "New family of simple solutions of relativistic perfect fluid hydrodynamics," *Physics Letters B*, vol. 663, no. 4, pp. 306–311, 2008.

[14] M. Csanád, M. I. Nagy, and S. Lökös, "Exact solutions of relativistic perfect fluid hydrodynamics for a QCD Equation of State," *The European Physical Journal A*, vol. 48, no. 11, pp. 173–178, 2012.

[15] T. Mizoguchi, H. Miyazawa, and M. Biyajima, "A potential including the Heaviside function in the 1 + 1 dimensional hydrodynamics by Landau : IIts basic properties and application to data at RHIC energies," *The European Physical Journal A*, vol. 40, no. 1, pp. 99–108, 2009.

[16] T. R. Taylor and C. Vafa, "Analytic solution for relativistic transverse flow at the softest point," *Physics Letters B*, vol. 474, no. 1-2, pp. 21–26, 2000.

[17] T. S. Bíró, "Generating new solutions for relativistic transverse flow at the softest point," *Physics Letters B*, vol. 487, no. 1-2, pp. 133–139, 2000.

[18] C.-Y. Wong, "Landau hydrodynamics reexamined," *Physical Review C: Nuclear Physics*, vol. 78, no. 5, Article ID 054902, 2008.

[19] A. Bialas and R. Peschanski, "Asymmetric (1+1)-dimensional hydrodynamics in high-energy collisions," *Physical Review C: Nuclear Physics*, vol. 83, no. 5, Article ID 054905, 2011.

[20] E. K. G. Sarkisyan and A. S. Sakharov, "Relating multihadron production in hadronic and nuclear collisions," *The European Physical Journal C*, vol. 70, no. 3, pp. 533–541, 2010.

[21] C. Gale, S. Jeon, and B. Schenke, "Hydrodynamic modeling of heavy-ion collisions," *International Journal of Modern Physics A*, vol. 28, no. 11, Article ID 1340011, 2013.

[22] U. Heinz and R. Snellings, "Collective flow and viscosity in relativistic heavy-ion collisions," *Annual Review of Nuclear and Particle Science*, vol. 63, pp. 123–151, 2013.

[23] A. N. Mishra, R. Sahoo, E. K. G. Sarkisyan, and A. S. Sakharov, "Effective-energy budget in multiparticle production in nuclear collisions," *The European Physical Journal C*, vol. 74, article 3147, 2014.

[24] Z. J. Jiang, Q. G. Li, and H. L. Zhang, "Revised Landau hydrodynamic model and the pseudorapidity distributions of charged particles produced in nucleus-nucleus collisions at maximum energy at the BNL Relativistic Heavy Ion Collider," *Physical Review C: Nuclear Physics*, vol. 87, no. 4, Article ID 044902, 2013.

[25] Z. J. Jiang, Y. Zhang, H. L. Zhang, and H. P. Deng, "A description of the pseudorapidity distributions in heavy ion collisions at RHIC and LHC energies," *Nuclear Physics A*, vol. 941, pp. 188–200, 2015.

[26] Z. W. Wang, Z. J. Jiang, and Y. S. Zhang, "The investigations of pseudorapidity distributions of final multiplicity in Au+Au collisions at high energy," *Journal of University of Shanghai for Science and Technology*, vol. 31, pp. 322–326, 2009.

[27] J. Qian and U. Heinz, "Hydrodynamic flow amplitude correlations in event-by-event fluctuating heavy-ion collisions," *Physical Review C: Nuclear Physics*, vol. 94, no. 2, Article ID 024910, 2016.

[28] E. K. G. Sarkisyan, A. N. Mishra, R. Sahoo, and A. S. Sakharov, "Multihadron production dynamics exploring the energy balance in hadronic and nuclear collisions," *Physical Review D: Particles, Fields, Gravitation and Cosmology*, vol. 93, no. 7, Article ID 079904, 2016.

[29] E. K. G. Sarkisyan, A. N. Mishra, R. Sahoo, and A. S. Sakharov, "Centrality dependence of midrapidity density from GeV to TeV heavy-ion collisions in the effective-energy universality picture of hadroproduction," *Physical Review D: Particles, Fields, Gravitation and Cosmology*, vol. 94, no. 1, Article ID 011501, 2016.

[30] J. Noronha-Hostler, M. Luzum, and J.-Y. Ollitrault, "Hydrodynamic predictions for 5.02 TeV Pb-Pb collisions," *Physical Review C nuclear physics*, vol. 93, no. 3, Article ID 034912, 2016.

[31] H. Niemi, K. J. Eskola, and R. Paatelainen, "Event-by-event fluctuations in a perturbative QCD + saturation + hydrodynamics model: Determining QCD matter shear viscosity in ultrarelativistic heavy-ion collisions," *Physical Review C: Nuclear Physics*, vol. 93, no. 2, Article ID 024907, 2016.

[32] F. G. Gardim, F. Grassi, M. Luzum, and J. Noronha-Hostler, "Hydrodynamic predictions for mixed harmonic correlations in 200 GeV Au+Au collisions," *Physical Review C: Nuclear Physics*, vol. 95, no. 3, Article ID 034901, 2017.

[33] M. Alqahtani, M. Nopoush, and M. Strickland, "Quasiparticle anisotropic hydrodynamics for central collisions," *Physical Review C: Nuclear Physics*, vol. 95, no. 3, Article ID 034906, 2017.

[34] F. Cooper and G. Frye, "Landau's hydrodynamic model of particle production and electron-positron annihilation into hadrons," *Physical Review D: Particles, Fields, Gravitation and Cosmology*, vol. 11, pp. 192–213, 1975.

[35] A. Berera, M. Strikman, W. Toothacker, W. Walker, and J. Whitmore, "The limiting curve of leading particles from hadron-nucleus collisions at infinite A," *Physics Letters B*, vol. 403, no. 1-2, pp. 1–7, 1997.

[36] J. J. Ryan, "Proceedings of the Annual Meeting of the Division of Particles and Fields of the APS," World Scientific, Singapore, 1993.

[37] A. E. Brenner, D. C. Carey, J. E. Elias et al., "Experimental study of single-particle inclusive hadron scattering and associated multiplicities," *Physical Review D: Particles, Fields, Gravitation and Cosmology*, vol. 26, no. 7, pp. 1497–1553, 1982.

[38] S. S. Adler and PHENIX collaboration, "Identified charged particle spectra and yields in Au+Au collisions at $\sqrt{s_{\mathrm{NN}}}$ = 200 GeV," *Physical Review C*, vol. 69, Article ID 034909, 2004.

[39] A. Adare and PHENIX Collaboration, "Scaling properties of azimuthal anisotropy in Au+Au and Cu+Cu collisions at $\sqrt{s_{\mathrm{NN}}}$ = 200 GeV," *Physical Review Letters*, vol. 98, Article ID 162301, 2007.

[40] L. N. Gao, Y. H. Chen, H. R. Wei, and F. H. Liu, "Speed of sound parameter from RHIC and LHC heavy-ion data," *Advances in High Energy Physics*, vol. 2013, Article ID 450247, 8 pages, 2013.

[41] S. Borsányi, G. Endrodi, Z. Fodor et al., "The QCD equation of state with dynamical quarks," *Journal of High Energy Physics*, vol. 2010, no. 11, article 77, pp. 1–31, 2010.

[42] Z.-J. Jiang, H.-L. Zhang, J. Wang, K. Ma, and L.-M. Cai, "The evolution-dominated hydrodynamics and the pseudorapidity distributions in nucleus-nucleus collisions at low energies at the BNL relativistic heavy ion collider," *Chinese Journal of Physics*, vol. 52, no. 6, pp. 1676–1685, 2014.

Hindawi
Advances in High Energy Physics
Volume 2018, Article ID 6307205, 7 pages
https://doi.org/10.1155/2018/6307205

Research Article

A Comparative Study of $K^{\pm}/\pi^{\pm}$ Ratio in Proton-Proton Collisions at Different Energies: Experimental Results versus Model Simulation

Swarnapratim Bhattacharyya,[1] **Maria Haiduc**,[2] **Alina Tania Neagu**,[2] **and Elena Firu**[2]

[1]*Department of Physics, New Alipore College, L Block, New Alipore, Kolkata 700053, India*
[2]*Institute of Space Science, Bucharest, Romania*

Correspondence should be addressed to Swarnapratim Bhattacharyya; swarna_pratim@yahoo.com

Received 14 July 2017; Revised 8 November 2017; Accepted 17 December 2017; Published 17 January 2018

Academic Editor: Bhartendu K. Singh

A detailed study of energy dependence of K^+/π^+, K^-/π^- and total kaon to pion multiplicity ratio $((K^+ + K^-)/(\pi^+ + \pi^-) = K/\pi)$ has been carried out in proton-proton (pp) collisions at $\sqrt{s}$ = 6.3, 17.3, 62.4, 200, and 900 GeV and also at $\sqrt{s}$ = 2.76 TeV and 7 TeV in the framework of UrQMD and DPMJET III model. Dependence of K^+/π^+ and K^-/π^- on energy shows different behavior for UrQMD and DPMJET III model. The presence of the horn-like structure in the variation of K^+/π^+ and K^-/π^- with energy for the experimental data is supported by the DPMJET III model. Experimentally it has been observed that as energy increases, the total kaon to pion multiplicity ratio $((K^+ + K^-)/(\pi^+ + \pi^-) = K/\pi)$ increases systematically for pp collisions at lower energies and becomes independent of energy in LHC energy regime. Our analysis on total kaon to pion multiplicity ratio $((K^+ + K^-)/(\pi^+ + \pi^-) = K/\pi)$ with UrQMD data is well supported by the experimental results obtained by different collaborations in different times. In case of DPMJET III data, the saturation of K/π ratio at LHC region has not been observed.

1. Introduction

The study of nucleus-nucleus interactions at high energies has been a subject of major interest to the theoretical and experimental physicists. The nucleus-nucleus interaction can provide valuable information on the spatiotemporal development of multiparticle production process, which is one of the prime interests in view of recent developments of quantum chromodynamics. Along with the study of nucleus-nucleus collisions, a thorough understanding of proton-proton (pp) collisions is also necessary both as input to detailed theoretical models of strong interactions and as a baseline for understanding the nucleus-nucleus collisions at relativistic and ultrarelativistic energies. Soft particle production from ultrarelativistic pp collisions is also sensitive to the flavor distribution within the proton, quark hadronization, and baryon number transport. The measurement of charged particle transverse momentum spectra in pp collisions serves as a crucial reference for particle spectra in nucleus-nucleus collisions. A proton-proton reference spectrum is needed for nucleus-nucleus collisions to investigate possible initial-state effects in the collision. The multiplicity distribution of particles produced in proton-proton (pp) collisions and the multiplicity dependence of other global event characteristics represent fundamental observables reflecting the properties of the underlying particle production mechanisms. In high-energy collisions along with the pions, kaons are also important as the strange particle production is a powerful probe into the hadronic interaction and the hadronization process in pp and heavy-ion collisions at relativistic energies. The study of K/π ratio in high-energy collisions is an important observable to be studied not only to address questions of the phase transition but also to obtain a better understanding of the pre-equilibrium dynamics, the hadronization processes, and dynamics of hadrons in the medium. It is well known that the strangeness enhancement in relativistic nucleus-nucleus collisions has been proposed as a signature of the Quark-Gluon Plasma (QGP) formation in the relativistic heavy-ion

collisions. The study of K/π ratio in pp collisions can provide a baseline to investigate the strangeness enhancement.

In this paper, we are presenting an analysis of energy dependence of K^+/π^+, K^-/π^- and total kaon to pion multiplicity ratio $((K^+ + K^-)/(\pi^+ + \pi^-) = K/\pi)$ at $\sqrt{s}$ = 6.3, 17.3, 62.4, 200, and 900 GeV and also at $\sqrt{s}$ = 2.76 TeV and 7 TeV in the framework of UrQMD and DPMJET III model in proton-proton (pp) collisions. We have also compared our results with available experimental results obtained so far. Before going into the details of the analysis it will be convenient for the readers to have brief introductions about the two models.

2. UrQMD and DPMJET III Model: A Brief Introduction

UrQMD model is a microscopic transport theory, based on the covariant propagation of all the hadrons on the classical trajectories in combination with stochastic binary scattering, colour string formation, and resonance decay. It represents a Monte Carlo solution of a large set of coupled partial integrodifferential equations for the time evolution of various phase space densities. The main ingredients of the model are the cross sections of binary reactions, the two-body potentials and decay widths of resonances. The UrQMD collision term contains 55 different baryon species (including nucleon, delta, and hyperon resonances with masses up to 2.25 GeV/c^2) and 32 different meson species (including strange meson resonances), which are supplemented by their corresponding antiparticle and all isospin-projected states. The states can either be produced in string decays, s-channel collisions, or resonance decays. This model can be used in the entire available range of energies from the Bevalac region to RHIC. For more details about this model, readers are requested to consult [1–3].

The Monte Carlo event generator DPMJET can be used to study particle production in high-energy nuclear collisions including photoproduction and deep inelastic scattering off the nuclei. It is a code system based on the Dual Parton Model and unifies all features of the DTUNUC-2, DPMJET-II, and PHOJET 1.12 event generators. DPMJET III allows the simulation of hadron-hadron, hadron-nucleus, nucleus-nucleus, photon-hadron, photon-photon, and photon-nucleus interactions from a few GeV up to the highest cosmic ray energies. DPMJET is an implementation of the two-component Dual Parton Model for the description of interactions involving nuclei. This model is based on the Gribov-Glauber [4–6] approach. Gribov theory of high-energy interactions of hadrons and nuclei is based on general properties of amplitudes in relativistic quantum theory and provides a unified approach to a broad class of processes. According to this theory, the Glauber approximation [6] to nuclear dynamics is valid in the region of not too high energies and should be modified at energies of RHIC and LHC. Gribov theory then allows determining the corrections to the Glauber approximation [6] for inclusive particle spectra by relating them to cross sections of large-mass diffraction. The technique has been applied to calculation of shadowing effects for structure functions of nuclei and a good agreement with experimental data on these processes has been obtained. The same approach predicts a strong reduction of particle densities at superhigh energies as compared to predictions of the Glauber approximation [6]. Since its first implementations [7, 8] DPMJET model uses the Monte Carlo realization of the Gribov-Glauber multiple scattering formalism according to the algorithms of [9] and allows the calculation of total, elastic, quasielastic, and production cross sections for any high-energy nuclear collision. DPMJET III is a string model and the generalization of the string model to hadron-nucleus and nucleus-nucleus collisions was done by the Glauber-Gribov theory [4–6]. DPMJET III model treats both soft and hard scattering processes in a unified way. Soft processes are parametrized according to Regge-phenomenology whereas lowest order perturbative QCD is used to simulate the hard component. In DPMJET III model multiple parton interactions in each individual hadron/nucleon/photon-nucleon interaction have been described by the PHOJET event generator and the fragmentation of parton configurations is treated by the Lund model PYTHIA. For more details about the model, one can consult [10, 11].

3. Analysis and Results

We have generated ten thousand events using the UrQMD (UrQMD-3.3p1) [1–3] and DPMJET III (DPMJET 3.06) [10, 11] model in pp collisions at $\sqrt{s}$ = 6.3, 17.3, 62.4, 200, and 900 GeV and also at $\sqrt{s}$ = 2.76 TeV and 7 TeV. However, as we are dealing with the RHIC and LHC data, these numbers cannot be taken as large. We have calculated the number of positive and negative kaons and the number of positive and negative pions from the generated output of the UrQMD and DPMJET III model for all the energies.

3.1. Energy Dependence Study of K^+/π^+ Ratio. The values of K^+/π^+ ratio have been calculated from the generated output of both UrQMD and DPMJET III model. Table 1 represents the values of K^+/π^+ ratio in pp collisions at $\sqrt{s}$ = 6.3, 17.3, 62.4, 200, and 900 GeV and also at $\sqrt{s}$ = 2.76 TeV and 7 TeV. From Table 1 it is reflected that DPMJET III model simulated values of K^+/π^+ ratio are higher than their UrQMD counterparts up to $\sqrt{s}$ = 62.4 GeV. From $\sqrt{s}$ = 200 GeV, UrQMD simulated values of K^+/π^+ ratio overestimate the DPMJET III simulated values.

For comparison in Table 1 we have shown the experimental values of K^+/π^+ ratio obtained from different experimental works at $\sqrt{s}$ = 6.3 GeV [12], $\sqrt{s}$ = 17.3 GeV [13], $\sqrt{s}$ = 62.4 GeV [14], $\sqrt{s}$ = 200 GeV [15], and $\sqrt{s}$ = 7000 GeV [16]. Pulawski presented [12] the experimental values of K^+/π^+ ratio at mid rapidity at $\sqrt{s}$ = 6.3 GeV [12] in case of inelastic pp collisions for the data of NA61/SHINE collaboration. The study of NA61/SHINE collaboration [12] reflected that the energy dependence of K^+/π^+ ratio exhibits rapid changes in the SPS energy range. Pulawski pointed out that [12] the EPOS, UrQMD, Pythia 8, and HSD model failed to describe the NA61/SHINE experimental results satisfactorily. The values of K^+/π^+ ratio $\sqrt{s}$ = 62.4 GeV and 7 TeV have been calculated from the dN/dy values at mid rapidity. The

Table 1: It represents the values of K^+/π^+ ratio in pp collisions at $\sqrt{s}$ = 6.3 GeV to 7 TeV in the framework of UrQMD, DPMJET III, and the experimental values.

Energy $\sqrt{s}$ GeV	UrQMD simulated value of K^+/π^+ ratio	DPMJET III model simulated value of K^+/π^+ ratio	Experimental values of K^+/π^+ ratio	Reference for the experimental values of K^+/π^+ ratio
6.3	.049 ± .001	.065 ± .002	.081 ± .002	[12]
17.3	.083 ± .003	.095 ± .003	.109 ± .003	[13]
62.4	.101 ± .002	.105 ± .002	.097 ± .002	[14]
200	.110 ± .008	.099 ± .005	.104 ± .008	[15]
900	.122 ± .004	.115 ± .006	.....	.....
2760	.124 ± .004	.116 ± .006	.....	.....
7000	.124 ± .005	.120 ± .007	.126 ± .006	[16]

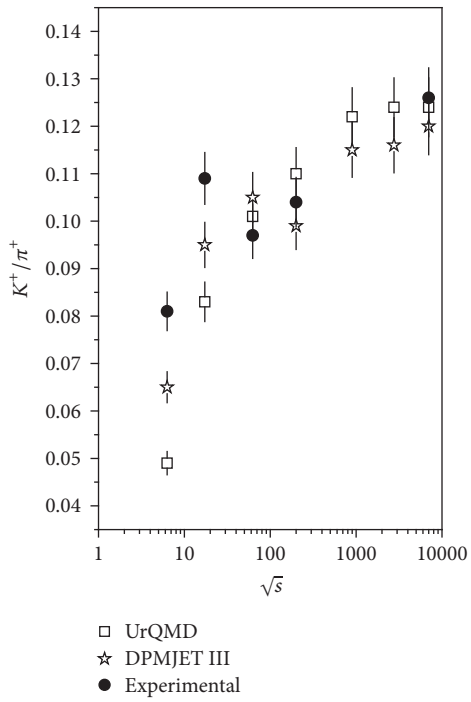

Figure 1: It represents the energy dependence of K^+/π^+ ratio in pp collisions at $\sqrt{s}$ = 6.3 GeV to 7 TeV of the UrQMD, DPMJET III, and experimental analysis.

dN/dy values at mid rapidity at $\sqrt{s}$ = 62.4 GeV and at $\sqrt{s}$ = 7 TeV are $|y| < 0.35$ and $|y| < 0.5$, respectively. K^+/π^+ ratios at other energies have been estimated with the help of a high accuracy digitized plot analyzer.

In Figure 1 we have presented the variation of K^+/π^+ ratio with energy for pp collisions in case of UrQMD simulated, DPMJET III simulated, and the experimental values. From the figure it can be seen that for UrQMD simulation the values of K^+/π^+ ratio increase smoothly with energy and after reaching at $\sqrt{s}$ = 900 GeV the ratio almost saturates, while in case of DPMJET III simulation the value of K^+/π^+ ratio shows a sudden decrease at $\sqrt{s}$ = 200 GeV. After the sudden decrease the K^+/π^+ values begin to increase with energy. No prominent saturation of K^+/π^+ ratio has been observed at LHC regime for DPMJET III model. The dependence of K^+/π^+ values with energy shows the presence of the horn-like structure in case of DPMJET III simulated events. The observed sudden decrease of K^+/π^+ ratio is completely absent in case of UrQMD simulation. The experimental studies of energy dependence of K^+/π^+ ratio also indicate that the K^+/π^+ values increase initially with energy, get a sudden drop at $\sqrt{s}$ = 62.4 GeV, and go on increasing again signifying the presence of the horn-like structure.

3.2. Energy Dependence Study of K^-/π^- Ratio. In order to study the energy dependence of K^-/π^- ratio in pp collisions we have calculated the values of K^-/π^- ratio obtained from the simulation of pp collisions at $\sqrt{s}$ = 6.3 GeV–7 TeV by UrQMD and DPMJET III model. Calculated values of K^-/π^- ratio for UrQMD and DPMJET III simulation have been presented in Table 2. From Table 2 it is seen that, from $\sqrt{s}$ = 900 GeV, UrQMD simulated values of K^-/π^- ratio overestimate the DPMJET III simulated values. In the same table the values of K^-/π^- ratio calculated from the different publications at $\sqrt{s}$ = 6.3 GeV [12], $\sqrt{s}$ = 17.3 GeV [13], $\sqrt{s}$ = 62.4 GeV [14], $\sqrt{s}$ = 200 GeV [15], $\sqrt{s}$ = 900 GeV [17], and $\sqrt{s}$ = 7000 GeV [16] have also been presented. As in the case of K^+/π^+ ratio, the values of K^-/π^- ratio have been calculated from the values of dN/dy at mid rapidity at $\sqrt{s}$ = 62.4 GeV ($|y| < 0.35$) and $\sqrt{s}$ = 7 TeV ($|y| < 0.5$).

In Figure 2 we have depicted the variation of K^-/π^- ratio with energy for UrQMD simulated, DPMJET III simulated, and the experimental values. From Figure 2 it may be noted that the values of K^-/π^- ratio for the UrQMD simulated events are found to increase smoothly with energy and after reaching $\sqrt{s}$ = 900 GeV, saturation of K^-/π^- ratio occurs. However in case of DPMJET III model a sudden drop of K^-/π^- ratio occurs at $\sqrt{s}$ = 900 GeV. The ratio then begins to rise again presenting a horn-like structure as observed in case of the energy dependence of K^+/π^+ values. The experimental values of K^-/π^- ratio also get a sudden drop at $\sqrt{s}$ = 62.4 GeV and increase again to construct a horn-like structure in the energy dependence of K^-/π^- values in pp collisions.

Thus it may be pointed out that the experimental study of energy dependence of both K^+/π^+ and K^-/π^- ratio shows a horn-like structure which is also shown by the DPMJET III model but UrQMD model fails to reproduce the horn-like

Table 2: It represents the values of K^-/π^- ratio in pp collisions at $\sqrt{s}$ = 6.3 GeV to 7 TeV in the framework of UrQMD, DPMJET III, and the experimental values.

Energy $\sqrt{s}$ GeV	UrQMD simulated value of K^-/π^- ratio	DPMJET III model simulated value of K^-/π^- ratio	Experimental values of K^-/π^- ratio	Reference for the experimental values of K^-/π^- ratio
6.3	.026 ± .001	.031 ± .002	.038 ± .001	[12]
17.3	.066 ± .003	.077 ± .003	.092 ± .003	[13]
62.4	.093 ± .004	.097 ± .002	.081 ± .005	[14]
200	.105 ± .005	.116 ± .005	.102 ± .005	[15]
900	.120 ± .007	.113 ± .006	.121 ± .013	[17]
2760	.123 ± .005	.115 ± .006	.....	.....
7000	.124 ± .006	.119 ± .007	.128 ± .004	[16]

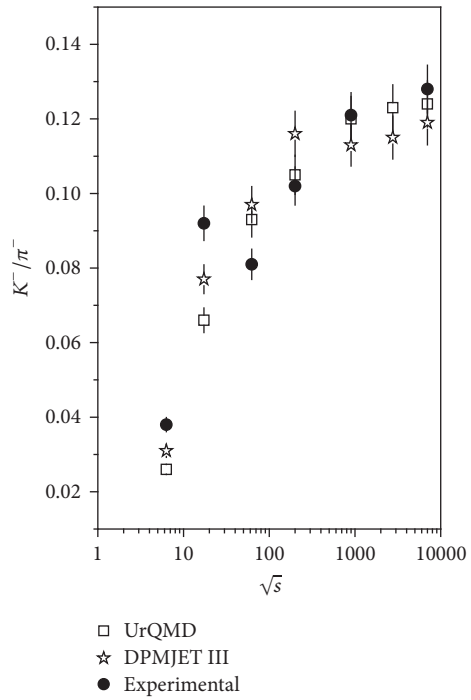

Figure 2: It represents the energy dependence of K^-/π^- ratio in pp collisions at $\sqrt{s}$ = 6.3 GeV to 7 TeV of the UrQMD, DPMJET III, and experimental analysis.

structure. The observed difference in the energy dependence of K^+/π^+ and K^-/π^- ratio between UrQMD and DPMJET III model is due to the basic difference between the two models. It may be mentioned here that both UrQMD and DPMJET III are microscopic Monte Carlo models. UrQMD is a hadronic transport model and DPMJET III is based on string interaction. String models describe the collision through the exchange of colour or momentum between partons in the projectile and target. As a consequence of these exchanges, these partons become joined by colourless objects which are called string, ropes, or flux tubes. UrQMD is a semiclassical hadronic transport model based on the concepts of kinetic theory, in which the evolution of a heavy-ion collision is described by the propagation of on-shell particles on relativistic trajectories in combination with a stochastic treatment of the individual particle scattering processes. The model offers an effective solution for the relativistic Boltzmann equation, where the collision term includes elastic and inelastic scatterings as well as resonance decays. To account for the quantum statistics, the hadrons are represented by Gaussian wave packets and effects such as Pauli blocking are included in this model.

It may be mentioned here that the horn-like structure of the experimental data occurs at different energy in comparison to the DPMJET III model for both K^+/π^+ and K^-/π^- ratio. In DPMJET III model at SPS energies two long strings with valence quarks at the end and SCET-soft sea quarks in the produced particles having a low $K^\pm/\pi^\pm$ ratio are given by a parameter in PYTHIA. The cross section fits dictate how at higher energies the additional strings enter. Their partons are considered as something like a minijet extension of pQCD events at large transverse momentum P_T. There should be something like a continuous transition at a cutoff P_T. It means the particles at the sea string ends have a larger P_T and a larger $\mathbf{K^\pm/\pi^\pm}$ ratio. At an energy where the new strings just come in, they are short and the fraction of particles containing the string end partons is sizable. With increasing energies the strings get longer and their influence gets diluted (i.e., $\mathbf{K^\pm/\pi^\pm}$ gets again lower). In heavy-ion scattering the production of new chains is enhanced as each projectile nucleon meets several target nucleons and vice versa. The new typically shorter strings now lead to an increase in the $\mathbf{K^\pm/\pi^\pm}$ ratio. The string fusion (available in DPMJET III) and rescattering effects (presumably necessary) do not have a significant effect. There is some uncertainty in the parameterization of sea strings energies and the position of the horn is not a firm prediction.

Comparing Tables 1 and 2 it may be said that significant differences between the values of K^+/π^+ and K^-/π^- exist for both the models up to $\sqrt{s}$ = 200 GeV. However, at the higher energy regime ($\sqrt{s}$ = 900 GeV–7 TeV), no significant difference occurs between the values of K^+/π^+ and K^-/π^- for both UrQMD and DPMJET III model. In case of the experimental data it can be seen that from $\sqrt{s}$ = 200 GeV the difference between the values of K^+/π^+ and K^-/π^- becomes insignificant. The difference between the K^+/π^+ and K^-/π^- values can be explained from the underlying physics of

Table 3: It represents the values oftotal kaon to pion multiplicity ratio $((K^+ + K^-)/(\pi^+ + \pi^-) = K/\pi)$ in pp collisions at $\sqrt{s}$ = 6.3 GeV to 7 TeV in the framework of UrQMD and DPMJET III model along with the experimentally obtained values.

Energy $\sqrt{s}$ GeV	Experimental value of K/π ratio	UrQMD model simulated Value of K/π ratio	DPMJET III model simulated value of K/π ratio	Reference for the experimental value
6.3	.045 ± .001	.046 ± .001	.052 ± .002	[18]
17.3	.082 ± .003	.075 ± .003	.087 ± .003	[13, 19, 20]
62.4	.094 ± .002	.097 ± .004	.101 ± .002	[14]
200	.103 ± .008	.108 ± .005	.109 ± .005	[15, 21]
900	.123 ± .004	.121 ± .007	.114 ± .006	[21]
2760	.124 ± .004	.123 ± .005	.116 ± .006	[16]
7000	.124 ± .005	.124 ± .006	.119 ± .007	[16]

kaon and antikaon production mechanism. Here it should be mentioned that there are two possible mechanisms of kaon production, the associated production mechanism and the pair production mechanism. According to the associated production mechanism only K^+ mesons are produced by the following two interactions: $N + N \rightarrow N + X + K^+$ and $\pi + N \rightarrow X + K^+$, where N is the nucleon and X is either Λhyperons or Ξ hyperons. On the other hand pair production mechanism produces K^+ and K^- according to the interaction given by $N + N \rightarrow N + N + K^+ + K^-$. At the lower energy, the associated production mechanism dominates. As the energy increases, the pair production, which produces the same number of K^+ and K^- becomes more significant. At higher energy the antikaon excitation function is steeper than that of the kaon because of a higher threshold. So at higher energy the antikaon production cross section increases faster than that of kaon and the K^-/π^- ratio increases.

3.3. Energy Dependence Studies of Total Kaon to Pion Multiplicity Ratio. We have also calculated the total kaon to pion multiplicity ratio $((K^+ + K^-)/(\pi^+ + \pi^-) = K/\pi)$ at these different collision energies for the proton-proton collisions and presented the values in Table 3 for both UrQMD and DPMJET III simulated events. It can be noticed from the table that as energy increases, the K/π ratio increases initially for both UrQMD and DPMJET III model. At higher energy in the LHC range the kaon to pion ratio becomes almost independent of energy in case of UrQMD model. But for DPMJET III simulation the values of K/π go on increasing slowly with energy. No clear energy independency is observed for DPMJET III model in LHC energy regime. Moreover, the observed sudden decrease of K^+/π^+ and K^-/π^- values vanishes in case of total kaon to pion multiplicity ratio $((K^+ + K^-)/(\pi^+ + \pi^-) = K/\pi)$ in DPMJET III simulation. From Table 3 it can be noted that the UrQMD simulated values of kaon to pion ratio are higher than the DPMJET III simulated values as energy increases from $\sqrt{s}$ = 200 GeV. At energy less than 200 GeV, however, DPMJET III model calculated values of kaon to pion ratio are higher in comparison to the UrQMD simulated values.

Experimental studies of total pion to kaon multiplicity ratio $((K^+ + K^-)/(\pi^+ + \pi^-) = K/\pi)$ in pp collisions have been reported by different collaborators in different times over a wide range of energy. From the report of the NA61 collaboration [18] we have calculated the values of K/π ratio in pp collisions at $\sqrt{s}$ = 6.3 GeV and presented the value in Table 3 along with the values obtained from our simulated analysis. From the study of NA49 collaboration [13, 19, 20] on pp collisions at $\sqrt{s}$ = 17.3 GeV, we have calculated the values of K/π ratio. In the regime of RHIC data, we extracted the values of K/π ratio from the analysis of PHENIX collaboration [14] at $\sqrt{s}$ = 62.4 GeV and from the analysis of STAR collaboration at $\sqrt{s}$ = 200 GeV [15]. At $\sqrt{s}$ = 900 GeV and $\sqrt{s}$ = 2.76 TeV, the K/π ratio has been calculated from the study of ALICE Collaboration [21]. ALICE Collaboration [17] studied the pion, kaon, and proton production in pp collisions at $\sqrt{s}$ = 7 TeV also. In that paper they calculated the values of K/π ratio in pp collisions. They have mentioned the values of K/π ratio in pp collisions at different energies studied earlier and presented a study of energy dependence. In [21] the values of K/π ratio at $\sqrt{s}$ = 200 GeV and $\sqrt{s}$ = 900 GeV have been mentioned in the text with proper references. The experimental values of K/π ratio at different energies have been calculated from the plot given in [16] with the help of a high accuracy digitized graphical software as mentioned earlier.

Experimentally calculated values of K/π ratio in pp collisions at $\sqrt{s}$ = 6.3, 17.3, 62.4, 200, and 900 GeV and also at $\sqrt{s}$ = 2.76 TeV and 7 TeV have been taken from these literatures and presented in Table 3. From Table 3 it can be seen that the experimentally obtained values of K/π ratio increase initially with the increase of energy up to 200 GeV. At energy greater than 200 GeV the K/π ratio becomes independent of energy. Moreover, Table 3 reflects that the experimentally obtained total kaon to pion multiplicity ratio agrees well with their UrQMD counterpart qualitatively and quantitatively over the entire energy range.

In comparison to the UrQMD analysis, DPMJET III model calculated values of K/π ratio are higher than the experimental data up to 200 GeV. As we enter in the LHC region (900 GeV to 7 TeV) DPMJET III simulated values of K/π ratio are found to be lower than the corresponding experimental values. We have also studied the variation of K/π ratio with energy graphically for the experimental events, UrQMD simulated events, and DPMJET III simulated events. Figure 3 depicts the variation of kaon to pion ratio

with energy in case of pp collisions from 6.3 GeV to 7 TeV for experimental, UrQMD simulated, and DPMJET III simulated events. From Figure 3 it can be noticed that no horn-like structure is observed for the experimental data when the energy dependence of total kaon to pion multiplicity ratio is studied.

It may be mentioned here that Long et al. [22] utilized the parton and hadron cascade model PACIAE based on PYTHIA to investigate the kaon to pion ratio in pp collisions at RHIC and LHC energy. They found that the PACIAE model calculated values of K/π at $\sqrt{s}$ = 17.2, 200, and 900 GeV agree with the NA49 [13, 19, 20], STAR [15], and ALICE data [21, 23]. With the inclusion of the results for $\sqrt{s}$ = 2.36, 7 and 14 TeV, it was found that the K/π ratio increases slightly from $\sqrt{s}$ = 0.2 to 0.9 TeV and then saturates. Our study with UrQMD model predicts the same result. It should be mentioned here that ALICE Collaboration also in their published papers [21, 23] studied the energy dependence of K/π ratio in pp collisions.

4. Conclusions

To summarize we recall that we have presented a systematic study of K^+/π^+, K^-/π^-, and $((K^+ + K^-)/(\pi^+ + \pi^-) = K/\pi)$ ratio in proton-proton collisions as a function of the bombarding energy from 6.3 GeV to 7 TeV using UrQMD model and DPMJET III model. Comparisons of the simulated results with the available experimental data have also been presented. Important findings of this analysis are given as follows:

(1) Values of K^+/π^+ and K^-/π^- differ from each other in the lower energy regime ($\sqrt{s}$ = 6.3 GeV–$\sqrt{s}$ = 200 GeV) for both UrQMD and DPMJET III model simulation. The difference becomes insignificant in the LHC energy range ($\sqrt{s}$ = 900 GeV–$\sqrt{s}$ = 7 TeV). Experimental study also supports this observation. This observation can be explained on the basis of Kaon production mechanism.

(2) In case of UrQMD model the values of K^+/π^+, K^-/π^-, and $((K^+ + K^-)/(\pi^+ + \pi^-) = K/\pi)$ increase with energy initially and then saturate in the LHC energy regime. DPMJET III simulated ratio of K^+/π^+, K^-/π^-, and $((K^+ + K^-)/(\pi^+ + \pi^-) = K/\pi)$ do not show any saturation at LHC region.

(3) A horn-like structure is observed in case of DPMJET III simulation during the variation of K^+/π^+ and K^-/π^- with energy. The horn-like structure is found to be wiped out when the total kaon to pion multiplicity ratio $((K^+ + K^-)/(\pi^+ + \pi^-) = K/\pi)$ was considered. No horn-like structure has been observed in case of UrQMD simulation.

(4) Comparison of our results with the experimental data of K^+/π^+, K^-/π^-, and total multiplicity ratio $((K^+ + K^-)/(\pi^+ + \pi^-) = K/\pi)$ has also been presented whenever available. Experimental study of energy dependence of K^+/π^+ and K^-/π^- shows the presence of horn-like structure. No horn-like structure is observed in case of energy dependence of total kaon to pion multiplicity ratio $((K^+ + K^-)/(\pi^+ + \pi^-) = K/\pi)$ for the experimental data.

(5) The experimental data was found to exhibit energy dependence at the lower energy regime but the values of K^+/π^+, K^-/π^-, and the K/π ratio become independent of energy as energy goes to the LHC range (900 GeV to 7 TeV). We have demonstrated that the experimentally obtained values of kaon to pion total multiplicity ratio (K/π values) are well reproduced by the UrQMD model. DPMJET III model simulated values of K/π ratio are little different from the experimental values of K/π ratio.

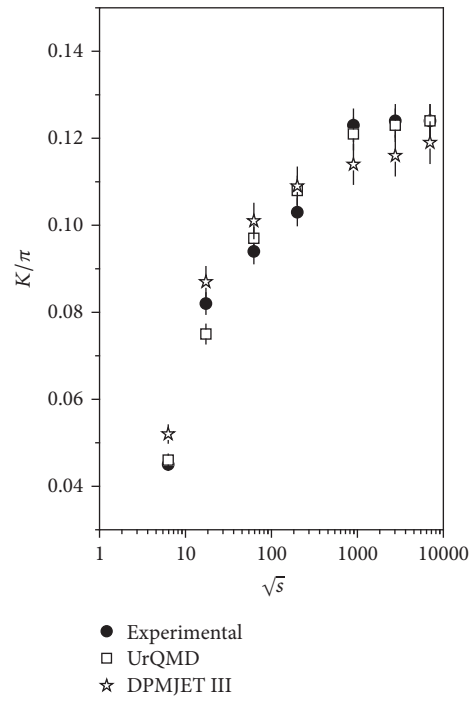

Figure 3: Variation of total kaon to pion multiplicity ratio $((K^+ + K^-)/(\pi^+ + \pi^-) = K/\pi)$ with energy $\sqrt{s}$ in pp collisions at $\sqrt{s}$ = 6.3 GeV to 7 TeV for the experimental data extracted from the papers of different collaborators, UrQMD model simulated values, and DPMJET III model simulated values.

Conflicts of Interest

There are no conflicts of interest in publishing the paper.

Acknowledgments

The corresponding author Dr. S. Bhattacharyya thanks Professor Nestor Armesto of Universidade de Santiago de Compostela, Spain, for helping in using the DPMJET III code, Professor F. W. Bopp, Department of Physics, University of Seigen, for useful discussions on the difference between UrQMD and DPMJET III models, Professor Dipak Ghosh, Department of Physics, Jadavpur University, and Professor Argha Deb, Department of Physics, Jadavpur University, for their inspiration in the preparation of this manuscript.

References

[1] M. Bleicher, E. Zabrodin, C. Spieles et al., "Relativistic hadron-hadron collisions in the ultra-relativistic quantum molecular dynamics model," *Journal of Physics G: Nuclear and Particle Physics*, vol. 25, no. 9, pp. 1859–1896, 1999.

[2] S. A. Bass, M. Belkacem, M. Bleicher et al., "Microscopic models for ultrarelativistic heavy ion collisions," *Progress in Particle and Nuclear Physics*, vol. 41, pp. 255–369, 1998.

[3] H. Petersen, M. Bleicher, S. A. Bass, and H. Stöcker, "UrQMD-2.3—changes and comparisons," https://arxiv.org/abs/0805.0567v1.

[4] V. N. Gribov, "Glauber corrections and the Interaction between high-energy Hadrons and Nuclei," *Soviet Journal of Experimental and Theoretical Physics*, vol. 29, no. 3, pp. 483–487, 1969, *Zhurnal Eksperimental'noi i Teoreticheskoi Fiziki*, vol. 56, no. 3, pp. 892-901, 1969.

[5] N. Armesto, A. B. Kaidalov, C. A. Salgado, and K. Tywoniuk, "Nuclear shadowing in Glauber-Gribov theory with Q^2-evolution," *The European Physical Journal C*, vol. 68, no. 3-4, pp. 447–457, 2010.

[6] R. J. Glauber, *Lectures on Theoretical Physics*, W. E. Britten and L. G. Duham, Eds., vol. 1, Interscience, New York, NY, USA, 1959.

[7] J. Ranft, "Dual parton model at cosmic ray energies," *Physical Review D*, vol. 51, no. 1, pp. 64–84, 1995.

[8] J. Ranft, "DPMJET version II.5, code manual," https://arxiv.org/abs/hep-ph/9911232.

[9] S. Y. Shmakov, V. V. Uzhinskii, and A. M. Zadoroshny, "DIAGEN—generator of inelastic nucleus-nucleus interaction diagrams," *Computer Physics Communications*, vol. 54, no. 1, pp. 125–135, 1989.

[10] S. Roesler, R. Engel, and J. Ranft, "The Monte Carlo event generator DPMJET-III," in *Advanced Monte Carlo for Radiation Physics, Particle Transport Simulation and Applications*, A. Kling, F. J. C. Barão, M. Nakagawa, L. Távora, and P. Vaz, Eds., Springer, Berlin, Germany, 2001.

[11] F. W. Bopp, J. Ranft, R. Engel, and S. Roesler, "Antiparticle to particle production ratios in hadron-hadron and *d*-Au collisions in the DPMJET-III Monte Carlo model," *Physical Review C*, vol. 77, no. 1, Article ID 014904, 9 pages, 2008.

[12] S. Pulawski, "Energy dependence of hadron spectra and multiplicities in p + p interactions," in *Proceedings of the 9th International Workshop on Critical point and Onset of Deconfinement (CPOD '14)*, Centre for Interdisciplinary Research, University of Bielefeld, Bielefeld, Germany, November 2014.

[13] T. Anticic, B. Baatar, J. Bartke et al., "Inclusive production of protons, anti-protons and neutrons in p + pp + p collisions at 158-GeV/cc beam momentum," *The European Physical Journal C*, vol. 65, pp. 9–63, 2010.

[14] A. Adare, S. Afanasiev, C. Aidala et al., "Identified charged hadron production in p + p collisions at $\sqrt{s}$ = 200 and 62.4 GeV," *Physical Review C*, vol. 83, no. 6, Article ID 064903, 29 pages, 2011.

[15] B. I. Abelev, M. M. Aggarwal, Z. Ahammed et al., "Systematic measurements of identified particle spectra in pp, d + Au, and Au + Au collisions at the STAR detector," *Physical Review C*, vol. 79, no. 3, Article ID 054323, 58 pages, 2009.

[16] J. Adam, D. Adamová, M. M. Aggarwal et al., "Measurement of pion, kaon and proton production in proton-proton collisions at $\sqrt{s}$ = 7 TeV," *The European Physical Journal C*, vol. 75, article 226, 2015.

[17] K. Aamodt, A. Abrahantes Quintana, D. Adamová et al., "Strange particle production in proton-proton collisions at $\sqrt{s}$ = 0.9 TeV with ALICE at the LHC," *The European Physical Journal C*, vol. 71, article 1594, 2011.

[18] A. Aduszkiewicz, Y. Ali, E. Andronov et al., "Status report to the proposal SPSCP330, Report from the NA61/SHINE experiment at the CERN SPS," NA61 Collaboration Report CERN-SPSC-2015-036/SPSC-SR-171, 2015.

[19] C. Alt, T. Anticic, B. Baatar et al., "Inclusive production of charged pions in p + p collisions at 158 GeV/c beam momentum," *The European Physical Journal C*, vol. 45, no. 2, pp. 343–381, 2006.

[20] T. Anticic, B. Baatar, J. Bartke et al., "Inclusive production of charged kaons in p + p collisions at 158 GeV/c beam momentum and a new evaluation of the energy dependence of kaon production up to collider energies," *The European Physical Journal C*, vol. 68, no. 1-2, pp. 1–73, 2010.

[21] K. Aamodt, N. Abel, U. Abeysekara et al., "Production of pions, kaons and protons in pp collisions at $\sqrt{s}$ = 900 GeV with ALICE at the LHC," *The European Physical Journal C*, vol. 71, article 1655, 2011.

[22] H.-Y. Long, S.-Q. Feng, D.-M. Zhou, Y.-L. Yan, H.-L. Ma, and B.-H. Sa, "Strange quark suppression and strange hadron production in pp collisions at energies available at the BNL Relativistic Heavy Ion Collider and the CERN Large Hadron Collider," *Physical Review C*, vol. 84, Article ID 034905, 2011.

[23] H. Oeschler, "Strange particle production in pp collisions at $\sqrt{s}$ = 0.9 and 7 TeV measured with the ALICE experiment," in *Proceedings of the 6th International Conference on Physics and Astrophysics of Quark Gluon Plasma (ICPAQGP '10)*, Goa, India, December 2010.

Hindawi
Advances in High Energy Physics
Volume 2017, Article ID 7374909, 5 pages
https://doi.org/10.1155/2017/7374909

Research Article

Mean Field Approximation for the Dense Charged Drop

S. Bondarenko and K. Komoshvili

Ariel University, Ariel, Israel

Correspondence should be addressed to S. Bondarenko; sergeyb@ariel.ac.il

Received 22 October 2017; Revised 29 November 2017; Accepted 6 December 2017; Published 31 December 2017

Academic Editor: Edward Sarkisyan-Grinbaum

We consider in this note the mean field approximation for the description of the probe charged particle in a dense charged drop. We solve the corresponding Schrödinger equation for the drop with spherical symmetry in the first order of mean field approximation and discuss the obtained results.

1. Introduction

Collisions of relativistic nuclei in the RHIC and LHC experiments at very high energies led to the discovery of a new state of matter named quark-gluon plasma (QGP). At the initial stages of the scattering, this plasma resembles almost an ideal liquid whose microscopic structure is not yet well understood [1–11]. The data obtained in the RHIC experiments is in good agreement with the predictions of the ideal relativistic fluid dynamics [12–32], which establishes fluid dynamics as the main theoretical tool to describe collective flow in collisions. As an input to the hydrodynamical evolution of the particles, it is assumed that, after a very short time, $\tau < 1$ fm/s [31, 32], the matter reaches a thermal equilibrium and expands with a very small shear viscosity [33–35].

In this paper, we continue to develop the model proposed in [36–39]. Namely, we assume that, at the local energy density fluctuations, hot drops [40–42] are created at the very initial stage of interactions at times $\tau < 0.5$ fm. These fireballs (hot drops) are very dense and small, their size is much smaller than the proton size (see [36–39]), and their energy density is much larger than the density achieved in high-energy interactions at the energies $\sqrt{s} < 100$ GeV. In our model, we assume that the fireballs consist of particles with weak interparticle interactions and have a nonzero charge. We consider this drop of charged particles from the point of view of quantum statistical physics. The most general Hamiltonian for this system can be written in the form which describes all possible interactions between the particles in the drop:

$$H = H^0 + V^1 + V^2 + \cdots + V^i + \cdots \quad (1)$$

(see [43]), where as usual V^1 is the energy of interaction of the particle with an external field, V^2 is the energy of pair-like interactions, and so forth. The mean field approximation for the probe particle in the system of charged particles, therefore, can be introduced by the following perturbative scheme. First of all, we can consider the motion of only one probe particle in the mean field of all other particles, which corresponds to preserving only the V^1 term in the expression of (1). This approximation will lead to the modification of the propagator of the particle, namely, from a free propagator to some "dressed" one. At the next step, we can take two probe particles, each of which will propagate in the mean field of the other charges of the system, similar to the first approximation, but additionally we can introduce the interaction of these two particles one with another in the mean field of the remaining charges in the drop, which requires introduction of one V^2 term in the expression of (1) in the mean field approximation. Further, we can increase the number of the probe particles in the system, considering, in addition to pair interactions, the interactions of free probe particles and so on.

In the present calculations, we limit ourselves to the first order of the mean field approach; namely, we will consider the motion of one nonrelativistic probe particle in the external mean field created by all other particles in the charged drop.

2. Mean Field Approximation for the Hamiltonian of the System

In the absence of the external field, we write the Hamiltonian of the system of charged particles as

$$H = -\frac{1}{2m}\int \Psi_\alpha^+\left(t,\vec{r}\right)\Delta\Psi_\alpha\left(t,\vec{r}\right)d^3x - \mu N + \frac{1}{2} \cdot \int \Psi_\beta^+\left(t,\vec{r}\right)\Psi_\alpha^+\left(t,\vec{r}\,'\right)U\left(\vec{r}-\vec{r}\,'\right)\Psi_\alpha\left(t,\vec{r}\,'\right) \cdot \Psi_\beta\left(t,\vec{r}\right)d^3x\,d^3x'. \tag{2}$$

Here,

$$N = \int \Psi_\alpha^+\left(t,\vec{r}\right)\Psi_\alpha\left(t,\vec{r}\right)d^3x \tag{3}$$

is a particle number operator. Considering the mean field approximation for a spherically symmetrical system, we introduce

$$\Psi_\alpha^+\left(t,\vec{r}\,'\right)\Psi_\beta\left(t,\vec{r}\right) \approx \left\langle \Psi_\alpha^+\left(t,\vec{r}\,'\right)\Psi_\beta\left(t,\vec{r}\right)\right\rangle = \delta_{\alpha\beta} f\left(r,r',r_0\right) \tag{4}$$

as some particles density for the droplet with characteristic size r_0; here, $r = |\vec{r}|$. The $f(r,r',r_0)$ function is a distribution function of the system of interest; it can be correctly determined by writing the corresponding Vlasov or Boltzmann equations coupled to system (1). In our case, we will not consider a particular form of this function, but instead we will discuss its form based on some physical assumptions only. Therefore, we obtain the following for the Hamiltonian:

$$H = -\frac{1}{2m}\int \Psi_\alpha^+\left(t,\vec{r}\right)\Delta\Psi_\alpha\left(t,\vec{r}\right)d^3x - \mu N + \frac{1}{2} \cdot \int \Psi_\alpha^+\left(t,\vec{r}\right)U\left(\vec{r}-\vec{r}\,'\right)f\left(r,r',r_0\right) \cdot \Psi_\alpha\left(t,\vec{r}\,'\right)d^3x\,d^3x', \tag{5}$$

which represents now the energy of the probe particle in the mean field created by the other particles of the system. Due to the spherical symmetry of the problem, we expand all the operators in the Hamiltonian expression in terms of spherical harmonic functions. We have the following for the two-particle interaction potential:

$$U\left(\vec{r}-\vec{r}\,'\right) = \sum_{l=0}^{\infty}\sum_{m=-l}^{l}\frac{4\pi q^2}{2l+1}\left(\theta\left(r'-r\right)\frac{r^l}{\left(r'\right)^{l+1}} + \theta\left(r-r'\right)\frac{r'^l}{r^{l+1}}\right)Y_{lm}^*\left(\Psi,\Phi\right)Y_{lm}\left(\psi,\phi\right) \tag{6}$$

with Ψ, Φ as spherical angles of r' vector, ψ, ϕ as spherical angles of r vector in some spherical coordinate system, and $\theta(r)$ as the step function. Correspondingly, we write the particle-field operator as

$$\Psi_\alpha\left(t,\vec{r}\right) = \sum_{l=0}^{\infty}\sum_{m=-l}^{l}\psi_{\alpha lm}\left(t,r\right)Y_{lm}\left(\psi,\phi\right). \tag{7}$$

Using the orthogonality property of the harmonic functions

$$\int Y_{lm}\left(\psi,\phi\right)Y_{l'm'}^*\left(\psi,\phi\right)d\Omega = \delta_{ll'}\delta_{mm'}, \tag{8}$$

with $d^3x = r^2dr\,d\Omega$, we rewrite the Hamiltonian equation (5) in a one-dimensional form as a function of r and r' only:

$$H = -\frac{1}{2m}\sum_{l=0}^{\infty}\sum_{m=-l}^{l}\int_0^\infty\left(\psi_{\alpha lm}^+\left(t,r\right)\Delta_r\psi_{\alpha lm}\left(t,r\right) - \frac{l\left(l+1\right)}{r^2}\psi_{\alpha lm}^+\left(t,r\right)\psi_{\alpha lm}\left(t,r\right)\right)r^2dr - \mu\sum_{l=0}^{\infty}\sum_{m=-l}^{l}\int_0^\infty\psi_{\alpha lm}^+\left(t,r\right)\psi_{\alpha lm}\left(t,r\right)r^2dr + \sum_{l=0}^{\infty}\sum_{m=-l}^{l}\frac{4\pi q^2}{2l+1} \cdot \int_0^\infty r^2dr\left(\int_r^\infty\frac{r^l}{r'^{(l+1)}}f\left(r,r',r_0\right)\psi_{\alpha lm}^+\left(t,r\right)\psi_{\alpha lm}\left(t,r'\right)r'^2dr' + \int_0^r\frac{r'^l}{r^{(l+1)}}f\left(r,r',r_0\right)\psi_{\alpha lm}^+\left(t,r\right)\psi_{\alpha lm}\left(t,r'\right)r'^2dr'\right). \tag{9}$$

In the next section, we solve Schrödinger's equation corresponding to this Hamiltonian.

3. Equations of Motion

We introduce the usual commutation relations for the fields of interest (see (7)):

$$\left\{\Psi_\alpha\left(t,\vec{r}\right),\Psi_\beta^+\left(t,\vec{r}\,'\right)\right\} = \delta_{\alpha\beta}\delta^3\left(\vec{t}-\vec{r}\,'\right). \tag{10}$$

Using the property of (8), we correspondingly obtain one-dimensional commutation relations for the new fields:

$$\left\{\psi_{\alpha lm}\left(t,r\right),\psi_{\beta l'm'}^+\left(t,r'\right)\right\} = \frac{1}{r^2}\delta_{\alpha\beta}\delta_{ll'}\delta_{mm'}\delta\left(r-r'\right). \tag{11}$$

The Schrödinger equation for $\psi_{\alpha lm}(t,r)$ field, therefore, has the following form:

$$\begin{aligned}\iota\frac{\partial}{\partial t}\psi_{\alpha lm}(t,r) &= \left(-\frac{1}{2m}\left(\Delta_r - \frac{l(l+1)}{r^2}\right) - \mu\right)\\ &\cdot \psi_{\alpha lm}(t,r)\\ &+ \frac{4\pi q^2}{2l+1}\left(\int_r^\infty \frac{r^l}{r'^{(l+1)}} f\left(r,r',r_0\right)\psi_{\alpha lm}\left(t,r'\right)r'^2 dr'\right.\\ &\left.+ \int_0^r \frac{r'^l}{r^{(l+1)}} f\left(r,r',r_0\right)\psi_{\alpha lm}\left(t,r'\right)r'^2 dr'\right).\end{aligned} \tag{12}$$

Rescaling the drop's density function and rewriting it in the dimensionless form as

$$f\left(r,r',r_0\right) \longrightarrow \frac{1}{r^{3/2}\left(r'\right)^{3/2}} f\left(r,r',r_0\right), \tag{13}$$

introducing a new variable in integrals in (12),

$$r' = xr, \tag{14}$$

we rewrite the integrals in (12) finally as

$$\begin{aligned}&\frac{4\pi}{r(2l+1)}\left(\int_1^\infty \frac{dx}{x^{l+1/2}} f(r,x,r_0)\,\psi_{\alpha lm}(t,x)\right.\\ &\left.+ \int_0^1 dx\, x^{l+1/2} f(r,x,r_0)\,\psi_{\alpha lm}(t,x)\right).\end{aligned} \tag{15}$$

For the case of the drop of small size, we can expand our ψ function in (15) around $x = 1$ in both terms; this point gives the main contribution to both integrals. Therefore, in the first approximation, we have the following for (15):

$$\begin{aligned}&\frac{4\pi}{r(2l+1)}\left(\int_1^\infty \frac{dx}{x^{l+1/2}} f(r,x,r_0)\,\psi_{\alpha lm}(t,xr)\right.\\ &\left.+ \int_0^1 dx\, x^{l+1/2} f(r,x,r_0)\,\psi_{\alpha lm}(t,xr)\right)\\ &\approx \psi_{\alpha lm}(t,r)\,\frac{4\pi}{r(2l+1)}\left(\int_1^\infty \frac{dx}{x^{l+1/2}} f(r,x,r_0)\right.\\ &\left.+ \int_0^1 dx\, x^{l+1/2} f(r,x,r_0)\right) = \frac{Q_l(r)}{r}\psi_{\alpha lm}(t,r),\end{aligned} \tag{16}$$

with Q_l as an l multipole moment of the drop. The Schrödinger equation (12) now acquires the following form:

$$\begin{aligned}&\iota\frac{\partial}{\partial t}\psi_{\alpha lm}(t,r)\\ &= \left(-\frac{1}{2m}\left(\Delta_r - \frac{l(l+1)}{r^2}\right) - \mu + \frac{q^2}{r}Q_l(r)\right)\\ &\cdot \psi_{\alpha lm}(t,r).\end{aligned} \tag{17}$$

Representing the wave function as

$$\psi_{\alpha lm}(t,r) = u_{\alpha lm}(r)\, e^{-\iota t(E-\mu)}, \tag{18}$$

we obtain the Schrödinger equation for the particle in the following form:

$$\left(\frac{1}{2m}\Delta_r - \frac{1}{2m}\frac{l(l+1)}{r^2} + E - \frac{q^2}{r}Q_l(r)\right)u_{\alpha lm}(r) = 0. \tag{19}$$

In general, we cannot solve this equation without knowledge of the form of $f(r,x,r_0)$ particles distribution function in integrals of (15). Nevertheless, we can guess the form of the function in the $r \le r_0$ region of the drop, mostly interesting for us. Indeed, at $r \gg r_0$, which is outside the drop region, the potential equation (16) is the usual Coulomb potential, but in the $r \le r_0$ region, the situation is different. The existence of the drop requires the presence of some potential well at $r \le r_0$ which will keep particles inside the drop for some (very short) time and, therefore, it must be the potential's minimum present somewhere between $r = 0$ and $r \propto r_0$. Hence, this minimum is the indication of the creation of the dense drop of finite size in the interaction system of interest and, consequently, we can write the potential energy from (19) in this region as

$$\begin{aligned}&\frac{1}{2m}\frac{l(l+1)}{r^2} + \frac{Q_l(r)\,q^2}{r}\\ &\approx \frac{1}{2m}\frac{l(l+1)}{r_{\min}^2} + \frac{Q_l(r_{\min})\,q^2}{r_{\min}}\\ &+ \frac{A_l(r_{\min})\,q^2}{2r_0^3}\left(r - r_{\min}\right)^2,\end{aligned} \tag{20}$$

where we assumed that the potential energy acquires its minimum at $r_{\min}$; $A_l(r_{\min})$ here are the positive coefficients of the potential's expansion around this minimum. This situation, in fact, is similar to the situation in the system of two-atom molecules (see [44] and the references therein), where two atoms are kept inside some mutual potential well. Inserting the expansion of (20) in (19), we obtain the following equation:

$$\begin{aligned}&\left(\frac{1}{2m}\Delta_r + E - \frac{1}{2m}\frac{l(l+1)}{r_{\min}^2} - Q_l(r_{\min})\frac{q^2}{r_{min}}\right.\\ &\left.- A_l(r_{\min})\frac{q^2}{2r_0^3}\left(r - r_{\min}\right)^2\right)u_{\alpha lm}(r) = 0.\end{aligned} \tag{21}$$

The solution of this equation is similar to the solution of the Schrödinger equation for the harmonic oscillator with energy levels defined by

$$E' = E - \frac{1}{2m}\frac{l(l+1)}{r_{\min}^2} - Q_l(r_{\min})\frac{q^2}{r_{\min}}, \tag{22}$$

and consequently the energy levels of the system are given by

$$\begin{aligned}E_{nl} &= \frac{1}{2m}\frac{l(l+1)}{r_{\min}^2} + Q_l(r_{\min})\frac{q^2}{r_{\min}}\\ &+ q\left(\frac{A_l(r_{\min})}{mr_0^3}\right)^{1/2}\left(n+\frac{1}{2}\right)\quad n = 0,1,2,\ldots,\end{aligned} \tag{23}$$

with the wave functions

$$u_{\alpha lm}(r) = c_{\alpha lm} \frac{e^{-(r-r_{\min})^2/(2R^2)}}{r\sqrt{R}} H_n\left(\frac{(r-r_{\min})}{R}\right), \quad (24)$$

where

$$R = \left(\frac{r_0^3}{mA_l(r_{\min})q^2}\right)^{1/4}. \quad (25)$$

We note that the obtained solution is indeed similar to the solution of the Schrödinger equation for the two-atom molecules (see, e.g., [44]).

4. Conclusion

In this note, we demonstrated that the spectrum of the charged nonrelativistic particle in the dense charged drop has a quantum structure (see (23)), and it is determined by three terms in the first mean field approximation. The first term in (23) can be considered as the quantized rotation energy of the drop; the second one is the quantized electrostatic energy due to the multipole moments of the charged drop. The third term in the expression of (23) is the usual quantum corrections to the energy due to the oscillation of the particle inside the drop with eigenfrequencies determined by the form of the distribution function of the particles in the drop. The presence of this minimum is a necessary condition of the drop's creation (see also [36–39]). The values of these corrections have an additional degeneracy of energy levels defined by l quantum number in comparison to the ordinary quantum oscillator. In this formulation, the considered problem is similar to the problem of the description of the system of the two-atom molecule (see [44]) (we note that the proposed approach can be used also for the description of bound states created at low energy interactions, and we plan to investigate this subject in a separate publication). Further development of the approach can include the consideration of higher orders of mean field approximation for the system and introduction of the kinetic equation for the distribution function of (4) coupled to the Hamiltonian; we plan to consider these problems in the following publications.

We conclude that our model can be useful for the clarification of the spectrum of the produced particles, which is influenced by the quantum-mechanical properties of the QCD fireball. We believe that this approach will provide the connection between the data, obtained in high-energy collisions of protons and nuclei in the LHC and RHIC experiments [12–32, 45–49], and microscopic fields inside the collision region.

Conflicts of Interest

The authors declare that there are no conflicts of interest regarding the publication of this paper.

References

[1] E. Shuryak, "Four lectures on strongly coupled Quark Gluon Plasma," *Nuclear Physics B*, vol. 195, pp. 111–156, 2009.

[2] E. Shuryak, "Physics of strongly coupled quark–gluon plasma," *Progress in Particle and Nuclear Physics*, vol. 62, no. 1, pp. 48–101, 2009.

[3] E. V. Shuryak and I. Zahed, "Toward a theory of binary bound states in the quark-gluon plasma," *Physical Review D: Particles, Fields, Gravitation and Cosmology*, vol. 70, Article ID 054507, 2004.

[4] B. Berdnikov and K. Rajagopal, "Slowing out of equilibrium near the QCD critical point," *Physical Review D: Particles, Fields, Gravitation and Cosmology*, vol. 61, Article ID 105017, 2000.

[5] V. Koch, A. Majumder, and J. Randrup, "Baryon-strangeness correlations: a diagnostic of strongly interacting matter," *Physical Review Letters*, vol. 95, Article ID 182301, 2005.

[6] J. Liao and E. V. Shuryak, "What do lattice baryonic susceptibilities tell us about quarks, diquarks, and baryons at $T > T_c$," *Physical Review D: Particles, Fields, Gravitation and Cosmology*, vol. 73, Article ID 014509, 2006.

[7] M. Nahrgang, C. Herold, and M. Bleicher, "Influence of an inhomogeneous and expanding medium on signals of the QCD phase transition," *Nuclear Physics A*, vol. 904-905, pp. 899c–902c, 2013.

[8] J. Steinheimer and J. Randrup, "Spinodal Amplification of Density Fluctuations in Fluid-Dynamical Simulations of Relativistic Nuclear Collisions," *Physical Review Letters*, vol. 109, Article ID 212301, 2012.

[9] V. V. Skokov and D. N. Voskresensky, "Hydrodynamical description of first-order phase transitions: Analytical treatment and numerical modeling," *Nuclear Physics A*, vol. 828, no. 3-4, pp. 401–438, 2009.

[10] V. V. Skokov and D. N. Voskresensky, "Hydrodynamical description of a hadron-quark first-order phase transition," *JETP Letters*, vol. 90, no. 4, pp. 223–227, 2009.

[11] J. Randrup, "Phase transition dynamics for baryon-dense matter," *Physical Review C: Nuclear Physics*, vol. 79, Article ID 054911, 2009.

[12] T. Ludlam and S. Aronson, "BRAHMS and STAR and PHOBOS and PHENIX collaborations," Tech. Rep. BNL-73847-2005, 2005.

[13] K. Adcox, S. S. Adler, S. Afanasiev et al., "Formation of dense partonic matter in relativistic nucleus-nucleus collisions at RHIC: experimental evaluation by the PHENIX collaboration," *Nuclear Physics A*, vol. 757, no. 1-2, pp. 184–283, 2005.

[14] J. Adams, M. M. Aggarwala, Z. Ahammed et al., "Experimental and theoretical challenges in the search for the quark–gluon plasma: the STAR Collaboration's critical assessment of the evidence from RHIC collisions," *Nuclear Physics A*, vol. 757, no. 1-2, pp. 102–183, 2005.

[15] I. Arsene, I. G. Bearden, D. Beavis et al., "Quark-gluon plasma and color glass condensate at RHIC? The perspective from the BRAHMS experiment," *Nuclear Physics A*, vol. 757, no. 1-2, pp. 1–27, 2005.

[16] C. Jena, in *Proceedings of the DAE Symposium on Nuclear Physics*, vol. 56, pp. 1180-1181, 2011.

[17] A. Jipa, O. Ristea, C. Ristea et al., "New information on the dynamics of relativistic nucleus-nucleus collisions," *Journal of Physics: Conference Series*, vol. 381, Article ID 012042, 2012.

[18] P. Steinberg, "What have we learned about the quark–gluon plasma with the ATLAS detector at the LHC?" *Nuclear Physics A*, vol. 932, pp. 9–16, 2014.

[19] J. Velkovska, "What have hard probes taught us about the quark–gluon plasma as measured in CMS?" *Nuclear Physics A*, vol. 932, pp. 17–24, 2014.

[20] I. Arsene, "BRAHMS collaboration results for relativistic heavy ion collisions," *Physics of Particles and Nuclei*, vol. 39, no. 7, pp. 1082–1086, 2008.

[21] M. Przybycien, "Recent results on soft probes of the Quark-Gluon Plasma from the ATLAS experiment at the LHC," *Nuclear and Particle Physics Proceedings*, vol. 273–275, pp. 1539–1545, 2016.

[22] J. Adam, D. Adamová, M. M. Aggarwal et al., "Production of light nuclei and anti-nuclei in *pp* and Pb-Pb collisions at energies available at the CERN Large Hadron Collider," *Physical Review C*, vol. 93, Article ID 024917, 2016.

[23] M. Chojnacki, "Soft probes of the Quark-Gluon Plasma measured by ALICE," *Nuclear and Particle Physics Proceedings*, vol. 273–275, pp. 1553–1558, 2016.

[24] CMS Collaboration, "Pseudorapidity distributions of charged hadrons in proton-lead collisions at $\sqrt{s_{NN}}$ = 5.02 and 8.16 TeV," Tech. Rep. CMS-PAS-HIN-16-021, 2017.

[25] B. Wosiek, "Measurements of hard probes of the quark-gluon plasma with the ATLAS experiment at the LHC," *Nuclear and Particle Physics Proceedings*, vol. 273–275, pp. 1546–1552, 2016.

[26] A. M. Sirunyan, W. Adam, F. Ambrogi, E. Asilar et al., "Pseudorapidity distributions of charged hadrons in proton-lead collisions at $\sqrt{s_{NN}}$ = 5.02 and 8.16 TeV," 2017, https://arxiv.org/abs/1710.09355.

[27] A. Barbano, "Heavy flavours as a probe for the Quark-Gluon Plasma with ALICE at the LHC," *IL NUOVO CIMENTO C*, vol. 40, no. 1, p. 27, 2017.

[28] B. Huang, "Overview of Recent Results from the STAR experiment," *Nuclear and Particle Physics Proceedings*, vol. 289–290, pp. 19–24, 2017.

[29] P. F. Kolb, P. Huovinen, U. Heinz, and H. Heiselberg, "Elliptic flow at SPS and RHIC: from kinetic transport to hydrodynamics," *Physics Letters B*, vol. 500, no. 3-4, pp. 232–240, 2001.

[30] D. Teaney, J. Lauret, and E. V. Shuryak, "Flow at the SPS and RHIC as a quark-gluon plasma signature," *Physical Review Letters*, vol. 86, no. 21, pp. 4783–4786, 2001.

[31] U. W. Heinz and P. F. Kolb, "Early thermalization at RHIC," *Nuclear Physics A*, vol. 702, no. 1–4, pp. 269–280, 2002.

[32] A. Peshier and W. Cassing, "The hot nonperturbative gluon plasma is an almost ideal colored liquid," *Physical Review Letters*, vol. 94, Article ID 172301, 2005.

[33] P. Romatschke and U. Romatschke, "Viscosity information from relativistic nuclear collisions: how perfect is the fluid observed at RHIC?" *Physical Review Letters*, vol. 99, no. 17, Article ID 172301, 2007.

[34] B. Schenke, S. Jeon, and C. Gale, "Higher flow harmonics from," *Physical Review C: Nuclear Physics*, vol. 85, Article ID 024901, 2012.

[35] D. Teaney, "Effect of shear viscosity on spectra, elliptic flow, and Hanbury Brown-Twiss radii," *Physical Review C: Nuclear Physics*, vol. 68, Article ID 034913, 2003.

[36] S. Bondarenko and K. Komoshvili, "Gas–liquid transition in the model of particles interacting at high energy," *The European Physical Journal C*, vol. 73, article 2624, 2013.

[37] S. Bondarenko and K. Komoshvili, "Transverse transport properties of a charged drop in an electric field," *International Journal of Modern Physics E*, vol. 24, no. 5, Article ID 1550034, 23 pages, 2015.

[38] S. Bondarenko, K. Komoshvili, and A. Prygarin, "Transport properties of a charged fireball in an external electromagnetic field," *Nuclear Physics A*, vol. 950, pp. 129–162, 2016.

[39] S. Bondarenko and K. Komoshvili, "Transverse kinetics of a charged drop in an external electric," *AIP Conference Proceedings*, vol. 1701, Article ID 060007, 2016.

[40] M. Gyulassy, D. H. Rischke, and B. Zhang, "Hot spots and turbulent initial conditions of quark-gluon plasmas in nuclear collisions," *Nuclear Physics A*, vol. 613, no. 4, pp. 397–434, 1997.

[41] G. Torrieri, "Quark fluids in heavy ion collisions," 2009, https://arxiv.org/abs/0911.5479.

[42] M. Stephanov, K. Rajagopal, and E. Shuryak, "Event-by-event fluctuations in heavy ion collisions and the QCD critical point," *Physical Review D: Particles, Fields, Gravitation and Cosmology*, vol. 60, Article ID 114028, 1999.

[43] L. D. Landau, E. M. Lifshitz, and L. P. Pitaevskii, *Statistical Physics, Part 1 (Course Theoretical Physics, Volume 5)*, Pergamon Press, 1980.

[44] M. H. Jeremy, "An Introduction to the dynamics of Van der Waals molecules," *Advances in Molecular Vibrations and Collision Dynamics 1A*, vol. 1, 1990.

[45] D. Kharzeev, E. Levin, and K. Tuchin, "Multiparticle production and thermalization in high-energy QCD," *Physical Review C: Nuclear Physics*, vol. 75, Article ID 044903, 2007.

[46] E. K. G. Sarkisyan and A. S. Sakharov, "Relating multihadron production in hadronic and nuclear collisions," *The European Physical Journal C*, vol. 70, no. 3, pp. 533–541, 2010.

[47] A. N. Mishra, R. Sahoo, E. K. G. Sarkisyan, and A. S. Sakharov, "Effective-energy budget in multiparticle production in nuclear collisions," *The European Physical Journal C*, vol. 74, article 3147, 2014, Erratum: [The European Physical Journal C 75, 70 (2015)].

[48] E. K. G. Sarkisyan, A. N. Mishra, R. Sahoo, and A. S. Sakharov, "Multihadron production dynamics exploring the energy balance in hadronic and nuclear collisions," *Physical Review D: Particles, Fields, Gravitation and Cosmology*, vol. 93, Article ID 079904, 2016, Addendum: [Physical Review D: Particles, Fields, Gravitation and Cosmology 93, no. 7, 079904 (2016)].

[49] E. K. G. Sarkisyan, A. N. Mishra, R. Sahoo, and A. S. Sakharov, "Centrality dependence of midrapidity density from GeV to TeV heavy-ion collisions in the effective-energy universality picture of hadroproduction," *Physical Review D: Particles, Fields, Gravitation and Cosmology*, vol. 94, Article ID 011501(R), 2016.

Hindawi
Advances in High Energy Physics
Volume 2017, Article ID 4135329, 7 pages
https://doi.org/10.1155/2017/4135329

Research Article

Chiral Phase Transition in Linear Sigma Model with Nonextensive Statistical Mechanics

Ke-Ming Shen, Hui Zhang, De-Fu Hou, Ben-Wei Zhang, and En-Ke Wang

Key Laboratory of Quark & Lepton Physics (MOE) and Institute of Particle Physics, Central China Normal University, Wuhan 430079, China

Correspondence should be addressed to Ben-Wei Zhang; bwzhang@mail.ccnu.edu.cn

Received 9 September 2017; Accepted 7 November 2017; Published 29 November 2017

Academic Editor: Edward Sarkisyan-Grinbaum

From the nonextensive statistical mechanics, we investigate the chiral phase transition at finite temperature T and baryon chemical potential μ_B in the framework of the linear sigma model. The corresponding nonextensive distribution, based on Tsallis' statistics, is characterized by a dimensionless nonextensive parameter, q, and the results in the usual Boltzmann-Gibbs case are recovered when $q \to 1$. The thermodynamics of the linear sigma model and its corresponding phase diagram are analysed. At high temperature region, the critical temperature T_c is shown to decrease with increasing q from the phase diagram in the (T, μ) plane. However, larger values of q cause the rise of T_c at low temperature but high chemical potential. Moreover, it is found that μ different from zero corresponds to a first-order phase transition while $\mu = 0$ to a crossover one. The critical endpoint (CEP) carries higher chemical potential but lower temperature with q increasing due to the nonextensive effects.

1. Introduction

Quantum Chromodynamics (QCD) is a basic theory of describing the strong interactions among quarks and gluons, the fundamental constituents of matter. More and more attentions have already been attracted to the QCD phase transition both theoretically and experimentally [1–8]. Though experimental studies and lattice Monte-Carlo simulations have made it possible to research on the phase diagram quantitatively, there still remains uncertainty at high baryon density region [9]. Consequently, the phase transition is also a vital topic in high-energy physics, where the thermal vacuum created by heavy-ion collisions differs from the one at zero temperature and chemical potential [7]. In order to study certain essential features of it, the linear sigma model has been proposed to illuminate the restoration of chiral symmetry and its spontaneous breaking [8].

Near the phase transition boundary, one should be cautious when using the Boltzmann-Gibbs (BG) statistics for the appearance of critical fluctuations due to a large correlation length [10]. It is of interest to investigate the phase transition in the formalism beyond conventional BG statistical mechanics. Recently nonextensive statistics firstly proposed in [11] has attracted a lot of attention and discussions [12]. In this formalism, instead of the exponential function, a generalized q-exponential function is defined as [11, 12]

$$\exp_q(x) \coloneqq \left[1 + (1-q)\,x\right]^{1/(1-q)}, \tag{1}$$

where the parameter q is called the nonextensive parameter, which accounts for all possible factors violating assumptions of the usual BG case. Its inverse function is also listed [11, 12]

$$\ln_q(x) \coloneqq \frac{x^{1-q} - 1}{1-q}. \tag{2}$$

Both of them return to the usual exponential and logarithm function with $q \to 1$.

The purpose of this paper is to clarify the nonextensive effects on physical quantities of the chiral phase transition in the generalized linear sigma model. We focus on the situations where both of temperature and chemical potential

are not vanished, which then indicates the influence of the Tsallis distribution on the whole phase diagram in the (T,μ) plane. Whereas the nonextensive parameter q is still a phenomenological parameter [12], not only the case of $q > 1$ but also $q < 1$, in this work, is computed. For comparisons, we have presented discussions on this issue for finite temperature but vanishing chemical potential [13, 14]. Given the consistency of nonextensive generalizations with the initial BG approaches, we also list the results of $q = 1$ which were investigated [15]. We close our researches with the comparisons to the nonextensive Nambu Jona-Lasinio model (q-NJL model) [16, 17] of the critical endpoint (CEP), whose location is still the hot topic for experiments as well as its theoretical researches [3, 5].

This paper is organized as follows. In Section 2 we introduce the theoretical framework, where the nonextensive q-linear sigma model is stated. Their consequences for various thermodynamic quantities with different nonextensive parameters, q, are explored in Section 3; more detailed discussions on the results are also contained. Section 4 is our brief summary and outlook.

2. Theoretical Framework

Within the linear sigma model, the chiral effective Lagrangian with quark degrees of freedom reads [15, 18, 19]

$$\begin{aligned}\mathscr{L} &= \overline{\psi}\left[i\gamma^{\mu}\partial_{\mu} - g\left(\sigma + i\gamma_5\vec{\tau}\cdot\vec{\pi}\right)\right]\psi \\ &\quad + \frac{1}{2}\left(\partial_{\mu}\sigma\partial^{\mu}\sigma + \partial_{\mu}\vec{\pi}\cdot\partial^{\mu}\vec{\pi}\right) - U\left(\sigma,\vec{\pi}\right),\end{aligned} \tag{3}$$

where $\psi = (u,d)$ stands for the spin-1/2 two flavors' light quark fields and the scalar field σ and the pion field $\vec{\pi} = (\pi_1,\pi_2,\pi_3)$ together form a chiral field $\Phi = (\sigma,\vec{\pi})$, with its potential

$$U\left(\sigma,\vec{\pi}\right) = \frac{\lambda^2}{4}\left(\sigma^2 + \vec{\pi}^2 - v^2\right)^2 - H\sigma. \tag{4}$$

Considering the obvious symmetry breaking term $H\sigma = 0$, $\mathscr{L}$ is invariant under chiral $\mathrm{SU}(2)_L \times \mathrm{SU}(2)_R$ transformations. The chiral symmetry is spontaneously broken in the vacuum with the expectation values: $\langle\sigma\rangle = f_\pi$ and $\langle\vec{\pi}\rangle = 0$, where $f_\pi = 93$ MeV is the pion decay constant. By the partially conserved axial vector current (PCAC) relation [15], the quantity $v^2 = f_\pi^2 - m_\pi^2/\lambda^2$ with the constant $H = f_\pi m_\pi^2$, where $m_\pi = 138$ MeV is the pion mass. The coupling constant λ^2 is fixed as 20 by $m_\sigma^2 = 2\lambda^2 f_\pi^2 + m_\pi^2$, where $m_\sigma = 600$ MeV is the sigma mass. Another coupling constant g is usually determined by the requirement of the constituent quark mass in vacuum, $M_{\mathrm{vac}} = gf_\pi$, which is about 1/3 of the nucleon mass, leading to $g \approx 3.3$. [15]

In order to investigate the temperature T and the chemical potential μ dependence in this model, let us consider a system of both quarks and antiquarks in the thermodynamical equilibrium. Here quark chemical potential $\mu \equiv \mu_B/3$. And the grand partition function goes like

$$\begin{aligned}\mathscr{Z} &= Tr\exp\left[-\frac{\mathscr{H}-\mu\mathscr{N}}{\mathrm{T}}\right] \\ &= \int \mathscr{D}\overline{\psi}\mathscr{D}\psi\mathscr{D}\sigma\mathscr{D}\vec{\pi}\exp\left[\int_x\left(\mathscr{L} + \mu\overline{\psi}\gamma^0\psi\right)\right],\end{aligned} \tag{5}$$

where $\int_x \equiv i\int_0^{1/T} dt\int_V d^3\vec{x}$ with V being the volume of the system.

Thus the grand canonical potential can be obtained

$$\Omega\left(T,\mu\right) = -\frac{T}{V}\ln\mathscr{Z} = U\left(\sigma,\vec{\pi}\right) + \Omega_{\overline{\psi}\psi} \tag{6}$$

with the (anti)quark contribution being

$$\begin{aligned}\Omega_{\overline{\psi}\psi}\left(T,\mu\right) &= -\nu\int\frac{d^3\vec{p}}{(2\pi)^3}\left\{E + T\ln\left[1 + e^{-(-\mu+E)/T}\right]\right. \\ &\quad \left. + T\ln\left[1 + e^{-(\mu+E)/T}\right]\right\},\end{aligned} \tag{7}$$

where $\nu = 12$ is the internal degrees of freedom of quarks and $E = \sqrt{p^2 + M^2}$ is the valence (anti)quark energy, with the mass of constituent (anti)quark defined as

$$M^2 = g^2\left(\sigma^2 + \vec{\pi}^2\right). \tag{8}$$

Here the first divergent term of E is absorbed in the coupling constant in the results which comes from the negative energy states of the Dirac sea.

It is inadequate to apply naively the BG statistics in such a system; critical fluctuations of energy and particle numbers will appear as well as a large correlation. In order to investigate the phase transition of systems departing from the classical thermal equilibrium, the nonextensive statistics [11] are introduced. The so-called Tsallis entropy and density matrix are given, respectively, as $S_q = k_B Tr(\rho - \rho^q)/(q-1)$ and $\rho = \exp_q(-E/T)/Z_q$, where k_B is the Boltzmann constant (set to 1 for simplicity next), q describes the degree of nonextensivity, and Z_q is the corresponding generalized partition function.

Recently these generalized statistics have been of great interest theoretically [20–22] and widely applied in many fields [23–26]. In the following, we investigate the linear sigma model within the nonextensive statistics. Firstly we rewrite the partition function of (5) as

$$\begin{aligned}\mathscr{Z}_q &= Tr\exp_q\left[-\frac{\mathscr{H}-\mu\mathscr{N}}{T}\right] \\ &= \int\mathscr{D}\overline{\psi}\mathscr{D}\psi\mathscr{D}\sigma\mathscr{D}\vec{\pi}\exp_q\left[\int_x\left(\mathscr{L} + \mu\overline{\psi}\gamma^0\psi\right)\right],\end{aligned} \tag{9}$$

where the q-exponential is seen in (1). Considering the q-thermodynamics [27], we have

$$\begin{aligned}\Omega_{\overline{\psi}\psi}(T,\mu,q) &= -\frac{T}{V}\ln_q \mathcal{Z}_q - U\left(\sigma,\vec{\pi}\right)\\ &= \sum_n\sum_p \left\{\ln_q\left[\beta^2\left(E_n^2+\left(E-\mu\right)^2\right)\right]\right.\\ &\left.+\ln_q\left[\beta^2\left(E_n^2+\left(E+\mu\right)^2\right)\right]\right\}.\end{aligned} \tag{10}$$

Before carrying it out, we give out the generalized identities with respect to q-sums and integrals

$$\begin{aligned}&\ln_q\left[\beta^2\left(E_n^2+\left(E\pm\mu\right)^2\right)\right]\\ &= \int_1^{\beta^2(E\pm\mu)^2}\frac{d\theta^2}{\left(\theta^2+\left(2n+1\right)^2\pi^2\right)^q}\\ &\quad+\ln_q\left[1+\left(2n+1\right)^2\pi^2\right]\end{aligned} \tag{11}$$

and the generalized sum over n, in our assumptions,

$$\begin{aligned}&\sum_n\frac{1}{\left(\theta^2+\left(2n+1\right)^2\pi^2\right)^q}\\ &\approx \frac{1}{\theta}\left(\frac{1}{2}-\frac{1}{\left(\exp_{2-q}(\theta)+1\right)^q}\right),\end{aligned} \tag{12}$$

where $E_n = (2n+1)\pi T$ is used and the index $2-q$ appears because of the duality

$$\begin{aligned}&\exp_q(-x)\cdot\exp_{2-q}(x)\\ &= \left[1-\left(1-q\right)x\right]^{1/(1-q)}\cdot\left[1+\left(q-1\right)x\right]^{1/(q-1)} = 1.\end{aligned} \tag{13}$$

Integrating over θ and dropping terms that are independent of β and μ, we finally obtain

$$\begin{aligned}\Omega_{\overline{\psi}\psi}(T,\mu,q) &= -\nu\int\frac{d^3\vec{p}}{(2\pi)^3}\left\{E\right.\\ &\quad+T\ln_q\left[1+\exp_q\left(-\frac{E-\mu}{T}\right)\right]\\ &\left.\quad+T\ln_q\left[1+\exp_q\left(-\frac{E+\mu}{T}\right)\right]\right\}.\end{aligned} \tag{14}$$

In our calculations within the mean-field approximation, we follow [15, 28] where the expectation value of the pion field is set to zero; $\vec{\pi}=0$. By solving the gap equation

$$\frac{\partial}{\partial\sigma}\Omega_{\overline{\psi}\psi}(T,\mu,q)\big|_{\sigma=\sigma_V} = 0, \tag{15}$$

the value for constituent (anti)quark mass $M = g\sigma_V$ can be determined, which will be also affected by different nonextensive parameters, q. Here we have replaced σ and $\vec{\pi}$ in the exponent by their expectation values in the mean-field approximation.

With such a q-thermal effective potential, we then explore the nonextensive effects on the physical quantities, as well as the phase transition, in the linear sigma model. The numerical results will be shown in the next section.

3. Results and Discussion

In virtue of the fact that there still exist fierce controversies over the possible interpretations of the nonextensive parameter q, we shall discuss the nonextensive effects in the q-linear sigma model for both the $q > 1$ and $q < 1$ case. Meanwhile, we give out the result of $q = 1$ as the baseline for better understanding.

It is worthy to note that the value of nonextensive parameter q cannot be much smaller than 1 since, in the expression of (14), the corresponding generalized exponential

$$\exp_q\left(-\frac{E+\mu}{T}\right) := \left[1-\left(1-q\right)\frac{\left(E+\mu\right)}{T}\right]^{1/(1-q)}, \tag{16}$$

where the part of the base should be larger than 0: $1-(1-q)((E+\mu)/T) > 0$; namely,

$$q > 1-\frac{T}{(E+\mu)}. \tag{17}$$

Thus some upper limitation of energy of the integral in (7) should be given in case of divergence when $q < 1$. On the other hand, too much smaller values of q are not necessary to be computed physically during our investigation on the nonextensive effects on the phase transition. Therefore, here we just list the results of $q = 1.1, 1.05, 0.95$ and $q = 1$ as baseline.

We start our discussions with presenting in Figure 1 the resulting thermodynamical potential Ω as a function of M, the constituent (anti)quark mass. Different q evidently results in a large change of the thermodynamical potential which shows that the effects caused by nonextensivity are quite strong whether the quark chemical potential vanishes or not.

In Figure 1(a), the potentials with different q are shown for $T = 148$ MeV and $\mu = 0$. Locations of its minimum become smaller when q gets larger. This means that, in the case of high temperature and low density, correlations with the nonextensive q-version shift the chiral condensation toward smaller M. On the other hand (in Figure 1(b)), at low temperature but high density ($T = 40$ MeV and $\mu = 286.8$ MeV), the gap of potential between local (near $M = 0$) and global (far from $M = 0$) vacuum also increases as q increases. It is worthy to note that, as seen in Figure 1(b), different q nearly does not affect the position of global vacuum which should have nothing to do with the model itself.

It is instructive to plot the q-effects on the constituent (anti)quark mass M under the temperature dependencies as well as the chemical potential dependencies, which are clearly shown in Figure 2. For the T-dependence ($\mu = 0$), the values of M change continuously with the temperature T, which describes a typical crossover transition, while, for the μ-dependence (where we set $T = 40$ MeV), it shows a jump over the values of M, demonstrating a first-order phase transition.

Figure 2(a), at low density, indicates that the temperature dependence of M for $q \neq 1$ is quite similar to the case of $q = 1$, the usual BG situation. Both the minimum and maximum

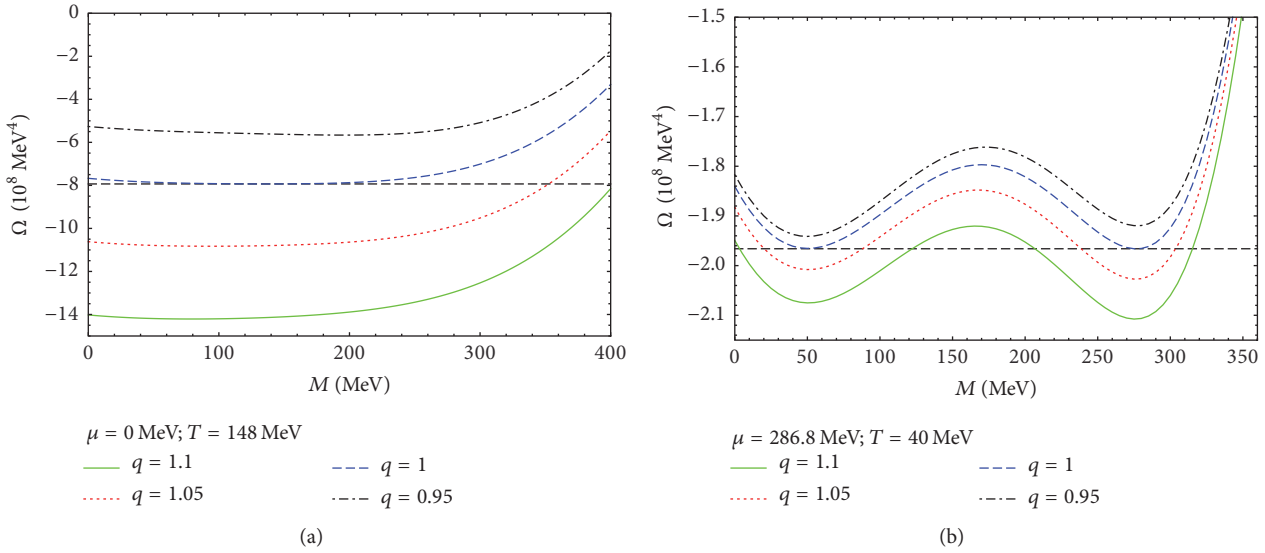

FIGURE 1: The thermodynamical potentials Ω (cf. (14) and (7)), with respect to the constituent (anti)quark mass M. (a) $T = 148$ MeV and $\mu = 0$. (b) $T = 40$ MeV and $\mu = 286.8$ MeV. We compare our results using the parameters near the phase boundaries. Both of them are analysed for $q = 1.1$, $q = 1.05$, and $q = 0.95$ with the case of $q = 1$ as comparisons.

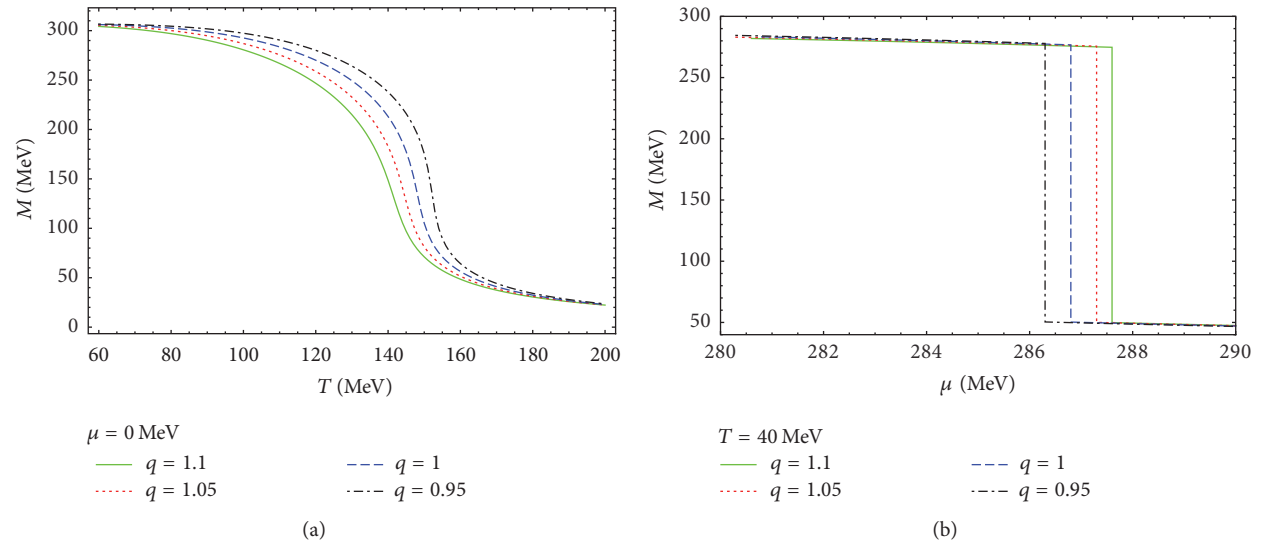

FIGURE 2: The constituent (anti)quark mass M as functions of the temperature T at $\mu = 0$ (a) and the chemical potential μ at $T = 40$ MeV (b) for different $q$as follows: $q = 1.1$, $q = 1.05$, and $q = 0.95$ as well as $q = 1$.

of M keep the same values for different q. Nevertheless, the behaviour of all curves tells us that high temperature is required to restore the chiral symmetry for small q, which agrees with the results of [13, 14].

At the same time, for the low temperature case, Figure 2(b) illustrates the μ-dependence of the constituent (anti)quark mass in the nonextensive linear sigma model for different nonextensive parameter q, which is not done in [13, 14]. One easily observes an analogous pattern characteristic to the above, while, for the μ-dependence, increasing q will also increase the value of phase transition chemical potential when $T = 40$ MeV is fixed. Moreover, for both of the cases, it is deserved to be mentioned that only the system near the chiral phase transition is well affected by nonextensive statistics.

In statistical physics, the critical properties of a thermodynamic system can be explored by studying the fluctuations of various observables. Particularly, the fluctuations of the order parameter probe the order of the phase transition and the position of a possible critical end point.

Then the negative partial derivative of M with respect to temperature T holding chemical potential μ constant, the susceptibility χ, is also investigated in this nonextensive linear sigma model, which describes the fluctuation of constituent (anti)quark mass. From the results seen in Figure 3, one can expect that, at the low density ($\mu = 0$), the location of peak

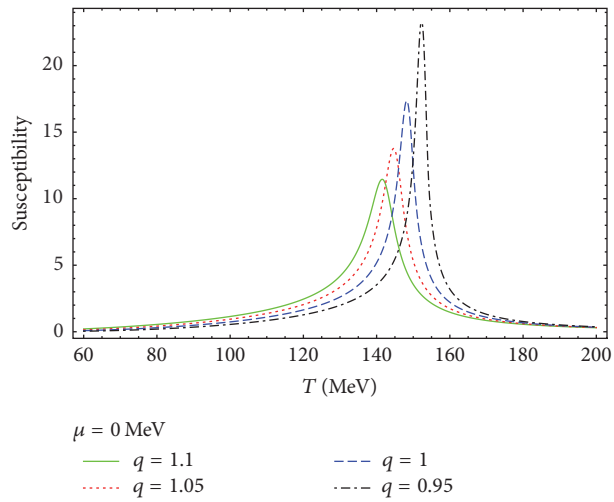

FIGURE 3: The nonextensive effects on susceptibility $\chi = -(\partial M/\partial T)|_{\mu}$ with temperature T at $\mu = 0$ are shown for various q values as shown in previous figures ($q = 1.1$, $q = 1.05$, and $q = 0.95$ as well as $q = 1$ for baseline).

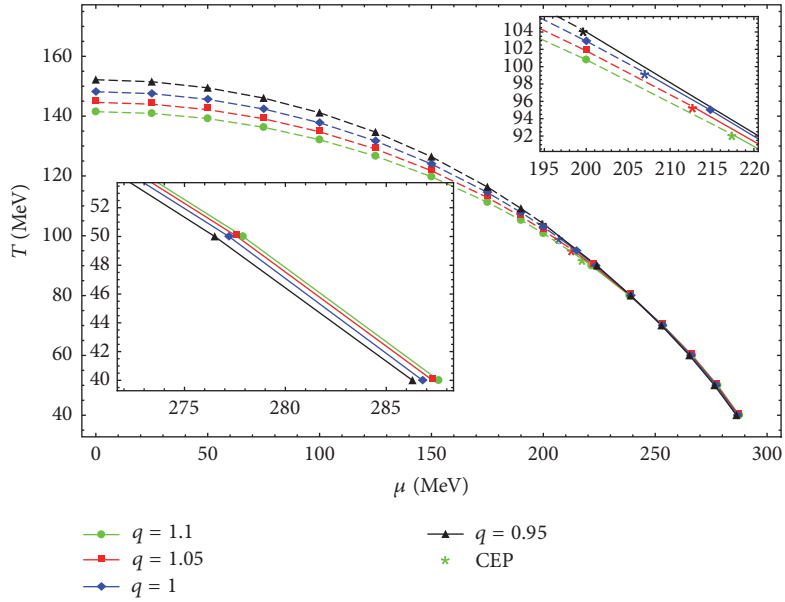

FIGURE 4: Phase diagram of the q-linear sigma model in the (T, μ) plane for various q values. The results are plotted for four different values of q with the vicinity of the q-dependent CEP and the low temperature part of the curves enlarged in the inset. For more details, the dashed line stands for crossover transition and the solid one the first-order transition. CEPs are shown as star points.

of susceptibility χ, as well as its own value, moves to the lower values of temperature T for larger q. This indicates that, with larger q, the critical temperature T_c gets smaller, which supports the fact that the nonextensive parameter q describes the departure of system from the conditions of BG situation.

Here we add a few remarks to better understand the results. Nonextensive dynamics develop the linear sigma model through the (anti)quark number distribution functions. These functions are connected with the thermal potential $\Omega_{\bar{\psi}\psi}(T, \mu, q)$ of (14), which modifies the fluctuations of fermions. The q-dependent chiral condensation can be obtained after solving out the gap equation in (15). From Figure 2(a), we can see that its shape with respect to T is strongly affected by the nonextensive parameter q. More specifically, q introduces differences of system itself from the usual BG one which decrease the values of critical temperature T_c, seen in Figure 3.

In order to explore the chiral phase transition in the q-linear sigma model more specifically, we also present the phase diagrams (seen in Figure 4) based upon the analysis above. It is easily seen that, indeed, at high temperature and low density region, it exhibits a crossover transition in the $(T - \mu)$ plane for different nonextensive parameters of q, with smaller nonextensive parameter q expanding the relative values of critical temperature and chemical potential. Meanwhile, a first-order phase transition is shown at low

temperature but high density region. And all the critical lines correspondingly develop differently, where larger q increases the position of T_c at the same μ_c.

As for the critical endpoint (CEP), which is located between the two kinds of phase transition, larger q occurs at higher chemical potential but lower temperature, which is also seen in the results of q-NJL model [16, 17]. This is because systems from fewer particles will encounter a larger value of q, whose phase transition takes place with higher number density in turn.

4. Summary and Outlook

To summarize, we have calculated the nonextensive thermodynamics of the chiral phase transition in the linear sigma model, to account for the sensitivity of the mean-field theory of the linear sigma model to the departure from the usual BG statistics. By the q-version, we have obtained generalized relations of the grand canonical potential Ω, the chiral condensation M, and susceptibility χ. Before that, we also analysed the values of nonextensive parameter q and reasonably considered the cases of $q = 1.1, 1.05, 0.95$ as well as $q = 1$.

Furthermore, we have investigated two scenarios, $\mu \neq 0$ and $\mu = 0$, respectively, which, as mentioned, correspond to different physical situations: a first-order and a crossover transition. For the studies of $\mu = 0$, it is found to be in agreement with the results obtained in [13, 14]. Besides, we discover that different values of q only influence the quantities near the phase boundary. This also proves that it is valuable and desirable to discuss the nonextensive effects on the chiral phase transition.

As expected, the observed nonextensive effects of both the potential Ω and the mass M lead to the fact that higher values of q shift all to an earlier state with other parameters fixed. In other words, the internal divergence from the classical thermal equilibrium really impacts the chiral phase transition. This is more illuminated in the phase diagrams of (T, μ) plane correspondingly. The CEP (see Figure 4) reveals a clear variation with different nonextensive parameters of q, namely, holding higher chemical potential but lower temperature with q increasing, which agrees with [16, 17]. As for the critical line in the diagram, as shown in Figure 4, q-effects derive different trends of it on the first-order and crossover phase transitions, whose physical mechanism needs from us more attention and investigations next.

Finally, it is worthy to mention that since CEP is still indistinct experimentally, our work may provide a possible intensive study of locating the CEP in high-energy physics [6]. Meanwhile, by comparing the results with experimental data, our researches could be of help to deeply understand the physical explanation of the Tsallis nonextensive parameter q, which is also what we will pay attention to in the future.

Conflicts of Interest

The authors declare that they have no conflicts of interest.

Acknowledgments

This research is partly supported by the Ministry of Science and Technology of China (MSTC) under the "973" Project nos. 2014CB845404 and 2015CB856904(4) and by NSFC under Grant nos. 11435004, 11322546, 11375070, and 11521064.

References

[1] A. Bazavov, H.-T. Ding, P. Hegde et al., "QCD Equation of State to $\partial(\mu_B^6)$ from Lattice QCD," *Physical Review D*, vol. 95, article 054504, 2017.

[2] H. Reinhardt and P. Vastag, "Chiral and deconfinement phase transition in the Hamiltonian approach to QCD in Coulomb gauge," *Physical Review D: Particles, Fields, Gravitation and Cosmology*, vol. 94, no. 10, 2016.

[3] R. A. Lacey, "Indications for a critical end point in the phase diagram for hot and dense nuclear matter," *Physical Review Letters*, vol. 114, article 142301, 2015.

[4] P. Braun-Munzinger and J. Wambach, "Colloquium: Phase diagram of strongly interacting matter," *Reviews of Modern Physics*, vol. 81, no. 3, pp. 1031–1050, 2009.

[5] C. S. Fischer, J. Luecker, and C. A. Welzbacher, "Locating the critical end point of QCD," *Nuclear Physics A*, vol. 931, pp. 774–779, 2014.

[6] J. Randrup, "Phase transition dynamics for baryon-dense matter," *Physical Review C: Nuclear Physics*, vol. 79, no. 5, 2009.

[7] M. Gyulassy and L. McLerran, "New forms of QCD matter discovered at RHIC," *Nuclear Physics A*, vol. 750, no. 1, pp. 30–63, 2005.

[8] M. Abu-Shady and H. M. Mansour, " Quantized linear ," *Physical Review C: Nuclear Physics*, vol. 85, no. 5, 2012.

[9] P. de Forcrand, "Simulating QCD at finite density," *PoS LAT*, vol. 010, 2009.

[10] M. Stephanov, K. Rajagopal, and E. Shuryak, "Signatures of the tricritical point in QCD," *Physical Review Letters*, vol. 81, no. 22, pp. 4816–4819, 1998.

[11] C. Tsallis, "Possible generalization of Boltzmann-Gibbs statistics," *Journal of Statistical Physics*, vol. 52, no. 1-2, pp. 479–487, 1988.

[12] Lists of many applications of non-extensive statistics are available at http://tsallis.cat.cbpf.br/biblio.htm.

[13] M. Ishihara, "Effects of the Tsallis distribution in the linear sigma model," *International Journal of Modern Physics E*, vol. 24, article 1550085, 2015.

[14] M. Ishihara, "Chiral phase transitions in the linear sigma model in the Tsallis nonextensive statistics," *International Journal of Modern Physics E*, vol. 25, article 1650066, 2016.

[15] O. Scavenius, Á. Mócsy, I. N. Mishustin, and D. H. Rischke, "Chiral phase transition within effective models with constituent quarks," *Physical Review C*, vol. 64, article 045202, 2001.

[16] J. Rozynek and G. Wilk, "Nonextensive effects in the Nambu–Jona-Lasinio model of QCD," *Journal of Physics G: Nuclear and Particle Physics*, vol. 36, article 125108, 2009.

[17] J. Rozynek and G. Wilk, "Nonextensive Nambu-Jona-Lasinio Model of QCD matter," *The European Physical Journal A*, vol. 52, no. 13, 2016.

[18] M. C. Birse and M. K. Banerjee, "A chiral soliton model of nucleon and delta," *Physics Letters B*, vol. 136, no. 4, pp. 284–288, 1984.

[19] M. C. Birse and M. K. Banerjee, "Chiral model for nucleon and delta," *Physical Review D: Particles, Fields, Gravitation and Cosmology*, vol. 31, no. 1, pp. 118–127, 1985.

[20] E. K. Lenzi, L. C. Malacarne, and R. S. Mendes, "Perturbation and variational methods in nonextensive tsallis statistics," *Physical Review Letters*, vol. 80, no. 2, pp. 218–221, 1998.

[21] C. Beck, "Dynamical foundations of nonextensive statistical mechanics," *Physical Review Letters*, vol. 87, no. 18, article 180601, 2001.

[22] F. D. Nobre, M. A. Rego-Monteiro, and C. Tsallis, "Nonlinear relativistic and quantum equations with a common type of solution," *Physical Review Letters*, vol. 106, no. 14, article 140601, 2011.

[23] T. S. Biro and G. Purcsel, "Non-extensive Boltzmann equation and hadronization," *Physical Review Letters*, vol. 95, article 162302, 2005.

[24] F. I. Pereira, R. Silva, and J. S. Alcaniz, "Nonextensive effects on the relativistic nuclear equation of state," *Physical Review C: Nuclear Physics*, vol. 76, no. 1, 2007.

[25] B. Liu and J. Goree, "Superdiffusion and Non-Gaussian Statistics in a Driven-Dissipative 2D Dusty Plasma," *Physical Review Letters*, vol. 100, no. 5, 2008.

[26] T. S. Biró and E. Molnár, "Fluid dynamical equations and transport coefficients of relativistic gases with non-extensive statistics," *Physical Review C: Nuclear Physics*, vol. 85, no. 2, 2012.

[27] C. Tsallis, *Introduction to Nonextensive Statistical Mechanics: Approaching a Complex World*, Springer, New York, NY, USA, 2009.

[28] L. P. Csernai, A. Mocsy, and I. N. Mishustin, "Microscopic model for rapid hadronization of supercooled Quark-Gluon Plasma," *Heavy Ion Physics*, vol. 3, no. 151, 1996.